BORANE-FUNCTIONALIZED POLYOLEFINS FOR CATALYSIS AND MATERIALS APPLICATION

by

HUINA LIN

A Dissertation submitted to the

Graduate School - Newark

Rutgers, The State University of New Jersey

in partial fulfillment of requirements

for the degree of

Doctor of Philosophy

Graduate Program in Chemistry

written under the direction of

Professor Frieder Jäkle

and approved by

_____

_____

_____

_____

Newark, New Jersey

October, 2020

ABSTRACT OF THE THESIS

BORANE-FUNCTIONALIZED POLYOLEFINS FOR CATALYSIS AND MATERIALS APPLICATION

By Huina Lin

Dissertation Director: Professor Frieder Jäkle

Boron-containing polymers have received tremendous attention over the past decades due to the diverse potential applications, including their use as polymer-supported catalysts, in drug delivery, optoelectronic materials, and sensors for anions. The ability of the empty p_B-orbital in tri-coordinate boranes to delocalize π–electrons and to form Lewis acid-base complexes is widely applied in Lewis acid catalysis, supramolecular assembly, and the development of luminescent materials. Here we focus on the incorporation of tri-coordinate borane moieties into the side chains of polystyrene (PS) and its derivatives for catalysis applications. An alternative strategy to incorporate boron into polymeric systems is the replacement of a C-C unit for an isosteric B-N unit. Nowadays, the study of carbon-boron-nitrogen (CBN) heterocycles has become one of the most popular topics in organic and materials chemistry. Numerous BN-embedded aromatic compounds have been synthesized. Thus, in a second direction of this thesis, we targeted new azaborine-substituted polymers,

with the goal of expanding the diversity and functionality of polystyrene *via* BN for CC substitution.

We designed a new class of polymers that feature bulkier groups in the *ortho*-position to boron to stabilize the borane moiety. The attachment of the tailored triarylborane moieties to the polyolefin backbone provides access to new polymer-supported Lewis acids with improved stability and recyclability that we applied in the catalytic hydrosilylation of unsaturated organic substrates. In addition, we discovered that both the model compounds and copolymers are strongly luminescent, and display thermally activated delayed fluorescence (TADF), a phenomenon that is attracting much current interest.

To expand the diversity and functionality of polystyrenes *via* BN for CC substitution, we successfully prepared a series of new isomeric azaborine-substituted polymers with high molecular weights *via* standard free-radical polymerization. Furthermore, we investigated the effects of the position of the vinyl group relative to the BN moiety on the polymerization reactivity and physical properties of the respective polymers. The results revealed that the reactivity and physical properties strongly depends on the substitution pattern. Lastly, the ring opening metathesis polymerization of BN Dewar isomers was accomplished with Grubbs 2nd generation catalyst. The synthesized polymer features four-membered BN-heterocycles alternating with vinylene groups in the main chain.

Acknowledgements

First and foremost, I would like to thank my supervisor and mentor, Prof. Frieder Jäkle, for his continuous support and guidance over the past years. His enthusiasm for research and discovery, along with his unmatched dedication to his students are what make him an excellent scientist, advisor, and person. He helped me to become a better researcher. I would also like to thank my research committee members Prof. John Sheridan, Prof. Michal Szostak and Prof. Elizabeth Elacqua (The Pennsylvania State University) for their help, advice and corrections to my thesis.

I am grateful for the wonderful time with many knowledgeable postdoctoral fellows and young talented chemists in the Jäkle group. I would like to thank Dr. Fernando Vidal who helped me with my research and interview. Thanks to Dr. Jiawei Chen, Dr. Xiaodong Yin and Dr. Yi Ren for their guidance and suggestions. In addition, I am thankful to all the past and present group members for their friendship and encouragement throughout my time in the Jäkle lab. I am also grateful to many of the faculty and staff at Rutgers University, especially Prof. Roger Lalancette for his help with single-crystal X-ray crystallography, Dr. Lazaros Kakalis for his expertise in NMR spectroscopy.

I am also appreciative of the many funding organizations that have supported me financially over the past years. These include the National Science Foundation under Grants CHE-1609043 and CHE-1904791. The Bruker 500 MHz NMR spectrometer used in this study was acquired with partial support by an NSF-MRI grant (CHE-1229030). Equipment in the Polymer and Nanomaterials Facility at Rutgers University Newark was acquired with support by the New Jersey Higher Education Equipment Leasing Fund (ELF III 047-04).

Last and certainly not least, I would like to thank my family and my sister for their support. Mon and dad always supported and encouraged me throughout all the good and bad times. I would also like to thank my friends Jingyao Zuo, Kanglei Liu and plenty of friends in China for their encouragement and support.

Table of Contents

List of Figures

List of Schemes

List of Tables

Chapter 1 General Introduction

1.1 Synthesis and Applications of Boron-containing Polyolefins

The incorporation of borane moieties into polymers has received tremendous attention over the past decades due to the diverse potential applications, including their use as polymer-supported catalysts, in drug delivery, optoelectronic materials, and sensors for anions. Figure 1-1 shows some of the most commonly studied architectures of boron-containing polymers.[1] The boron element can be either embedded into the main chain of conjugated polymers or as pendant groups; the attachment of organoborane moieties as side chains or as end groups to polyolefins has also been studied extensively.[2] Although a lot of synthetic routes have been developed to incorporate boron into the polymer main chain, the challenges in achieving control over the molecular weight and polymer architecture still present an obstacle. In contrast, the functionalization of polyolefins offers some advantages such as excellent solubility, easier access to materials of controlled molecular weight and architecture, and the facile combination with other functional groups. Thus, diverse methods for the preparation of borane-functionalized polyolefins have been introduced, including systems with tricoordinate and tetracoordinate borane moieties. Here, we will mainly focus on the attachment of borane moieties to the side chains of soluble polyolefins. The different synthetic routes to these tricoordinate organoborane polymers will be presented, followed by a brief overview of their applications.

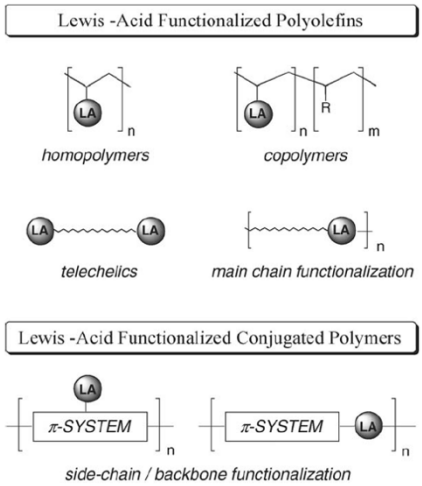

Figure 1-1. Selected architectures of boron-containing polymers.[1] [Adapted with permission from reference 1. Copyright © 2006 Elsevier B.V.]

1.1.1 Synthesis of polymers with tri-coordinate organoborane pendant groups

Organoborane-functionalized polyolefins are generally synthesized either by direct polymerization of boron-functionalized monomers or *via* so-called post-modification of pre-formed functional polymers. Both methods have been applied successfully for the attachment of boron substituents to the side chains of polyolefins.[3]

1.1.1.1 Direct polymerization

The direct polymerization approach requires the preparation of boron-functionalized monomers that contain polymerizable groups, most commonly vinyl functional groups. Conventional free radical polymerization and controlled free radical polymerization both work well for the polymerization of boron-containing monomers, since the synthetic

protocols are straightforward and the compatibility of the propagating radicals with B-C bonds tends to be reasonably good. Meanwhile, Ziegler-Natta polymerization is also well suited, especially for strongly Lewis acidic monomers. In addition, ring-opening metathesis polymerization can be applied for the polymerization of cyclic olefinic monomers with pendent borane groups.

Conventional free radical polymerization has been frequently used for monomers that feature air-stable borane moieties, such as boronic acids and esters.[4] Even some more unusual monomers such as 1-hydro-2-vinyl-1,2-azaborine and 1-hydro-2-styryl-1,2-azaborine have successfully been polymerized by thermally induced radical polymerization with AIBN (azobisisobutyronitrile), BPO (benzoyl peroxide) or ACHN (1,1'-azobis(cyclohexanecarbonitrile) as initiators (Scheme 1-1a).[5] "Living" free radical polymerization has also been applied to the preparation of organoboron polymers with controlled molecular weight and end groups. Moreover, this is the most common strategy for the preparation of block copolymer architectures. Our group presented the first example of controlled polymerization of a boron-containing monomer to achieve homopolymers and block copolymers with styrene *via* atom transfer free radical polymerization (ATRP) (Scheme 1-1b).[6] Later on, we demonstrated the direct and controlled polymerization of dimesitylborane-substituted styrenes *via* reversible addition-fragmentation chain transfer (RAFT). A block copolymer with PNIPAM (poly(N-isopropylacrylamide)) was used to detect fluoride anions in aqueous solution at a remarkably low level of less than one ppm (Scheme 1-1c).[7]

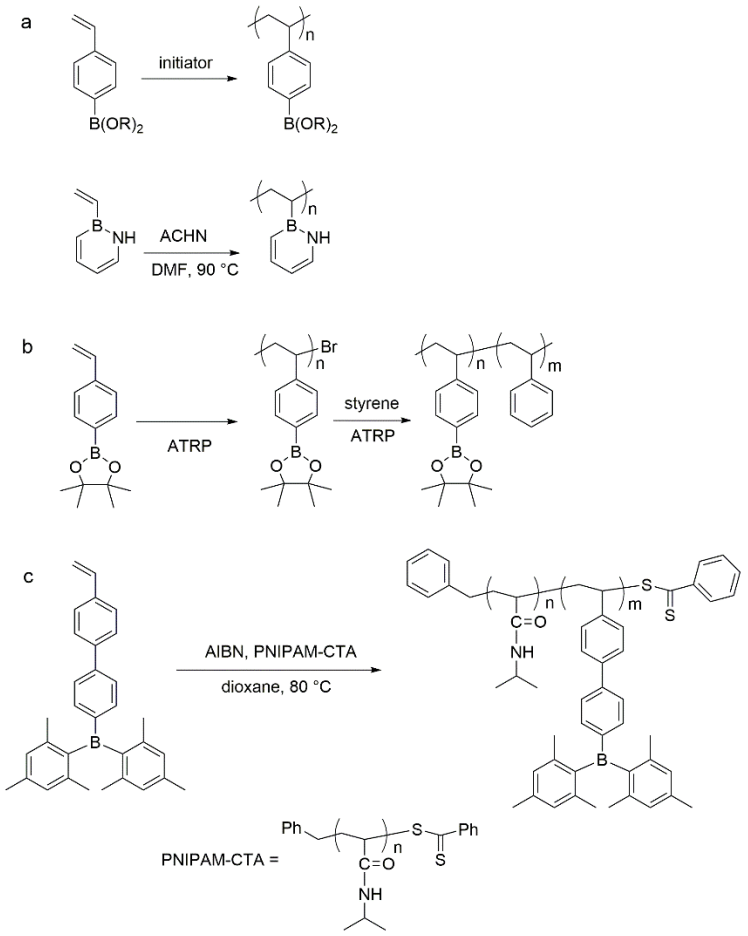

Scheme 1-1. Examples of standard free radical polymerization (a), ATRP (b), and RAFT (c) polymerization of organoboron monomers.[4-7]

Ziegler-Natta polymerization presents a powerful method that has commonly been employed to polymerize α-olefins with high linearity and stereoselectivity. This method is compatible with highly reactive and strongly Lewis acidic organoboron species. Chung and coworkers reported the copolymerization of propylene with hexenyl-9-BBN (9-BBN = 9-borabicyclononane) in toluene with $TiCl_3$ as catalyst and Et_2AlCl as cocatalyst.[8] The direct copolymerization of ethylene with a triarylborane monomer has been studied by Do and Lee and coworkers to prepare a luminescent polyethylene derivative in the presence of

$Me_2Si(\eta^5\text{-}C_5Me_4)(\eta^1\text{-N-}t\text{-Bu})TiCl_2$/methylaluminoxane (MAO) as the catalyst system.[9] More recently, Klausen and coworkers investigated the Ziegler-Natta polymerization of BN-substituted 2-vinylnaphthalene (BN2VN). The polymerization with Cp^*TiMe_3 as the catalyst and $B(C_6F_5)_3$ as the cocatalyst proceeded in a syndioselective fashion (Scheme 1-2). Syndiotactic poly(vinyl alcohol) was prepared by stereoretentive post-polymerization oxidation of the pendent organoborane units using NaOOH.[10]

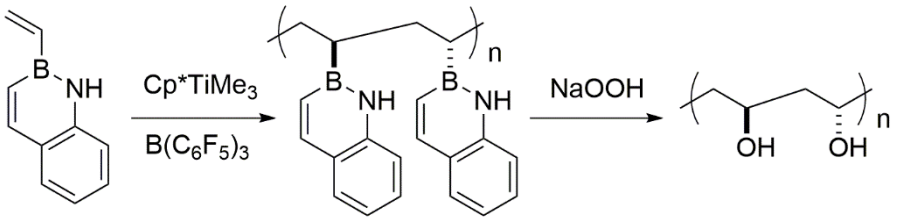

Scheme 1-2. Synthesis of syndiotactic poly(vinyl alcohol) *via* Ziegler-Natta polymerization of BN2VN by Klausen.[10]

Chung and coworkers have extended the toolbox to ring-opening metathesis polymerization (ROMP) to achieve boron-containing polymers. The $WCl_6/SnMe_4$-catalyzed ROMP of monomers such as 9-BBN-norbornene (1) produced polymers with an equal ratio of *cis/trans* isomer composition (Figure 1-2).[11] More recently, Gilroy and coworkers polymerized a novel norbornene-based boron difluoride formazante monomer (2) by ROMP. The resulting polymer retained the unique characteristics of the monomers with large Stokes shifts and the ability to serve as electron reservoirs.[12] Other cyclic olefins that possess considerable ring strain include 6-(cyclooctenyl)decaborane (3).[13] The scope of ring-opening polymerizations (ROP) is not limited to cyclic olefins. Manners and Braunschweig explored the synthesis of ferrocenylborane polymers *via* the ROP of boron-

bridged [1] ferrocenophanes (4), which show tilt-angles between the planes of two cyclopentadienyl rings of up to 32º. The high strain energy within the organoborane monomers results in the ring-opening reaction of these boracycles.[14]

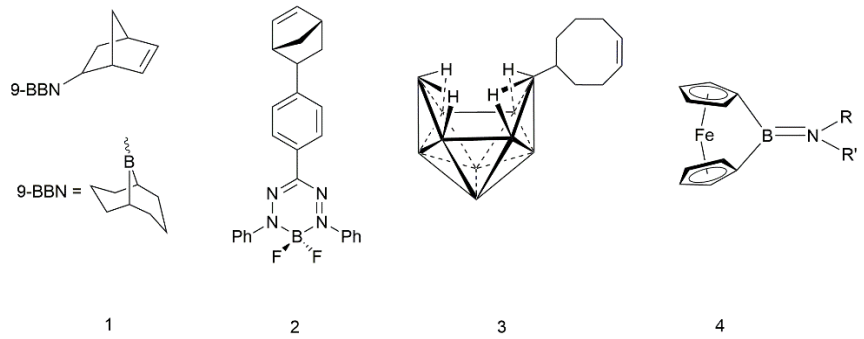

Figure 1-2. Examples of boron-containing monomers for ROMP and ROP studied by Chung[11] (1), Gilroy[12] (2), Sneddon[13] (3), and Manners[14] (4, R = R' = $SiMe_3$/R = Si, R' = *t*Bu/R = R' = *i*Pr).

1.1.1.2 Post-polymerization modification approaches

Post-polymerization modification represents an alternative to direct polymerization that has proved to be highly versatile for attachment of organoborane moieties to polyolefins. Hydroboration, modification based on organolithium or organomercury intermediates, and later on developed borylation of silylated polystyrene, are among the most versatile synthetic methods for the preparation of borane-containing polymers. Besides, unfunctionalized polyolefins have been borylated *via* transition metal-catalyzed C-H activation procedures.

Hydroboration of vinyl-functionalized polyolefins is an efficient method for the synthesis of organoborane-substituted polyolefins. In the 1990s, early studies of the hydroboration of polyolefins with unsaturation in either the main chain or side chain were reported by

Ramakrishnan and Chung.[15, 16] After the hydroboration, the borane moiety can be replaced by other functional groups. For instance, Studer and coworkers reported the synthesis of functionalized poly(alkoxyamine)s by hydroboration of polyolefins with catecholborane and subsequent oxidation by nitroxides (Scheme 1-3).[17]

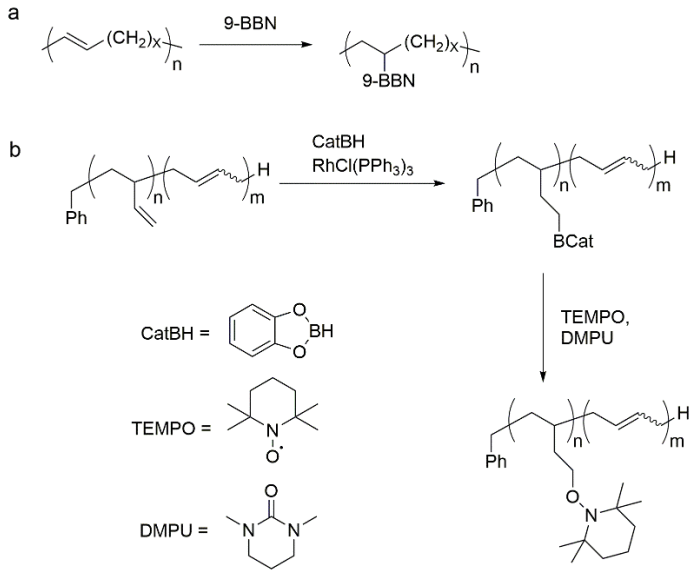

Scheme 1-3. Hydroboration of polyolefins with unsaturated groups and further oxidation by Studer.[17]

Early work of post-polymerization modification also relied on lithiated and mercuriated polymers. However, the obstacles of low selectivity, low conversion, and crosslinking issues limited applications. To solve these issues, our group has demonstrated a strategy using silylated polystyrenes instead. This approach consists of three steps: the preparation of the trimethylsilyl-functionalized polystyrene, the exchange of the trimethylsilyl groups for dibromoboryl groups, and the replacement of the bromines with other functional groups. The advantages of this strategy are: (1) silylated polymers and copolymers of well-controlled architecture, molecular weight, and degree of functionalization can be accessed;

(2) the boron-silicon exchange occurs under mild reaction conditions; (3) facile fine-tuning of the Lewis acidity of the boron centers can be achieved by introducing different substituents (Scheme 1-4, Figure 1-3).[3, 18, 19]

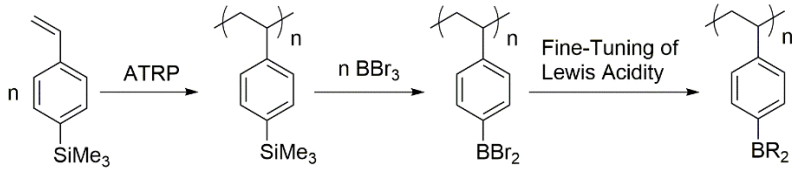

Scheme 1-4. General methods for the synthesis of organoboron polymers of varying Lewis acidity by Jäkle.[18]

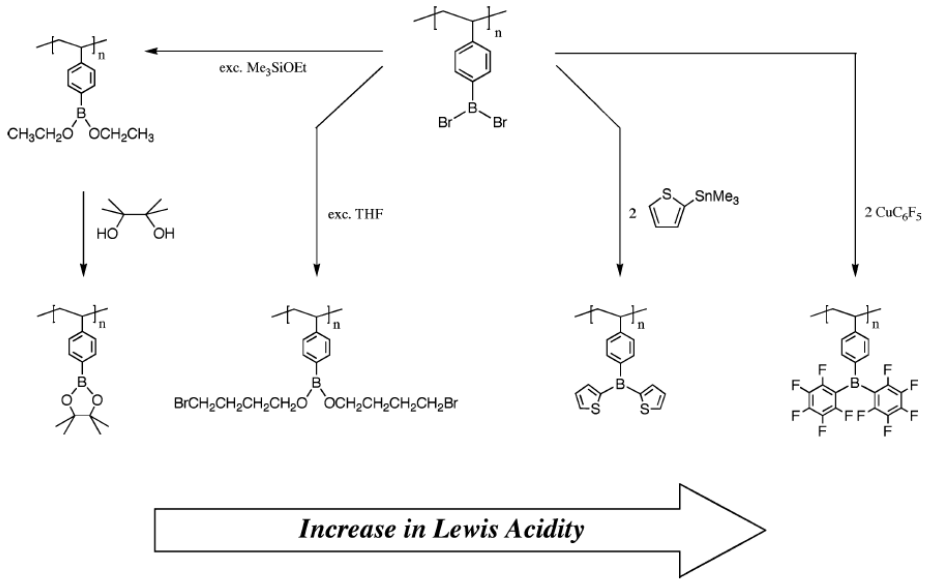

Figure 1-3. Formation of organoboron polymers from dibromoborylated polystyrene.[3] [Adapted with permission from reference 3. Copyright © 2005 Springer Science+Business Media, Inc.]

In 2005, Hillmyer and coworkers reported the transition metal-catalyzed C-H activation of polyolefins. The regioselective functionalization of polypropylenes of varying tacticity was achieved using Cp*Rh(C_6Me_6) as the catalyst. In this process the methyl C-H bonds are

functionalized with Bpin (pin = pinacolato) groups.[20] Aromatic C-H activation is also possible; for instance, Bae's group reported a highly effective borylation of polystyrene using bis(pinacolato)diboron (B_2pin_2) in the presence of $[IrCl(COD)]_2$ (COD = cyclooctadiene) under mild conditions while tolerating various functional groups (Scheme 1-5). Aromatic ionomers were pursued by subsequent Suzuki-Miyaura coupling between sulfonated phenyl bromides and the boron-containing polystyrene.[21]

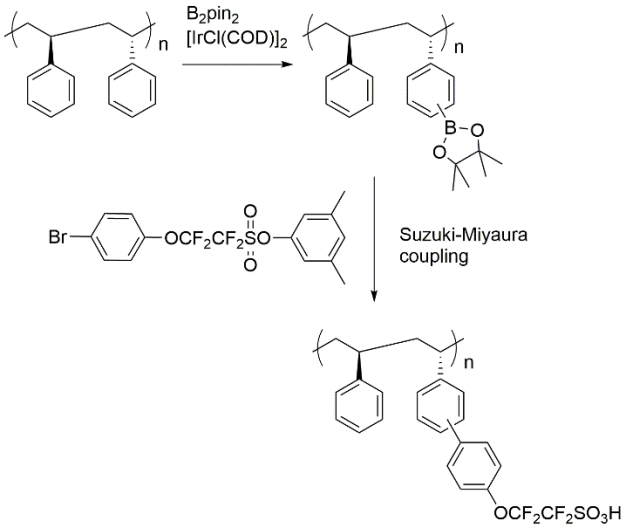

Scheme 1-5. Synthesis of syndiotactic polystyrene ionomers functionalized with sulfonic acid groups *via* transition metal-catalyzed C-H activation of polyolefins by Bae.[21]

1.1.2 Applications

Due to the ability of the empty p_B-orbital of boron to delocalize π–electrons and to form Lewis acid-base complexes, organoboranes are widely applied in catalysis, the formation of supramolecular materials, and luminescent materials.

1.1.2.1 Lewis acids in catalysis

Over the past decade, frustrated Lewis pair (FLP) chemistry has emerged and is nowadays widely applied in catalysis. This concept is based on the notion that the reactivity of an unquenched Lewis pair, consisting of a Lewis acid and a Lewis base, can be harnessed to activate a third molecule. The potent boron Lewis acid $B(C_6F_5)_3$ (Figure 1-4) was first prepared back in the early 1960s, without a specific purpose, until Marks and coworkers found that electron deficient-boranes are excellent cocatalysts in metallocene-mediated alkene polymerization.[22] The catalytic ability of $B(C_6F_5)_3$, by itself, was discovered in the late 1990s by Piers and coworkers in the $B(C_6F_5)_3$-catalyzed hydrosilylations of C=X bonds (Scheme 1-6a).[23] Catalytic applications of Lewis acids developed relatively slowly until 2006 when Stephan and coworkers first introduced the concept of FLPs. This concept represents a fundamental and novel strategy to develop catalysts for small molecule activation (Scheme 1-6b).[24] Following the successful implementation of organoboranes in FLP chemistry by Stephan, numerous catalytic processes, including hydrogenation, hydroamination, and CO_2 reduction, have been explored. Meanwhile, organoborane-promoted hydrosilylation reactions have also been further investigated, including many different substrates.

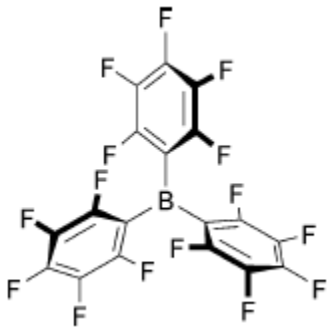

Figure 1-4. Tris(pentafluorophenyl)borane [$B(C_6F_5)_3$].

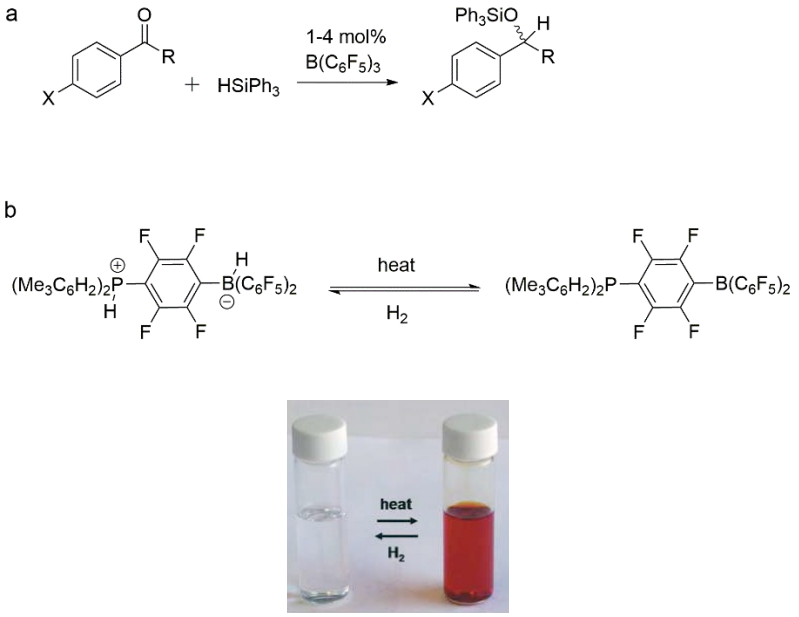

Scheme 1-6. (a) Lewis acid catalyzed hydrosilylation by Piers[23] and (b) FLP activation of dihydrogen by Stephan[24]; the photograph illustrates the color changes observed upon hydrogenation and dehydrogenation of the boron-phosphorous Lewis pair.

Metal-free hydrogenation catalysis is an essential application of FLPs. Over the past decade, the scope of the substrate has been expanded dramatically to more polar substrates, including enamines, silyl enol ethers, enones, oximes, olefins, and polyaromatics. As the most common and privileged Lewis acid, the applicability of $B(C_6F_5)_3$ is restricted owing to its relatively low functional group tolerance and moisture sensitivity. Two strategies have been successfully implemented to reduce the incompatibility of $B(C_6F_5)_3$ with substrates encompassing oxygen or nitrogen-centered Lewis base sites. One is the mitigation of electron-deficiency of the boron, and the other is the size-exclusion approach (Figure 1-5). In this way, Soós and coworkers developed a series of well-tuned Lewis acidic boranes that serve as more tolerant FLP catalysts for hydrogenation[25-27] (Figure 1-

6). In addition to hydrogenation, the hydroamination of alkynes with arylamines can be used to produce the corresponding aryl enamines.[28] Beyond the activation of H_2, a variety of other small molecules are captured by FLPs. An example is the reduction of CO_2. Since Ashley and O'Hare discovered the potential of FLPs to promote the reduction of CO_2 to methanol,[29] more diverse FLPs for CO_2 capture and reduction have been exploited.

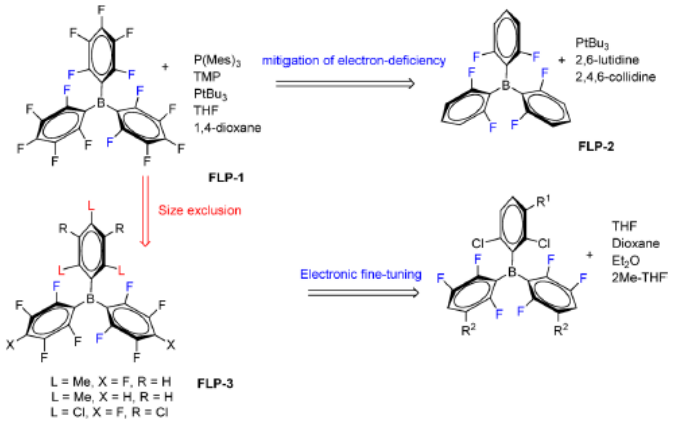

Figure 1-5. Design concepts for moisture-tolerant FLP hydrogenation by Soós.[27] [Adapted with permission from Ref. 27. Copyright © 2015, American Chemical Society]

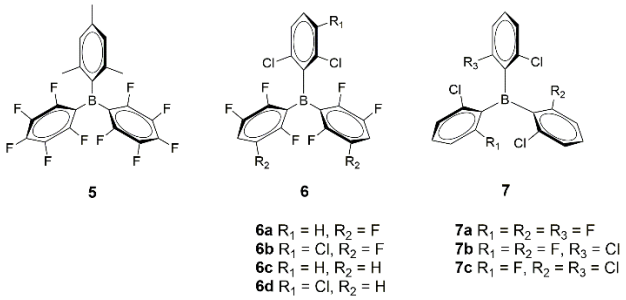

Figure 1-6. Examples of well-tuned Lewis acidic boranes by Soós.[25-27]

Without additional Lewis bases, electron-deficient boranes as Lewis acids catalyze the hydrosilylation of C=X bonds by a counterintuitive mechanism shown in Scheme 1-7.[30]

That is, the Lewis acid activates the hydrosilane through reversible η^1 coordination, rather than the Lewis basic sites in the substrate, to form intermediate **IV**. The nucleophilic attack by the Lewis basic atom in **I** is then facilitated by the enhanced Lewis acidity of the silicon atom in **IV**. The hydride migration from silicon to boron generates an ion pair **VI**. Transfer of the hydride from the borohydride to the electrophilic substrate completes the catalytic cycle. Piers and coworkers found that $B(C_6F_5)_3$ is a suitable catalyst for the activation of the Si-H bond. Various aromatic and aliphatic carbonyl compounds were hydrosilylated by Ph_3SiH. These findings encouraged the exploration of new electron-deficient boranes that have higher functional group tolerance. The extension of this carbonyl reduction chemistry to thioketones, imines, and alkenes was successfully achieved. Oestreich and coworkers also established cyclohexa-1,4-diene- and cyclohexa-1,3-diene-based trimethylsilane as new platforms for ionic transfer hydrosilylation of alkenes (Scheme 1-8). The hydrosilane is released in *situ* by $B(C_6F_5)_3$–promoted decomposition of silylated cyclohexadiene.[31, 32] This approach avoids the usage of gaseous hydrosilanes, such as Me_3SiH.

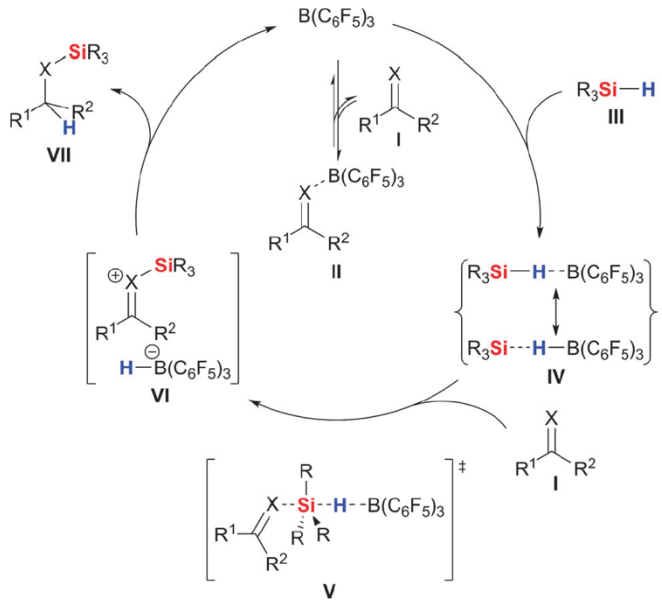

Scheme 1-7. Mechanism of the $B(C_6F_5)_3$-catalyzed hydrosilylation of ketones (X = O) and imines (X = NR^3).[30] [Adapted with permission from Ref. 30. Copyright © The Royal Society of Chemistry 2015]

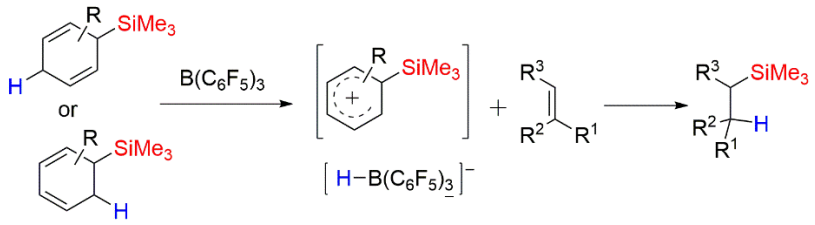

Scheme 1-8. Cyclohexa-1,4-dienes and cyclohexa-1,3-dienes as hydrosilane surrogates in $B(C_6F_5)_3$-catalyzed transfer processes to alkenes.[31, 32]

The attachment of tricoordinate borane moieties to polyolefins produces polymeric Lewis acids[1] and allows for the separation and recovery of the Lewis acid catalysts.[33] Although the idea of using polymer-supported Lewis acids as catalysts in these transformations is appealing, only very few efforts have been reported to date. In 2002, Piers and coworkers reported the first example of a dendrimer-supported Lewis acid catalyst. The carbosilane

dendrimers capped with 4, 8, 12 perfluoroarylborane Lewis acids were prepared and successfully utilized as catalysts in the catalytic hydrosilylation of acetophenone.[34] As an alternative, embedding Lewis base into polymer networks was studied by Thomas and coworkers. The combination of porous polymeric Lewis base and Lewis acid $B(C_6F_5)_3$ yields semi-immobilized FLPs, which are capable of splitting dihydrogen and catalyze hydrogenation at ambient temperature and low hydrogen pressure.[35] Very recently, Yan and coworkers found a new CO_2-responsive system for the catalytic formylation of N-H bonds based on two complementary Lewis acidic and basic block copolymers (Figure 1-7). Interestingly, CO_2 acts as a cross-linker that enables the formation of micelles as recyclable nanocatalysts in this system.[36] The group of Fontaine reported in 2019 the preparation of alkylammoniotrifluoroborate functionalized polystyrenes. These polymeric FLPs were tested as heterogeneous pre-catalysts for the borylation of heteroarenes, and the reusability of the polymers may lead to greener processes for these catalytic C-H borylation processes (Figure 1-8).[37]

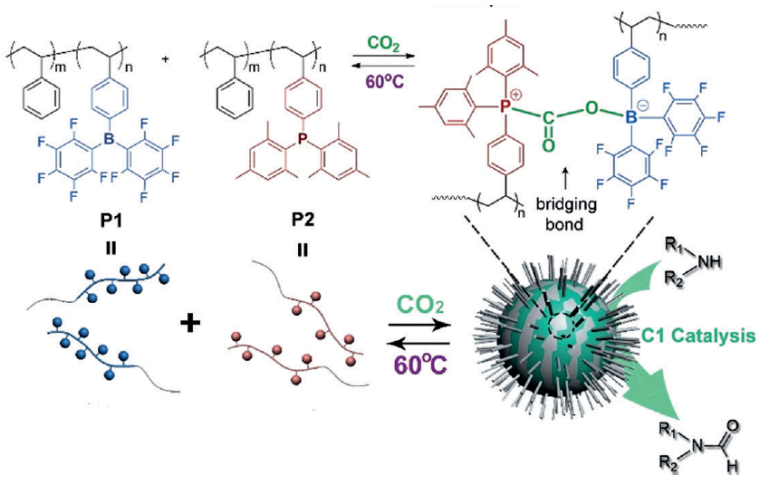

Figure 1-7. Poly(FLPs) as a second-generation CO_2-responsive system designed by Yan.[36] [Adapted with permission from Ref. 36. Copyright © 2018 Wiley-VCH Verlag GmbH & Co. KGaA, Weinheim]

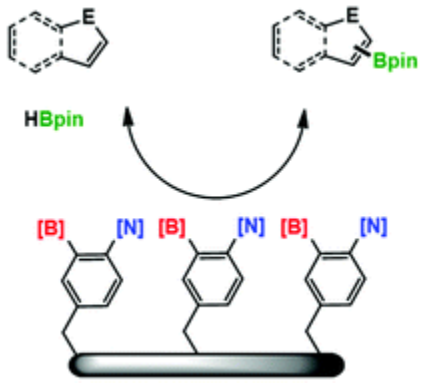

Figure 1-8. Poly(FLPs) as pre-catalysts for the C-H borylation of heteroarenes designed by Fontaine.[37] [Adapted with permission from Ref. 37. Copyright © The Royal Society of Chemistry 2019]

1.1.2.2 Supramolecular materials

Researchers have recently started to explore organoborane polymers as macromolecular building blocks for advanced supramolecular materials. The dative interaction between LAs and LBs offers potential benefit relative to other approaches. A particular benefit of classical LPs for applications in supramolecular polymeric materials is that a vast range of binding strengths is accessible *via* simple substituent variation. Brook and coworkers reported the first example of thermoreversible cross-linked polymer networks that build on the dative LP interactions by use of terminal or pendant functionalized silicone boronates and amines.[38] Our group reported the construction of transient polymer networks promoted by unhindered LPs as the crosslinking points. Matching of polymers with appended weak/strong organoborane LAs and amine LBs offered access to dynamic materials with

mechanical properties that are tunable over a wide range (Figure 1-9).[39] The formation of the first silicone elastomers based on dynamic B-N crosslinks was demonstrated as well. Different from the approach described above, extending the concept of FLPs with latent reactivity to polymer science permits the development of yet another new class of responsive, functional, self-healing materials. The combination of sterically hindered Lewis acids and bases has been used as a platform for the formation of dynamic polymer networks in the presence of small molecules like carbon dioxide[36] and diethyl azodicarboxylate (DEAD). Shaver and coworkers reported a poly(FLP) system comprised of B- and P-functionalized polystyrene (Figure 1-10). The addition of DEAD triggered rapid network formation. The resulting gel is dynamic, self-healable, heat-responsive, and can be reshaped by post-gelation processing.[40]

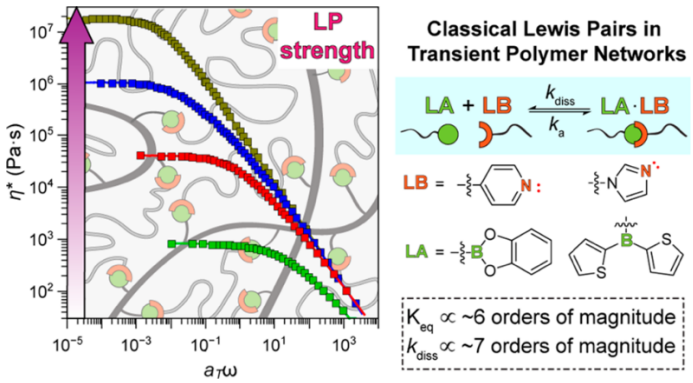

Figure 1-9. Classical Lewis pairs in transient polymer networked reported by Jäkle.[39] [Adapted with permission from Ref. 39. Copyright © 2019 American Chemical Society]

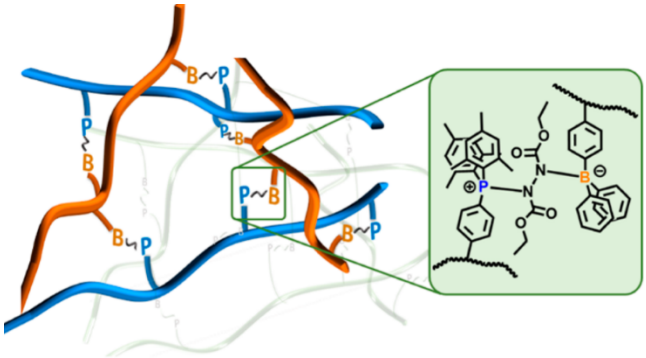

Figure 1-10. Poly(FLPs) as responsive self-healing gels reported by Shaver.[40] [Adapted with permission from Ref. 40. Copyright © 2017 American Chemical Society]

1.1.2.3 Luminescent materials

With the vacant p_z orbital on boron, tri-coordinated organoboron moieties serve as excellent electron acceptors. However, in the absence of stabilization by the binding of a Lewis base, the empty p-orbital also renders tri-coordinate organoboranes often unstable to air and moisture. Steric protection of the boron center with bulky aromatic substituents can be used to increase the stability of organoboranes towards nucleophilic attacks. The most common substituents used for steric protection strategies are 2,4,6-trimethylphenyl (Mes), 2,4,6-tri-iso-propylphenyl (Tip) and 2,4,6-tri-tert-butylphenyl (Mes*). Numerous triarylboron compounds have been explored for applications in optoelectronic devices (OLEDs, FETs, photovoltaics, *etc*.) and anion sensing. Organic light emitting diodes (OLEDs) have attracted considerable interest because of their potential application in flat panel displays and solid-state lighting.[41] Since the first demonstration by Shirota and coworkers that bithiophene or terthiophene with Mes_2B substituents can be used as efficient electron-transporting materials in OLEDs,[42] many different luminescent materials

based on tri-coordinate organoboranes have been designed.[43] More recently, Marder and coworkers[44] studied the difference between $(Mes)_2B$ and $(FMes)_2B$ moieties (FMes = 2,4,6-tris(trifluoromethyl)phenyl), finding that the much enhanced acceptor strength makes $(FMes)_2B$-substituted derivatives promising for OLEDs application (Figure 1-11).

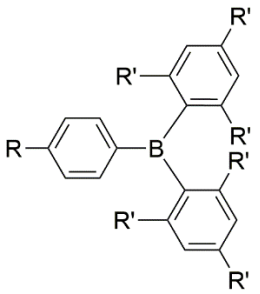

8a, R = H, R' = CF_3
8b, R = $(CH_3)_3C$, R' = CF_3
8c, R = $(C_6H_5)_2C$, R' = CF_3
8d, R = $(C_6H_5)_2C$, R' = CH_3

Figure 1-11. Luminescent triaryboranes for OLEDs application by Marder.[44]

On the other hand, the binding of anions, such as fluoride and cyanide, to boron results in quenching of luminescence or a shift in the emission wavelength, which allows the use of triarylboranes for anion sensing.[45] Yamaguchi and coworkers reported the first organoborane system for fluoride detection in 2001. They developed a highly sterically hindered tris(9-anthryl)borane, which is stable toward air and moisture, but readily binds the small fluoride anion. The addition of fluoride switched the color from orange to colorless (Figure 1-12a).[46] More recently, polymeric materials have also been developed (Figure 1-12b), including systems that show amplified sensory responses and operate in aqueous solution (see also Scheme 1-1c).[7, 47]

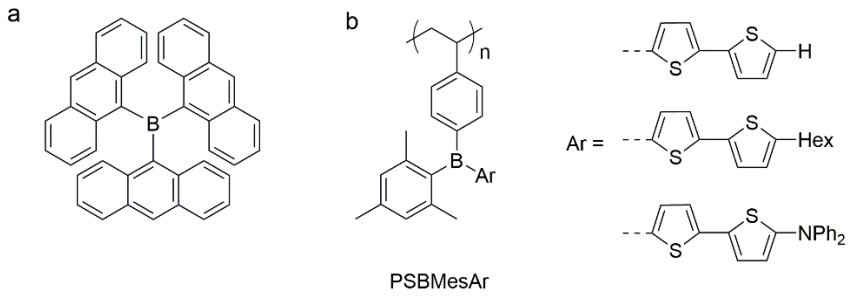

Figure 1-12. (a) The first triarylborane for fluoride sensing by Yamaguchi[46] and (b) triarylborane polymers PSBMesAr for fluoride and cyanide sensing by Jäkle.[47]

Organoborane polymers that show changes in their emission upon application of other stimuli (temperature, solvent polarity, photoirradiation, additives) have also been developed. In a recent example, Li and Wang introduced a new class of multi-emissive/responsive polymers based on a methacrylate monomer containing a switchable boron chromophore (Figure 1-13a). The internal B←O bond in the chromophore can undergo structural switching between a blue-emitting open form and a red-emitting closed form. The degree of polymerization greatly influences the ratio of the open and closed form, leading to tunable multicolor fluorescence (Figure 1-13b).[48]

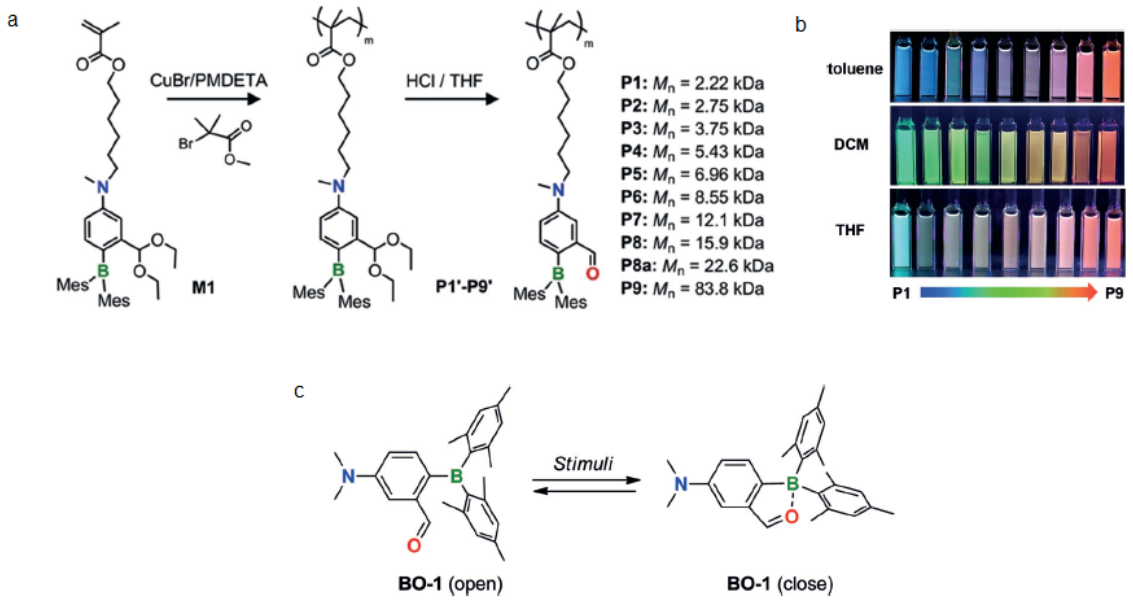

Figure 1-13. (a) Synthetic route to methacrylate polymers with a switchable boron chromophore. (b) Photographs showing the emission colors of the homopolymers (P1 to P9) in toluene (top), DCM (middle), and THF (bottom) under 365 nm UV irradiation. (c) Illustration of the switching of the boron chromophore based on the reversible intramolecular B←O bond.[48] [Adapted with permission from reference 48. Copyright © 2019 Wiley-VCH Verlag GmbH & Co. KGaA, Weinheim]

1.1.2.4 Synthesis of polymers with tetra-coordinate organoborane pendant groups

Tetra-coordinate organoboranes are also attractive as chromophores due to their typically high stability. These chromophores can be embedded in the polymer main chain or side chain. Our group reported a one-pot approach to achieve well-defined organoboron quinolate polymers. Their photoluminescence can be tuned from the blue to the red region by adjusting the quinoline substituents from electron-withdrawing to electron-donating groups (Figure 1-14).[49] In another example, Wang and Li developed the first examples of

organoboron-based photochromic polymers. The copolymer bearing a photochromic B(ppy)Mes_2 unit (ppy = 2-phenylpyridyl, Mes = mesityl) undergoes photoisomerization upon 365 nm irradiation, leading to switchable color and fluorescence as shown in Scheme 1-9.[50]

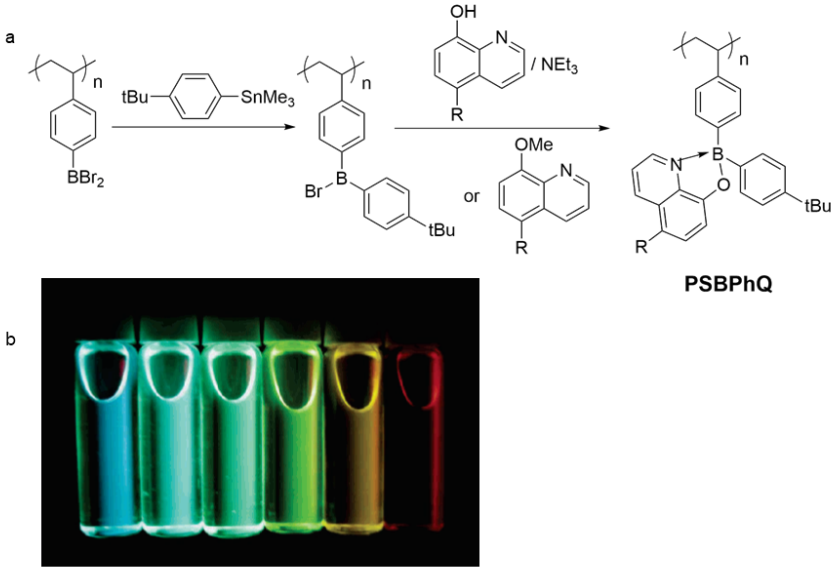

Figure 1-14. (a) Synthesis of organoboron quinolate polymers. (b) Photographs of solutions of PSBPhQ in THF (ca. $2*10^{-3}$ M) excited with black light at 365 nm[49] (from left to right: R = Bpin, C_6F_5, H, Cl, C_6H_4OMe, $C_6H_4NMe_2$, respectively). [Adapted with permission from reference 49. Copyright © 2006 American Chemical Society]

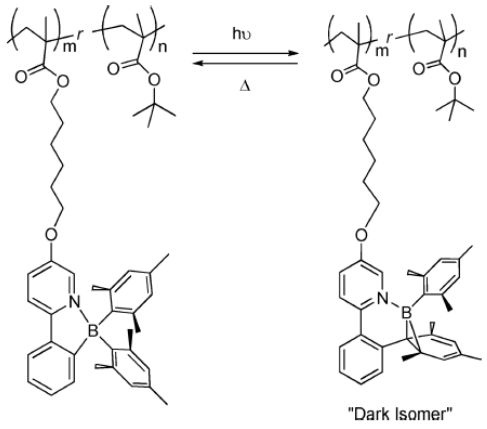

Scheme 1-9. Photochromic random copolymers with B(ppy)Mes_2 as the pendant unit designed by Wang and Li.[50] [Adapted with permission from reference 50. Copyright © 2017 American Chemical Society]

In Chapter 2 of this thesis, we demonstrate the preparation of a new class of polystyrene-based triarylborane polymers. The exploration of their catalysis applications and the investigation of their photophysical properties are discussed. The results indicate the strong potential of these polymeric Lewis acids as catalysts in the hydrosilylation of unsaturated organic substrates and their potential utility as luminescent materials.

1.2 Boron-Nitrogen-Doped Aromatic Compounds and Polymers

Boron and nitrogen-doped aromatic systems generated by replacing a C-C unit with B-N unit have recently received significant attention. Despite the fact that a B-N unit is an isosteric replacement of a C-C unit, having the same number of valence electrons as a pair of carbon atoms, differences can be expected in molecular and electronic properties of BN-doped aromatic compounds due to the dipolar nature of the BN bond. The first example of BN/CC isosterism of an arene to give borazine (*c*-$B_3N_3H_6$) was reported by Alfred Stock in 1926 (**9**).[51] In 1958, Dewar successfully synthesized the first BN-substituted aromatic compound 9,10-azaboraphenathrene (**10**) by replacing a single C=C bond in a polycyclic aromatic hydrocarbon (PAH) with a BN bond.[52] Dewar and White later prepared the first monocyclic 1,2-azaborines (**11**, **12**).[53, 54] Nowadays, the study of carbon-boron-nitrogen (CBN) heterocycles has become one of the most popular topics in organic chemistry and material chemistry. Numerous BN-embedded aromatic compounds have been synthesized. Monocyclic azaborines (more precisely named azaborinines), the isosteres of benzene, can

be categorized into three isomers referred to as 1,2-azaborine, 1,3-azaborine, and 1,4-azaborine according to the particular substitution pattern.

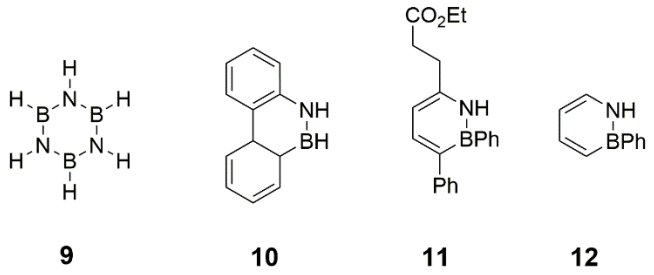

Figure 1-15. Early examples of BN arenes by Stock[51] (**9**), Dewar[52, 53] (**10, 11**) and White[54](**12**).

1.2.1 Azaborines as BN-Isosters of Benzene

The stability of the different azaborine isomers decreases in the order of 1,2-azaborine > 1,4-azaborine > 1,3-azaborine, and all of them are relatively less stable than benzene (Figure 1-16).[55] Following a breakthrough in the mild synthesis of monocyclic 1,2-azaborine achieved by Ashe's group in 2000,[56] 1,2-azaborine as the most stable isomer has attracted considerable interest as a versatile aromatic building block. Meanwhile, efforts by the Liu and Braunschweig groups also resulted in significant progress in the synthesis of 1,3-azaborines and 1,4-azaborines. Overall, numerous synthetic reports for azaborines support further investigations into the functional utility in biochemistry and pharmacology, material science, and transition-metal-based catalysis.

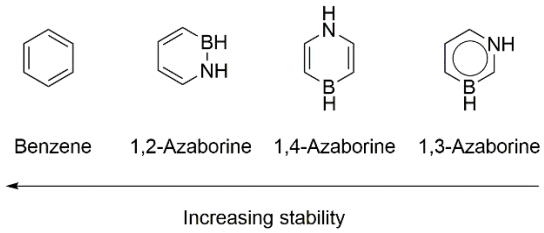

Figure 1-16. Calculated stability trends of benzene and azaborine isomers.[55]

1.2.1.1 1,2-Azaborines

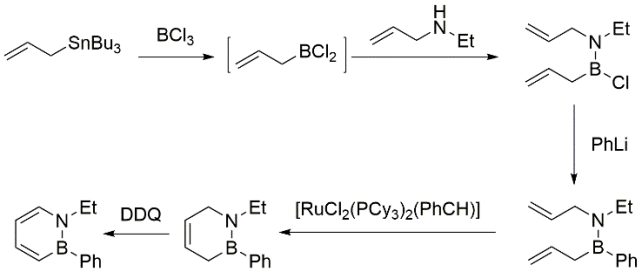

Scheme 1-10. Mild synthesis of 1,2-azaborine by Ashe.[56]

In 2000, Ashe and coworkers developed a ring-closing metathesis/oxidation procedure that enabled the mild and efficient formation of 1,2-azaborines (Scheme 1-10). Liu and coworkers subsequently introduced an important innovation to Ashe's method that allows the synthesis of 1,2-azaborines comprising various substituents on boron by preserving the reactivity of the B-Cl bond.[57] Additionally, Liu's group demonstrated post-functionalization methods for each of the ring positions, paving the way to a greater diversity of 1,2-azaborines. The C(3) and C(6)-substitutions were achieved by a series of versatile coupling reactions. Diverse C(3) functionalization has been accomplished by the Negishi coupling reaction (Scheme 1-11a).[58] Substitution at C(6) has been realized through iridium-catalyzed borylation, followed by palladium-catalyzed (hetero)arylation (Scheme

1-11b).[59] More recently, methods for further functionalization of the previously inaccessible C(4) and C(5)-positions of the 1,2-azaborine heterocycle have been introduced (Scheme 1-11c). Although the product of C-H borylation consists of a mixture of C(4) and C(5)-borylated 1,2-azaborines, the distinct electronic properties of the C(4) and C(5)-positions enable their isolation *via* resolution chemistry. For example, the oxidation by N-methylmorpholine-N-oxide (NMP) is selective for the C4-borylated 1,2-azaborine and the Ir-catalyzed deborylation occurs selectively for the C5-borylated 1,2-azaborine. These two new 1,2-azaborine building blocks are anticipated to expand the diversity and functionality of 1,2-azaborines greatly.[60]

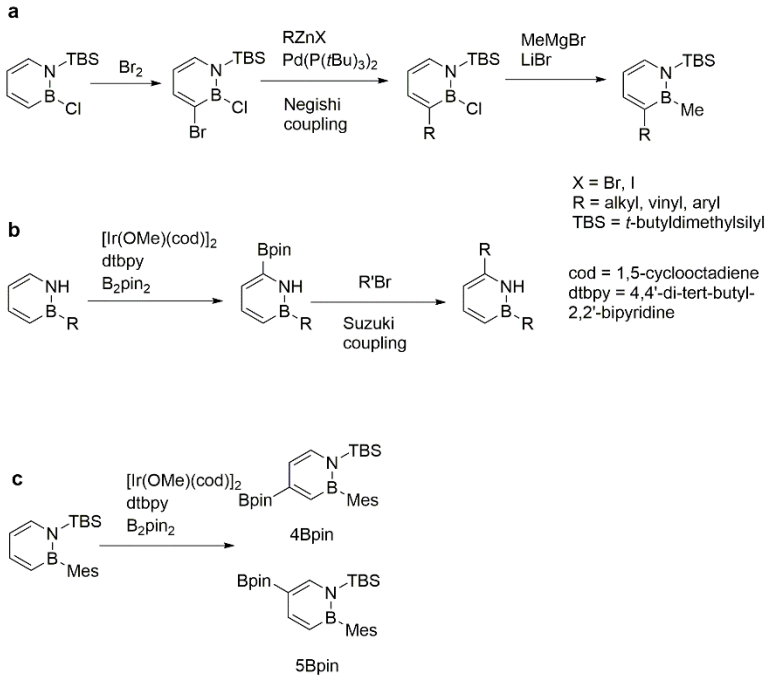

Scheme 1-11. Late-stage functionalization of monocyclic 1,2-azaborines at different positions by Liu.[58-60]

Besides these synthetic advances, many studies on the fundamental properties and reactivities have been pursued. For example, Liu's group demonstrated the first example of a Diels-Alder reaction with 1,2-azaborines (Scheme 1-12).[61] A variety of electron-deficient dienophiles were shown to react with N-TBS-B-Me-1,2-azaborine to produce cycloadducts with high functional complexity.

Scheme 1-12. Diels-Alder reaction between 1,2-azaborine and maleic anhydride by Liu.[61]

Another exciting advance is the photoisomerization of 1,2-azaborines, studied by Bettinger and Liu. The Dewar isomer of the parent 1,2-azaborine was only achieved by irradiation with UV light under matrix isolation conditions (Scheme 1-13a), but B- and N-substituted derivatives could be generated in solution and isolated under ambient conditions (Scheme 1-13b).[62, 63] They proposed that the energy that is reversibly stored in this Dewar valence isomer could be utilized in molecular solar-thermal system applications. They also extended this strategy to synthesize 1,2-substituted cyclobutanes (Scheme 1-13c),[64] first using photoinduced valence isomerization of 1,2-azaborines to furnish the corresponding BN isosteres of Dewar benzene, followed by the cleavage of the B-N bond to furnish an unfused cyclobutane substituted with boron and nitrogen. Ultimately, a diverse set of 1,2-substituted cyclobutanes rings could be easily generated *via* further functionalization at boron-bound carbon.

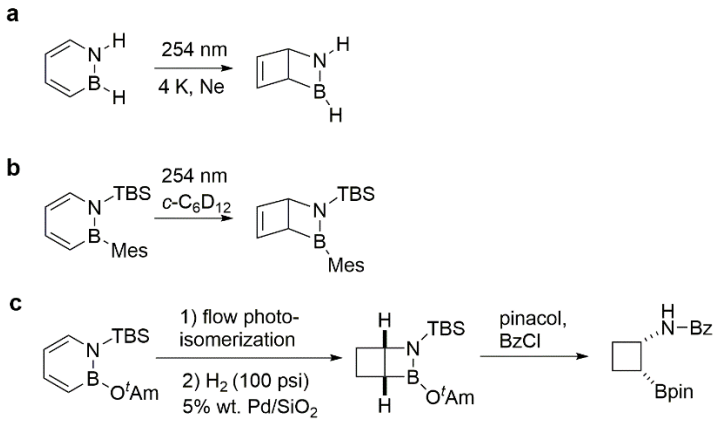

Scheme 1-13. a) Photoisomerization of 1,2-dihydro-1,2-azaborine in matrix;[62] b) photoisomerization of 1,2-dihydro-1-tert-butyldimethylsilyl-2-mesityl-1,2-azaborine in solution;[63] c) synthesis of aminoborylated cyclobutane.[64]

1.2.1.2 1,3-Azaborines

Due to the low stability of 1,3-azaborines, only one synthetic route is available that was introduced by Liu in 2011. Cyclization is achieved through ring-closing metathesis, followed by catalytic dehydrogenation to afford the desired 1,3-azaborines (Scheme 1-14).[65] A general method to diversify the substituent on boron was reported,[66] but the modification of other positions of the 1,3-azaborine ring remains to be developed, except for the single isolated example of electrophilic aromatic substitution at C(6) using Böhme's salt (Scheme 1-14).[65]

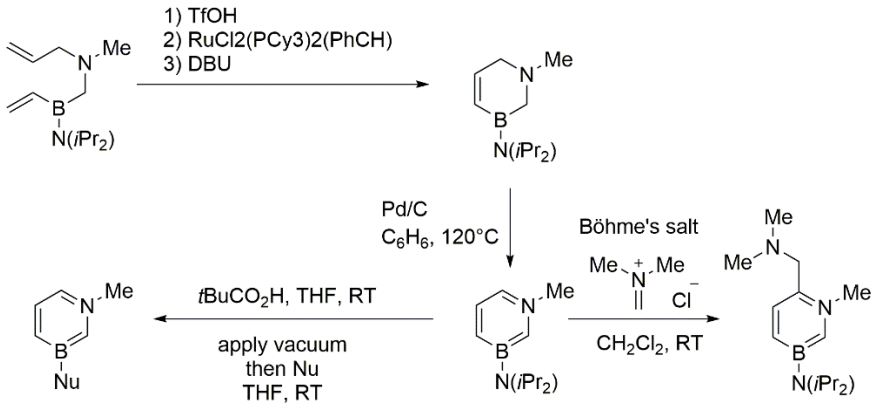

Scheme 1-14. Synthesis and post-functionalization of 1,3-azaborines by Liu.[65, 66]

1.2.1.3 1,4-Azaborines

For 1,4-azaborine, most of the pioneering work has centered on polycyclic dibenzo-fused derivatives. In 2012, Braunschweig and coworkers reported the first synthesis and isolation of a monocyclic 1,4-azaborine *via* a Rh-mediated cyclization. Liu and coworkers developed a more versatile three-step synthetic route to access a wide range of substituted monocyclic 1,4-azaborine derivatives (Scheme 1-15). They also found that the placement of donor and acceptor substituents on the boron and nitrogen atoms dramatically affects the optical properties of the corresponding 1,4-azaborines.[67]

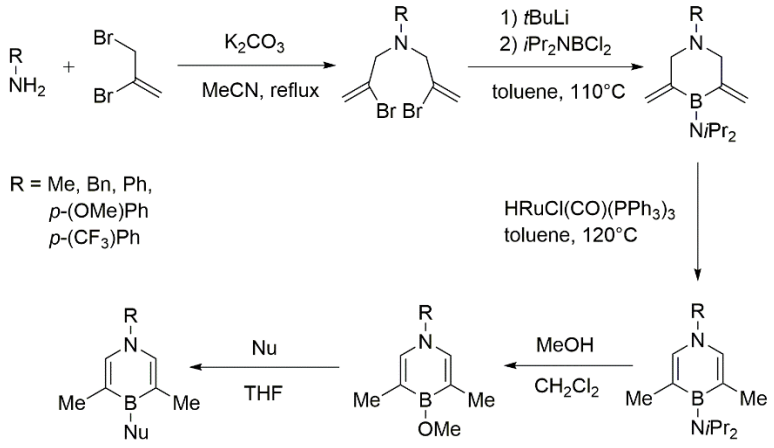

Scheme 1-15. Synthesis and post-functionalization of 1,4-azaborines by Liu.[67]

1.2.2 BN-Substituted Polymers

With a long-standing interest in the isoelectronic relationship between boron-nitrogen and carbon-carbon bonds, and increasing research efforts to create analogues, the placement of boron-nitrogen in the main chain and side chain of polymers is receiving ever increasing attention as an alternative to hydrocarbon-based materials.[68, 69] The implications on the materials' properties, both chemical and physical, are profound, which suggests intriguing characteristics and novel applications that are not accessible to traditional materials.

Polymers with B-N units as an inorganic backbone are interesting as they are isoelectronic with C-C units but strongly polarized. Manners pioneered the substitution of B-N for C-C units in the main chain of polyolefins, giving rise to exciting new classes of polymeric materials. The unsubstituted poly(aminoborane)s with the general formula $[NH_2\text{-}BH_2]_n$ is the most investigated polymer in this class of materials.[70, 71] However, a synthetic route to give access to soluble, well defined, and high-molecular-weight polymers remained elusive,

until Manners and coworkers demonstrated the catalytic dehydropolymerization of a series of alkylamine-boranes, using IrH_2POCOP (POCOP = κ^3-1,3-$(tBu_2PO)_2C_6H_3$) as the catalyst (Scheme 1-16a).[72] Since then many catalysts have been explored for this reaction. Later, Helten and coworkers reported the synthesis of linear poly(iminoborane)s, which can be regarded as the inorganic analogues of poly(acetylene) (Scheme 1-16b).[73]

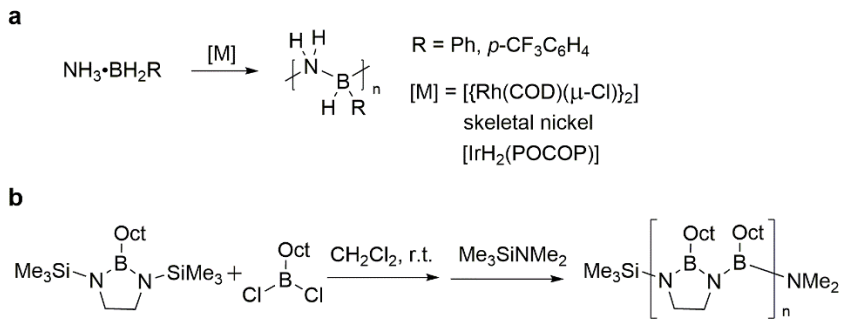

Scheme 1-16. a) Synthesis of poly(aminoborane)s by Manners; [72] b) synthesis of poly(iminoborane)s by Helten.[73]

An alternative strategy to generate BN-substituted polymers is to embed boron and nitrogen in the backbone of conjugated polymers. In 2015, our group reported the first example of an azaborine-based conjugated polymer (**13**). Although the polymer main chain is isoelectronic to poly(*p*-phenylene), the photophysical experimental observation and computational studies suggest that the polymers more closely resemble a B-N bridged polyacetylene rather than a poly(*p*-phenylene).[74] In 2016, Helten and coworkers developed a new organic-inorganic hybrid polymer, a poly[N-(para-phenylene)diimidoborane] (**14**), which comprises alternating NBN and para-phenylene units.[75] In another example, Helten's group replaced the vinylene groups in poly(phenylene vinylene) with boron-

nitrogen units. The B-N bonds in compound **15** are polarized and only exhibit partial double bond character.[76]

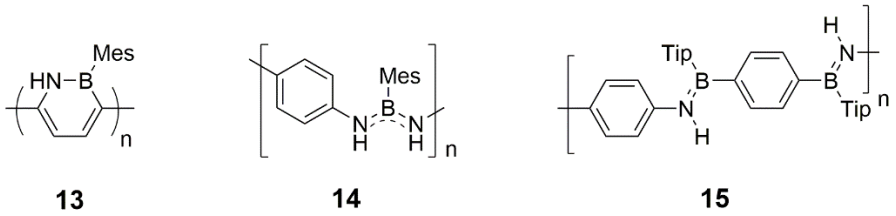

Figure 1-17. Examples of B-N units embedded in conjugated polymers by Jäkle[74] (**13**) and by Helten[75, 76] (**14**, **15**).

The isosteric replacement of C-C with BN moieties in the side chains of polyolefins has also recently been developed. In earlier work, a few studies on borazine-functionalized polyolefins (**16**, **17**) have been reported by Sneddon and Allen.[77, 78] In 2016, the first synthesis of azaborine-substituted polystyrene (BN-PS, **18**) as well as its phenylene-expanded congener (BN-PVBP, **19**) were reported by our group. The increased polarity of the side groups and the presence of N-H moieties completely altered the physical properties of the polymers, such as solubility characteristics and thermal behavior.[5] Several related works have appeared in the literature. Staubitz reported a high molecular weight poly(N-methyl-B-vinylazaborine) (**20**) as a B-N analogue of poly(methylstyrene);[79] Klausen developed a gram-scale synthesis of the BN-substituted vinylnaphthalene polymer **21** and of corresponding copolymers with styrene. Most importantly, they also demonstrated that the oxidative cleavage of the BN-naphthalene moieties results in poly(styrene-co-vinylalcohol) copolymers that are desirable as compatibilizers because of the additional polar functional groups.[80]

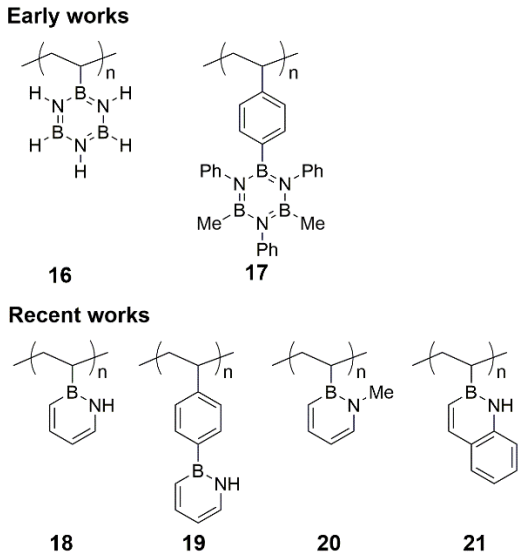

Figure 1-18. Examples of B-N embedded in polymer side chain by Sneddon[77] (**16**), Allen[78] (**17**), Jäkle[5] (**18**, **19**), Staubitz[79] (**20**)， and Klausen[80] (**21**).

In Chapter 3 of this thesis, the preparation of a series of new isomeric azaborine-substituted polymers is reported. Detailed investigations into the effects of the substitution pattern of vinylated B-mesityl azaborines on the polymerization reactivity and physical properties of the respective polymers are discussed. Both computational studies and experimental results demonstrate that the attachment of the vinyl groups to different carbon atoms in the heterocycle results in tunable reactivity.[81] Chapter 4 expands the investigation on the polymerization of a Dewar isomer of a 1,2-azaborine derivative. The first synthesis of poly(BN-Dewar benzene) *via* ROMP is demonstrated. The Grubbs 2nd generation catalyst is found to successfully catalyze the polymerization to give a product that features four-membered BN-heterocycles alternating with vinylene groups in the main chain.

1.3 References

1.Jäkle, F., Lewis acidic organoboron polymers. *Coordination Chemistry Reviews* **2006,** *250* (9), 1107-1121.

2.Jäkle, F., Advances in the Synthesis of Organoborane Polymers for Optical, Electronic, and Sensory Applications. *Chemical Reviews* **2010,** *110* (7), 3985-4022.

3.Jäkle, F., Borylated Polyolefins and their Applications. *Journal of Inorganic and Organometallic Polymers and Materials* **2005,** *15* (3), 293-307.

4.Lennarz, W.; Snyder, H., Arylboronic Acids. III. Preparation and Polymerization of p-Vinylbenzeneboronic Acid 1. *Journal of the American Chemical Society* **1960,** *82*.

5.Wan, W.-M.; Baggett, A. W.; Cheng, F.; Lin, H.; Liu, S.-Y.; Jäkle, F., Synthesis by free radical polymerization and properties of BN-polystyrene and BN-poly(vinylbiphenyl). *Chemical Communications* **2016,** *52* (93), 13616-13619.

6.Qin, Y.; Sukul, V.; Pagakos, D.; Cui, C.; Jäkle, F., Preparation of Organoboron Block Copolymers via ATRP of Silicon and Boron-Functionalized Monomers. *Macromolecules* **2005,** *38* (22), 8987-8990.

7.Cheng, F.; Bonder, E. M.; Jäkle, F., Electron-Deficient Triarylborane Block Copolymers: Synthesis by Controlled Free Radical Polymerization and Application in the Detection of Fluoride Ions. *Journal of the American Chemical Society* **2013,** *135* (46), 17286-17289.

8.Ramakrishnan, S.; Berluche, E.; Chung, T. C., Functional group-containing copolymers prepared by Ziegler-Natta process. *Macromolecules* **1990,** *23* (2), 378-382.

9.Park, M. H.; Kim, T.; Huh, J. O.; Do, Y.; Lee, M. H., Luminescent polyethylene with side-chain triarylboranes: Synthesis and fluoride sensing properties. *Polymer* **2011,** *52* (7), 1510-1514.

10.Mendis, S. N.; Zhou, T.; Klausen, R. S., Syndioselective Polymerization of a BN Aromatic Vinyl Monomer. *Macromolecules* **2018,** *51* (17), 6859-6864.

11.Ramakrishnan, S.; Chung, T. C., Poly(exo-5-hydroxynorbornene): a functional polymer using metathesis polymerization of an organoborane derivative. *Macromolecules* **1989,** *22* (7), 3181-3183.

12.Novoa, S.; Paquette, J. A.; Barbon, S. M.; Maar, R. R.; Gilroy, J. B., Side-chain boron difluoride formazanate polymers via ring-opening metathesis polymerization. *Journal of Materials Chemistry C* **2016,** *4* (18), 3987-3994.

13.Wei, X.; Carroll, P. J.; Sneddon, L. G., New Routes to Organodecaborane Polymers via Ruthenium-Catalyzed Ring-Opening Metathesis Polymerization. *Organometallics* **2004,** *23* (2), 163-165.

14.Berenbaum, A.; Braunschweig, H.; Dirk, R.; Englert, U.; Green, J. C.; Jäkle, F.; Lough, A. J.; Manners, I., Synthesis, Electronic Structure, and Novel Reactivity of Strained, Boron-Bridged [1]Ferrocenophanes. *Journal of the American Chemical Society* **2000,** *122* (24), 5765-5774.

15.Ramakrishnan, S., Well-defined ethylene-vinyl alcohol copolymers via hydroboration: control of composition and distribution of the hydroxyl groups on the polymer backbone. *Macromolecules* **1991,** *24* (13), 3753-3759.

16.Chung, T. C.; Lu, H. L.; Li, C. L., Synthesis and Functionalization of Unsaturated Polyethylene: Poly(ethylene-co-1,4-hexadiene). *Macromolecules* **1994,** *27* (26), 7533-7537.

17.Wagner, C. B.; Studer, A., Oxidation of Alkylcatecholboranes with Functionalized Nitroxides for Chemical Modification of Cyclohexene, Perallylated Polyglycerol and of Poly(butadiene). *European Journal of Organic Chemistry* **2010,** *2010* (30), 5782-5786.

18.Qin, Y.; Cheng, G.; Achara, O.; Parab, K.; Jäkle, F., A New Route to Organoboron Polymers via Highly Selective Polymer Modification Reactions. *Macromolecules* **2004,** *37* (19), 7123-7131.

19.Qin, Y.; Cheng, G.; Sundararaman, A.; Jäkle, F., Well-Defined Boron-Containing Polymeric Lewis Acids. *Journal of the American Chemical Society* **2002,** *124* (43), 12672-12673.

20.Bae, C.; Hartwig, J. F.; Boaen Harris, N. K.; Long, R. O.; Anderson, K. S.; Hillmyer, M. A., Catalytic Hydroxylation of Polypropylenes. *Journal of the American Chemical Society* **2005,** *127* (2), 767-776.

21.Chang, Y.; Brunello, G. F.; Fuller, J.; Hawley, M.; Kim, Y. S.; Disabb-Miller, M.; Hickner, M. A.; Jang, S. S.; Bae, C., Aromatic Ionomers with Highly Acidic Sulfonate Groups: Acidity, Hydration, and Proton Conductivity. *Macromolecules* **2011,** *44* (21), 8458-8469.

22.Chen, E. Y.-X.; Marks, T. J., Cocatalysts for Metal-Catalyzed Olefin Polymerization: Activators, Activation Processes, and Structure−Activity Relationships. *Chemical Reviews* **2000,** *100* (4), 1391-1434.

23.Parks, D. J.; Piers, W. E., Tris(pentafluorophenyl)boron-Catalyzed Hydrosilation of Aromatic Aldehydes, Ketones, and Esters. *Journal of the American Chemical Society* **1996,** *118* (39), 9440-9441.

24.Welch, G. C.; Juan, R. R. S.; Masuda, J. D.; Stephan, D. W., Reversible, Metal-Free Hydrogen Activation. *Science* **2006,** *314* (5802), 1124.

25.Dorkó, É.; Szabó, M.; Kótai, B.; Pápai, I.; Domján, A.; Soós, T., Expanding the Boundaries of Water-Tolerant Frustrated Lewis Pair Hydrogenation: Enhanced Back Strain in the Lewis Acid Enables the Reductive Amination of Carbonyls. *Angewandte Chemie International Edition* **2017,** *56* (32), 9512-9516.

26.Erős, G.; Mehdi, H.; Pápai, I.; Rokob, T. A.; Király, P.; Tárkányi, G.; Soós, T., Expanding the Scope of Metal-Free Catalytic Hydrogenation through Frustrated Lewis Pair Design. *Angewandte Chemie International Edition* **2010,** *49* (37), 6559-6563.

27.Gyömöre, Á.; Bakos, M.; Földes, T.; Pápai, I.; Domján, A.; Soós, T., Moisture-Tolerant Frustrated Lewis Pair Catalyst for Hydrogenation of Aldehydes and Ketones. *ACS Catalysis* **2015,** *5* (9), 5366-5372.

28.Mahdi, T.; Stephan, D. W., Frustrated Lewis Pair Catalyzed Hydroamination of Terminal Alkynes. *Angewandte Chemie International Edition* **2013,** *52* (47), 12418-12421.

29.Ashley, A. E.; Thompson, A. L.; O'Hare, D., Non-Metal-Mediated Homogeneous Hydrogenation of CO2 to CH3OH. *Angewandte Chemie International Edition* **2009,** *48* (52), 9839-9843.

30.Oestreich, M.; Hermeke, J.; Mohr, J., A unified survey of Si–H and H–H bond activation catalysed by electron-deficient boranes. *Chemical Society Reviews* **2015,** *44* (8), 2202-2220.

31.Keess, S.; Simonneau, A.; Oestreich, M., Direct and Transfer Hydrosilylation Reactions Catalyzed by Fully or Partially Fluorinated Triarylboranes: A Systematic Study. *Organometallics* **2015,** *34* (4), 790-799.

32.Yuan, W.; Orecchia, P.; Oestreich, M., Cyclohexa-1,3-diene-based dihydrogen and hydrosilane surrogates in B(C6F5)3-catalysed transfer processes. *Chemical Communications* **2017,** *53* (75), 10390-10393.

33.Bergbreiter, D. E., Soluble Polymers as Tools in Catalysis. *ACS Macro Letters* **2014,** *3* (3), 260-265.

34.Roesler, R.; Har, B. J. N.; Piers, W. E., Synthesis and Characterization of (Perfluoroaryl)borane-Functionalized Carbosilane Dendrimers and Their Use as Lewis

Acid Catalysts for the Hydrosilation of Acetophenone. *Organometallics* **2002,** *21* (21), 4300-4302.

35.Trunk, M.; Teichert, J. F.; Thomas, A., Room-Temperature Activation of Hydrogen by Semi-immobilized Frustrated Lewis Pairs in Microporous Polymer Networks. *Journal of the American Chemical Society* **2017,** *139* (10), 3615-3618.

36.Chen, L.; Liu, R.; Yan, Q., Polymer Meets Frustrated Lewis Pair: Second-Generation CO2-Responsive Nanosystem for Sustainable CO2 Conversion. *Angewandte Chemie International Edition* **2018,** *57* (30), 9336-9340.

37.Bouchard, N.; Fontaine, F.-G., Alkylammoniotrifluoroborate functionalized polystyrenes: polymeric pre-catalysts for the metal-free borylation of heteroarenes. *Dalton Transactions* **2019,** *48* (15), 4846-4856.

38.Dodge, L.; Chen, Y.; Brook, M. A., Silicone Boronates Reversibly Crosslink Using Lewis Acid– Lewis Base Amine Complexes. *Chemistry – A European Journal* **2014,** *20* (30), 9349-9356.

39.Vidal, F.; Gomezcoello, J.; Lalancette, R. A.; Jäkle, F., Lewis Pairs as Highly Tunable Dynamic Cross-Links in Transient Polymer Networks. *Journal of the American Chemical Society* **2019,** *141* (40), 15963-15971.

40.Wang, M.; Nudelman, F.; Matthes, R. R.; Shaver, M. P., Frustrated Lewis Pair Polymers as Responsive Self-Healing Gels. *Journal of the American Chemical Society* **2017,** *139* (40), 14232-14236.

41.Fu, G.-L.; Zhang, H.-Y.; Yan, Y.-Q.; Zhao, C.-H., p-Quaterphenyls Laterally Substituted with a Dimesitylboryl Group: A Promising Class of Solid-State Blue Emitters. *The Journal of Organic Chemistry* **2012,** *77* (4), 1983-1990.

42.Noda, T.; Shirota, Y., 5,5‘-Bis(dimesitylboryl)-2,2‘-bithiophene and 5,5‘‘-Bis(dimesitylboryl)-2,2‘:5‘,2‘‘-terthiophene as a Novel Family of Electron-Transporting Amorphous Molecular Materials. *Journal of the American Chemical Society* **1998,** *120* (37), 9714-9715.

43.Mellerup, S. K.; Wang, S., Boron-Doped Molecules for Optoelectronics. *Trends in Chemistry* **2019,** *1* (1), 77-89.

44.Zhang, Z.; Edkins, R. M.; Nitsch, J.; Fucke, K.; Steffen, A.; Longobardi, L. E.; Stephan, D. W.; Lambert, C.; Marder, T. B., Optical and electronic properties of air-stable organoboron compounds with strongly electron-accepting bis(fluoromesityl)boryl groups. *Chemical Science* **2015,** *6* (1), 308-321.

45.Wade, C. R.; Broomsgrove, A. E. J.; Aldridge, S.; Gabbaï, F. P., Fluoride Ion Complexation and Sensing Using Organoboron Compounds. *Chemical Reviews* **2010,** *110* (7), 3958-3984.

46.Yamaguchi, S.; Akiyama, S.; Tamao, K., Colorimetric Fluoride Ion Sensing by Boron-Containing π-Electron Systems. *Journal of the American Chemical Society* **2001,** *123* (46), 11372-11375.

47.Parab, K.; Venkatasubbaiah, K.; Jäkle, F., Luminescent Triarylborane-Functionalized Polystyrene: Synthesis, Photophysical Characterization, and Anion-Binding Studies. *Journal of the American Chemical Society* **2006,** *128* (39), 12879-12885.

48.Wang, J.; Wang, N.; Wu, G.; Wang, S.; Li, X., Multicolor Emission from Non-conjugated Polymers Based on a Single Switchable Boron Chromophore. *Angewandte Chemie International Edition* **2019,** *58* (10), 3082-3086.

49.Qin, Y.; Kiburu, I.; Shah, S.; Jäkle, F., Synthesis and Characterization of Organoboron Quinolate Polymers with Tunable Luminescence Properties. *Macromolecules* **2006,** *39* (26), 9041-9048.

50.Wang, J.; Jin, B.; Wang, N.; Peng, T.; Li, X.; Luo, Y.; Wang, S., Organoboron-Based Photochromic Copolymers for Erasable Writing and Patterning. *Macromolecules* **2017,** *50* (12), 4629-4638.

51.Stock, A.; Pohland, E., Borwasserstoffe, IX.: B3N3H6. *Berichte der deutschen chemischen Gesellschaft (A and B Series)* **1926,** *59* (9), 2215-2223.

52.Dewar, M. J. S.; Kubba, V. P.; Pettit, R., 624. New heteroaromatic compounds. Part I. 9-Aza-10-boraphenanthrene. *Journal of the Chemical Society (Resumed)* **1958,** (0), 3073-3076.

53.Dewar, M. J. S.; Marr, P. A., A Derivative of Borazarene. *Journal of the American Chemical Society* **1962,** *84* (19), 3782-3782.

54.White, D. G., 2-Phenyl-2,1-borazarene and Derivatives of 1,2-Azaboracycloalkanes. *Journal of the American Chemical Society* **1963,** *85* (22), 3634-3636.

55.Ghosh, D.; Periyasamy, G.; Pati, S. K., Density functional theoretical investigation of the aromatic nature of BN substituted benzene and four ring polyaromatic hydrocarbons. *Physical Chemistry Chemical Physics* **2011,** *13* (46), 20627-20636.

56.Ashe, A. J.; Fang, A Synthesis of Aromatic Five- and Six-Membered B−N Heterocycles via Ring Closing Metathesis. *Organic Letters* **2000,** *2* (14), 2089-2091.

57.Marwitz, A. J. V.; Abbey, E. R.; Jenkins, J. T.; Zakharov, L. N.; Liu, S.-Y., Diversity through Isosterism: The Case of Boron-Substituted 1,2-Dihydro-1,2-azaborines. *Organic Letters* **2007,** *9* (23), 4905-4908.

58.Brown, A. N.; Li, B.; Liu, S.-Y., Negishi Cross-Coupling Is Compatible with a Reactive B–Cl Bond: Development of a Versatile Late-Stage Functionalization of 1,2-Azaborines and Its Application to the Synthesis of New BN Isosteres of Naphthalene and Indenyl. *Journal of the American Chemical Society* **2015,** *137* (28), 8932-8935.

59.Baggett, A. W.; Vasiliu, M.; Li, B.; Dixon, D. A.; Liu, S.-Y., Late-Stage Functionalization of 1,2-Dihydro-1,2-azaborines via Regioselective Iridium-Catalyzed C–H Borylation: The Development of a New N,N-Bidentate Ligand Scaffold. *Journal of the American Chemical Society* **2015,** *137* (16), 5536-5541.

60.McConnell, C. R.; Haeffner, F.; Baggett, A. W.; Liu, S.-Y., 1,2-Azaborine's Distinct Electronic Structure Unlocks Two New Regioisomeric Building Blocks via Resolution Chemistry. *Journal of the American Chemical Society* **2019,** *141* (22), 9072-9078.

61.Burford, R. J.; Li, B.; Vasiliu, M.; Dixon, D. A.; Liu, S.-Y., Diels–Alder Reactions of 1,2-Azaborines. *Angewandte Chemie International Edition* **2015,** *54* (27), 7823-7827.

62.Brough, S. A.; Lamm, A. N.; Liu, S.-Y.; Bettinger, H. F., Photoisomerization of 1,2-Dihydro-1,2-Azaborine: A Matrix Isolation Study. *Angewandte Chemie International Edition* **2012,** *51* (43), 10880-10883.

63.Edel, K.; Yang, X.; Ishibashi, J. S. A.; Lamm, A. N.; Maichle-Mössmer, C.; Giustra, Z. X.; Liu, S.-Y.; Bettinger, H. F., The Dewar Isomer of 1,2-Dihydro-1,2-azaborinines: Isolation, Fragmentation, and Energy Storage. *Angewandte Chemie International Edition* **2018,** *57* (19), 5296-5300.

64.Giustra, Z. X.; Yang, X.; Chen, M.; Bettinger, H. F.; Liu, S.-Y., Accessing 1,2-Substituted Cyclobutanes through 1,2-Azaborine Photoisomerization. *Angew Chem.Int.Ed* **2019,** *58* (52), 18918-18922.

65.Xu, S.; Zakharov, L. N.; Liu, S.-Y., A 1,3-Dihydro-1,3-azaborine Debuts. *Journal of the American Chemical Society* **2011,** *133* (50), 20152-20155.

66.Xu, S.; Mikulas, T. C.; Zakharov, L. N.; Dixon, D. A.; Liu, S.-Y., Boron-Substituted 1,3-Dihydro-1,3-azaborines: Synthesis, Structure, and Evaluation of Aromaticity. *Angewandte Chemie International Edition* **2013,** *52* (29), 7527-7531.

67.Liu, X.; Zhang, Y.; Li, B.; Zakharov, L. N.; Vasiliu, M.; Dixon, D. A.; Liu, S.-Y., A Modular Synthetic Approach to Monocyclic 1,4-Azaborines. *Angewandte Chemie International Edition* **2016,** *55* (29), 8333-8337.

68.Manners, I., Synthetic Metal-Containing Polymers. **2004**.

69.Vidal, F.; Jäkle, F., Functional Polymeric Materials Based on Main-Group Elements. *Angewandte Chemie International Edition* **2019,** *58* (18), 5846-5870.

70.Staubitz, A., Generation of High-Molecular-Weight Polymers with Diverse Substituents:AnUnusual Metal-Free Synthesis of Poly(aminoborane)s. *Angew.Chem.Int. Ed.* **2018,** *57*, 5990 –5992.

71.Staubitz, A.; Robertson, A. P. M.; Sloan, M. E.; Manners, I., Amine- and Phosphine-Borane Adducts: New Interest in Old Molecules. *Chem. Rev.* **2010**, (110), 4023–4078.

72.Resendiz-Lara, D., A. ; Stubbs, N. E.; Arz, M. I.; Pridmore, N. E.; Sparkes, H. A.; Manners, I., Boron–nitrogen main chain analogues of polystyrene: poly(B-aryl)aminoboranes via catalytic dehydrocoupling. *Chem. Commun.* **2017**, (53), 11701--11704.

73.Ayhan, O.; Eckert, T.; Plamper, F. A.; Helten, H., Poly(iminoborane)s:AnElusiveClass of Main-GroupPolymers? *Angew.Chem. Int.Ed.* **2016**, 55, 13321 –13325.

74.Baggett, A. W.; Guo, F.; Li, B.; Liu, S.-Y.; Jäkle, F., Regioregular Synthesis of Azaborine Oligomers and a Polymer with a syn Conformation Stabilized by N•H···π Interactions. *Angewandte Chemie International Edition* **2015,** *54* (38), 11191-11195.

75.Lorenz, T.; Lik, A.; Plamper, F. A.; Helten, H., Dehydrocoupling and Silazane Cleavage Routes to Organic–Inorganic Hybrid Polymers with NBN Units in the Main Chain. *Angewandte Chemie International Edition* **2016,** *55* (25), 7236-7241.

76.Lorenz, T.; Crumbach, M.; Eckert, T.; Lik, A.; Helten, H., Poly(p-phenylene iminoborane): A Boron–Nitrogen Analogue of Poly(p-phenylene vinylene). *Angewandte Chemie International Edition* **2017,** *56* (10), 2780-2784.

77.Kai Su, E. E. R., * Helen M. Thompson, Larry G. Sneddon*, Syntheses and Properties of PoIy(B-vinylborazine) and Poly(styrene-co-B-vinylborazine) Copolymers. *Macromolecules* **1991,** (24), 3760-3766.

78.LOGAN A. JACKSON, C. W. A., Organoborazines. 111. Homo- and Copolymerization of p-Vinylphenylcyclotriborazines*. *Journal of Polymer Science: Part A Polymer Chemistry* **1992,** *30*, 577-581.

79.Thiedemann, B.; Gliese, P. J.; Hoffmann, J.; Lawrence, P. G.; Sönnichsen, F. D.; Staubitz, A., High molecular weight poly(N-methyl-B-vinylazaborine) – a semi-inorganic B–N polystyrene analogue. *Chemical Communications* **2017,** *53* (53), 7258-7261.

80.van de Wouw, H. L.; Lee, J. Y.; Klausen, R. S., Gram-scale free radical polymerization of an azaborine vinyl monomer. *Chemical Communications* **2017,** *53* (53), 7262-7265.

81.Lin, H.; McConnell, C. R.; Jilus, B.; Liu, S.-Y.; Jäkle, F., Changing up BN-Polystyrene: Effect of Substitution Pattern on the Free-Radical Polymerization and Polymer Properties. *Macromolecules* **2019,** *52* (12), 4500-4509.

Chapter 2 Tailored Triarylborane Polymeric Lewis Acids as Supported Catalysts and Luminescent Materials with TADF Characteristics

2.1 Introduction

Benefiting from a readily accessible low-lying vacant p_z orbital on boron, triarylboranes serve important roles both as electron acceptors and as powerful Lewis acids.[1] Their electron-deficient character and desirable photophysical properties are exploited in applications ranging from nonlinear optics to organic light-emitting diodes (OLEDs), organic field-effect transistors (OFETs), and organic photovoltaics (OPVs).[2] The tunable Lewis acidity of triarylboranes is advantageous in anion sensing, catalysis and small molecule activation. Following the successful implementation of organoboranes in "frustrated Lewis pairs" (FLPs) chemistry by Stephan[3] they have been applied in numerous catalytic processes including hydrogenation,[4] hydroamination,[5] and CO_2 reduction.[6] The high Lewis acidity of organoboranes also facilitates catalytic hydrosilylation based on a weak Lewis acid (LA)-Lewis base (LB) interaction between boron and hydrosilanes.[7]

The attachment of borane moieties to polyolefins offers access to polymer-supported Lewis acids (PLAs, Figure 2-1), potentially providing an opportunity to take advantage of the reusability of the polymers after catalysis.[8] On the other hand, organoborane-based fluorescent polymers are also promising as optoelectronic materials.[9] Polymers with tunable emission color, intensity, and delayed fluorescence characteristics are highly sought after for display applications.[10] In 2002, we first reported on the introduction of

Lewis acidic boranes into the side chains of polystyrene via facile substituent exchange reactions on boron, leading to a family of well-defined PLAs (**A**).[11] Straightforward substituent exchange reactions also provided access to borane polymers with π-conjugated bithiophene, carbazole and fluorene pendent groups that are both Lewis acidic and strongly fluorescent (**B**).[12] These polymers were applied as ratiometric sensors for small anions such fluoride or cyanide. We later demonstrated the controlled polymerization of a dimesitylborane (Mes_2B)-substituted vinylbiphenyl monomer via reversible addition fragmentation chain transfer (RAFT) and discovered that a luminescent block copolymer with PNIPAM (**C**) can be used to detect fluoride anions in aqueous solution at a remarkably low level of less than 1 ppm.[13] More recently, researchers have explored Lewis acidic organoborane polymers as macromolecular building blocks for advanced supramolecular materials. For instance, Shaver and coworkers demonstrated that the addition of a small molecule, such as diethyl azodicarboxylate, can promote rapid and reversible network formation between Lewis acidic Ph_2B- (**D**) and Lewis basic Mes_2P-substituted polystyrenes.[14] In the absence of the additive, the LA and LB groups do not interact due to the large steric hindrance on the P sites, instead acting as FLPs. Dithienylborane-substituted polystyrenes (**E**) have also proven to be excellent building blocks for the formation of transient polymer networks and recyclable elastomers via reversible formation of B-N classical Lewis pairs (CLPs).[15]

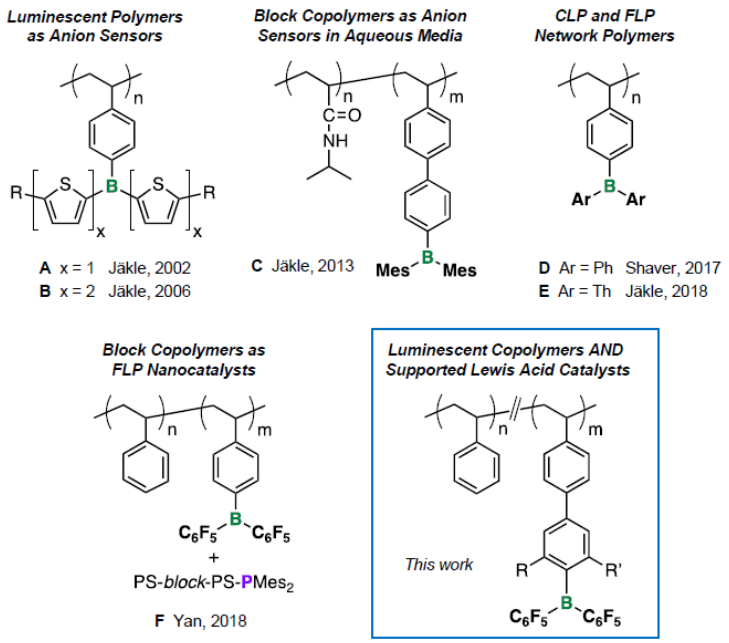

Figure 2-1. Triarylborane Lewis acid-functionalized polymers and their applications.

Applications of soluble organoborane polymers in catalysis remain scarce.[16] Very recently, Yan and coworkers found a new CO_2-responsive system for the catalytic formylation of N-H bonds based on two complementary Lewis acidic organoborane (**F**) and Lewis basic organophosphine block copolymers. Interestingly, in their system CO_2 acts as a cross-linker that enables micelle formation as recyclable nanocatalysts.[17] However, one of the obstacles to broader implementation of polymer-supported borane LAs and FLPs is that sterically unprotected arylboranes, such as Ph_3B or $PhB(C_6F_5)_2$, undergo gradual hydrolysis and are easily deactivated by Lewis base impurities or substrate functionalities that form strong Lewis pair complexes. The stability of organoboranes can be effectively enhanced by two strategies: the mitigation of the electron-deficiency and the introduction of bulky substituents on the boron atom. Recognizing these issues, Soos,[18] Wildgoose,[19]

and Ashley[20] tailored molecular organoborane LAs, optimizing the steric and electronic properties by judicial introduction of substituents (CH_3, CF_3, Cl) in *ortho*-position of the B-aryl substituents.

In a first foray into tailor-made luminescent PLAs and FLPs that are more robust, yet highly active, we set out to prepare copolymers that feature an additional benzene ring between the borane functional group and the polymerizable styryl group. This allows us to stabilize the borane moiety with bulkier groups in *ortho*-position while also tuning the Lewis acidity. We designed two systems to match these requirements. The *ortho*-methyl groups in **P1** are expected to sterically retard the binding of Lewis bases (including water) to the Lewis acidic center; similarly, the introduction of a chlorine atom in *ortho* position in **P2** provides some steric hindrance, but also enhances the electron-deficient character. The attachment of these tailored triarylborane moieties to a polyolefin backbone offers access to new polymer-supported Lewis acids with potential for recyclability.[21] These polymers also display intriguing luminescent properties that could not only prove advantageous for visual observation of the catalyst state (bound vs unbound)[22] but also enable applications as new materials in optoelectronic devices.

2.2 Results and Discussion

Synthesis of Copolymers and Molecular Model Systems. Precursor **1** was prepared by lithiation of 5-bromo-2-iodo-1,3-dimethylbenzene followed by quenching with Me_3SiOTf according to a method reported in the patent literature,[23] and a similar synthesis was developed for **2** starting from 4-bromo-2-chloro-1-iodobenzene. These silylated arenes

were converted to monomers **M1** and **M2** by Suzuki-Miyaura coupling with 4-vinylphenylboronic acid (Scheme 2-1). The monomers were purified by column chromatography on alumina using hexanes as the eluent, and **M2** was further recrystallized from MeOH. The products were isolated as white solids in 47% and 53% yield, respectively. Similarly, Suzuki-Miyaura coupling of **M1** and **M2** with 4-*tert*-butylphenylboronic acid gave the model compounds **Mod1-Si** and **Mod2-Si** as white solid in 44% and 55% yield. The monomers **M1** and **M2** were then copolymerized with styrene in a 1:5 molar ratio in anisole with 1,1'-azobisisobutyronitrile (AIBN) as the initiator. After 24 h at 110 ºC, ^{1}H NMR analyses showed that the copolymers **P1-Si** and **P2-Si** contain ca. 17 and 13 mol% of –$SiMe_3$ pendant group respectively, which matches well the monomer feed ratio. GPC analyses in THF gave estimated molecular weights of M_n = 18.8 kDa ($Đ$ = 1.65) for **P1-Si** and M_n = 39.3 kDa ($Đ$ = 2.09) for **P2-Si** relative to narrow polystyrene standards.

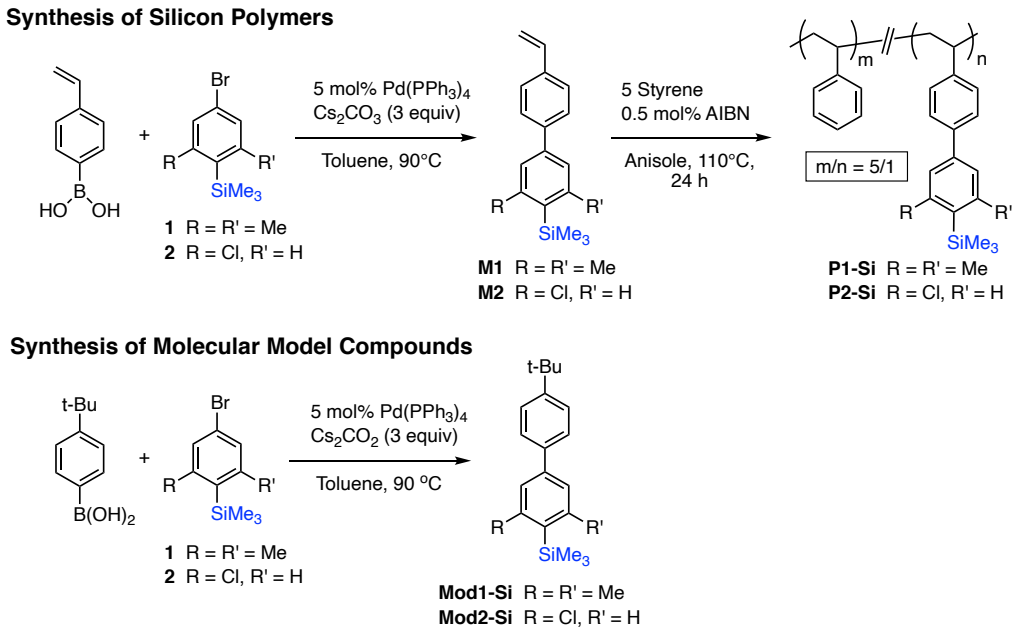

Scheme 2-1. Synthesis of Silane-functionalized Polymers and Model Compounds.

The subsequent silicon-boron exchange to introduce the borane functional groups was first investigated on the molecular model compounds (Scheme 2-2). For **Mod1-Si**, the trimethylsilyl (TMS) groups were readily replaced with BBr_2 groups upon reaction with BBr_3 in a concentrated toluene solution at room temperature over 12 h. In contrast, the conversion of **Mod2-Si** to **Mod2-BBr2** required addition of an excess of BBr_3 (3 equiv.) and heating of the mixture to 80 ºC, because the inductive electron-withdrawing (–I) influence of the Cl substituent in *ortho* position slows down the electrophilic borylation. The disappearance of the TMS group in the ^{1}H NMR and the appearance of a signal at 63.0 and 57.4 ppm respectively in the ^{11}B NMR spectra both indicate that the Si-B exchange reactions proceeded successfully. As shown in Scheme 2-2, **Mod1-BPf2** and **Mod2-BPf2** were obtained by subsequent reaction with bis(pentafluorophenyl)zinc ($Zn(C_6F_5)_2$). Higher temperatures (80 ºC) and reaction times (48 hours) were required for the functionalization

of **Mod1-BBr2** with $Zn(C_6F_5)_2$ (1.5 equivs.), while conversion of **Mod2-BBr2** to the product proceeded at room temperature over 24 hours with 1.05 equivs. of $Zn(C_6F_5)_2$. The structures of these model compounds were confirmed by ^{1}H, ^{11}B, ^{19}F, and ^{13}C NMR spectroscopy (Figures 2-S25-28 and Figures 2-S36-39 in the appendix). The ^{11}B NMR spectra showed broad downfield signals at 69.6 ppm (**Mod1-BPf2**) and 63.3 ppm (**Mod2-BPf2**), respectively, which are consistent with the expected chemical shifts of the tricoordinate arylboranes, and slightly downfield from those of the BBr_2-functionalized intermediates (63.0, 57.4 ppm). The typical patterns were observed in the ^{19}F NMR spectra with three separate signals for the *ortho*-, *meta*-, and *para*-F atoms on the C_6F_5 groups. A larger separation between the *para*- and *meta*-F atoms for **Mod1-BPf2** ($\Delta\delta$ = 15.4 ppm) in comparison to **Mod2-BPf2** ($\Delta\delta$ = 14.4 ppm) is consistent with the expected more electron-deficient character of **Mod2-BPf2**. The ^{1}H NMR spectra are also consistent with the expected structures. In addition, high-resolution MALDI-TOF MS data were acquired of the corresponding fluoride anion complexes generated by addition of an excess of $[Bu_4N]F$ to solutions of the boranes in THF.

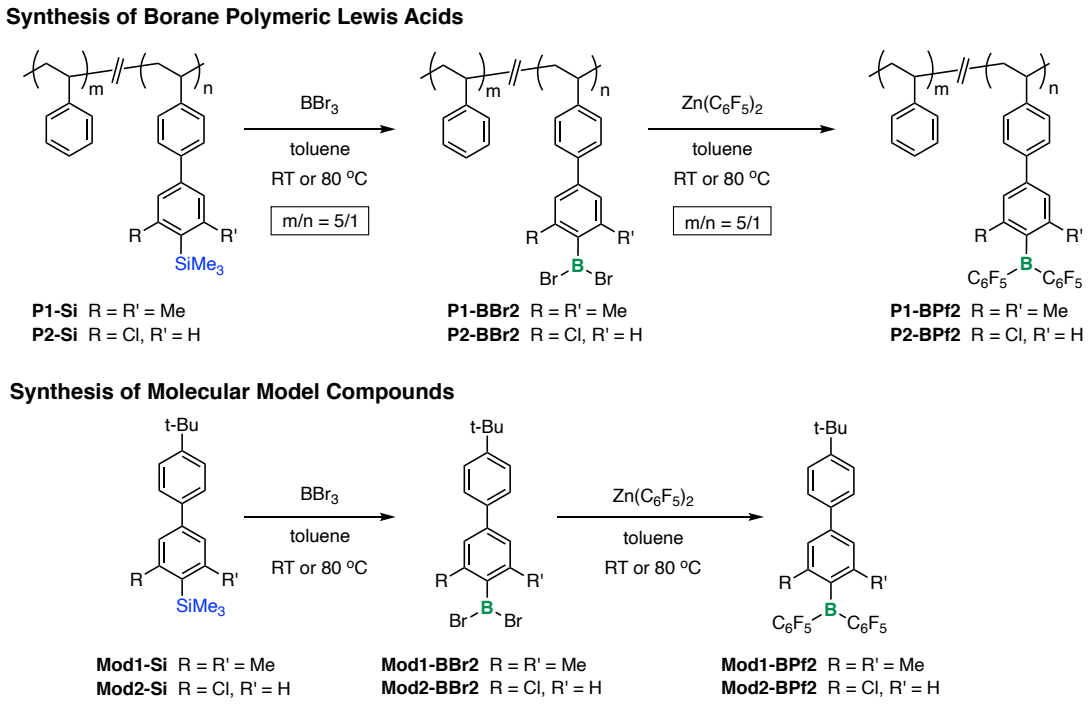

Scheme 2-2. Conversion to Arylborane-functionalized Polymers and Model Compounds.

With this information in hand, we pursued the polymer modification of **P1-Si** and **P2-Si**. Using similar methods as for the model compounds the TMS groups were selectively exchanged with BBr_3 in toluene. As in the case of the model compound, for **P2-BBr2** an excess of BBr_3 and heating to 80 ºC were required to achieve close to quantitative borylation. The conversion to **P1-BBr2/P2-BBr2** was verified by the disappearance of the signal for the TMS groups in the ^{1}H NMR spectra and the appearance of a signal at ~60 and ~55 ppm in the ^{11}B NMR spectra respectively. For **P1-BBr2**, the signals for the methyl groups on the functional units shift from 2.52 to 2.39 ppm with only a small residual signal remaining at 2.60 ppm (< 5%) (Figure S9). The ratio between the ^{1}H NMR integrals for the methyl and aromatic protons of **P1-BBr2** is in line with the expected ca. 5:1 ratio of styryl and borane-functionalized styryl units. Similarly, for **P2-BBr2** the integral ratio

between three protons on the borane-attached phenyl rings and backbone protons is consistent with the proposed structure (Figure S16). The polymer **P1-BBr2** was used in situ for the subsequent arylation reaction, but **P2-BBr2** was first precipitated into anhydrous hexanes to remove the excess of BBr_3. The dibromoborylated polymers were converted to the target polymers **P1-BPf2** and **P2-BPf2** by reaction with $Zn(C_6F_5)_2$. Under the conditions established for the model systems, **P1-BBr2** was reacted with 1.5 equivs. of $Zn(C_6F_5)_2$ at 80 ºC for 48 h and **P2-BBr2** with 1.05 equivs. of $Zn(C_6F_5)_2$ at room temperature for 24 h. The final products were isolated in 64 and 56% yield by repeated precipitation into hexanes and dried under high vacuum. The structures of the copolymers were confirmed by ^{1}H, ^{11}B and ^{19}F NMR spectroscopy (Figure 2-2). The ^{19}F NMR spectra of **P1-BPf2** and **P2-BPf2** both show the typical set of three peaks for the *ortho*-, *meta*- and *para*-position fluorines on the C_6F_5 groups; the signals appear at chemical shifts that are similar to those of the model compounds but are slightly broadened. The ^{11}B NMR signals at 68.3 ppm and 62.9 ppm for **P1-BPf2** and **P2-BPf2**, respectively, are also consistent with those of the model compounds. In addition, a characteristic upfield shift of the methyl protons to 2.17 ppm for **P1-BPf2** from 2.52 ppm for **P1-SiMe3** is consistent with shifts seen for the model compounds. The GPC traces of the triarylboranes substituted copolymers are very broad, indicating a small degree of crosslinking of the copolymers, likely due to the presence of a few Ar_2B-O-BAr_2 linkages as suggested by very minor signals in the ^{11}B NMR spectra at ca. 40 ppm. The possible formation of B-OH/B-O-B species due to the presence of trace amounts of water during the synthesis or isolation processes was further examined by studying the stability of the compounds in wet $CDCl_3$

by ^{19}F and ^{11}B NMR spectroscopy in air. Gradual conversion to borinate species was observed over a period of four days for the model compounds (Figures 2-S43- 46 in the appendix). For the polymers, precipitation occurred within 30 mins (Figures 2-S47-49 in the appendix), suggesting that even a small extent of hydrolysis results in an insoluble crosslinked material. Although the crosslinked material is still catalytically active (*vide infra*), these findings suggest that, in the absence of Lewis base stabilization, the polymers are best handled in the absence of air and moisture.

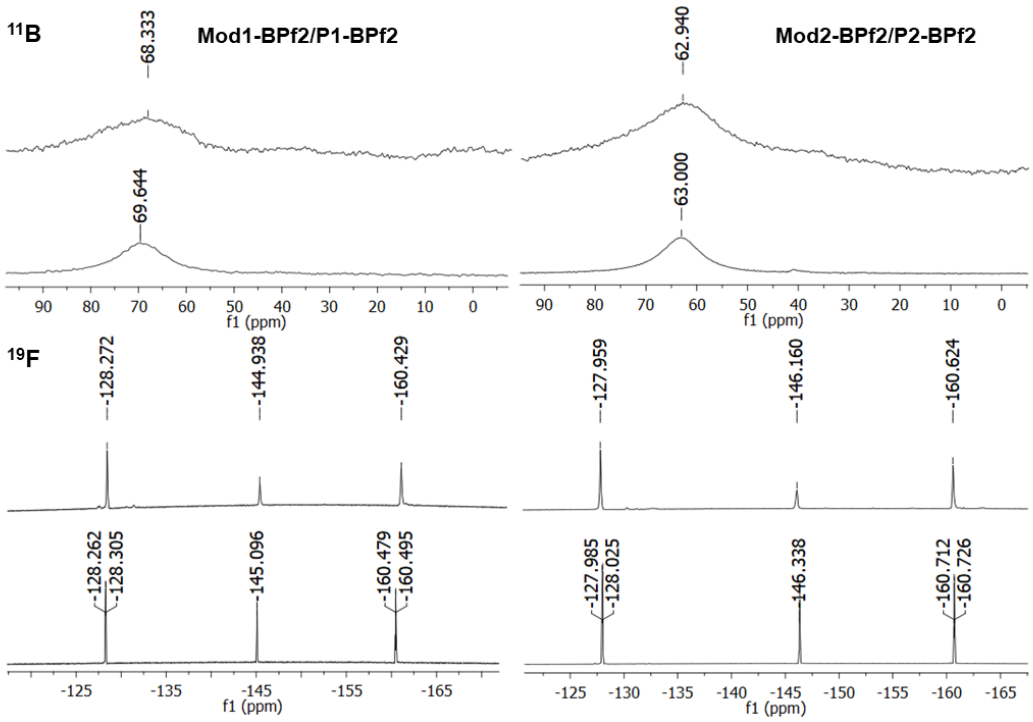

Figure 2-2. ^{19}F and ^{11}B NMR spectra of model compounds (bottom) and polymers (top) in $CDCl_3$.

Determination of Lewis Acid Strength. The relative Lewis acidity of the boron centers in the model compounds and polymers were estimated by treatment with triethylphosphine

oxide (Et_3PO) according to the Gutmann-Beckett[24] method. The ^{31}P NMR shifts of the Et_3PO-borane complexes are summarized in Table 2-1 and compared to the adduct (Et_3PO)-$B(C_6F_5)_3$. All model compounds and copolymers are high Lewis acidic, having around 90% relative Lewis acid strength compared with $B(C_6F_5)_3$. **Mod2-BPf2** and **P2-BPf2** display relatively higher Lewis acidity than **Mod1-BPf2** and **P1-BPf2** due to the more electron-withdrawing chlorine substituent in *ortho*-position to the boron center. The complex formation for **Mod1-BPf2** and **P1-BPf2** proved to be dynamic at room temperature. Hence the studies were performed at low temperature (-20 ºC) where the equilibrium between free acid and Et_3PO is sufficiently slow to accurately determine the ^{31}P NMR chemical shift of the complex.

Table 2-1. Gutmann-Becket analysis of organoborane model compounds and polymers

Compound	$\delta(^{31}P)$ for adduct (ppm) [a]	$\Delta\delta(^{31}P)$ [b]	Lewis acidity relative to B(C6F5)3 (%)	Acceptor number (AN) [c]
Mod1-BPf2 [d]	74.0	21.3	90	72.9
P1-BPf2 [d]	74.1	21.4	91	73.2
Mod2-BPf2	74.3	21.6	92	73.5
P2-BPf2	74.6	21.8	93	74.2
$B(C_6F_5)_3$	76.2	23.5	100	77.8

[a] ^{31}P NMR shifts are recorded in $CDCl_3$ relative to H_3PO_4 (δ = 0.00 ppm) as internal standard. [b] $\Delta\delta(^{31}P) = \delta(^{31}P)$ adduct - 52.7 ppm. [c] Gutmann–Beckett method: AN = $2.21\times(\delta^{31}_{LA\cdot Et3PO} - 41)$. [d] Data acquired at –20 ºC.

Applications as Catalysts in Hydrosilylation Reactions. The observed high Lewis acidity prompted us to explore applications in the Lewis acid catalyzed hydrosilylation of unsaturated organic substrates. The objective of these investigations was to test the capacity of these novel Lewis acids as recyclable catalysts. To explore the feasibility, we initially

tested the borane model compounds in the catalyzed hydrosilylation of benzaldehyde (**1a**), acetophenone (**1b**), N-benzylideneaniline (**1c**), and styrene (**1d**). When using 10 mol% of the model compounds as catalysts, quantitative conversion of **1a** was achieved within 10 min (Table 2-2, entry 1, 2), demonstrating the high reactivity of these Lewis acids. This result suggested that even at much lower catalyst loading the reactivity in the catalytic hydrosilylation reaction may be retained. Gratifyingly, both **Mod1BPf2** and **Mod2-BPf2** were found to promote carbonyl hydrosilylation with 0.5 mol% model catalysts loading, reaching high conversions within short reaction time (Table 2-2, entry 3-6). When directly comparing their catalytic performance, **Mod2-BPf2** showed relatively higher efficiency. This efficiency difference becomes more pronounced in the hydrosilylation of imine **1c** (Table 2-2, entry 7, 8). While 2 mol% of **Mod1-BPf2** resulted in 69% conversion at 50 ºC after 48 h, the more Lewis acidic **Mod2-BPf2** gave full conversion at ambient temperature over 24 h. Finally, the hydrosilylation of styrene was probed. Even with 10 mol% **Mod1-BPf2** no conversion of the relatively less nucleophilic styrene could be achieved over 48 hours at 60 ºC. In contrast, when applying 10 mol% of **Mod2-BPf2** 29% conversion was reached at 30 ºC after 48 hours. In all cases was the structure of hydrosilylated products confirmed by comparison with ^{1}H NMR data reported in the literature. For the hydrosilylation of styrene only one isomer was detected, consistent with the results reported when using $B(C_6F_5)_3$ as the catalyst.[7b] Having identified the catalytic efficiency of the borane model systems, we next focused on exploring the polymeric Lewis acids in the hydrosilylation of **1a**, **1b** and **1c**. When keeping the loading of the active borane moieties in the polymer constant loading, **P1-BPf2** and **P2-BPf2** display similar catalytic

efficiency as the corresponding model compounds (Table 2-2, entry 11-15). The hydrosilylation of **1c** was only carried out with **P2-BPf2**, because the lower reactivity of **Mod1-BPf2** toward **1c** that forecast a low efficiency of **P1-BPf2**. An important aspect is the reusability of the polymeric Lewis acids. Using **P2-BPf2** as an example, we found that by simply precipitating and washing the product mixture with hexanes the polymeric catalyst could be separated (confirmed by ^{1}H NMR) from the final product and the catalytic processes repeated for at least 5 times. The catalytic activity towards benzaldehyde was retained, achieving 95% conversion in the fifth cycle (Figure 2-S55 in the appendix). Thus, these polymeric Lewis acids are well suited as reusable Lewis acid catalysts for hydrosilylation reactions.

Table 2-2. Investigation of Lewis acids in catalytic hydrosilylation of selected substrates

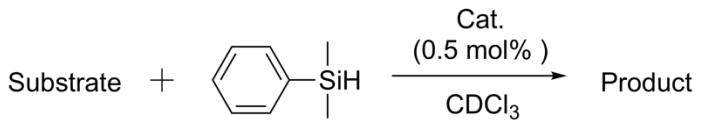

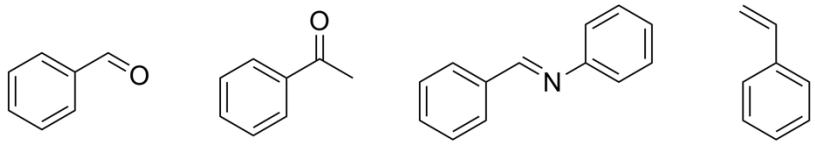

entry	substrate	catalyst	cat. loading (mol%)	temp / time (ºC / h)	conversion (%)
1	1a	Mod1-BPf2	10	25 / 10 min	100
2	1a	Mod2-BPf2	10	25 / 10 min	100
3	1a	Mod1-BPf2	0.5	25 / 0.5	85
4	1a	Mod2-BPf2	0.5	25 / 0.5	100
5	1b	Mod1-BPf2	0.5	25 / 2.5	98
6	1b	Mod2-BPf2	0.5	25 / 2.5	100
7	1c	Mod1-BPf2	2	50 / 48	69
8	1c	Mod2-BPf2	0.5	25 / 24	100
9	1d	Mod1-BPf2	10	60 / 48	0
10	1d	Mod2-BPf2	10	30 / 48	29
11	1a	P1-BPf2	0.5	25 / 0.5	80
12	1a	P2-BPf2	0.5	25 / 0.5	100
13	1b	P1-BPf2	0.5	25 / 2	77
14	1b	P2-BPf2	0.5	25 / 2	85
15	1c	P2-BPf2	0.5	25 / 24	100

Photophysical Properties. During the course of our studies we noticed that both the organoborane model compounds and the copolymers are strongly luminescent in solution. This suggests potential utility also as materials for optoelectronic device or imaging applications. Since the first demonstration by Shirota and coworkers that bithiophene or terthiophene with Mes_2B substituents can be used as efficient electron-transporting materials in OLEDs,[25] many different luminescent materials based on tricoordinate organoboranes have been designed.[2] More recently, researchers have discovered organoborane donor-acceptor systems that exhibit highly effective thermally activated delayed fluorescence (TADF).[26] Relevant to our studies is the work by Zhao and coworkers who reported that triarylborane-triarylamine systems with [2.2]paracyclophane, twisted biphenyl or binaphthyl backbones display charge transfer emissions that, depending on the system, are temperature-dependent, circularly polarized, or exhibit TADF characteristics.[27] Of note is also work by Thilagar and coworker who designed simple structures exhibiting TADF, which encompass tridurylboranes with NR_2 (R = H, Me) donor moieties.[26d] In all these compounds, the spatial separation of the donor-centered HOMO and acceptor-centered LUMO plays an important role in enabling the TADF behavior.[28] While most studies have focused on Mes_2B groups as acceptors, Marder and coworkers found that the much enhanced acceptor strength of $(FMes)_2B$ (FMes = 2,4,6-tris(trifluoromethyl)phenyl) derivatives can be beneficial for optoelectronic application.[27b,29] These findings prompted us to investigate the photophysical properties of our polymers and model compounds in more detail.

As seen in Table 2-3, the absorption and emission data for the copolymers **P1/P2-BPf2** closely track those of the molecular model compounds **Mod1/Mod2-BPf2**. This is expected considering that the functional group loading for the polymers is about 20%, thus spacing out the chromophores. The UV-visible absorption spectra of **Mod1-BPf2** and **Mod2-BPf2** in DCM show maxima at 386 and 363 nm, respectively (Figure 2-3). The absorptions for **Mod1**/**P1-BPf2** are redshifted relative to those of **Mod2**/**P2-BPf2**, likely due to elevation of the HOMO in the presence of the more electron-rich dimethylphenyl compared to the chlorophenyl group. The presence of a second band at around 260–270 nm for all compounds may indicate additional transitions that involve predominantly orbitals localized on the *para*-substituted phenyl ring that is common to both systems.

In DCM solution, **Mod1**/**P1-BPf2** give rise to green emissions with maxima at 538 / 543 nm, while **Mod2**/**P2-BPf2** are blue-emissive with maxima at 483 / 490 nm. The fluorescence quantum yields of **Mod1**/**P1-BPf2** (Φ_{FL} = 0.34 / 0.31) are higher than those of **Mod2**/**P2-BPf2** (Φ_{FL} = 0.14 / 0.22), and the fluorescence lifetimes measured for **Mod1**/**P1-BPf2** (τ_{FL} = 35.6 / 34.6 ns) are significantly longer than those of **Mod2**/**P2-BPf2** (τ_{FL} = 6.9 / 8.4 ns, averaged for two components). From the τ_{FL} and Φ_{FL} values, the radiative (k_r) and nonradiative (k_{nr}) decay rate constants were calculated. **Mod2**/**P2-BPf2** show relatively larger k_r and k_{nr} values than **Mod1**/**P1-BPf2**. The only slightly larger k_r values but significantly larger k_{nr} values for **Mod2**/**P2-BPf2** lead to the observation of lower quantum yields for the chlorinated derivatives. A possible explanation is that intersystem crossing (ISC) is facilitated by the chlorine heavy atom effect. The small k_r values, together with the large Stokes shifts, may also suggest a twisted excited state structure for these

compounds.[27b, c] The excited state structure of **Mod1-BPf2** is expected to be more distorted compared to that of **Mod2-BPf2**, because the *ortho*-methyl groups are sitting below and above the boron center, generating more steric hindrance.

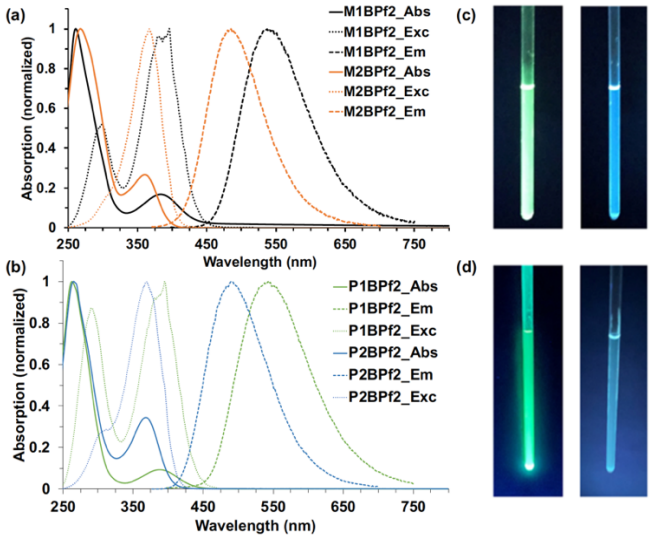

Figure 2-3. (a, b) UV-vis absorption, excitation and emission spectra of borane model compounds and polymers in DCM solution. Photographs of solutions of (c) **Mod1-BPf2** / **Mod2-BPf2** (right), (d) **P1-BPf2** (left) / **P2-BPf2** (right) in CDCl3 irradiated with a handheld UV lamp (254 nm).

Table 2-3. Comparison of Photophysical Data of Model Compounds and Polymers

Compound	λ_{Abs}[a] (nm)	λ_{Exc}[b] (nm)	λ_{FL}[c] (nm)	Stokes shift (cm^{-1})	τ_{FL}[d] (ns)	Φ_{FL}[e]	k_r/k_{nr}[f] (10^7 s^{-1})
Mod1-BPf2	386, 260	392, 300	538	7300	τ_1 = 35.6, 100% (χ^2 = 1.28)	0.34	0.95/1.8
P1-BPf2	388, 263	389, 293	543	7300	τ_1 = 34.6, 100% (χ^2 = 1.26)	0.31	0.89/2.0
Mod2-BPf2	363, 270	369, 302	483	6800	τ_1 = 1.7, 20% τ_2 = 8.2, 80%	0.14	2.0/12.4

					(χ^2 = 1.59) [g]		
P2-BPf2	367, 265	369, 305	490	6800	τ_1 = 7.9, 95% τ_2 = 18.6, 5% (χ^2 = 1.44)	0.22	2.6/9.3

[a] In DCM solution. [b] Excitation data for maximum emission. [c] Excited at the lowest energy absorption maxima. [d] Excited with a nanoLED at 390 nm. [e] Absolute quantum yield determined using an integrating sphere. [f] Radiative (k_r) and nonradiative (k_{nr}) decay rate constants are calculated using the equations $k_r = \Phi/\tau$, $k_{nr} = (1 - \Phi)/\tau$. [g] For triple-exponential fit: **Mod2-BPf2**: τ_1 = 6.7 ns, 64 %; τ_2 = 11.2 ns, 22 %; τ_3 = 1.2 ns, 14 % (χ^2 = 1.42).

Considering the likely role of intramolecular charge transfer (ICT) in the excited state, we investigated the effects of changes in solvent polarity on the absorption and emission spectra. These studies were performed on the model compounds, because the range of suitable solvents is larger. The data are illustrated in Figure 2-4 and summarized in Table 2-S1 (appendix). While the absorption spectra are only slightly dependent on solvent polarity, the emission spectra exhibit a distinct positive solvatochromism. Upon changing the solvent from hexane to DCM, the emission maximum shifted from 469 to 538 nm for **Mod1-BPf2** and from 413 to 483 nm for **Mod2-BPf2**, indicative of a more polarized first excited state in comparison to the ground state.

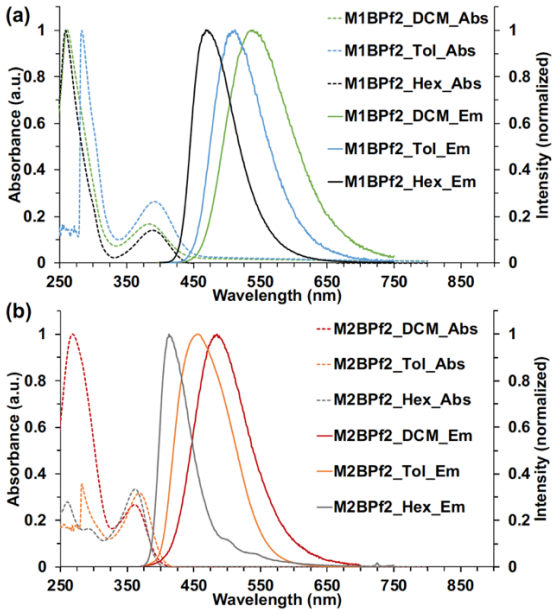

Figure 2-4. (a) UV-vis absorption and emission spectra of **Mod1-BPf2** in DCM (black), toluene (green) and hexanes (blue) solution. (b) UV-vis absorption and emission spectra of **Mod2-BPf2** in DCM (red), toluene (orange) and hexanes (gray) solution.

Time-gated spectroscopic studies were carried out at room temperature in DCM solution with a 0.1 ms delay time, revealing the presence of additional slower emission pathways. As seen in Figure 2-5, the prompt and gated emission spectra of **Mod1-BPf2** and **Mod2-BPf2** are virtually identical with maxima around 538 nm and 483 nm, respectively. This strongly suggests TADF to be operative. The lifetime of the delayed component is 54.9 µs for **Mod1-BPf2** and 0.73 ms for **Mod2-BPf2**, while the prompt fluorescence lifetime is 35.6 ns and 6.9 ns respectively (Figure 2-6). Similar measurements were also performed for the copolymers, revealing long lifetimes due to TADF components of 62.4 µs for **P1-BPf2** and 0.66 ms for **P2-BPf2**, which are similar to those of the corresponding model compounds.

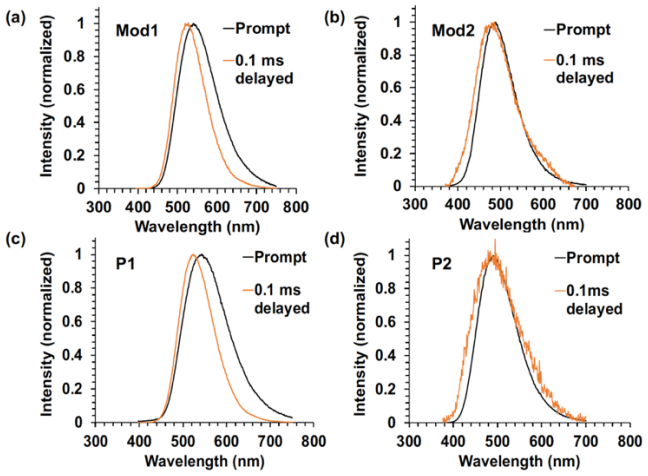

Figure 2-5. Fluorescence (black) and delayed fluorescence (orange) emission spectra of (a) **Mod1-BPf2**, (b) **Mod2-BPf2**, (c) **P1-BPf2**, and (d) **P2-BPf2** in DCM solution.

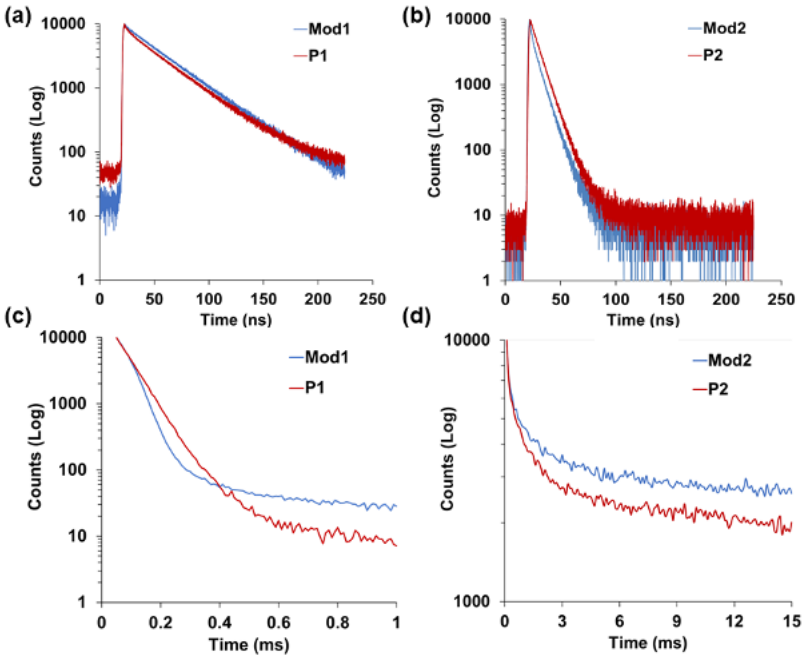

Figure 2-6. Prompt fluorescence emission decay curves of (a) **Mod1/P1-BPf2** and (b) **Mod2/P2-BPf2** in DCM solution. Delayed emission decay curves of (c) Single-exponential fit of **Mod1-BPf2**: τ_1 = 54.9 µs, 100 % and **P1-BPf2**: τ_1 = 62.4 µs, 100 % and (d) double-exponential fit of **Mod2-BPf2**: τ_1 = 0.16 ms, 74 %; τ_2 = 2.34 ms, 26 % and **P2-BPf2**: τ_1 = 0.16 ms, 72 %; τ_2 = 1.95 ms, 28 % in DCM solution.

In TADF-active molecules, thermal repopulation of the S_1 state from the T_1 state takes place, which requires a fluorophore to have a small energy gap (ΔE_{ST}) between S_1 and T_1, typically within 0.3 eV and ideally less than 0.1 eV.[28b] The longer TADF lifetimes of **Mod2**/**P2-BPf2** compared to **Mod1**/**P1-BPf2** indicate a lower ΔE_{ST} for **Mod2**/**P2-BPf2**. To further investigate this aspect, the energy gaps of the model compounds were studied by DFT and TD-DFT calculations as discussed in the following.

Theoretical calculations. The electronic structures of the model compounds and the orbitals involved in the electronic transitions were computed at the b3lyp/6-31g(d) level of theory using the polarizable continuum model (PCM) for solvation in DCM. As seen in Figure 2-7, for **Mod1-BPf2** and **Mod2-BPf2**, the HOMO is localized mainly on the 4-(*tert*-butyl)-1,1'-biphenyl groups, with a small contribution from the nominally empty p-orbital on the boron atom. The LUMO is localized primarily on the boryl group, with some contribution from the boron-bound phenyl ring. The HOMO and LUMO energy levels are -5.90 and -2.53 eV for **Mod1-BPf2**, but significantly lower at -6.25 and -2.65 eV for **Mod2-BPf2**. TD-DFT calculations (rcam-b3lyp/6-31g(d)) suggest a small oscillator strength of f = 0.0992 for the S_0-S_1 transition of **Mod1-BPf2**, in good agreement with the weak intensity of the lowest energy absorption. However, a much larger f = 0.6619 was found for **Mod2-BPf2**, which clearly overestimates the intensity of the experimental lowest-energy absorption of the latter (Table 2-S3 in the appendix). To address this apparent discrepancy, we carried out a single-point TD-DFT calculation for **Mod2-BPf2** using the optimized **Mod1-BPf2** geometry as a starting point, but with the methyl groups replaced for –H and –Cl at a distance of 1.771 Å. Using this geometry, an oscillator strength of f = 0.1300 for

the lowest energy absorption of **Mod2-BPf2** was found, which is in good agreement with the experimental data (Table 2-S3 in the appendix). The computed excitation wavelengths for the S_0-S_1 transition are calculated to be 353 nm (**Mod1-BPf2**) and 326 nm (**Mod2-BPf2**; 324 nm for the modified structure using the geometry of **Mod1-BPf2**) (Table 2-4). These values are reasonably consistent with the experimental lowest-energy absorption maxima[30] The relatively larger HOMO-LUMO energy gap for **Mod2-BPf2** correlates well with the longer wavelength absorption maxima of **Mod1-BPf2** in comparison to **Mod2-BPf2**. For both, the HOMO and LUMO predominantly contribute to the excitation to S_1 (Table 2-S3 in the appendix), suggesting significant intramolecular charge transfer (ICT) character for this process. This also supports the experimentally observed emission solvatochromism of these compounds. [29]

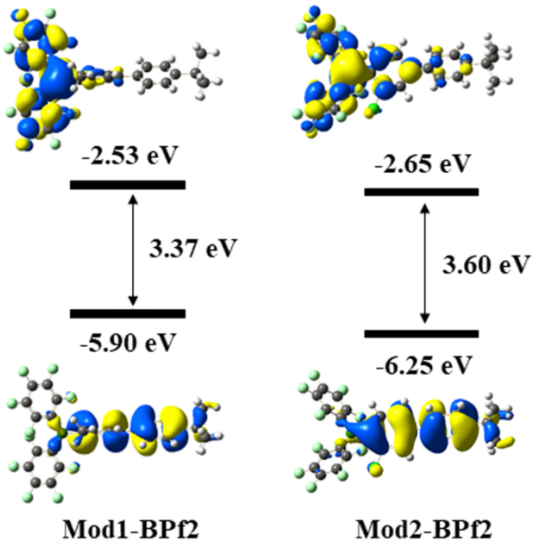

Figure 2-7. DFT calculated frontier orbitals for Mod1-BPf2 and Mod2BPf2 (rb3lyp/6-31g(d), DCM solvation model, isovalue = 0.02).

Table 2- 4. TD-DFT calculated photophysical data for Mod1-BPf2 and Mod2-BPf2 (rcam-b3lyp/6-31g(d), DCM solvation model)

	Transition (*f*)	E_{ex}[a] (eV)	λ[a] (nm)	Dominant components[b] (%)
		Absorption		
Mod1-BPf2	$S_0 \rightarrow S_1$ (0.0992)	3.51 (3.21)	353 (386)	HOMO-5 → LUMO (18) HOMO → LUMO (77)
Mod2-BPf2	$S_0 \rightarrow S_1$ (0.6619)	3.81 (3.41)	326 (363)	HOMO → LUMO (74)
		Emission[c]		
Mod1-BPf2	$S_1 \rightarrow S_0$ (0.0126)	2.94 (2.30)	421 (538)	H-SOMO-4 → L-SOMO (10) H-SOMO → L-SOMO (84)
Mod2-BPf2	$S_1 \rightarrow S_0$ (0.0406)	3.27 (2.57)	379 (483)	H-SOMO → L-SOMO (84)

[a] Values in parentheses are experimental longest-wavelength absorption or emission maxima in DCM. [b] Components with greater than 10% contribution shown. Percentage contribution approximated by $2 \times (c_i)^2 \times 100\%$, where c_i is the coefficient for the particular 'orbital rotation'. [c] Taken as the reverse of excitation to S_1 from S_0 at the optimized S_1 geometry.

We also carried out TD-DFT optimizations of the S_1 states for both model compounds to investigate the structural relaxation in the excited state. The DFT b3lyp/6-31g(d) calculated ground-state optimized geometries were used as the input, and the rcam- b3lyp/6-31g(d) level of theory was employed using a DCM solvation model. In both cases, a distortion of the $(C_6F_5)_2B$ group occurs, in which a reduction of the dihedral angles between the C_6F_5 planes and the BC_3 plane leads to enhanced conjugation between the C_6F_5 groups with the p-orbital of the boron atom. In addition, the two methyl groups and chlorine substituted phenyl rings of **Mod1-BPf2** and **Mod2-BPf2** twist out of conjugation from 71.6 to 80.9º and 43.1 to 78.6 º respectively, forming a more twisted intramolecular charge transfer (TICT) state, with an elongation of the B-C_{Ph} bond by 0.034 and 0.043 Å (Table 2-5). To support these results, we performed TD-DFT calculations (rcam-b3lyp/6-31g(d), DCM

solvation) to compute the emission properties. The simulated fluorescence emissions are again slightly higher in energy,[30] but overall consistent with the experimental data (Table 2-3). Moreover, the small calculated oscillator strength for **Mod1-BPf2** and **Mod2-BPf2** reflects that the luminescence spectra of these compounds are indeed composed of the sum of both fluorescence and delayed fluorescence components.

Table 2-5. Comparison of structural parameters at the S_0 (rb3lyp/6-31g(d)) and S_1 (rcam-b3lyp/6-31g(d)) states

Compound	B-C_{Ph}	B-C_{Pf}	Ph_1//Ph_2	Ph_2//BC_3	Pf//BC_3
Mod1-BPf2$_{S0}$	1.572	1.577, 1.575	35.3	71.6	36.7, 37.0
Mod1-BPf2$_{S1}$	1.606	1.550, 1.551	18.6	80.9	27.0, 27.8
Mod2-BPf2$_{S0}$	1.560	1.571, 1.576	34.7	43.1	36.7, 41.9
Mod2-BPf2$_{S1}$	1.603	1.548, 1.549	16.9	78.6	25.7, 28.8

One of the determining factors regarding the delayed fluorescence is the energy difference between the S_1 and T_1 states. An investigation of the first triplet excited state (T_1) was attempted for both model compounds using the ub3lyp functional with a 6-31g(d) basis set and DCM solvation. The estimated difference in vertical transition energies ΔE_{ST} between the singlet (S_1) and triplet (T_1) excited states is extremely small for **Mod1-BPf2** (0.089 eV), but more substantial for **Mod2-BPf2** (0.242 eV) (Figure 2-8). These results correlate well with the experimental observations, i.e., the lower ΔE_{ST} of **Mod1-BPf2** enhances the

reverse intersystem crossing (RISC), resulting in more efficient upconversion from T_1 to S_1 that leads to a shorter lifetime for the delayed fluorescence. In contrast, the relatively larger ΔE_{ST} of **Mod2-BPf2** results in slower RISC and a longer lifetime.

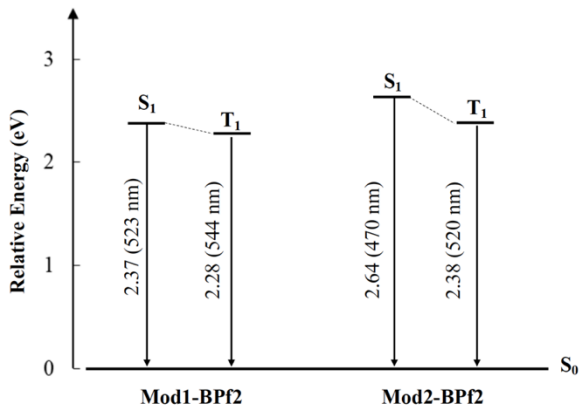

Figure 2-8. Comparison of the energy of the excited states S_1, T_1 and relative to the S_0 ground state for model compounds computed in DCM solvent.

2.3 Conclusions

To summarize, one part of our investigations was dedicated to the design of new polymeric Lewis acids for catalytic hydrosilylation. Two novel copolymers and their corresponding model compounds have been developed and employed as catalysts for the hydrosilylation of C=O or C=N bonds. These systems encompass either two *ortho*-methyl or an *ortho*-chlorine substituent to provide steric and electronic fine-tuning of the Lewis acidic component. In this way, the high Lewis acidity required for efficient catalysis is maintained while expanding the substrate scope. The polymer-supported Lewis acids present excellent recyclability, as they can be recovered by simple washing with hexanes.

Another part of the present work comprised an investigation of the electronic structure and photophysical properties through a combination of experimental and computational studies. We found that the photophysical properties also vary with the substituents in the *ortho*-positions. The methyl groups in the bridge render **Mod1**/**P1-BPf2** more electron-rich than **Mod2**/**P2-BPf2** with a chlorine substituent. As a result, in DCM solution **Mod1**/**P1-BPf2** show green emission, while **Mod2**/**P2-BPf2** are blue-emissive. In addition, **Mod1**/**P1-BPf2** display longer fluorescence lifetimes and higher quantum yields than **Mod2**/**P2-BPf2**. Using time-gated spectroscopy we found evidence of an additional slower component of the emission that was attributed to TADF processes involving a twisted intramolecular charge transfer state. The much longer delayed fluorescence lifetime of **Mod2**/**P2-BPf2** than **Mod1**/**P1-BPf2** suggests a smaller gap between S_1 and T_1, which was further confirmed by TD-DFT calculations.

Overall, our results indicate the strong potential of structurally fine-tuned polymer-supported Lewis acids as catalysts in the hydrosilylation of C=X bonds (X = O, N) with excellent recyclability, whereas the intriguing emissive properties suggest potential utility as luminescent materials.

2.4 Experimental

General Method. NMR data were acquired at 25 ºC. 500.0 MHz ^{1}H, 160.4 MHz ^{11}B, and 470.3 MHz ^{19}F NMR data were recorded on a 500 MHz Bruker AVANCE spectrometer; 500.2 MHz ^{1}H and 125.8 MHz ^{13}C NMR data on a 500 MHz Bruker Auto AVANCE spectrometer; and 599.7 MHz ^{1}H, 150.8 MHz ^{13}C and 192.4 MHz ^{11}B NMR data on a

Varian INOVA 600 spectrometer. ^{11}B NMR spectra were acquired with boron-free quartz NMR tubes either on the Varian INOVA 600 with a boron-free 5 mm dual broadband gradient probe (Nalorac, Varian Inc., Martinez, CA) or the 500 MHz Bruker Auto Avance with a 5mm PH SEX 500S1 11B-H/F-D probe. ^{1}H and ^{13}C NMR spectra were referenced internally to solvent signals ($CDCl_3$: 7.26 ppm for ^{1}H NMR, 77.16 ppm for ^{13}C NMR) and all other NMR spectra externally to $SiMe_4$ (0 ppm).

UV-visible absorption data were acquired on a Varian Cary 5000 UV-Vis/NIR spectrophotometer or a Cary 60 UV-Vis spectrophotometer. The fluorescence data and lifetimes were measured using a Horiba Fluorolog-3 spectrofluorometer equipped with a 390 nm nanoLED and a FluoroHub R-928 detector. The thermally activated delayed fluorescent lifetimes were measured using a FL-1040A phosphorimeter incorporated into the Fluorolog setup. The excitation source was a pulsed xenon flash lamp, the full-width half-maximum of each pulse is 3 μs. A delay of 0.1 ms was used to ensure full decay of the prompt fluorescent response and the Xe lamp output. Absolute quantum yields (Φ_F) were measured on the HORIBA Fluorolog-3 using a pre-calibrated Quanta-φ integrating sphere. Light from the sample compartment is directed into the sphere via a fiber-optic cable and an F-3000 Fiber-Optic Adapter, and then returned to the sample compartment (and to the emission monochromator) via a second fiber-optic cable and an F-3000 Fiber-Optic Adapter.

GC-MS data were acquired on an Agilent HP6890 GC System with an HP-5MS 5% phenyl methyl siloxane column and Agilent 5973A inert XL EI/CI MSD using helium as the carrier gas at a flow rate of 1 mL/min. The initial oven temperature was 50 °C, after holding

for 3 mins the temperature was increased with a 10 °C/min ramp to a final temperature of 220 °C, then held at 220 °C for 15 min (splitless mode of injection, total run time of 22.0 min). MALDI-TOF MS measurements were performed on a Bruker Ultraflextreme in reflection mode with delayed extraction. Red phosphorus was used for calibration.

GPC-RI analyses were performed in THF (1.0 mL/min, 35 °C) using a Viscotek GPCmax with a VE 2001 GPC solvent/sample module, a 2600 UV-PDA detector, and a TDA 305 triple detector array. A set of two columns consisting of one PLgel 5 mm mixed-D and one PLgel 5 mm mixed-C column was used for separation and ten narrow polystyrene standards (580 Da – 364000 Da, Polymer Laboratories, Varian Inc.) for calibration.

All calculations (DFT and TD-DFT) were carried out with the program package Gaussian 16 (Rev. B.01 or Rev. D.01) and were performed on a parallel cluster system. The input files were generated from Chem3D and pre-optimized in Spartan '08 V 1.2.0. Ground state geometries were then optimized in Gaussian 16 using the hybrid density functional b3lyp with a 6-31g(d) basis set. Frequency calculations were performed to confirm the presence of local minima (only positive frequencies). Vertical excitations were calculated by TD-DFT methods at the rcam-b3lyp/6-31g(d) and rb3lyp/6-31g(d) level. First triplet excited state geometries were optimized by DFT methods at the ub3lyp/6-31g(d) level and first singlet excited state geometries were optimized by TD-DFT methods at the b3lyp/6-31g(d) level. All calculations were performed using the polarizable continuum model (PCM) for solvation in DCM.

Materials. Toluene and hexanes were purified using a solvent purification system (Innovative Technologies) and stored over Na/K alloy. Diethyl ether was distilled from Na/benzophenone; anisole and all chlorinated solvents were distilled from CaH_2. Azobisisobutyronitrile (AIBN) initiator was recrystallized in methanol. All other chemicals were purchased from commercial sources and directly used without further purification. All oxygen- and moisture-sensitive manipulations were carried out under an inert atmosphere using either standard Schlenk techniques or a glove box. Reactions involving BBr_3 were conducted in Teflon-stoppered Schlenk tubes, avoiding the use of silicone grease.

Synthesis of (3,5-Dimethyl-4'-vinyl-[1,1'–biphenyl]-4-yl)trimethylsilane (Monomer M1). In a 250 mL Schlenk flask, 5-bromo-2-iodo-1,3-dimethylbenzene (5.00 g, 16.1 mmol) was dissolved in diethyl ether (200 mL). Under N_2 flow, a solution of n-butyl lithium (1.6 M in hexanes, 10.6 mL, 17.0 mmol, 1.05 equiv.) was added dropwise at -78 °C and the mixture was kept stirring at -78 °C for 1 h. Trimethylsilyl trifluoromethanesulfonate (3.49 mL, 19.3 mmol, 1.2 equiv.) was dropwise added at -78 °C. The temperature was raised to room temperature and the reaction mixture stirred overnight. The product, (4-bromo-2,6-dimethylphenyl)trimethylsilane, was extracted with diethyl ether and then purified by fractional distillation. Yield: 3.43 g (83%). ^{1}H NMR (500.0 MHz, $CDCl_3$): δ = 7.12 (s, 2H, Ph), 2.41 (s, 6H, Me), 0.38 (s, 9H, $SiMe_3$).[23] GC-MS (retention time 12.3 min) calcd. for $C_{11}H_{17}BrSi$ (m/z) 256.0, found 256.1.

In an oven-dried 250 mL Schlenk flask were dissolved (4-bromo-2,6-dimethylphenyl)trimethylsilane (3.00 g, 11.7 mmol) and 4-vinylphenylboronic acid (2.07

g, 14.0 mmol, 1.2 equiv.) with toluene (90 mL). Then Cs_2CO_3 was added (11.4 g, 35.0 mmol, 3 equiv.). The mixture was degassed by 3 freeze-pump-thaw procedures. A solution of the catalyst $Pd(PPh_3)_4$ (0.67 g, 0.58 mmol, 5 mol%) in toluene (10 mL) was added and the reaction mixture was kept stirring under N_2 flow overnight at 90 °C. After aqueous workup and extraction with DCM the solvent was removed under vacuum to give a brownish oil. The crude product was purified by column chromatography on alumina with hexanes as the eluent and then recrystallized from MeOH at room temperature by slow solvent evaporation. Yield: 1.53 g (47%). ^{1}H NMR (500.0 MHz, $CDCl_3$): δ = 7.57 (d, J = 8.5 Hz, 2H, Ph), 7.47 (d, J = 8.5 Hz, 2H, Ph), 7.22 (s, 2H, Ph), 6.76 (dd, J = 17.5, 10.5 Hz, 1H, vinyl), 5.79 (d, J = 17.5 Hz, 1H, vinyl), 5.27 (d, J = 11.0 Hz, 1H, vinyl), 2.53 (s, 6H, Me), 0.44 (s, 9H, $SiMe_3$). ^{13}C NMR (150.8 MHz, $CDCl_3$): δ = 144.9, 141.0, 140.3, 136.8, 136.6, 135.9, 127.3, 126.7, 113.9, 25.2, 3.7. GC-MS (retention time 19.4 min) calcd. for $C_{19}H_{24}Si$ (m/z) 280.2, found 280.2. Elemental analysis: Calcd for $C_{19}H_{24}Si$: C 81.36; H 8.63%. Found: C 81.23; H 8.53%.

Synthesis of (3-Chloro-4'-vinyl-[1,1'-biphenyl]-4-yl)trimethylsilane (Monomer M2). 4-Bromo-2-chloro-1-iodobenzene (10.0 g, 31.5 mmol) was charged into a 500 mL Schlenk flask under nitrogen, followed by adding of 200 mL of degassed diethyl ether, and the mixture was cooled to -78 °C. A solution of n-butyl lithium (2.5 M in hexanes, 13.2 mL, 33.0 mmol, 1.05 equiv.) was added dropwise and the mixture was stirred at -78 °C for 1 h. Then trimethylsilyl trifluoromethanesulfonate (8.40 g, 37.8 mmol, 1.2 equiv.) was added dropwise at -78 °C. The temperature was raised to room temperature and the reaction mixture kept stirring overnight. The product, (4-bromo-2-chlorophenyl)trimethylsilane,

was extracted with diethyl ether, and then purified by fractional distillation. Yield: 5.10 g (61%). ^{1}H NMR (500.0 MHz, $CDCl_3$): δ = 7.50 (s, 1H, Ph), 7.36 (d, J = 8.0 Hz, 1H, Ph), 7.29 (d, J = 7.0 Hz, 1H, Ph), 0.36 (s, 9H, $SiMe_3$). GC-MS (retention time 10.5 min) calcd. for $C_9H_{12}BrClSi$ (m/z) 262.0, found 264.0.

4-Vinylphenylboronic acid (737 mg, 4.98 mmol), (4-bromo-2-chlorophenyl)trimethylsilane (1.10 g, 4.17 mmol), and Cs_2CO_3 (4.10 g, 12.6 mmol, 2.5 equiv.) were charged into a 50 mL Schlenk flask. After adding 25 mL of toluene, the mixture was degassed by 3 freeze-pump-thaw procedures. A solution of the catalyst $Pd(PPh_3)_4$ (241 mg, 209 μmol, 5 mol%) in toluene (5 mL) was added to the Schlenk flask by syringe. The mixture was stirred overnight at 90 °C under nitrogen flow. The reaction was worked up with water and extracted with dichloromethane. The solvent was removed under vacuum and the residue was purified by column chromatography (alumina gel, hexanes) to give the product as a white solid. Yield: 0.63 g (53%). ^{1}H NMR (500.0 MHz, $CDCl_3$): δ = 7.59 (s, 1H, Ph), 7.56 (d, J = 8.5 Hz, 2H, Ph), 7.53 (d, J = 8.0 Hz, 1H, Ph), 7.50 (d, J = 8.0 Hz, 2H, Ph), 7.47 (d, J = 7.5 Hz, 1H, Ph), 6.77 (dd, J = 17.5, 11.0 Hz, 1H, vinyl), 5.82 (d, J = 17.0 Hz, 1H, vinyl), 5.31 (d, J = 11.0 Hz, 1H, vinyl), 0.42 (s, 9H, $SiMe_3$). ^{13}C NMR (150.8 MHz, $CDCl_3$): δ = 143.3, 141.7, 139.1, 137.4, 136.4, 136.2, 127.6, 127.3, 126.9, 124.5, 114.0, 25.2, -0.6. GC-MS (retention time 18 min) calcd. for $C_{17}H_{19}ClSi$ (m/z) 286.1, found 286.2. Elemental analysis: Calcd for $C_{17}H_{19}ClSi$: C 71.18; H 6.68%. Found: C 71.28; H 6.75%.

Synthesis of Poly((3,5-dimethyl-4'-vinyl-[1,1'-biphenyl]-4-yl)trimethylsilane)-co-Polystyrene (P1-Si). In a glovebox, monomer **M1** (1.00 g, 3.57 mmol), styrene (1.86 g,

17.9 mmol), azobisisobutyronitrile (17.7 mg, 0.108 mmol, 0.5 mol%), and 2.8 mL of anisole were charged into a 10 mL Schlenk flask. The flask was then taken outside the glovebox, the mixture subjected to three freeze-pump-thaw cycles, and subsequently immersed in an oil bath preset at 110 °C. After stirring for 24 h the flask was cooled to room temperature, one drop of the polymer solution was taken to determine the monomer conversion of **M1** (92%) and styrene (85%) by ^{1}H NMR integration of the residual vinyl group signals of the monomers relative to the Me group signal of anisole. The reaction mixture was precipitated into methanol. The precipitate was collected by filtration and then redissolved in toluene. The copolymer was recovered by repeated reprecipitation from toluene into hexanes (twice) and dried under vacuum. Yield: 1.60 g (56%). ^{1}H NMR (500 MHz, $CDCl_3$): δ = 7.4 - 6.2 (overlapped aromatic protons), 2.52 (broad s, Me), 2.3 - 1.3 (overlapped backbone protons), 0.44 (broad s, $SiMe_3$). GPC-RI: M_n = 34200 g mol^{-1}, M_w = 127600 g mol^{-1}, $Đ$ = 3.7; $X(\mathbf{M1})_{n\ GPC}$ = 45, $X(St)_{n\ GPC}$ = 208. The product contains 18 mol% Si monomer based on ^{1}H NMR integration of the $SiMe_3$ signal relative to aromatic signals (17mol% based on the feed ratio).

Conversion to Poly((3,5-dimethyl-4'-vinyl-[1,1'-biphenyl]-4yl)bis(pentafluorophenyl)-borane)-co-Polystyrene (P1-BPf2). In a glovebox, **P1-Si** (250.0 mg, 0.327 mmol $SiMe_3$ groups) was dissolved in toluene (3 mL). A solution of BBr_3 (90.1 mg, 0.360 mmol) in 0.2 mL of toluene was added dropwise, and the mixture was allowed to stir at room temperature for 12 h. The formation of the dibromoborylated intermediate was confirmed by ^{1}H and ^{11}B NMR spectroscopy of the crude mixture: ^{1}H NMR (500.0 MHz, $CDCl_3$): δ = 7.2 - 6.3 (overlapped aromatic protons, 5m+6n H, relative

integration: 29.14), 2.4 (broad s, Me, 6n H, relative integration: 6), 2.2 - 1.3 (overlapped backbone protons), 0.67 (s, Me_3SiBr); ^{11}B NMR (160.4 MHz, $CDCl_3$): δ = 59.6. The polymer mixture was diluted with 10 mL toluene, then, a solution of $Zn(C_6F_5)_2$ (195.6 mg, 0.490 mmol) in toluene (0.1 mL) was added dropwise at room temperature. The mixture was kept stirring at 80 °C for 48 h. A solid precipitate formed and was removed by filtration through a small pad of celite. The solvent was removed under high vacuum. Purification by reprecipitation from toluene into hexanes (three times) and drying under high vacuum gave the product as a light yellow fluorescent solid. Yield: 0.218 g (64%). ^1H NMR (500 MHz, $CDCl_3$): δ = 7.4 – 6.2 (overlapped aromatic protons, 5m+6n H, relative integration: 29.17), 2.20 (broad s, Me, 6n H, relative integration: 6), 2.0 – 1.2 (overlapped backbone protons). ^{19}F NMR (470.3 MHz, $CDCl_3$): δ = -128.3 (4n F, Pf), -145.0 (2n F, Pf), -160.4 (4n F, Pf). ^{11}B NMR (160.4 MHz, $CDCl_3$): δ = 68 (very broad).

Synthesis of Poly((3-chloro-4'-vinyl-[1,1'-biphenyl]-4-yl)trimethylsilane)-co-PS (P2-Si). In a glovebox, monomer **M2** (1.00 g, 3.49 mmol), styrene (1.81 g, 17.4 mmol), azobisisobutyronitrile (17.2 mg, 0.105 mmol, 0.5 mol%), and 2.8 mL of anisole were charged into a 10 mL Schlenk flask. The flask was then taken outside the glovebox, the mixture subjected to three freeze-pump-thaw cycles, and subsequently immersed in an oil bath preset at 110 °C. After stirring for 24 h the flask was cooled to room temperature and one drop of the polymer solution was taken to determine the monomer conversion of **M2** (75%) and styrene (68%) by ^1H NMR integration of the residual vinyl group signals of the monomers relative to the Me group signal of anisole. The reaction mixture was precipitated into methanol. The precipitate was collected by filtration and then redissolved in toluene.

The copolymer was recovered by repeated reprecipitation from toluene into hexanes (twice) and dried under high vacuum. Yield: 1.72 g (61%). ^{1}H NMR (500 MHz, $CDCl_3$): δ = 7.6 – 7.3 (aromatic protons of functional monomer), 7.3 – 6.2 (overlapped aromatic protons), 2.3 – 1.2 (overlapped backbone protons), 0.45 (broad s, $SiMe_3$). GPC-RI: M_n = 31500 g mol^{-1}, M_w = 97400 g mol^{-1}, $Đ$ = 3.09; $X(M2)_{n\ GPC}$ = 31, $X(St)_{n\ GPC}$ = 217. The product contains 13 mol% Si monomer based on ^{1}H NMR integration of the $SiMe_3$ signal relative to the aromatic signals (17 mol% based on the feed ratio).

Conversion to Poly((3-chloro-4'-vinyl-[1,1'-biphenyl]-4-yl)bis(pentafluoro-phenyl)borane)-co-PS (P2-BPf2). In a glovebox, **P2-Si** (500.0 mg, 0.492 mmol) was dissolved in toluene (3 mL), followed by dropwise addition of a solution of BBr_3 (0.370 g, 1.48 mmol) in toluene (0.2 mL). The mixture was allowed to stir at 80 ºC for 24 h. The formation of the dibromoborylated intermediate was confirmed by ^{1}H and ^{11}B NMR spectroscopy. ^{1}H NMR (500.0 MHz, $CDCl_3$): δ = 7.5 - 7.3 (aromatic protons of borane monomer, 3n H, relative integration: 3), 7.3 – 6.2 (overlapped aromatic protons), 2.3 – 1.2 (overlapped backbone protons, 3m+3n H, relative integration: 25.28); ^{11}B NMR (160.4 MHz, $CDCl_3$): δ = 55.1. The polymer was precipitated into dry hexanes to remove the excess of BBr_3. The precipitate was redissolved in toluene (20 mL), a solution of $Zn(C_6F_5)_2$ (0.206 g, 0.516 mmol) in toluene (5 mL) was added dropwise, and stirring was continued at room temperature for 24 h. A white precipitate formed that was removed by filtration through a small pad of celite. The solvent was evaporated under high vacuum. Purification by repeated reprecipitation from toluene into hexanes (three times) and drying under high vacuum gave the product as a light yellow solid. Yield: 0.350 g (56%). ^{1}H NMR (500 MHz,

$CDCl_3$): δ = 7.7 – 7.4 (aromatic protons of borane monomer, 3n H, relative integration: 3), 7.3 – 6.2 (overlapped aromatic protons), 2.3 – 1.2 (overlapped backbone protons, 3m+3n H, relative integration: 25.22). ^{19}F NMR (470.3 MHz, $CDCl_3$): δ = -128.0 (4n F, Pf), -146.2 (2n F, Pf), -160.6 (4n F, Pf). ^{11}B NMR (160.4 MHz, $CDCl_3$): δ = 62.9.

Synthesis of (4'-(*tert*-Butyl)-3,5-dimethyl-[1,1'-biphenyl]-4-yl)trimethylsilane (Mod1-Si). In a 250 mL dry Schlenk flask, (4-bromo-2,6-dimethylphenyl)trimethylsilane (2.00 g, 7.77 mmol) and 4-*tert*-butylphenylboronic acid (1.66 g, 9.32 mmol, 1.2 equiv.) were dissolved in toluene (90 mL). Cs_2CO_3 was added (7.60 g, 23.3 mmol, 3 equiv.) and the mixture was degassed by purging with N_2 for 30 min. A solution of the catalyst $Pd(PPh_3)_4$ (0.45 g, 0.39 mmol, 5 mol%) in toluene (10 mL) was added and the reaction mixture was kept stirring under N_2 flow overnight at 90 °C. After aqueous workup and extraction with DCM the solvent was removed under vacuum to give a brownish oil. The crude product was recrystallized from hexanes by slow evaporation of the solvent at room temperature. Yield: 1.05 g (44%). ^{1}H NMR (500.2 MHz, $CDCl_3$): δ = 7.52 (d, J = 8.5 Hz, 2H, Ph), 7.44 (d, J = 8.5 Hz, 2H, Ph), 7.20 (s, 2H, Ph), 2.52 (s, 6H, Me), 1.36 (s, 9H, *t*-Bu), 0.43 (s, 9H, $SiMe_3$). ^{13}C NMR (125.8 MHz, $CDCl_3$): δ = 150.4, 144.8, 141.4, 138.1, 135.4, 126.9, 126.9, 125.7, 34.7, 31.5, 25.2, 3.7. GC-MS (retention time 20.1 min) calcd. for $C_{21}H_{30}Si$ (m/z) 310.2, found 310.3. Elemental analysis: Calcd for $C_{21}H_{30}Si$: C 81.22; H 9.74%. Found: C 81.07; H 9.65%.

Synthesis of (4'-*tert*-Butyl-3,5-dimethyl-[1,1'-biphenyl]-4-yl)bis(pentafluorophenyl)borane (Mod1-BPf2). In a glovebox, to a toluene (0.5 mL) solution of **Mod1-Si** (50.0 mg, 0.161 mmol) in a reaction tube was added the solution of

BBr_3 (44.4 mg, 0.177 mmol, 1.1 equiv.) in 0.2 toluene dropwise. The mixture was allowed to stir at room temperature overnight. The formation of the dibromoborylated intermediate was confirmed by ^1H and ^{11}B NMR spectroscopy of the crude mixture: ^1H NMR (500.0 MHz, $CDCl_3$): δ = 7.51 (d, J = 8.5 Hz, 2H, Ph), 7.46 (d, overlapped with residual toluene), 2.41 (s, 6H, Me), 1.37 (s, 9H, *t*-Bu) , 0.60 (Me_3SiBr); ^{11}B NMR (160.4 MHz, $CDCl_3$): δ = 63.0. Then a solution of $Zn(C_6F_5)_2$ (67.5 mg, 0.169 mmol) in 0.5 mL of toluene was added dropwise at room temperature. The mixture was kept stirring at 80 °C for 48 h. A solid precipitate formed that was removed by filtration through a small pad of celite. The solvent was removed under vacuum. Purification by recrystallization from hexanes gave the product as a yellow fluorescent solid. Yield: 54.4 mg (58%). ^1H NMR (500.0 MHz, $CDCl_3$): δ = 7.55 (d, J = 8.5 Hz, 2H, Ph), 7.45 (d, J = 8.5 Hz, 2H, Ph), 7.22 (s, 2H, Ph), 2.17 (s, 6H, Me), 1.36 (s, 9H, *t*-Bu). ^{19}F NMR (470.3 MHz, $CDCl_3$): δ = -128.2 (m, 4F, Pf), -145.1 (tt, J = 20.0, 5.9 Hz, 2F, Pf), -160.5 (m, 4F, Pf). ^{11}B NMR (160.4 MHz, $CDCl_3$): δ = 69.6. ^{13}C NMR (150.8 MHz, $CDCl_3$): δ = 150.8, 148.0 (d, J = 241 Hz), 144.5 (d, J = 271 Hz), 142.9, 140.9 (br, B-C), 138.2, 137.8, 137.6 (d, J = 256 Hz), 126.8, 125.9, 125.8, 114.9 (br, B-C), 34.7, 31.5, 22.7. High-resolution MALDI-TOF mass spectrum (anthracene, neg. mode): m/z = 601.1569 ($[M]^-$: 100 %, calcd for $C_{30}H_{21}BF_{11}^-$ 601.1560). Elemental analysis: Calcd for $C_{30}H_{21}BF_{10}$: C 61.88; H 3.64; for $C_{30}H_{21}BF_{10}$ * 0.3 toluene (C_7H_8): C 63.21; H 3.87%. Found: C 63.23; H 4.06%.

Synthesis of (4'-*tert*-Butyl-3-chloro-[1,1'-biphenyl]-4-yl)trimethylsilane (Mod2-Si). In an oven-dried 250 mL Schlenk flask, (4-bromo-2,6-dimethylphenyl)trimethylsilane (1.60 g, 6.07 mmol) and 4-*tert*-butylphenylboronic acid (1.30 g, 7.30 mmol, 1.2 equiv.) were

dissolved in toluene (90 mL). Then Cs_2CO_3 was added (5.93 g, 18.2 mmol, 3 equiv.). The mixture was degassed by purging with N_2 for 30 min. A solution of the catalyst $Pd(PPh_3)_4$ (0.35 g, 0.30 mmol, 5 mol%) in 10 mL toluene was added and the reaction mixture was kept stirring under N_2 flow overnight at 90 °C. After aqueous workup and extraction with DCM the solvent was removed under vacuum to give a brownish oil. The crude product was recrystallized from hexanes by slow evaporation of the solvent at room temperature. Yield: 1.06 g (55%). ^{1}H NMR (500.2 MHz, $CDCl_3$): δ = 7.56 (d, J = 1.5 Hz, 1H, Ph), 7.52 (d, J = 8.5 Hz, 2H, Ph), 7.49 (s, 1H, Ph), 7.47 (d, J = 8.5 Hz, 2H, Ph), 7.45 (dd, J = 7.8, 1.5 Hz, 1H, Ph), 1.36 (s, 9H, *t*-Bu), 0.40 (s, 9H, $SiMe_3$). ^{13}C NMR (125.8 MHz, $CDCl_3$): δ = 151.2, 143.7, 141.6, 136.9, 136.1, 127.7, 126.9, 126.0, 124.6, 34.7, 31.5, -0.6. GC-MS (retention time 19.4 min) calcd. for $C_{19}H_{25}ClSi$ (m/z) 316.1, found 316.2. Elemental analysis: Calcd for $C_{19}H_{25}ClSi$: C 72.00; H 7.95%. Found: C 71.99; H 7.73%.

Synthesis of (4'-*tert*-Butyl-3-chloro-[1,1'-biphenyl]-4-yl)bis(pentafluorophenyl)borane (Mod2-BPf2). In a glovebox, to a solution of **Mod2-Si** (50.0 mg, 0.158 mmol) in toluene (0.5 mL) was added dropwise a solution of BBr_3 (0.118 g, 0.471 mmol, 3.0 equiv.) in toluene (0.2 mL). The mixture was allowed to stir at 80 °C for 24 h. After removal of all volatile components in high vacuum, including the excess of BBr_3, the product was obtained as a brown oil. The formation of the dibromoborylated intermediate was confirmed by ^{1}H and ^{11}B NMR spectroscopy of the crude mixture: ^{1}H NMR (500.0 MHz, $CDCl_3$): δ = 7.90 (d, J = 8.0 Hz, 1H, Ph), 7.68 (s, 1H, Ph), 7.59 (d, J = 8.0 Hz, 2H, Ph), 7.58 (d, overlapped, 1H, Ph), 7.54 (d, J = 8.0, 2H, Ph), 1.41 (s, 9H, *t*-Bu). ^{11}B NMR (160.4 MHz, $CDCl_3$): δ = 57.4. The product was redissolved in toluene (0.3 mL)

and a solution of $Zn(C_6F_5)_2$ (66.2 mg, 0.166 mmol) in toluene (0.2 mL) was added dropwise with stirring. The mixture was kept stirring at room temperature for 24 h. A white precipitate formed that was removed by filtration through a small pad of celite. The solvent was removed under high vacuum. Extraction with toluene and subsequent recrystallization from hexanes gave the product as a white solid. Yield: 41.8 mg (45%). ^{1}H NMR (500.0 MHz, $CDCl_3$): δ = 7.69 (s, 1H, Ph), 7.58 (d, J = 8.0 Hz, 2H, Ph), 7.55 (d, J = 8.0, 1H, Ph), 7.51 (d, J = 8.5, 2H, Ph), 7.43 (d, J = 8.0, 1H, Ph), 1.37 (s, 9H, *t*-Bu). δ = -128.0 (m, 4F, Pf), -146.3 (tt, J = 20.2, 5.3 Hz, 2F, Pf), -160.7 (m, 4F, Pf). ^{11}B NMR (160.4 MHz, $CDCl_3$): δ = 63.3. ^{13}C NMR (150.8 MHz, $CDCl_3$): δ = 152.6, 148.0, 147.6 (d, J = 249 Hz), 144.1 (d, J = 260 Hz), 141.1, 138.0, 137.6 (d, J = 254 Hz), 135.7, 128.5, 127.1, 126.3, 125.0, 114.7, 34.9, 31.4. High-resolution MALDI-TOF mass spectrum (anthracene, neg. mode): m/z = 607.0873 ($[M]^-$, 100 %, calcd for $C_{28}H_{16}BClF_{11}^-$ 607.0857). Elemental analysis: Calcd for $C_{28}H_{16}BClF_{10}$: C 57.13; H 2.74. Found: C 56.26; H 2.99.

2.5 References

1.L. Ji, S. Griesbeck and T. B. Marder, *Chem. Sci.* **2017**, *8*, 846-863.

2.a) S. K. Mellerup and S. Wang, *Trends in Chemistry* **2019**, *1*, 77-89; b) J. Huo, H. Wang, S. Li, H. Shi, Y. Tang and B. Z. Tang, *Chem. Rec.* **2019**, *19*, DOI: 10.1002/tcr.201900068.

3.a) D. W. Stephan, *Accounts of Chemical Research* **2015**, *48*, 306-316; b) D. W. Stephan, *Science* **2016**, *354*, aaf7229; c) A. R. Jupp and D. W. Stephan, *Trends in Chemistry* **2019**, *1*, 35-48.

4.D. W. Stephan and G. Erker, *Angew Chem Int Ed Engl* **2010**, *49*, 46-76.

5.T. Mahdi and D. W. Stephan, *Angewandte Chemie International Edition* **2013**, *52*, 12418-12421.

6.M.-A. Courtemanche, M.-A. Légaré, L. Maron and F.-G. Fontaine, *Journal of the American Chemical Society* **2013**, *135*, 9326-9329.

7.a) D. J. Parks and W. E. Piers, *J. Am. Chem. Soc.* **1996**, *118*, 9440-9441; b) M. Rubin, T. Schwier and V. Gevorgyan, *The Journal of Organic Chemistry* **2002**, *67*, 1936-1940; c) S. Rendler and M. Oestreich, *Angewandte Chemie-International Edition* **2008**, *47*, 5997-6000; d) W. E. Piers, A. J. V. Marwitz and L. G. Mercier, *Inorg. Chem.* **2011**, *50*, 12252-12262; e) A. Y. Houghton, J. Hurmalainen, A. Mansikkamaki, W. E. Piers and H. M. Tuononen, *Nature Chemistry* **2014**, *6*, 983-988; f) S. Keess, A. Simonneau and M. Oestreich, *Organometallics* **2015**, *34*, 790-799; g) W. Yuan, P. Orecchia and M. Oestreich, *Chemical Communications* **2017**, *53*, 10390-10393.

8.a) S. Itsuno in *Polymer-Supported Metal Lewis Acids*, *Vol. 2* (Ed. H. Yamamoto), Wiley VCH, Weinheim, New York, Chichester, Brisbane, Singapore, Toronto, **2000**, pp. 945-979; b) F. Jäkle, *Coord. Chem. Rev.* **2006**, *250*, 1107-1121; c) F. Vidal and F. Jakle, *Angewandte Chemie-International Edition* **2019**, *58*, 5846-5870; d) F. Jäkle in *Borylated Polystyrenes as Versatile Functional Materials*, (Ed. Y. Chujo), Springer Singapore, Singapore, **2019**, pp. 59-76.

9.a) N. Matsumi and Y. Chujo, *Polym. J.* **2008**, *40*, 77-89; b) F. Jäkle, *Chem. Rev.* **2010**, *110*, 3985-4022; c) A. Nagai and Y. Chujo, *Chem. Lett.* **2010**, *39*, 430-435; d) K. Tanaka and Y. Chujo, *Macromol. Rapid Comm.* **2012**, *33*, 1235-1255.

10.A. M. Polgar, J. Poisson, N. R. Paisley, C. J. Christopherson, A. C. Reyes and Z. M. Hudson, *Macromolecules* **2020**, *53*, 2039-2050.

11.a) Y. Qin, G. Cheng, A. Sundararaman and F. Jäkle, *Journal of the American Chemical Society* **2002**, *124*, 12672-12673; b) Y. Qin, G. Cheng, O. Achara, K. Parab and F. Jäkle, *Macromolecules* **2004**, *37*, 7123-7131.

12.a) K. Parab, K. Venkatasubbaiah and F. Jäkle, *J. Am. Chem. Soc.* **2006**, *128*, 12879-12885; b) K. Parab, A. Doshi, F. Cheng and F. Jäkle, *Macromolecules* **2011**, *44*, 5961-5967.

13.F. Cheng, E. M. Bonder and F. Jäkle, *Journal of the American Chemical Society* **2013**, *135*, 17286-17289.

14.M. Wang, F. Nudelman, R. R. Matthes and M. P. Shaver, *Journal of the American Chemical Society* **2017**, *139*, 14232-14236.

15.a) F. Vidal, H. Lin, C. Morales and F. Jäkle, *Molecules* **2018**, *23*, 405; b) F. Vidal, J. Gomezcoello, R. A. Lalancette and F. Jakle, *Journal of the American Chemical Society* **2019**, *141*, 15963-15971.

16.a) s. systems in *2020semiimmobilized systems*, *Vol.* **2020**; b) M. Trunk, J. F. Teichert and A. Thomas, *Journal of the American Chemical Society* **2017**, *139*, 3615-3618; c) A. Willms, H. Schumacher, T. Tabassum, L. Qi, S. L. Scott, P. J. C. Hausoul and M. Rose, *Chemcatchem* **2018**, *10*, 1835-1843; d) Y. Y. Ma, S. Zhang, C. R. Chang, Z. Q. Huang, J. C. Ho and Y. Q. Qu, *Chemical Society Reviews* **2018**, *47*, 5541-5553.

17.L. Chen, R. Liu and Q. Yan, *Angewandte Chemie International Edition* **2018**, *57*, 9336-9340.

18.a) G. Eros, H. Mehdi, I. Papai, T. A. Rokob, P. Kiraly, G. Tarkanyi and T. Soos, *Angew. Chem., Int. Ed.* **2010**, *49*, 6559-6563; b) Á. Gyömöre, M. Bakos, T. Földes, I. Pápai, A. Domján and T. Soós, *ACS Catalysis* **2015**, *5*, 5366-5372; c) É. Dorkó, M. Szabó, B. Kótai, I. Pápai, A. Domján and T. Soós, *Angewandte Chemie International Edition* **2017**, *56*, 9512-9516.

19.) R. J. Blagg, E. J. Lawrence, K. Resner, V. S. Oganesyan, T. J. Herrington, A. E. Ashley and G. G. Wildgoose, *Dalton Transactions* **2016**, *45*, 6023-6031; b) R. J. Blagg, T. R. Simmons, G. R. Hatton, J. M. Courtney, E. L. Bennett, E. J. Lawrence and G. G. Wildgoose, *Dalton Transactions* **2016**, *45*, 6032-6043.

20.D. J. Scott, M. J. Fuchter and A. E. Ashley, *Chemical Society Reviews* **2017**, *46*, 5689-5700.

21.a) D. E. Bergbreiter, J. H. Tian and C. Hongfa, *Chemical Reviews* **2009**, *109*, 530-582; b) J. Lu and P. H. Toy, *Chemical Reviews* **2009**, *109*, 815-838; c) D. E. Bergbreiter, *Acs Macro Letters* **2014**, *3*, 260-265.

22.a) J. R. Gaffen, J. N. Bentley, L. C. Torres, C. Chu, T. Baumgartner and C. B. Caputo, *Chem* **2019**, *5*, 1567-1583; b) B. L. Thompson, C. R. Simons and Z. M. Heiden, *Chemical Communications* **2019**, *55*, 11430-11433.

23.N. Iwama, T. Tayano and H. Ohtaki in Catalyst component for olefin polymerization, catalyst for α-olefin polymerization and process for the production of α-olefin polymer, Vol. Japan Polypropylene Corporation, Japan . **2005**, p. 23 pp.

24.M. A. Beckett, G. C. Strickland, J. R. Holland and K. Sukumar Varma, *Polymer* **1996**, *37*, 4629-4631.

25.T. Noda and Y. Shirota, *Journal of the American Chemical Society* **1998**, *120*, 9714-9715.

26.a) T. Hatakeyama, K. Shiren, K. Nakajima, S. Nomura, S. Nakatsuka, K. Kinoshita, J. Ni, Y. Ono and T. Ikuta, *Advanced Materials* **2016**, *28*, 2777-2781; b) T. Agou, K. Matsuo, R. Kawano, I. S. Park, T. Hosoya, H. Fukumoto, T. Kubota, Y. Mizuhata, N. Tokitoh and T. Yasuda, *ACS Materials Letters* **2020**, *2*, 28-34; c) M.-Y. Zhang, Z.-Y. Li, B. Lu, Y.

Wang, Y.-D. Ma and C.-H. Zhao, *Organic Letters* **2018**, *20*, 6868-6871; d) S. Pagidi, N. K. Kalluvettukuzhy and P. Thilagar, *Inorganic Chemistry* **2020**, *59*, 3142-3151.

27.a) G.-L. Fu, H.-Y. Zhang, Y.-Q. Yan and C.-H. Zhao, *The Journal of Organic Chemistry* **2012**, *77*, 1983-1990; b) Z. Zhang, R. M. Edkins, J. Nitsch, K. Fucke, A. Steffen, L. E. Longobardi, D. W. Stephan, C. Lambert and T. B. Marder, *Chemical Science* **2015**, *6*, 308-321; c) Z.-B. Sun, J.-K. Liu, D.-F. Yuan, Z.-H. Zhao, X.-Z. Zhu, D.-H. Liu, Q. Peng and C.-H. Zhao, *Angewandte Chemie International Edition* **2019**, *58*, 4840-4846; d) C. Wang, Q.-W. Xu, W.-N. Zhang, Q. Peng and C.-H. Zhao, *J. Org. Chem.* **2015**, *80*, 10914-10924.

28.a) H. Uoyama, K. Goushi, K. Shizu, H. Nomura and C. Adachi, *Nature* **2012**, *492*, 234–238; b) X.-K. Chen, D. Kim and J.-L. Brédas, *Acc. Chem. Res.* **2018**, *51*, 2215-2224.

29.H. Belaidi, F. Rauch, Z. Zhang, C. Latouche, A. Boucekkine, T. B. Marder and J.-F. Halet, *ChemPhotoChem* **2020**, *4*, 173-180.

30.a) 2020camb3lyp in *2020camb3lyp*, *Vol.* **2020**; b) N. S. Makarov, S. Mukhopadhyay, K. Yesudas, J.-L. Brédas, J. W. Perry, A. Pron, M. Kivala and K. Müllen, *The Journal of Physical Chemistry A* **2012**, *116*, 3781-3793.

2.6 Appendix

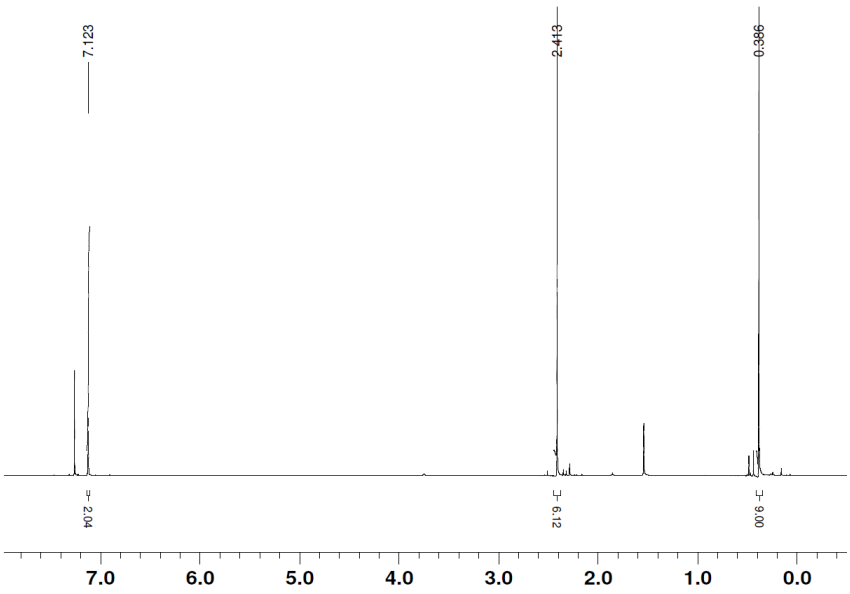

Figure 2-S1. ^{1}H NMR spectrum of (4-bromo-2,6-dimethylphenyl)trimethylsilane (1) in $CDCl_3$.

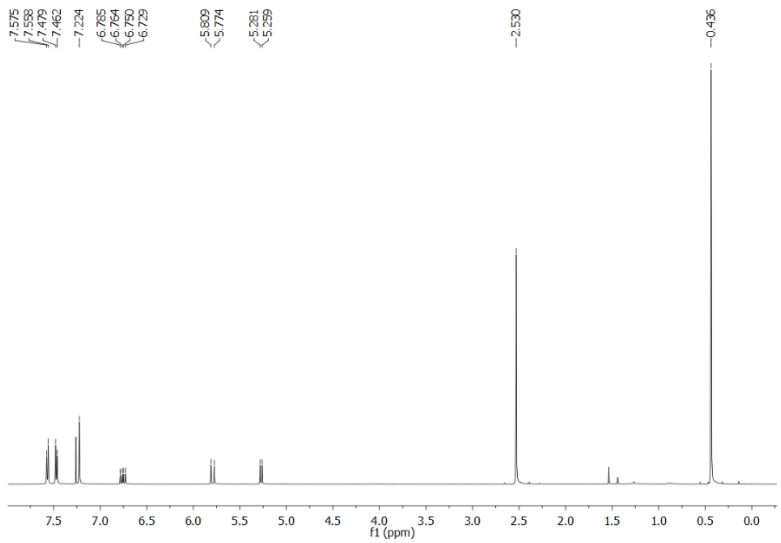

Figure 2-S2. ^{1}H NMR spectrum of monomer **M1** in $CDCl_3$.

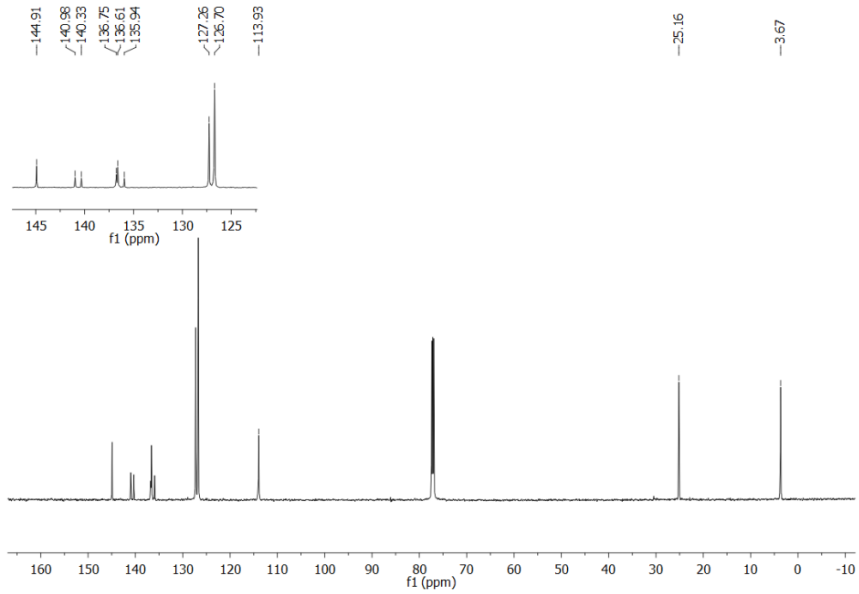

Figure 2-S3. ^{13}C NMR spectrum of monomer **M1** in $CDCl_3$.

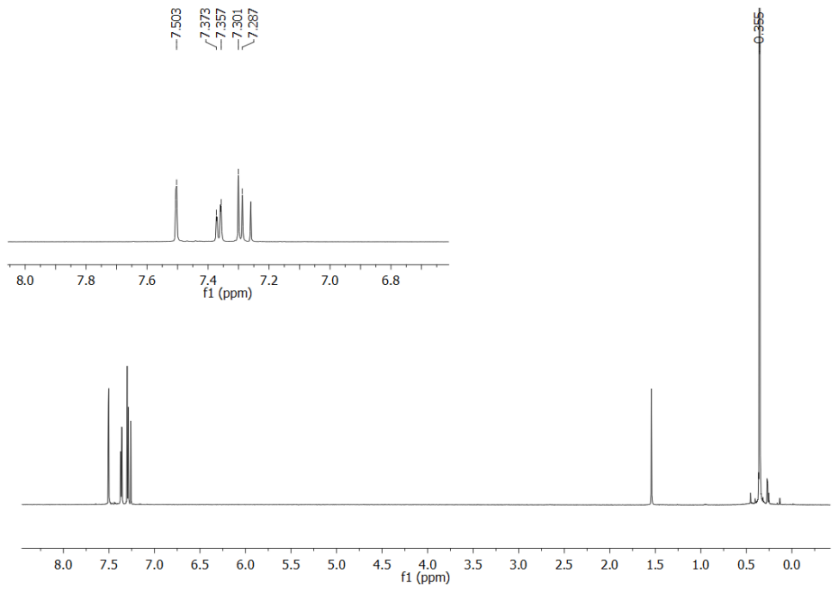

Figure 2-S4. ^{1}H NMR spectrum of (4-bromo-2-chlorophenyl)trimethylsilane (2) in $CDCl_3$.

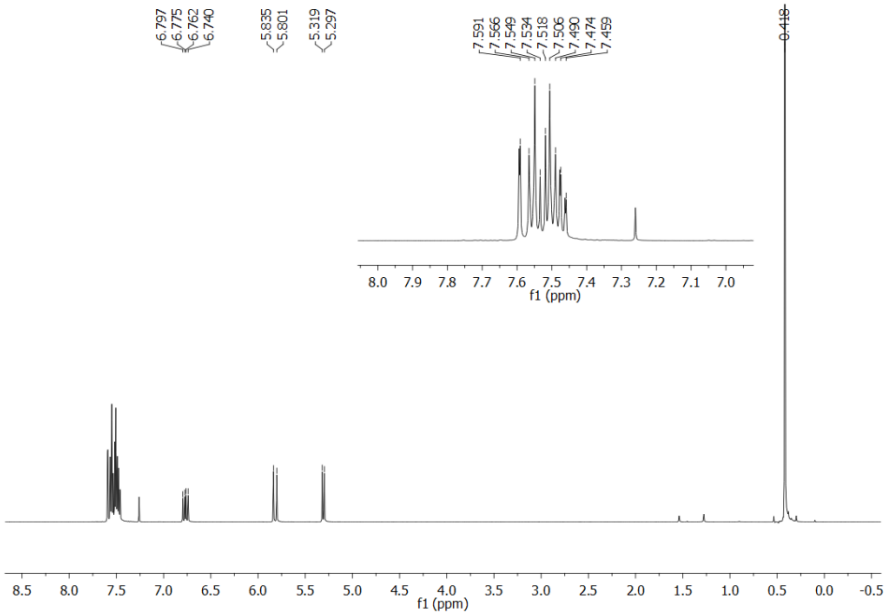

Figure 2-S5. ^{1}H NMR spectrum of monomer **M2** in $CDCl_3$.

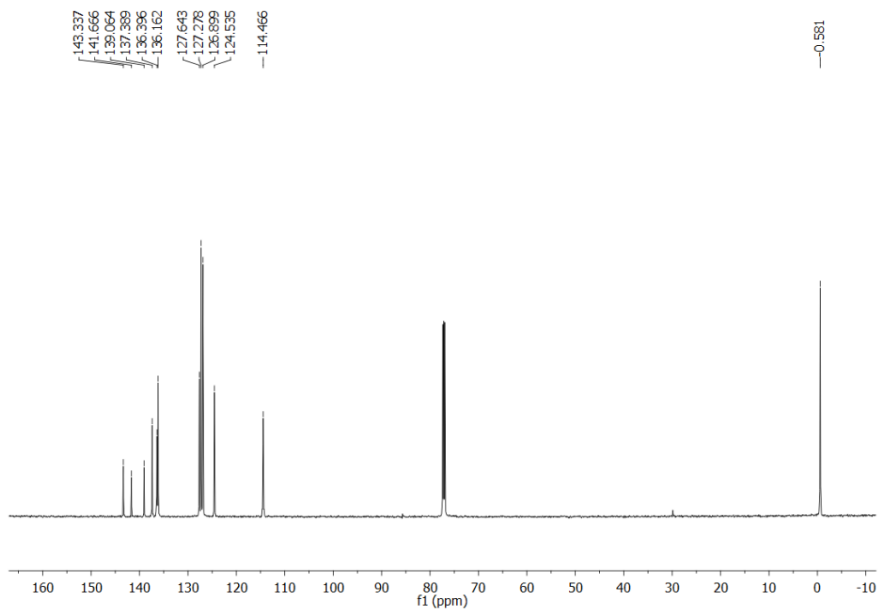

Figure 2-S6. ^{13}C NMR spectrum of monomer **M2** in $CDCl_3$.

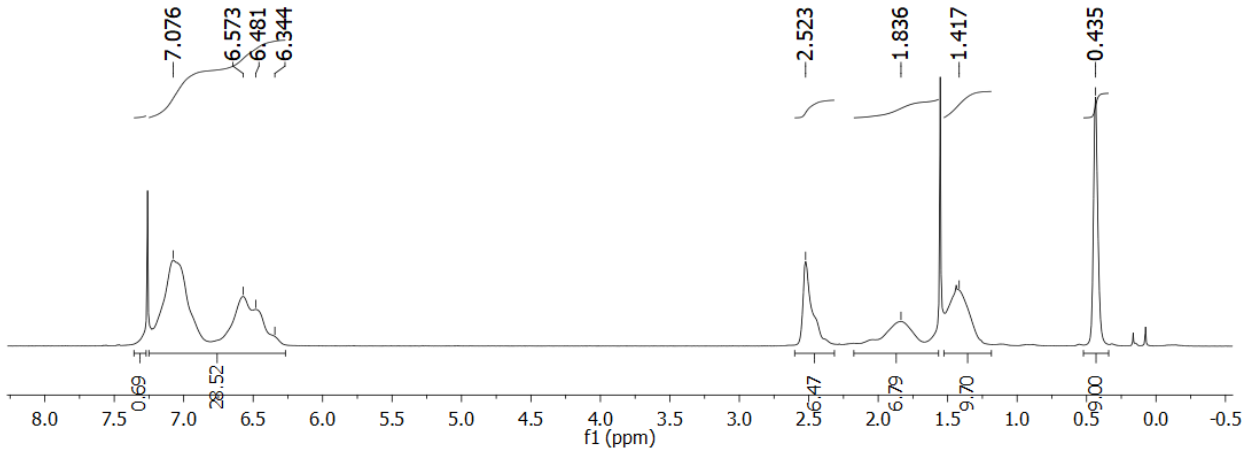

Figure 2-S7. ^{1}H NMR spectrum of **P1-Si** in $CDCl_3$.(the signal at ca. 1.5 ppm is due to a trace of water in the solvent)

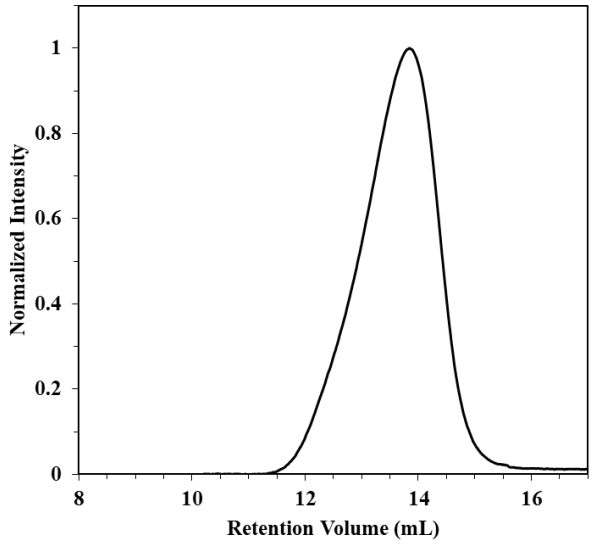

Figure 2-S8. GPC trace of **P1-Si** obtained from conventional free radical polymerization, eluent: THF, 1 mL·min^{-1}.

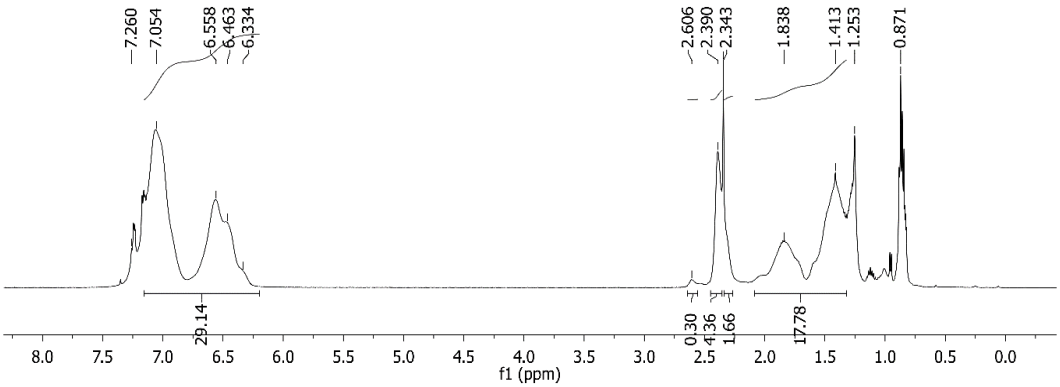

Figure 2-S9. ^{1}H NMR spectrum of **P1-BBr2** after precipitation into hexanes in $CDCl_3$ (the signals at ca. 0.87 and 1.25 ppm are attributed to residual hexanes and the sharp signal at 2.34 ppm to residual tolene). The integral ratio between aryl and methyl protons is consistent with a ratio of m/n = 5 (from integration m/n = 4.64)

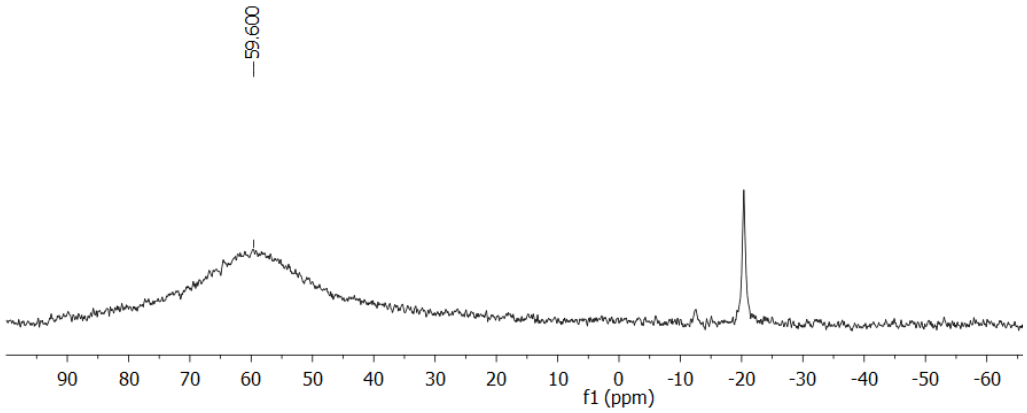

Figure 2-S10. ^{11}B NMR spectrum of **P1-BBr2** (after precipitation into hexanes) in $CDCl_3$.

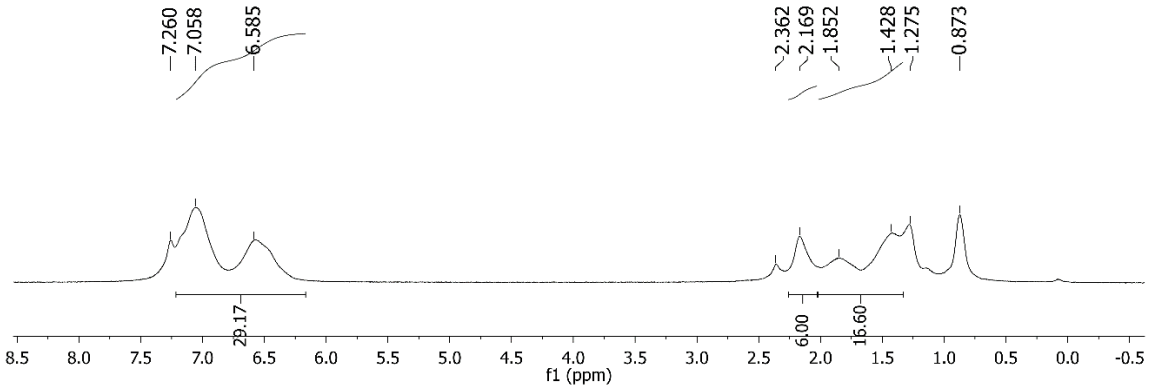

Figure 2-S11. ^{1}H NMR spectrum of **P1-BPf2** in $CDCl_3$ (the signals at 0.87 and 1.27 ppm are attributed to residual hexanes solvent and the small signal at 2.36 ppm to as residual toluene).

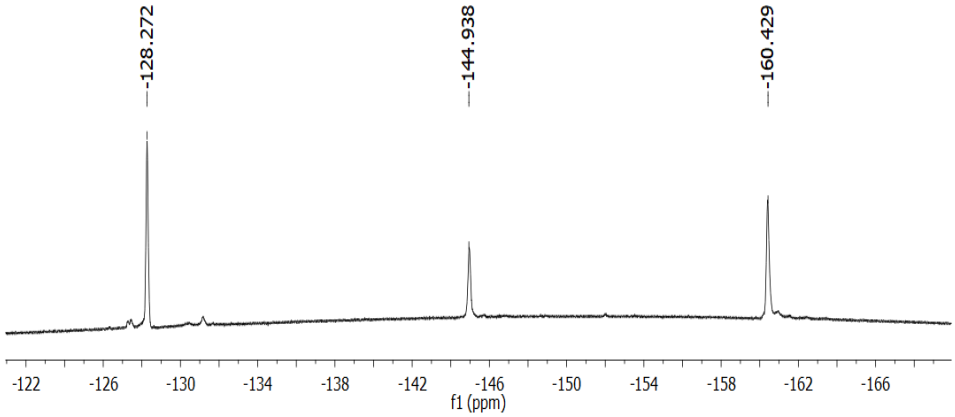

Figure 2-S12. ^{19}F NMR spectrum of **P1-BPf2** in $CDCl_3$.

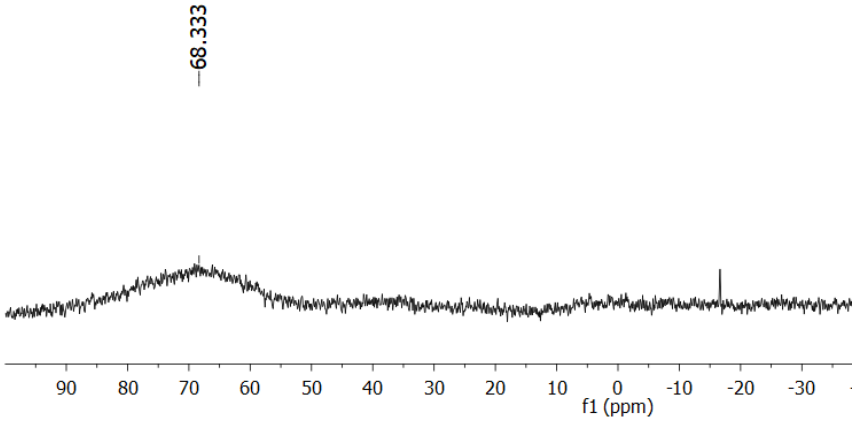

Figure 2-S13. ^{11}B NMR spectrum of **P1-BPf2** in $CDCl_3$.

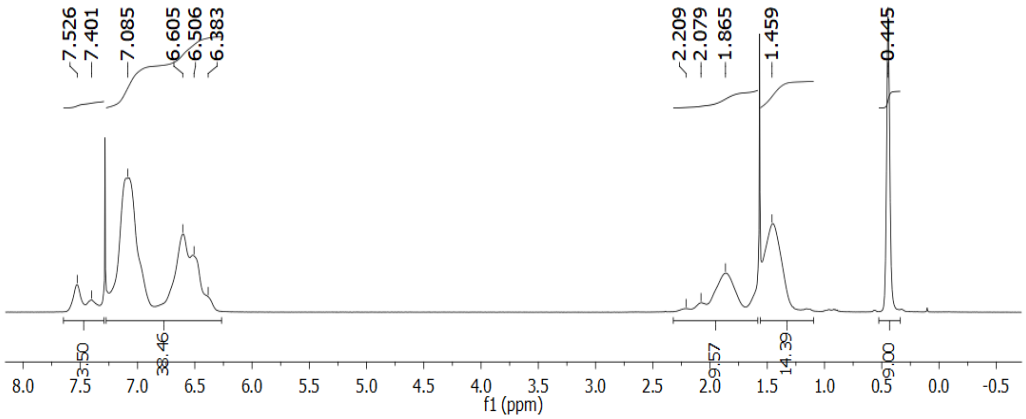

Figure 2-S14. ^{1}H NMR spectrum of **P2-Si** in $CDCl_3$.

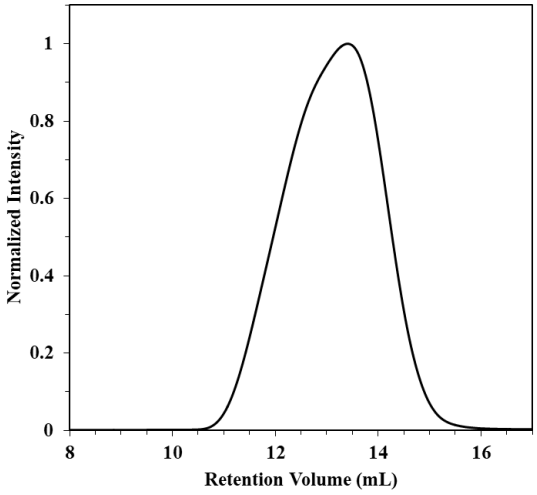

Figure 2-S15. GPC trace of **P2-Si** obtained from conventional free radical polymerization, eluent: THF, 1 mL·min^{-1}.

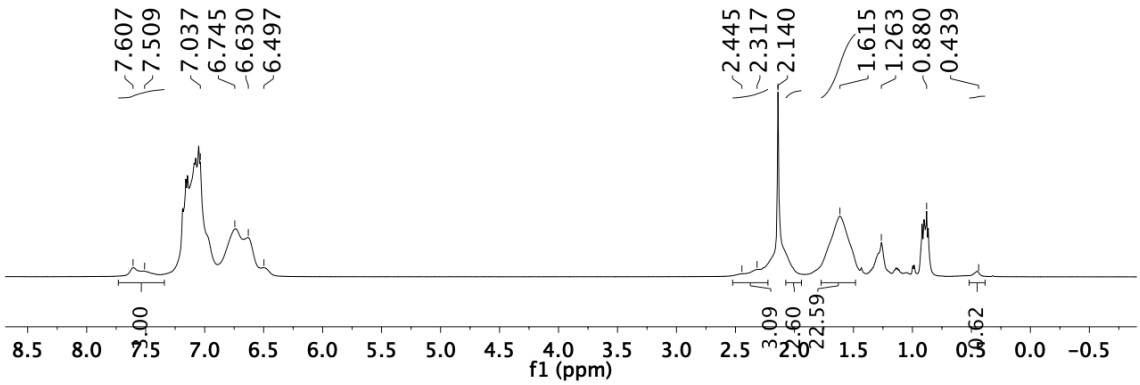

Figure 2-S16. ^{1}H NMR spectrum of **P2-BBr2** (after precipitation into hexanes) in $CDCl_3$ (the signals at 2.14 and ca. 7.2-7.3 ppm are attritubuted to residual toluene solvent, those at 0/88 and 1.26 ppm to hexanes and the signal at 0.44 ppm to a small number of residual Si-bound methyl groups). The integral ratio between protons on the boron-substituted aryl ring (3n H) and methylene backbone protons (3m+3n H) is consistent with a ratio of m/n = 5 (from integration m/n = 6.98)

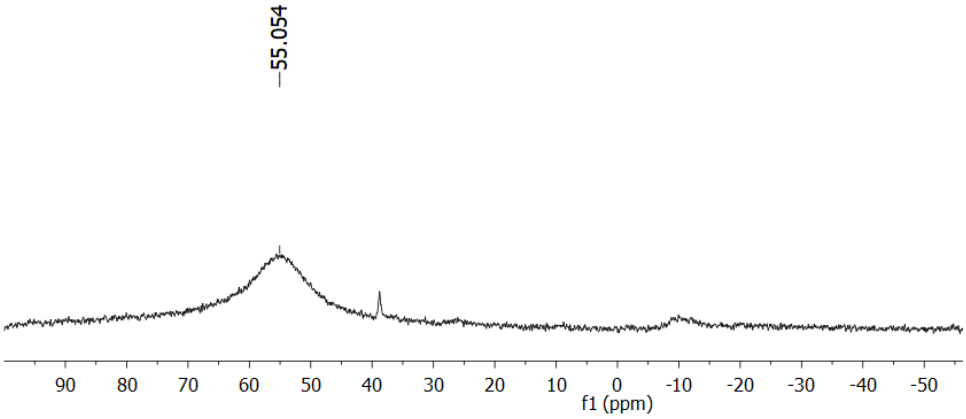

Figure 2-S17. ^{11}B NMR spectrum of **P2-BBr2** (after precipitation into hexanes) in $CDCl_3$.

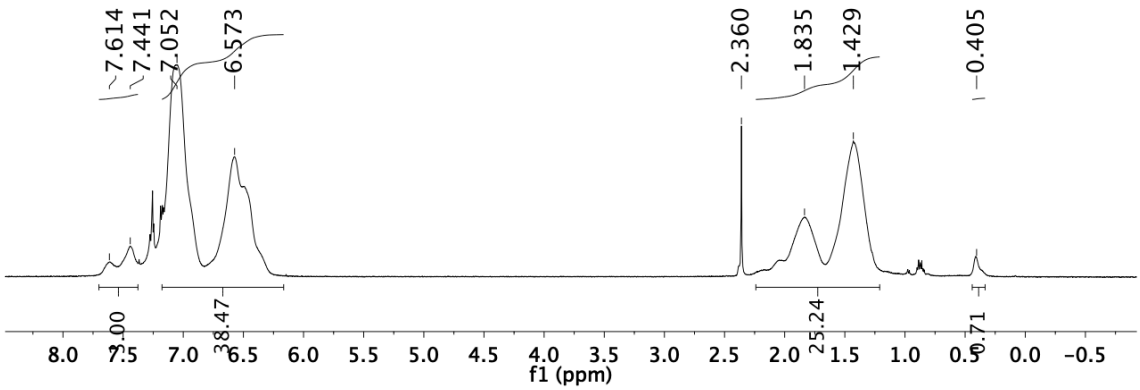

Figure 2-S18. ^{1}H NMR spectrum of **P2-BPf2** in $CDCl_3$. (the signals at 2.36 and ca. 7.2-7.3 ppm are attributed to residual toluene solvent, those at 0.8 ppm to hexanes and that at 0.40 ppm to 7% of residual Si-bound methyl groups). The integral ratio between protons on the boron-substituted aryl ring (3n H) and methylene/methine backbone protons (3n + 3m H) is consistent with a ratio of m/n = 5 (from integration m/n = 6.98)

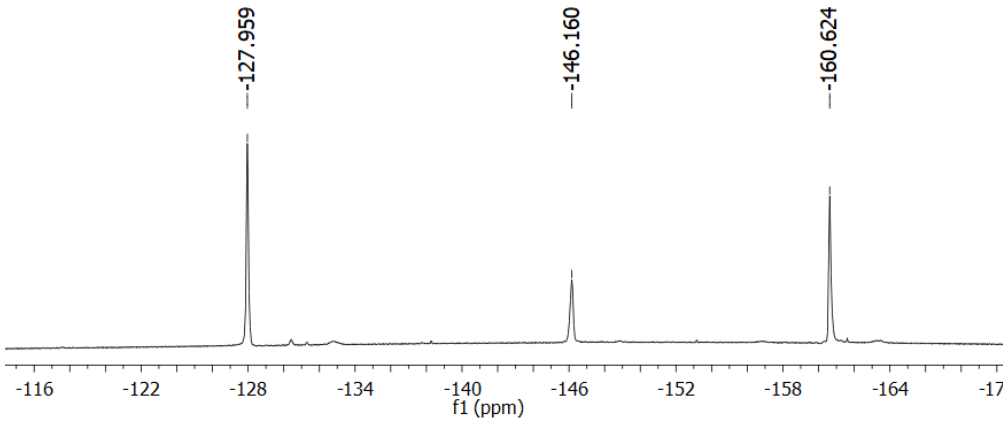

Figure 2-S19. ^{19}F NMR spectrum of **P2-BPf2** in $CDCl_3$.

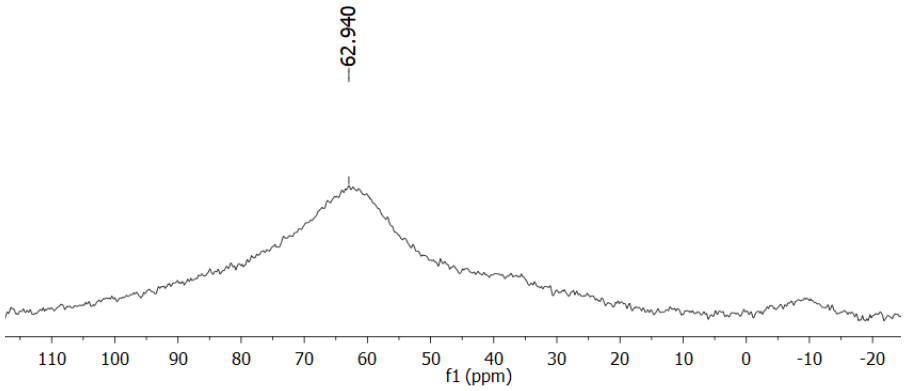

Figure 2-S20. ^{11}B NMR spectrum of **P2-BPf2** in $CDCl_3$.

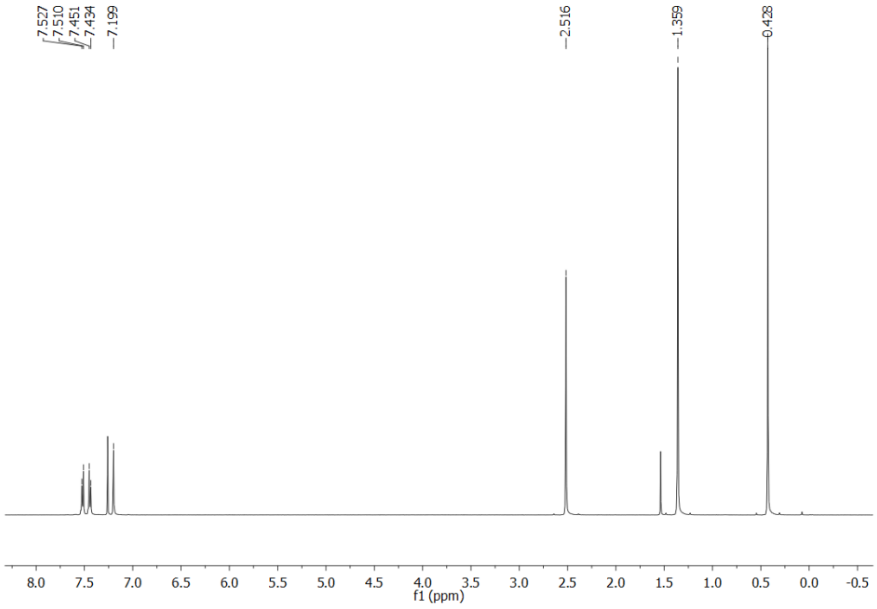

Figure 2-S21. ^{1}H NMR spectrum of **Mod1-Si** in $CDCl_3$.

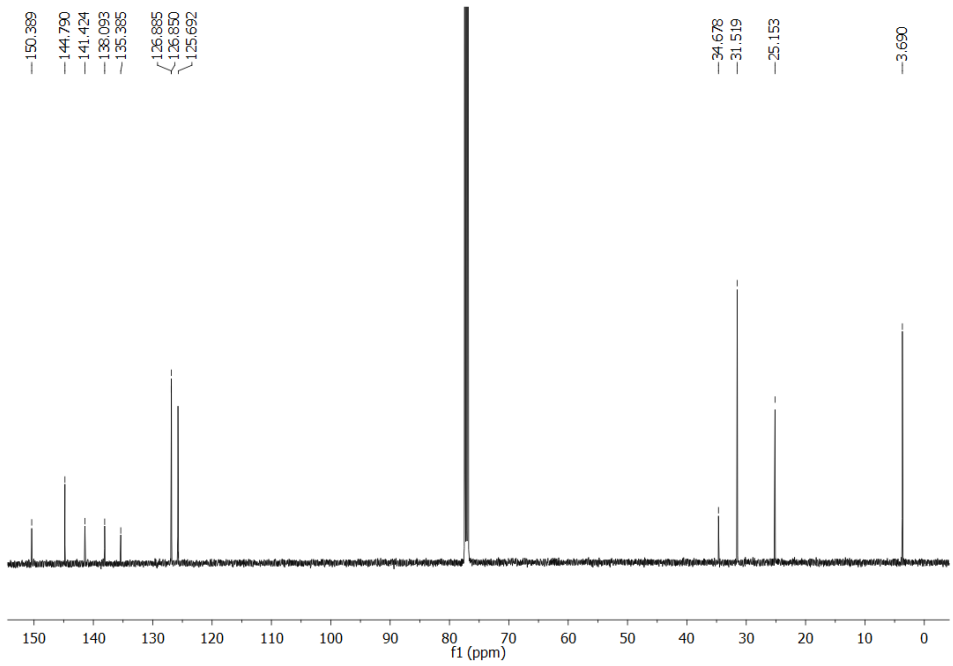

Figure 2-S22. ^{13}C NMR spectrum of **Mod1-Si** in $CDCl_3$.

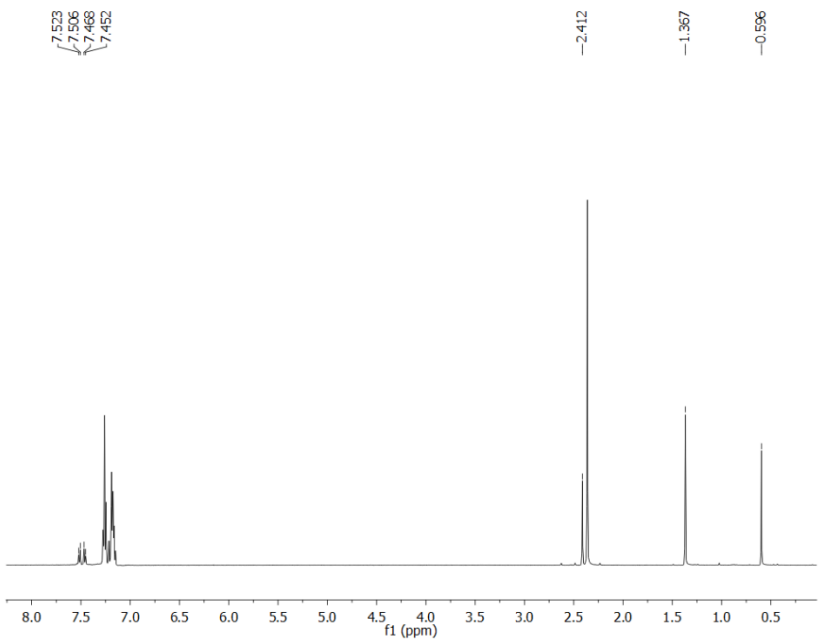

Figure 2-S23. ^{1}H NMR spectrum of the reaction solution of **Mod1-BBr2** in $CDCl_3$. (the signal at 0.60 ppm is attributed to Me_3SiBr that is generated as by-product, the signals at 2.43 and in part those at 7.1-7.3 ppm are attributed to toluene).

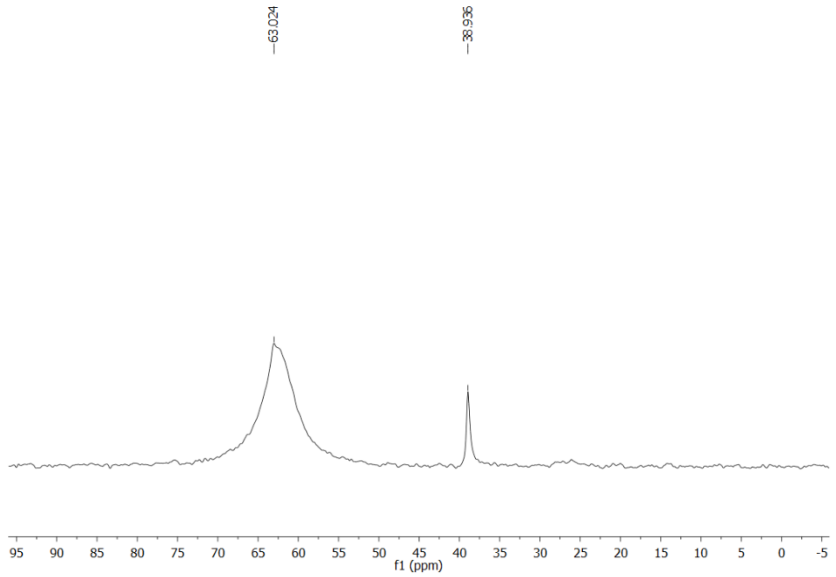

Figure 2-S24. ^{11}B NMR spectrum of the reaction solution of **Mod1-BBr2** in $CDCl_3$ (signal at 38.9 ppm due to excess BBr_3).

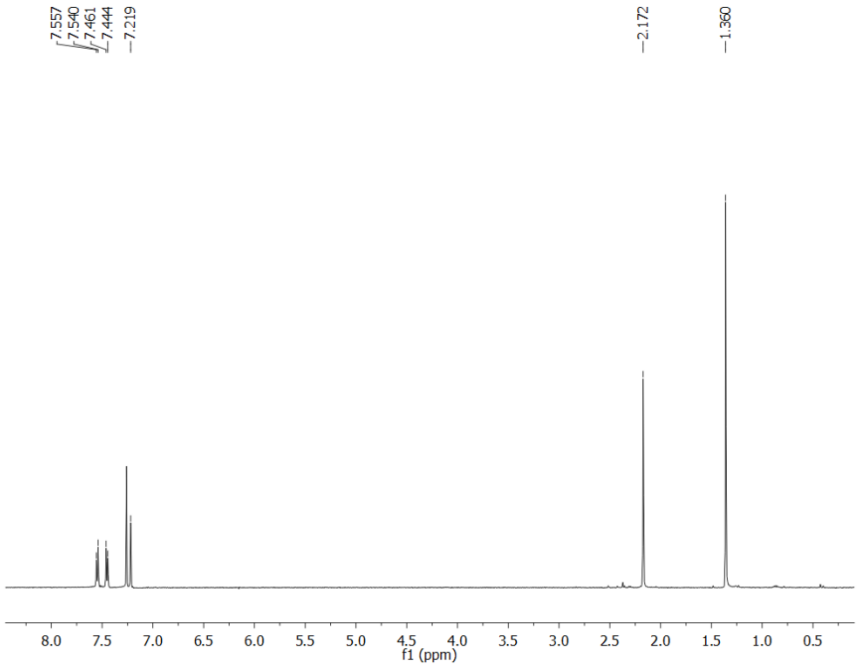

Figure 2-S25. ^{1}H NMR spectrum of **Mod1-BPf2** in $CDCl_3$.

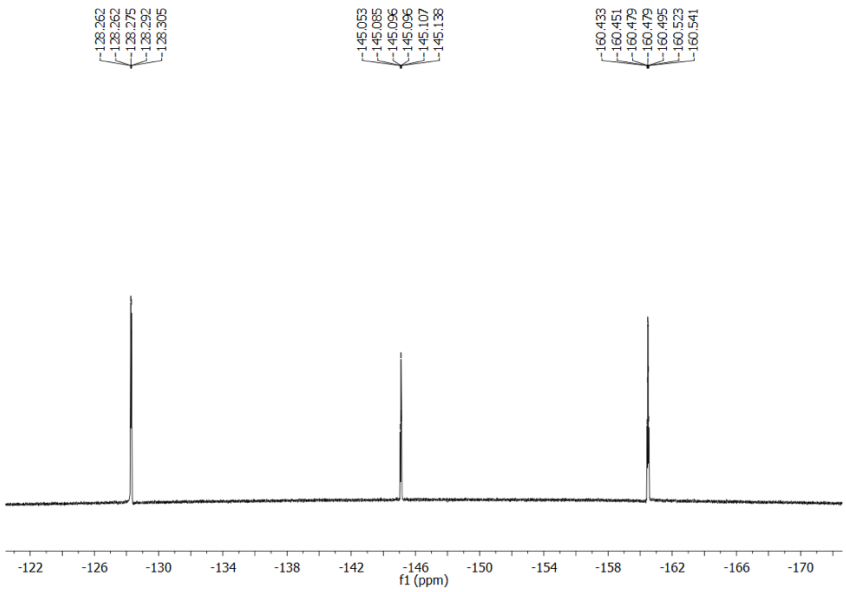

Figure 2-S26. ^{19}F NMR spectrum of **Mod1-BPf2** in $CDCl_3$.

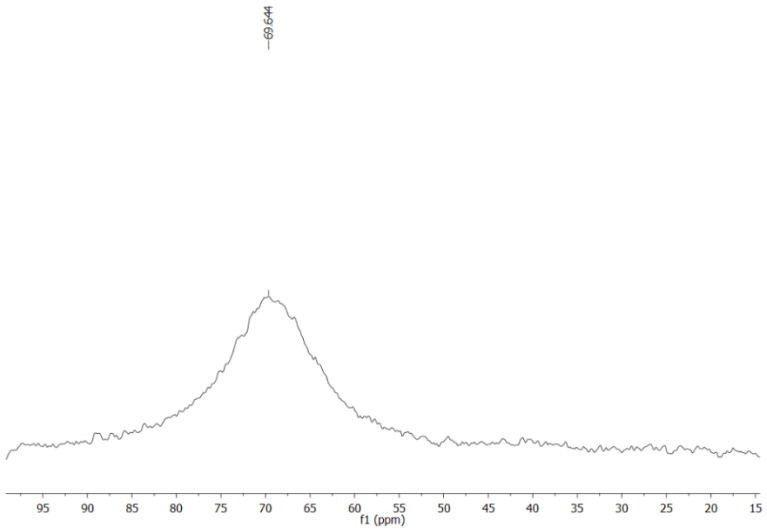

Figure 2-S27. ^{11}B NMR spectrum of **Mod1-BPf2** in $CDCl_3$.

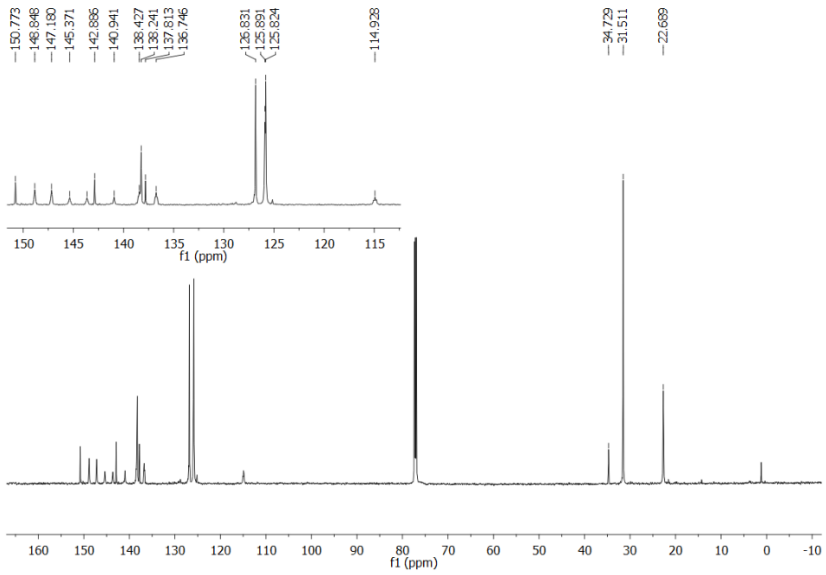

Figure 2-S28. ^{13}C NMR spectrum of **Mod1-BPf2** in $CDCl_3$.

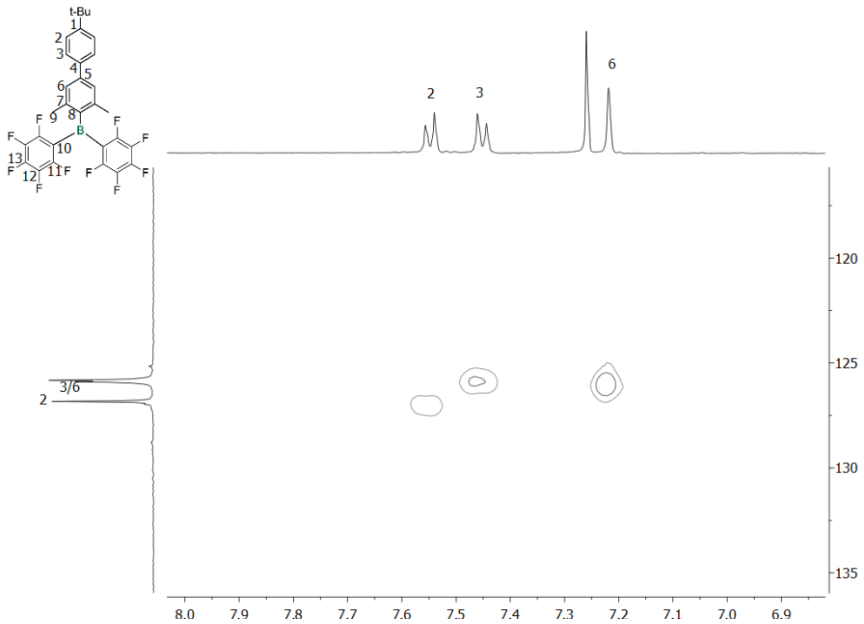

Figure 2-S29. ^{1}H, ^{13}C-HSQC NMR spectrum of **Mod1-BPf2** in $CDCl_3$.

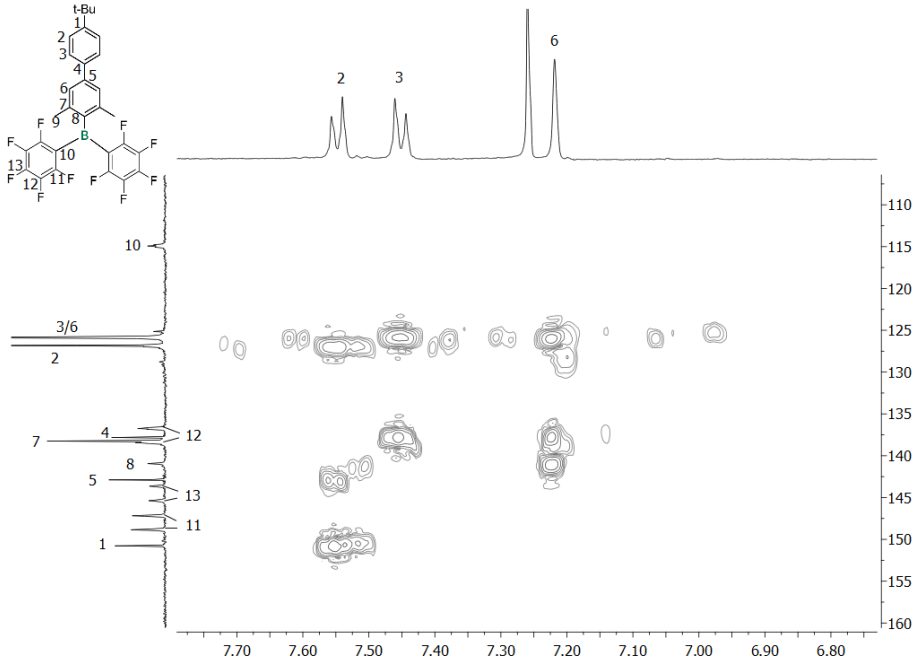

Figure 2-S30. ^{1}H, ^{13}C-HMBC NMR spectrum of **Mod1-BPf2** in $CDCl_3$.

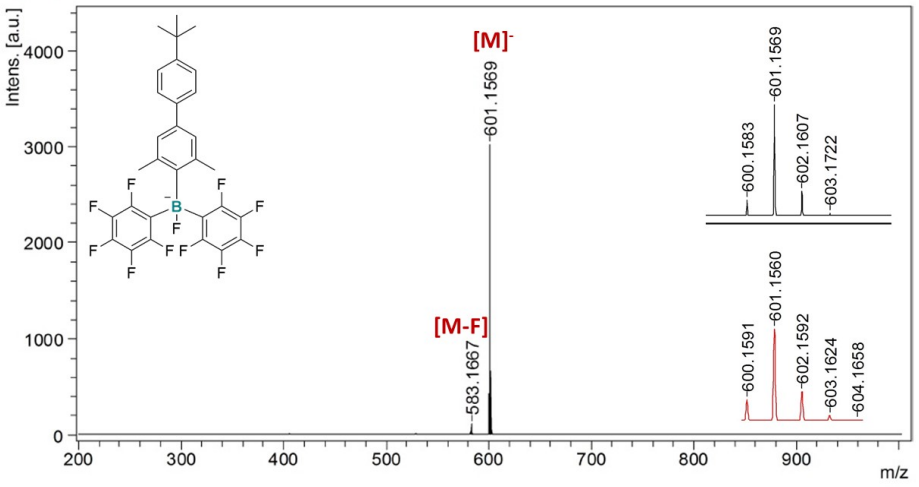

Figure 2-S31. MALDI-TOF MS data of [**Mod1-BPf2**]**F**$^{-}$ generated by addition of TBAF to **Mod1-BPf2** (anthracene, neg. mode).

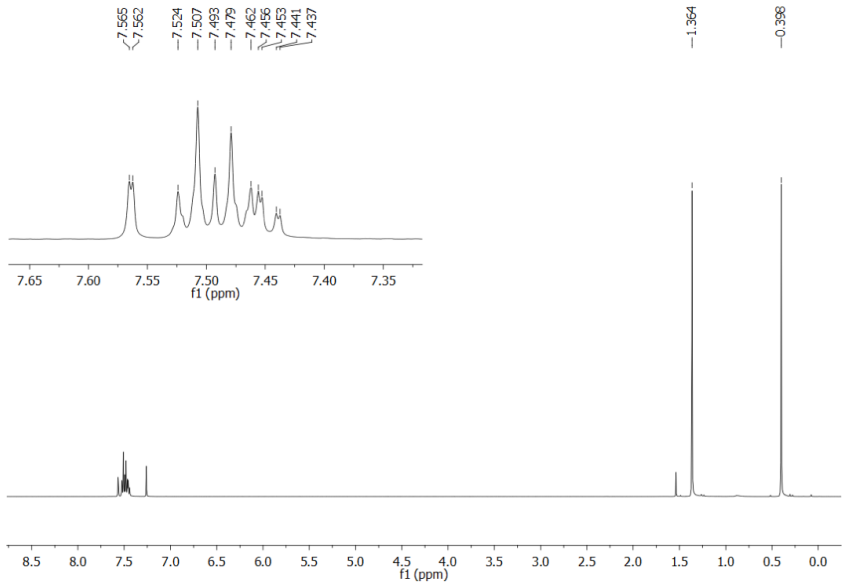

Figure 2-S32. ^{1}H NMR spectrum of **Mod2-Si** in $CDCl_3$.

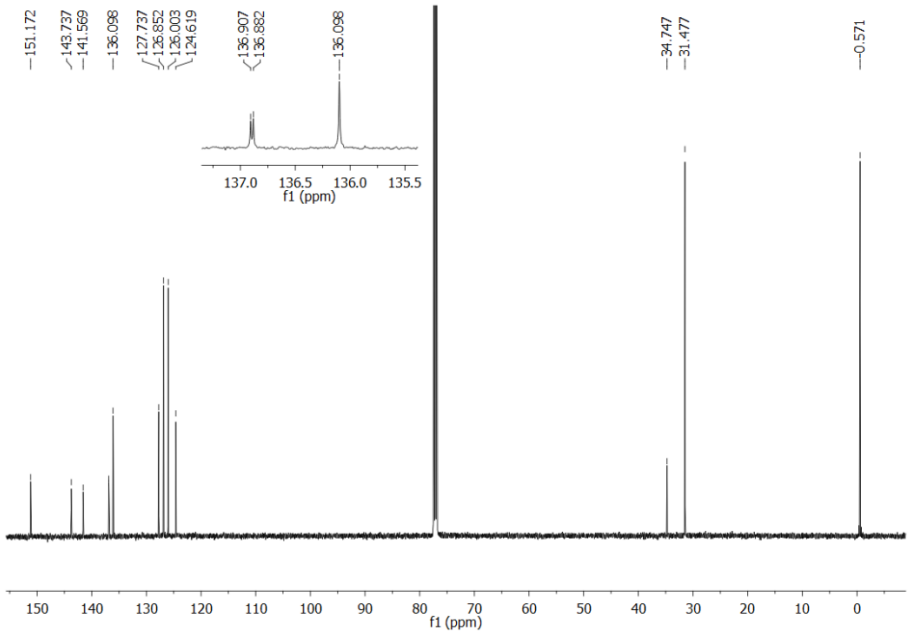

Figure 2-S33. ^{13}C NMR spectrum of **Mod2-Si** in $CDCl_3$.

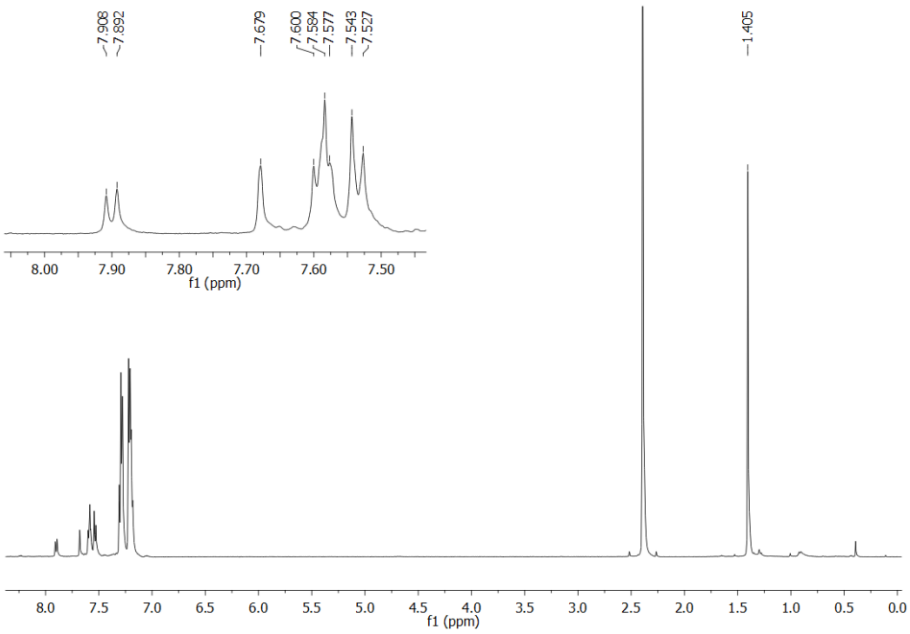

Figure 2-S34. ^{1}H NMR spectrum of the reaction solution of **Mod2-BBr2** in $CDCl_3$ (the signals at 2.40 and 7.1-7.4 ppm are attributed to toluene).

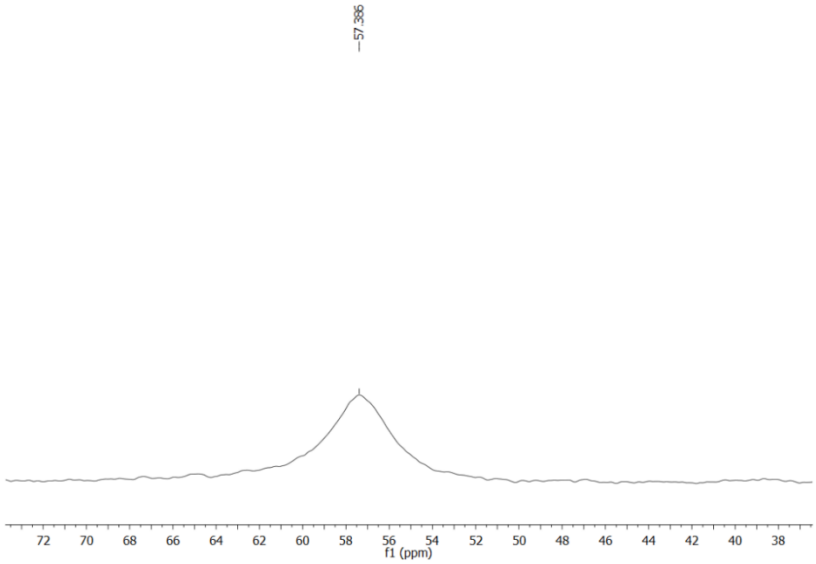

Figure 2-S35. ^{11}B NMR spectra of the reaction solution of **Mod2-BBr2** in $CDCl_3$ after removal of volatile components.

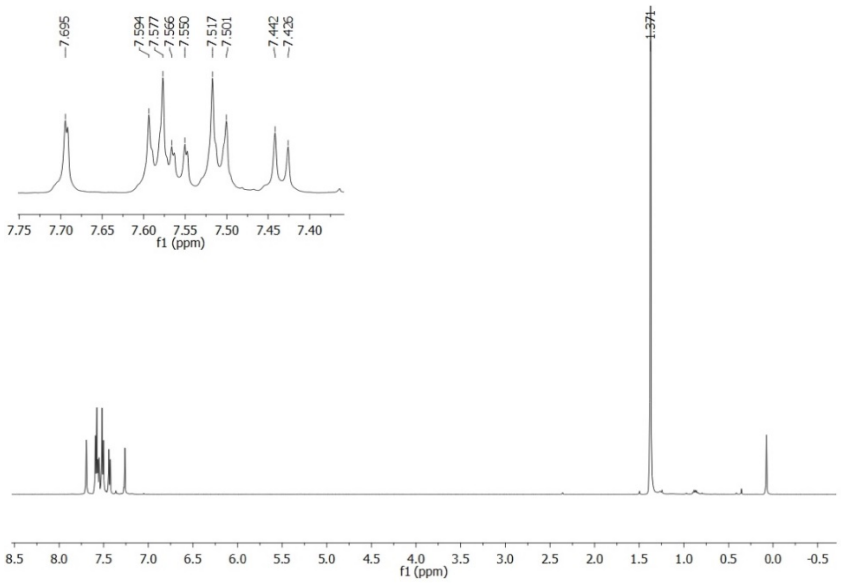

Figure 2-S36. ^{1}H NMR spectrum of **Mod2-BPf2** in $CDCl_3$.

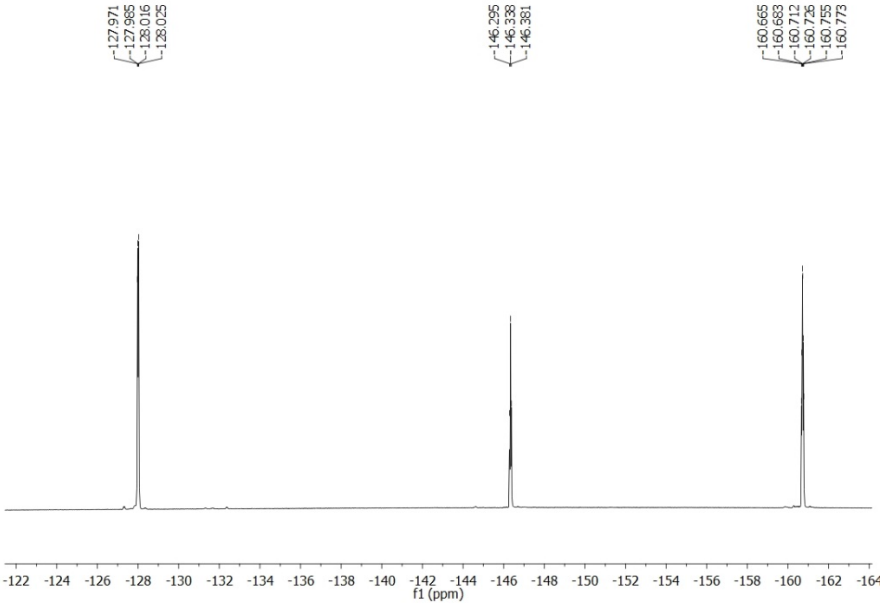

Figure 2-S37. ^{19}F NMR spectrum of **Mod2-BPf2** in $CDCl_3$.

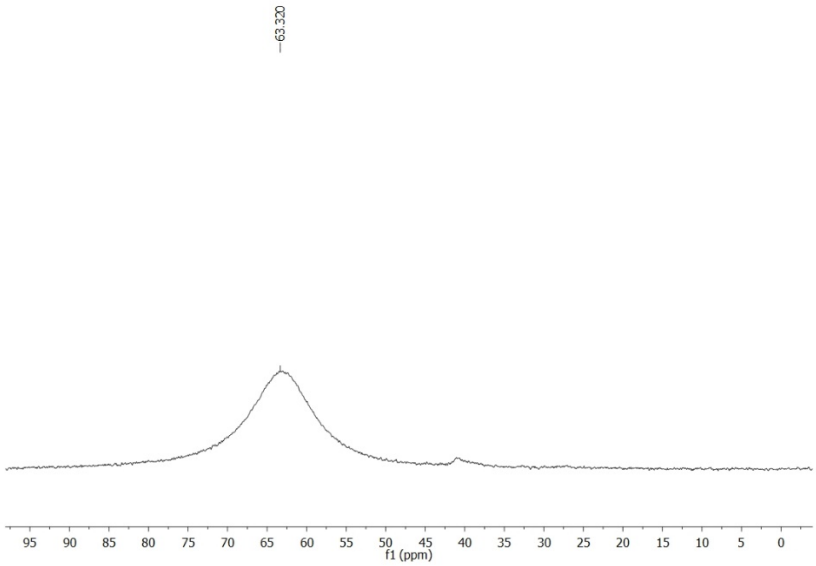

Figure 2-S38. ^{11}B NMR spectrum of **Mod2-BPf2** in $CDCl_3$.

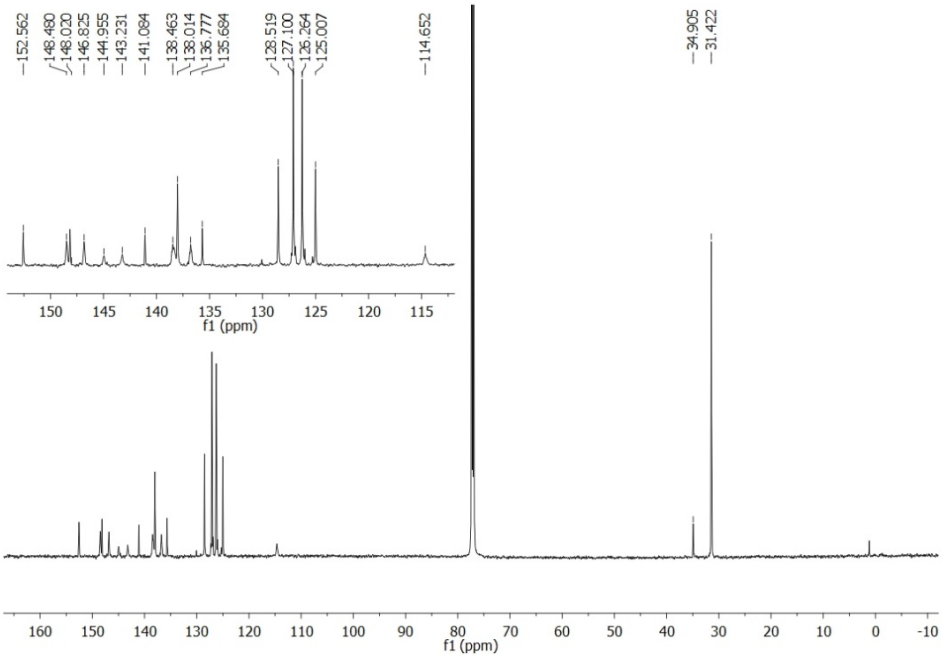

Figure 2-S39. ^{13}C NMR spectrum of **Mod2-BPf2** in $CDCl_3$.

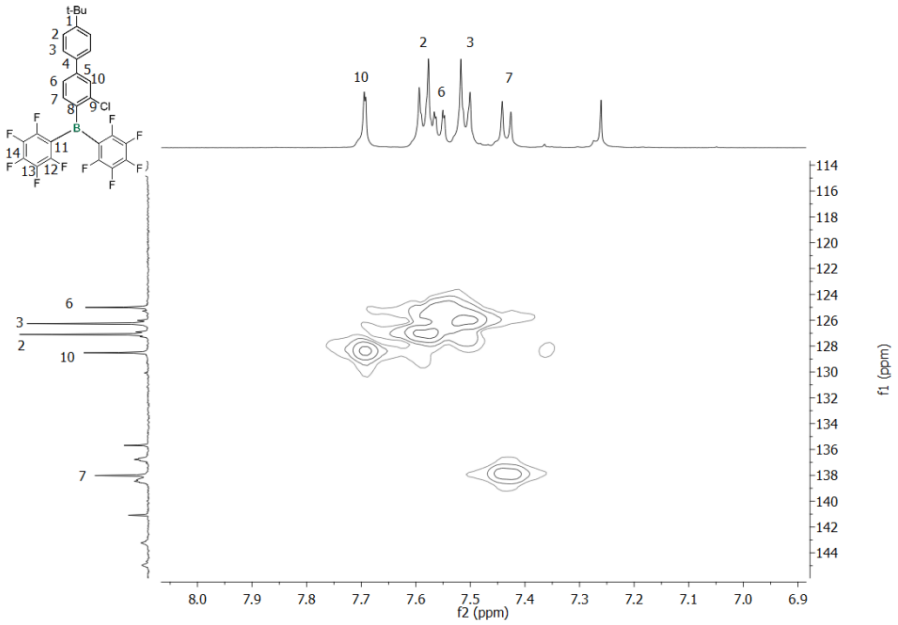

Figure 2-S40. ^{1}H, ^{13}C-HSQC NMR spectrum of **Mod2-BPf2** in $CDCl_3$.

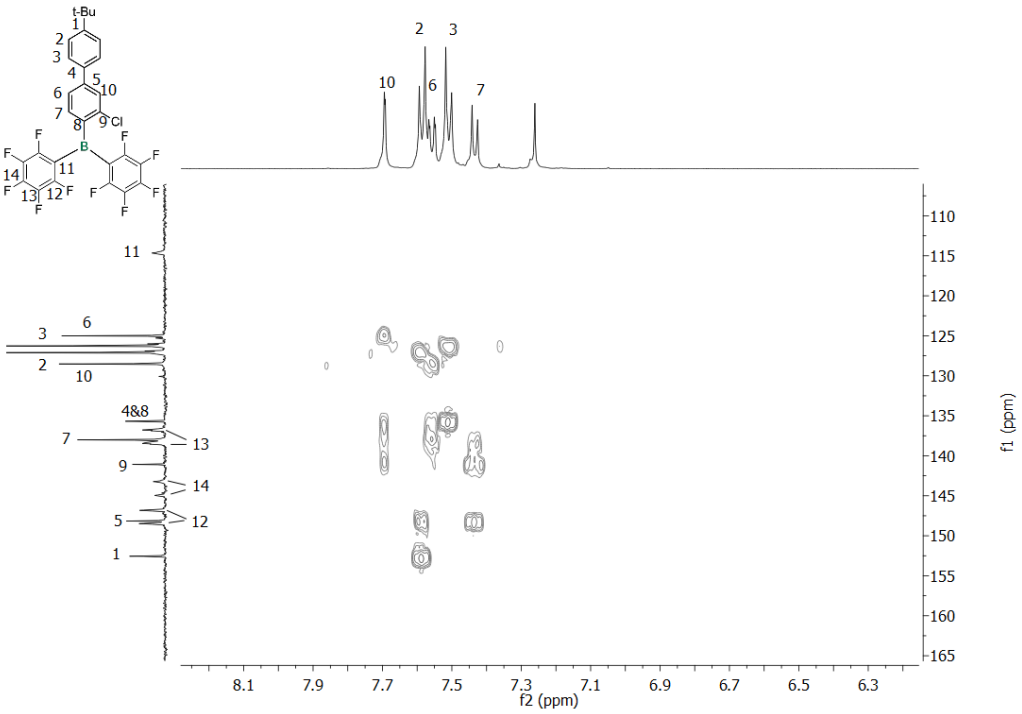

Figure 2-S41. ^{1}H, ^{13}C-HMBC NMR spectrum of **Mod2-BPf2** in $CDCl_3$.

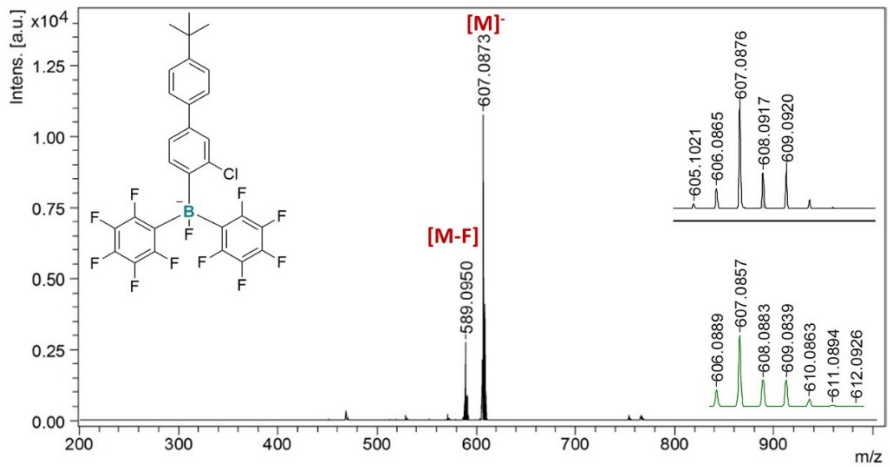

Figure 2-S42. MALDI-TOF MS data of [**Mod2-BPf2**]**F**$^-$ generated by addition of TBAF to **Mod2-BPf2** (anthracene, neg. mode).

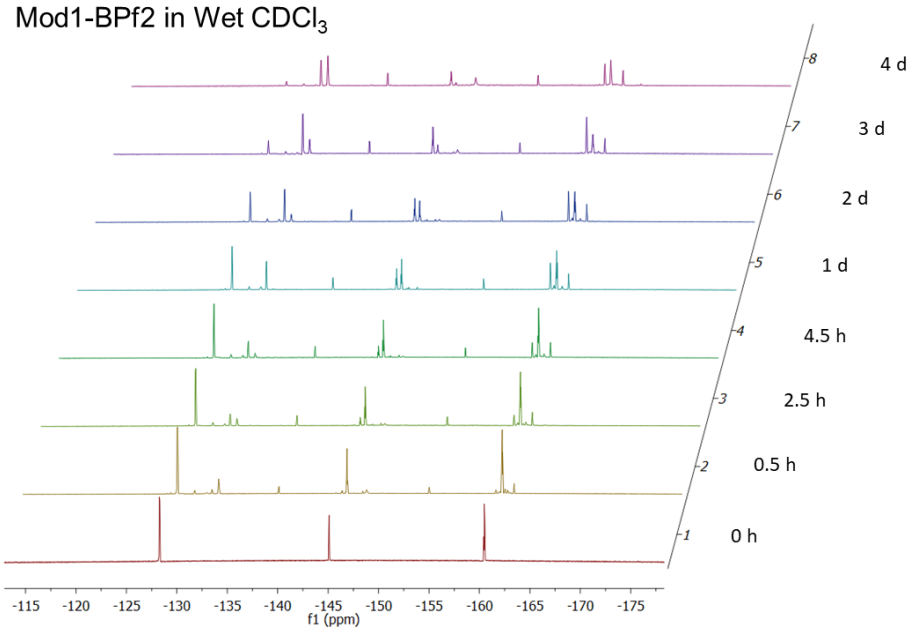

Figure 2-S43. ^{19}F NMR spectra of **Mod1-BPf2** in wet $CDCl_3$.

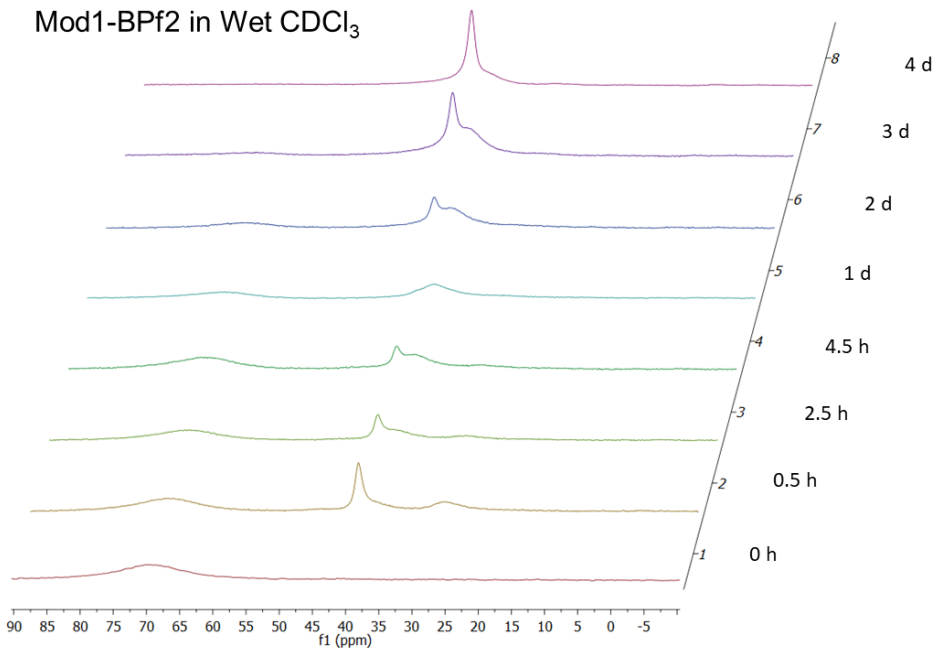

Figure 2-S44. ^{11}B NMR spectra of **Mod1-BPf2** in wet $CDCl_3$.

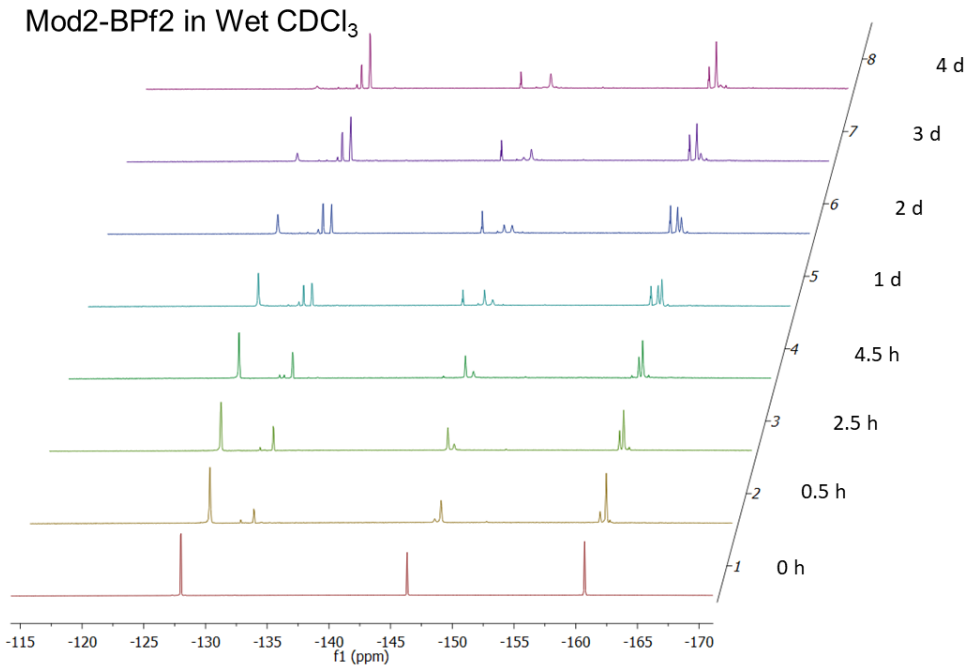

Figure 2-S45. ^{19}F NMR spectra of **Mod2-BPf2** in wet $CDCl_3$.

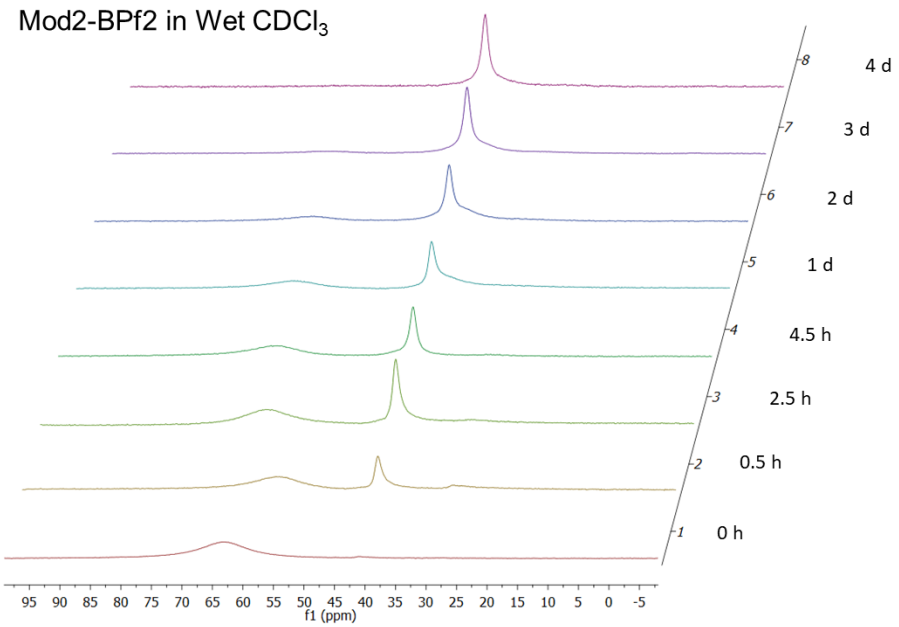

Figure 2-S46. ^{11}B NMR spectra of **Mod2-BPf2** in wet $CDCl_3$.

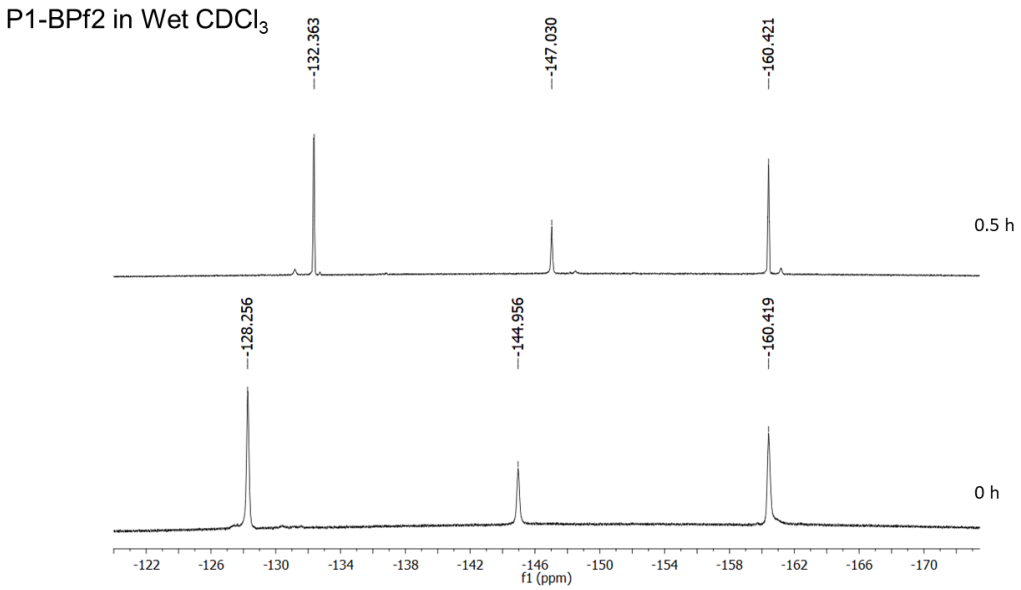

Figure 2-S47. ^{19}F NMR spectra of **P1-BPf2** in wet $CDCl_3$ (polymer precipitation was observed).

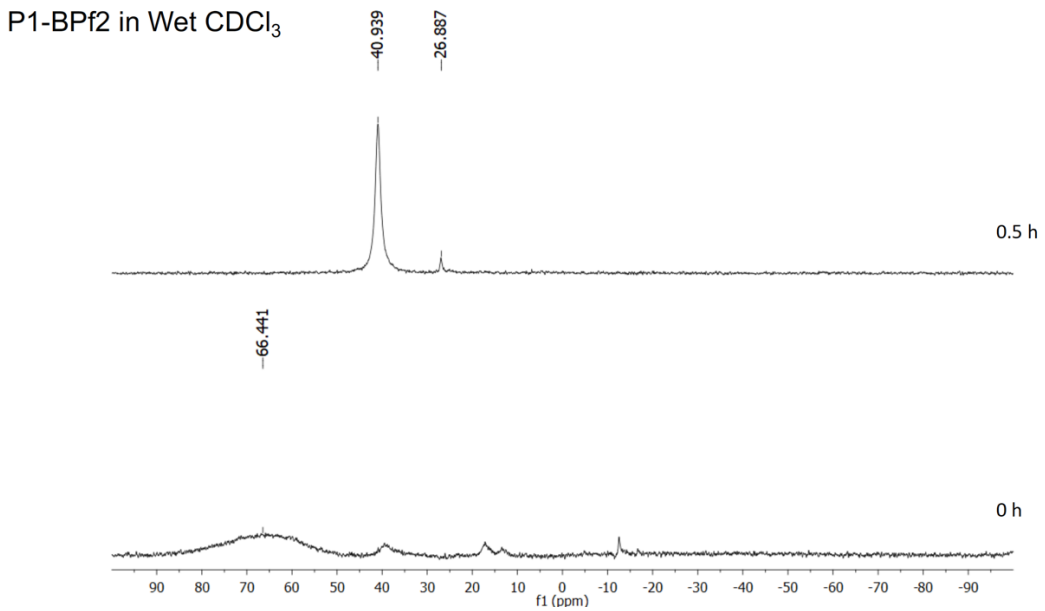

Figure 2-S48. ^{11}B NMR spectra of **P1-BPf2** in wet $CDCl_3$ (polymer precipitation was observed).

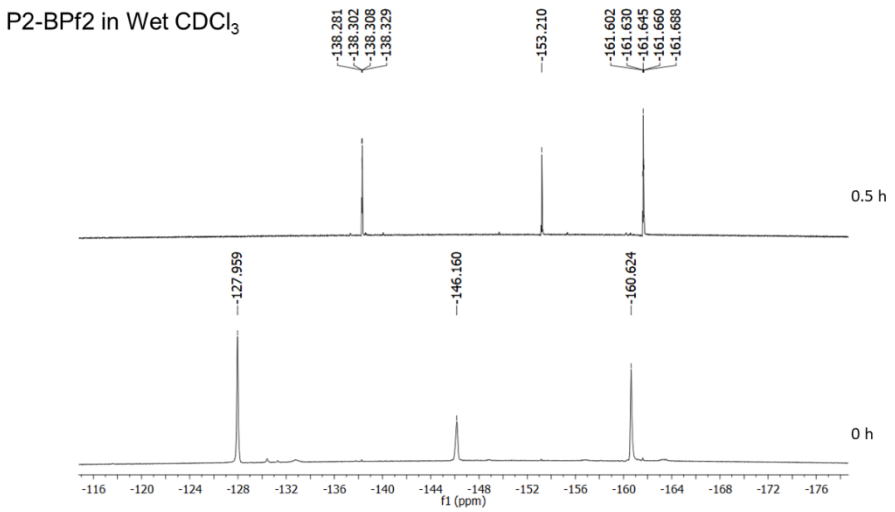

Figure 2-S49. ^{19}F NMR spectra of **P2-BPf2** in wet $CDCl_3$ (polymer precipitation was observed).

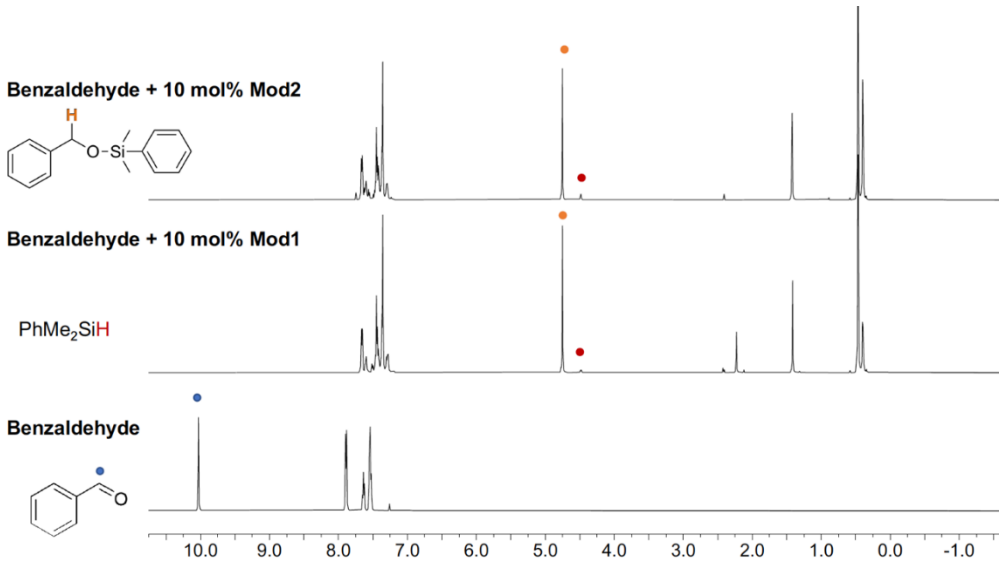

Figure 2-S50. ^{1}H NMR spectra for the hydrosilylation of benzaldehyde catalyzed by 10 mol% of the model compounds in $CDCl_3$.

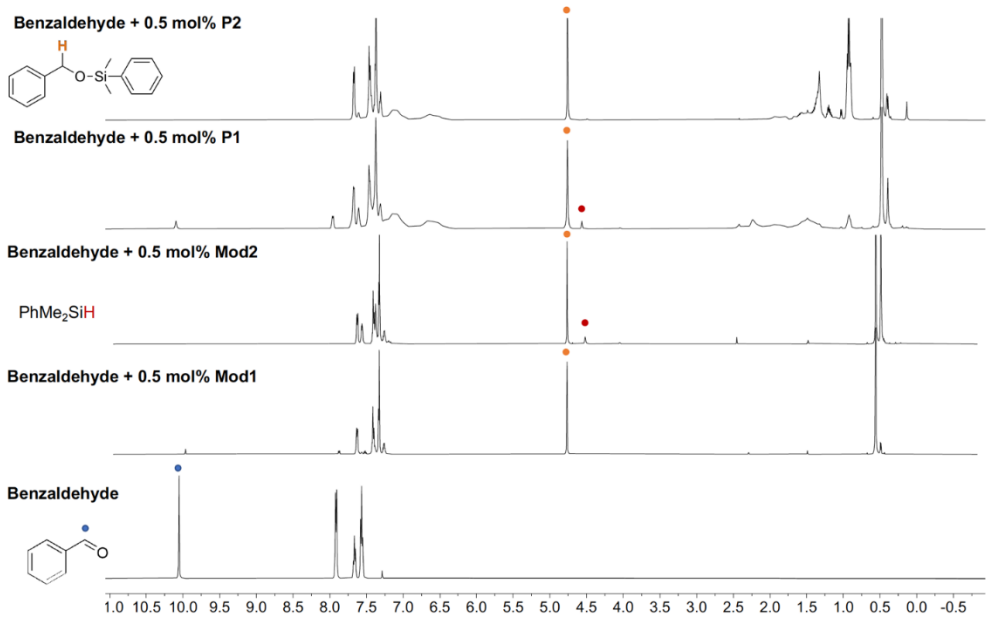

Figure 2-S51. ^{1}H NMR spectra for the hydrosilylation of benzaldehyde catalyzed by Lewis acids in $CDCl_3$.

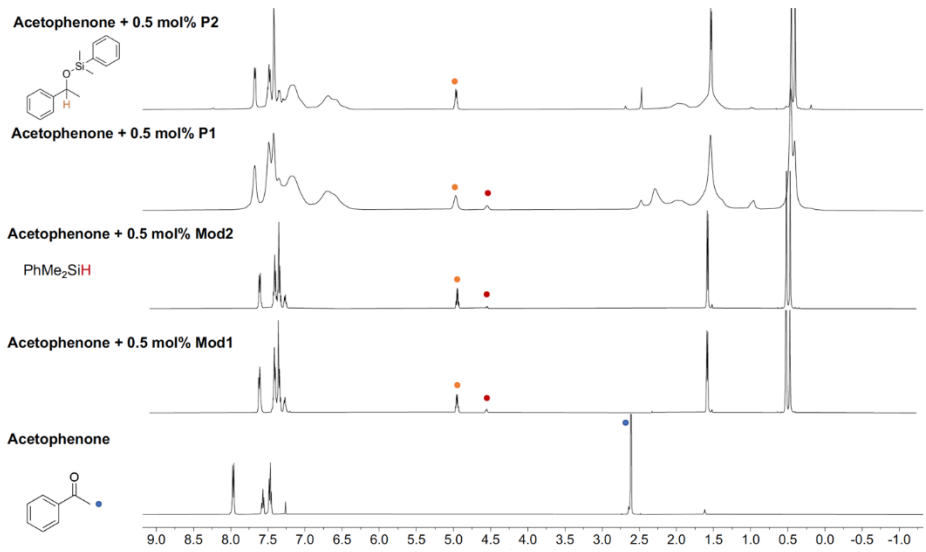

Figure 2-S52. ^{1}H NMR spectra for the hydrosilylation of acetophenone catalyzed by Lewis acids in $CDCl_3$.

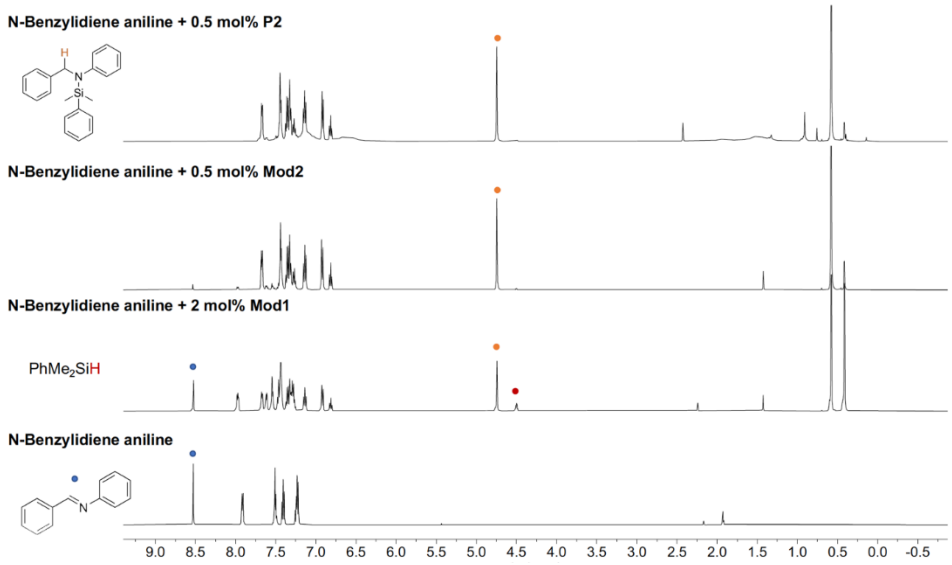

Figure 2-S53. ^{1}H NMR spectra for the hydrosilylation of N-benzylidiene aniline catalyzed by Lewis acids in $CDCl_3$.

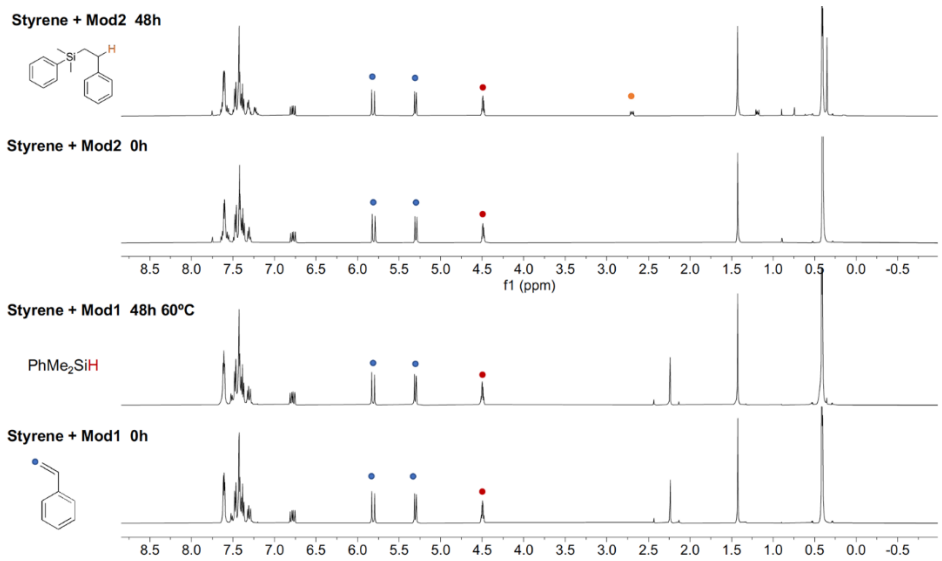

Figure 2-S54. ^{1}H NMR spectra for the hydrosilylation of styrene catalyzed by 10 mol% of the model compounds in $CDCl_3$.

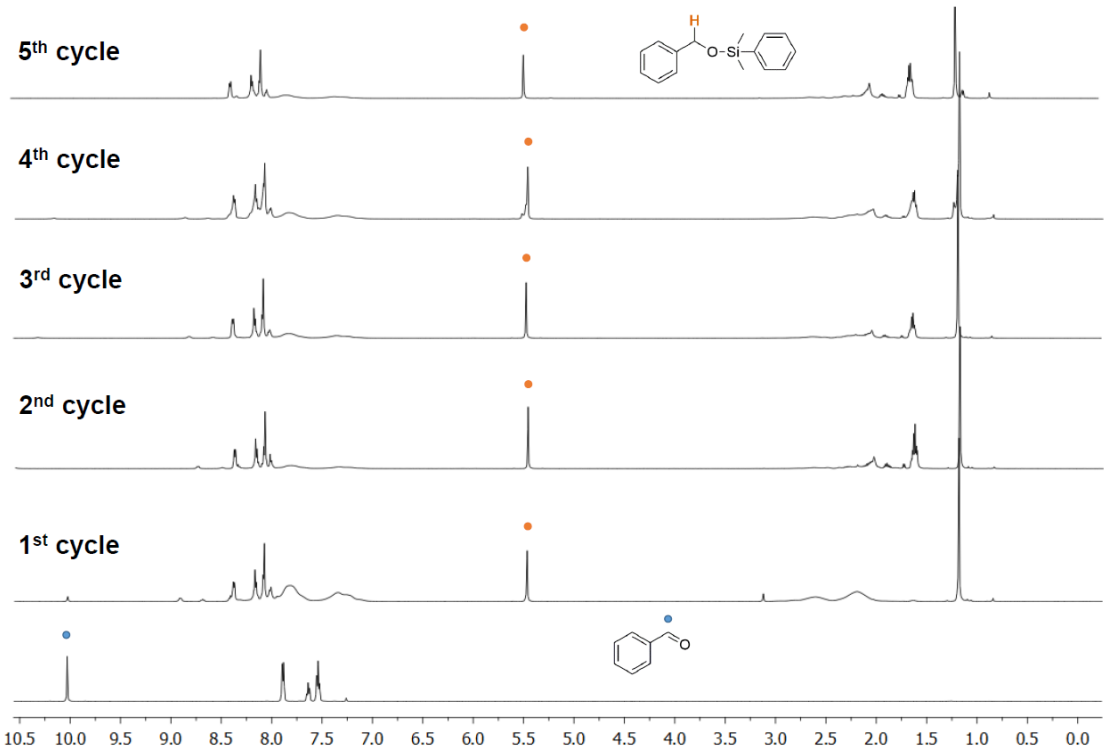

Figure 2-S55. Recyclability of **P2-BPf2** catalyzed hydrosilylation of benzaldehyde in $CDCl_3$.

Table 2-S1. UV-vis Absorption and Fluorescence Data of Model Compounds in Various Solvents

Compound	Solvent	λ_{Abs}[a] (nm)	λ_{FL}[b] (nm)	Stokes shift (cm^{-1})
Mod1-BPf2	hexane	389	469	4400
	toluene	392	512	6000
	DCM	386	538	7300
Mod2-BPf2	hexane	362	413	3400
	toluene	368	456	5200
	DCM	363	483	6800

[a] Only the lowest energy absorption maxima are given. [b] Excited at the lowest energy absorption maxima.

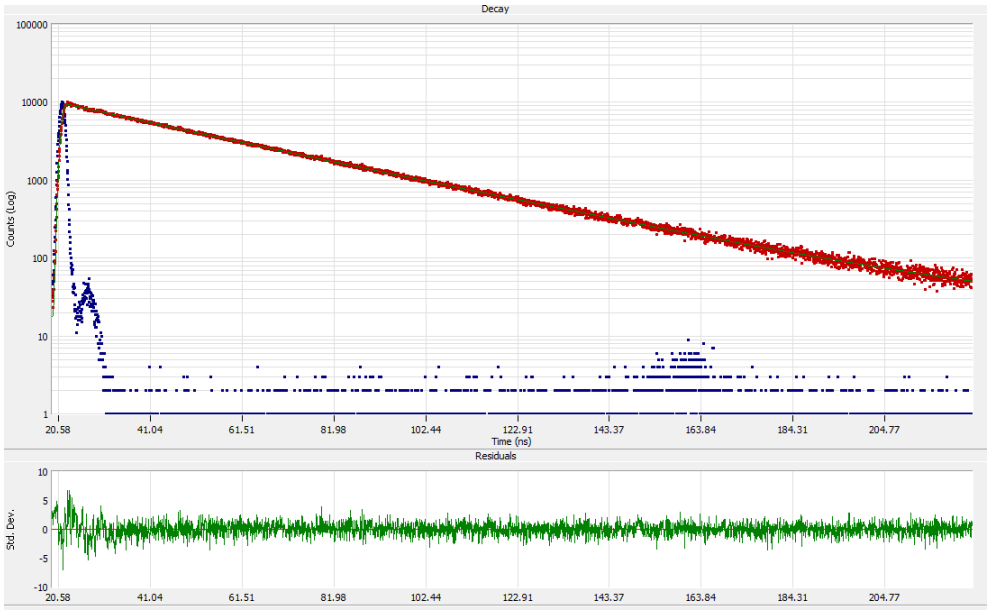

Figure 2-S56. Single-exponential fit of fluorescence decay of **Mod1-BPf2** in degassed DCM excited with a 390 nm nanoLED.

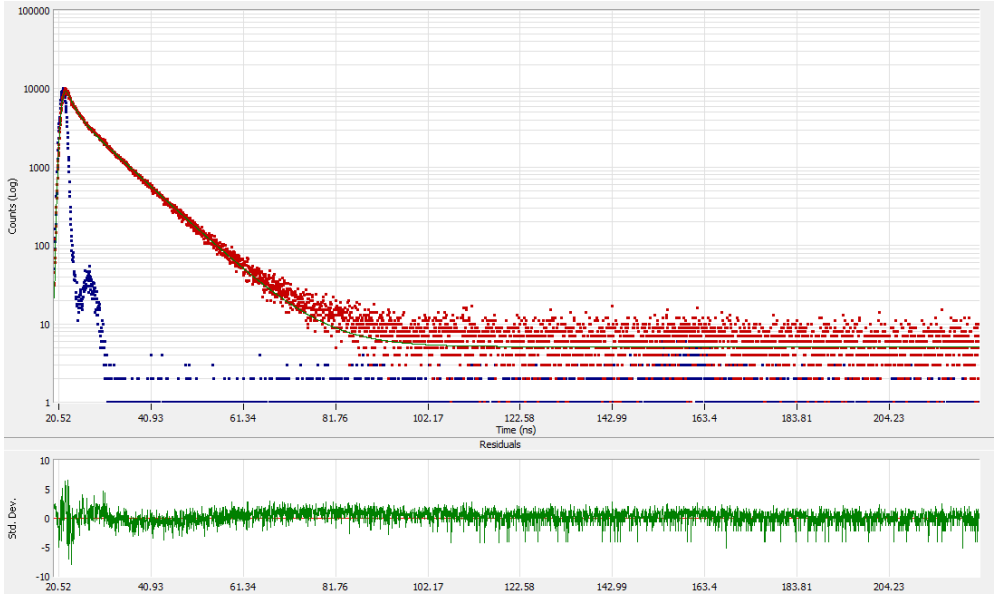

Figure 2-S57. Triple-exponential fit of fluorescence decay of **Mod2-BPf2** in degassed DCM excited with a 390 nm nanoLED.

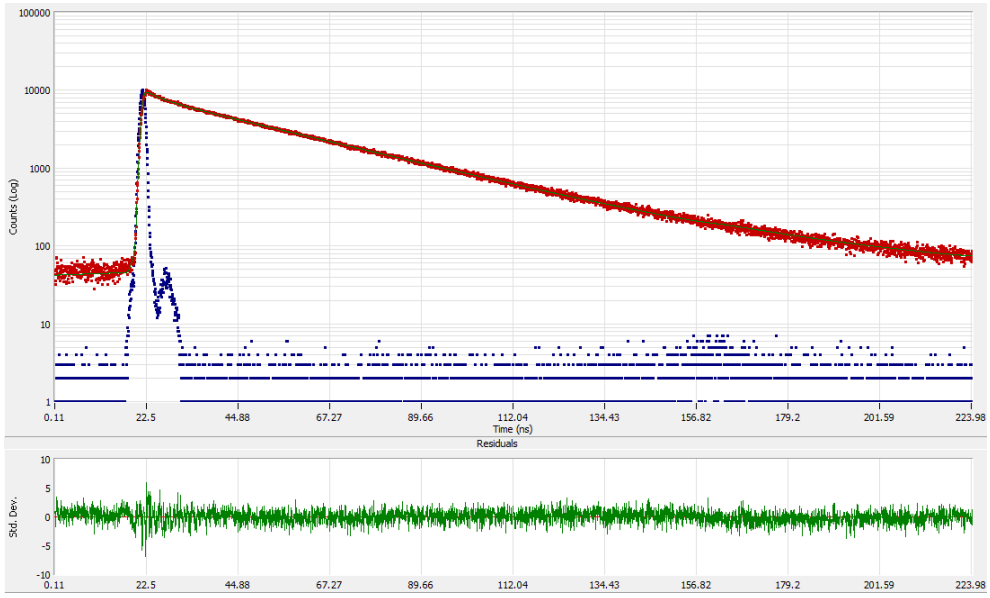

Figure 2-S58. Single-exponential fit of fluorescence decay of **P1-BPf2** in degassed DCM excited with a 390 nm nanoLED.

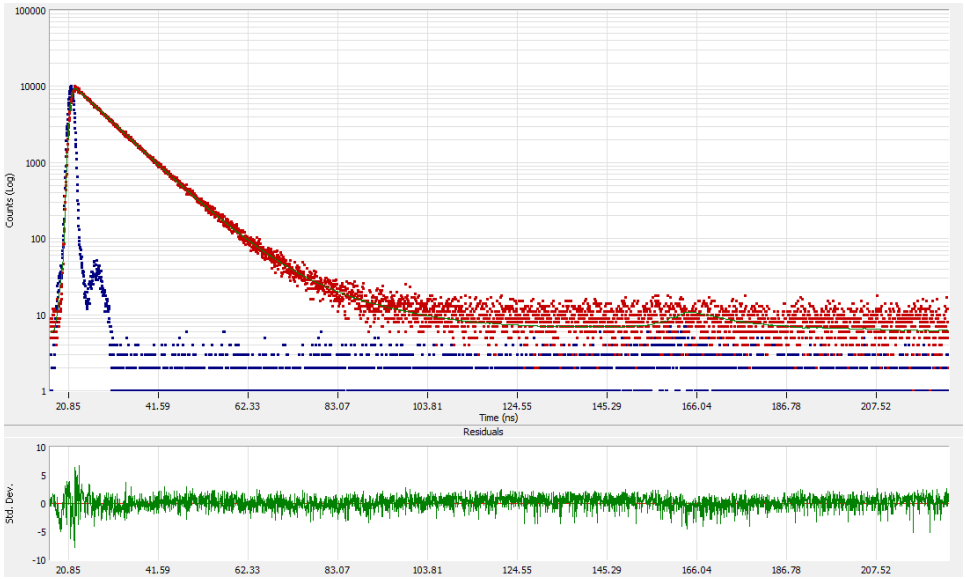

Figure 2-S59. Double-exponential fit of fluorescence decay of **P2-BPf2** in degassed DCM excited with a 390 nm nanoLED.

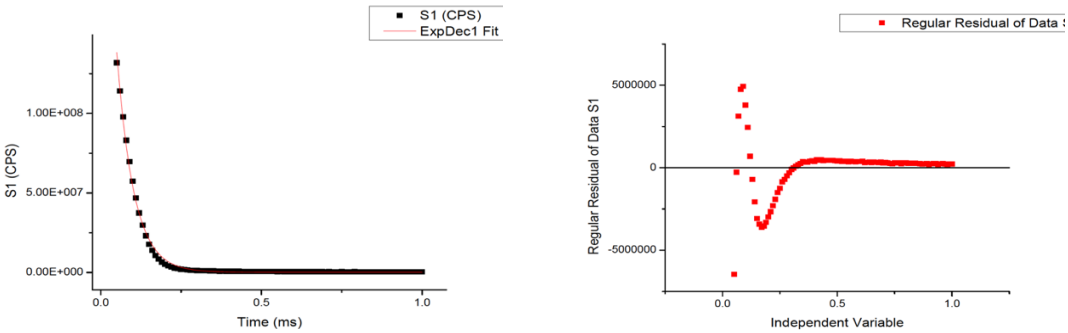

Figure 2-S60. Single-exponential fit of TADF of **Mod1-BPf2** in degassed DCM excited with pulsed Xe lamp.

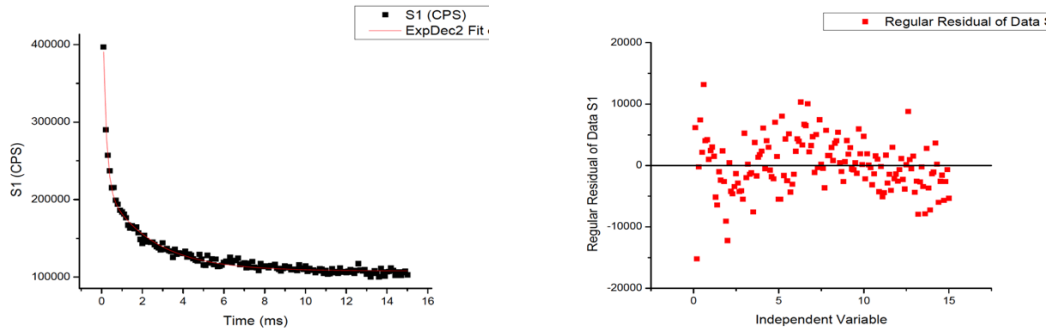

Figure 2-S61. Double-exponential fit of TADF of **Mod2-BPf2** in degassed DCM excited with pulsed Xe lamp.

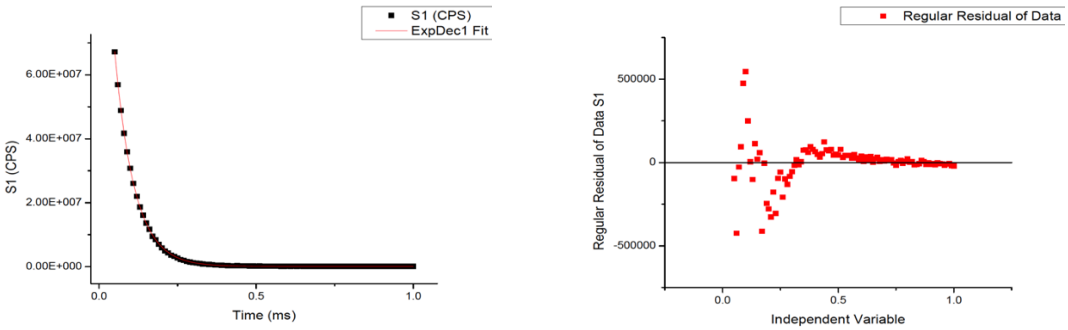

Figure 2-S62. Single-exponential fit of TADF of **P1-BPf2** in degassed DCM excited with pulsed Xe lamp.

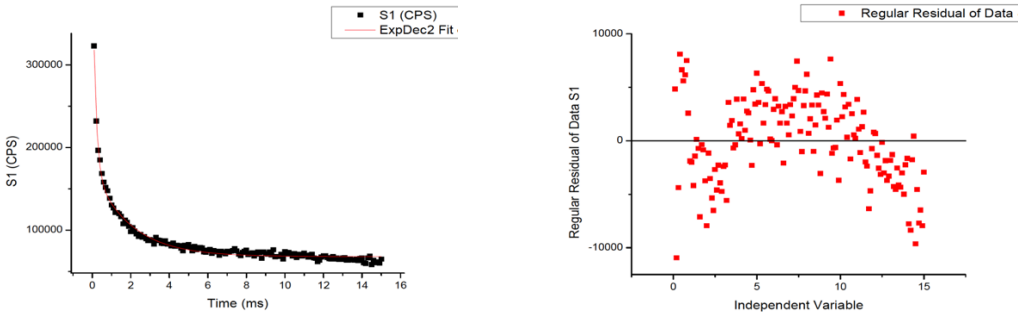

Figure 2-S63. Double-exponential fit of TADF of **P2-BPf2** in degassed DCM excited with pulsed Xe lamp.

Table 2-S2. Summary of TD-DFT data (rb3lyp/6-31g(d))

Compound	Transition [a]	E_{ex} (eV)	λ (nm)	Oscillator strength f	Assignment (%)
Mod1-BPf2	$S_0 \rightarrow S_1$	2.74	452.8	0.0640	H-5 → L (0.13) H → L (0.69)
	$S_0 \rightarrow S_7$	4.02	308.5	0.3069	H-6 → L (0.68) H-5 → L (0.11)
	$S_0 \rightarrow S_8$	4.48	278.4	0.7229	H-7 → L (0.55) H → L+2 (0.43)
	$S_0 \rightarrow S_{10}$	4.62	268.1	0.3511	H-7 → L (-0.41) H → L+2 (0.55)
Mod2-BPf2	$S_0 \rightarrow S_1$	3.11	397.9	0.4667	H → L (0.69)
	$S_0 \rightarrow S_6$	3.90	318.0	0.2523	H-5 → L (0.69)
	$S_0 \rightarrow S_7$	4.19	296.1	0.1065	H-6 → L (0.69)
	$S_0 \rightarrow S_9$	4.73	262.1	0.5111	H-7 → L (-0.23) H → L+1 (0.64)
Mod2-BPf2[b]	$S_0 \rightarrow S_1$	2.97	417.6	0.0734	H-6 → L (-0.12) H → L (0.69)
	$S_0 \rightarrow S_6$	4.00	310.1	0.3387	H-5 → L (0.69)
	$S_0 \rightarrow S_8$	4.43	279.7	0.5470	H-7 → L (0.61) H → L+1 (-0.33)
	$S_0 \rightarrow S_9$	4.62	268.2	0.4919	H-7 → L (0.31) H → L+1 (0.61)

[a] Only transition from S_0 to S_1 and transitions with oscillator strength > 0.1 are presented.
[b] The ground-state molecule structure of Mod2-BPf2 was obtained from modifying the optimized Mod1-BPf2 geometry by replacing two methyl groups with –H and –Cl in 1.771 Å distance as starting geometry.

Table 2-S3. Summary of TD-DFT data (rcam-b3lyp/6-31g(d))

Compound	Transition [a]	E_{ex} (eV)	λ (nm)	Oscillator strength f	Assignment (%)
Mod1-BPf2	$S_0 \rightarrow S_1$	3.51	353.0	0.0992	H-5 → L (0.30)

					H → L (0.62)
	$S_0 \rightarrow S_5$	4.49	276.2	0.3330	H-6 → L (0.62) H-3 → L (0.26)
	$S_0 \rightarrow S_6$	4.92	251.7	1.1423	H-7 → L (0.29) H → L+1 (0.61)
Mod2-BPf2	$S_0 \rightarrow S_1$	3.81	325.6	0.6619	H-7 → L (-0.11) H-6 → L (0.20) H-2 → L (-0.11) H-1 → L (-0.12) H → L (0.61) H → L+1 (0.11)
	$S_0 \rightarrow S_2$	4.31	287.7	0.1003	H-3 → L (0.17) H-2 → L (0.40) H-1 → L (0.48)
	$S_0 \rightarrow S_5$	4.44	279.4	0.2543	H-6 → L (-0.11) H-5 → L (0.57) H-4 → L (-0.27) H-3 → L (-0.21)
	$S_0 \rightarrow S_8$	5.18	239.3	0.4323	H-7 → L (0.40) H → L+1 (0.49) H → L+2 (0.12)
Mod2-BPf2[b]	$S_0 \rightarrow S_1$	3.82	324.4	0.1300	H-6 → L (0.28) H-2 → L (-0.15) H → L (0.61)
	$S_0 \rightarrow S_4$	4.47	277.3	0.3844	H-5 → L (0.64) H-3 → L (0.13) H-2 → L (-0.17)
	$S_0 \rightarrow S_6$	4.94	250.8	1.0526	H-7 → L (0.38) H-2 → L+1 (0.56)

[a] Only transition from S_0 to S_1 and transitions with oscillator strength > 0.1 are presented. [b] The ground-state molecule structure of Mod2-BPf2 was obtained from modifying the optimized Mod1-BPf2 geometry by replacing two methyl groups with –H and –Cl in 1.771 Å distance as starting geometry.

Table 2-S4. Comparison of the calculated singlet state and triplet state energies for **Mod1-BPf2** and **Mod2-BPf2**

Compound	S_0[a] (Hartree)	T_1[a] (Hartree)	S_1[b] (Hartree)	$\Delta E_{ad}(S_1\text{-}S_0)$ (eV/kJ mol^{-1})	$\Delta E_{ad}(T_1\text{-}S_0)$ (eV/kJ mol^{-1})	$\Delta E_{ad}(S_1\text{-}T_1)$ (eV/kJ mol^{-1})
Mod1-BPf2	-2178.671863	-2178.588064	-2178.584775	2.370/228.6	2.280/220.0	0.089/8.635
Mod2-BPf2	-2559.701063	-2559.613454	-2559.604114	2.638/254.5	2.384/230.0	0.242/23.33

[a] S_0 optimized a rb3lyp/6-31g(d), T_1 optimized a ub3lyp/6-31g(d) level of theory. [b] From TD-DFT optimization of S_1 state at b3lyp/6-31g(d) level of theory.

Table 2-S5. Kohn-Sham HOMO and LUMO orbital plots for Mod1-BPf2 and Mod2-BPf2 (rb3lyp/6-31g(d)

Mod1-BPf2	S_0	S_1
LUMO	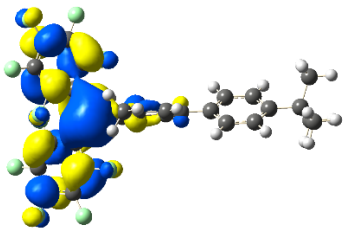 -2.53 eV	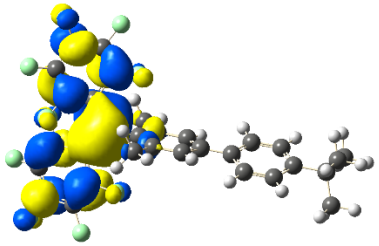 -2.77 eV
HOMO	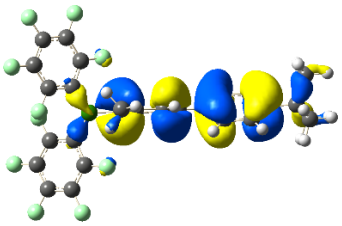 -5.90 eV	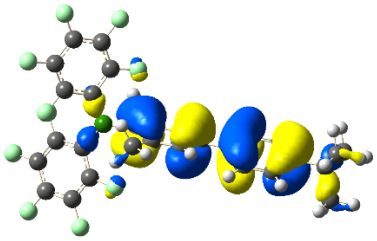 -5.51 eV
Mod2-BPf2	S_0	S_1
LUMO	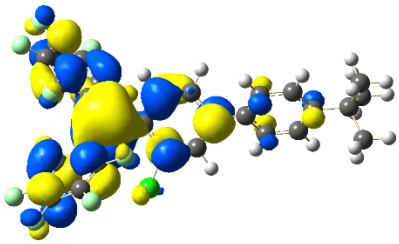 -2.65 eV	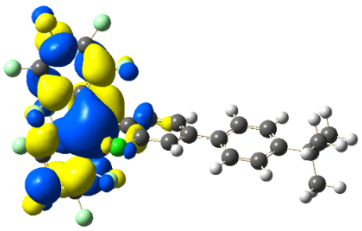 -2.83 eV
HOMO	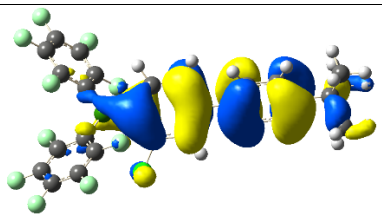 -6.25 eV	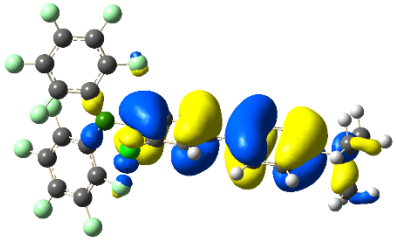 -5.78 eV

Table 2-S6. Kohn-Sham HOMO and LUMO orbital plots for Mod1-BPf2 and Mod2-BPf2 (rcam-b3lyp/6-31g(d)

Mod1-BPf2	S_0	S_1
LUMO	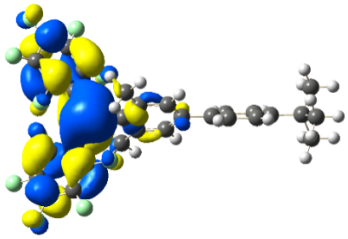 -1.38 eV	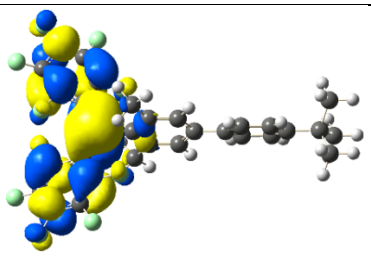 -1.64 eV
HOMO	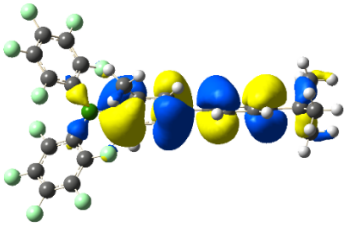 -7.23 eV	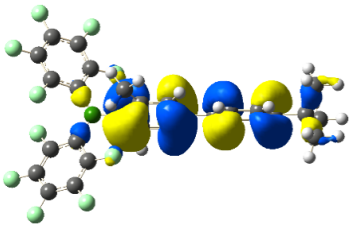 -6.81 eV
Mod2-BPf2	S_0	S_1
LUMO	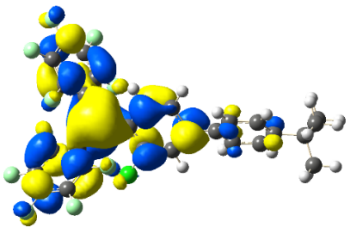 -1.55 eV	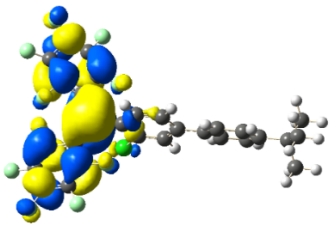 -1.71 eV
HOMO	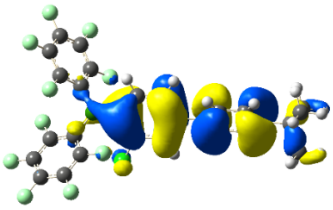 -7.57 eV	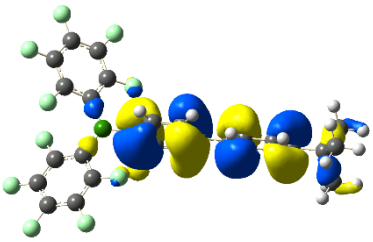 -7.07 eV

Chapter 3 Changing up BN-Polystyrene: Effect of Substitution Pattern on the Free-Radical Polymerization and Polymer Properties[a]

3.1 Introduction

The isoelectronic and isosteric replacement of C=C for B-N units in conjugated organic systems has attracted tremendous recent interest as novel electronic properties, reactivity, and applications are achieved.[1-8] Fundamental studies on the replacement of ubiquitous benzene moieties for 1,2-dihydro-1,2-azaborinines, in particular, have revealed significant differences in the aromatic delocalization (the B-N bond shows partial double bond character), whereas the polarity of the azaborinine molecule and increased acidity of the N-H proton tend to also influence intermolecular interactions.[9, 10] These differences have been exploited in diverse applications ranging from conjugated materials for use in luminescent imaging, field effect transistors and organic solar cells,[11-16] to the development of new ligands for catalysis,[17] and even the biomedical field in the form of enzyme inhibitors[18, 19].

In the realm of polymeric materials,[20-27] Manners pioneered the substitution of B-N and B-P for C-C units in the backbone of polyolefins, giving rise to exciting new classes of polymeric materials (**A**, Figure 3-1).[28-31] Expanding on this theme, Helten recently reported the first B-N analog of polyacetylene (**B**).[32] We envisioned a strong potential impact of

[a] Lin, H.; McConnell, C. R.; Jilus, B.; Liu, S.-Y.; Jäkle, F., *Macromolecules* **2019,** *52* (12), 4500-4509.

materials in which benzene rings are replaced by azaborinine moieties, given that aromatic groups play a major role in polymer science. In earlier work, Sneddon had examined the polymerization of vinylborazines in an effort to generate boron-containing ceramics.[33] We reported in 2015 the first example of an azaborinine-based conjugated polymer (BN-PPP, **C**),[9] a B-N analog of poly(*p*-phenylene), and in 2016 an example of a B-N substituted polystyrene (BN-PS, **D**) as well as its phenylene-expanded congener (BN-PVBP, **E**).[34] Higher molecular weights were achieved for **E** compared to **D**, and this difference was tentatively attributed to the direct attachment of the vinyl group to boron in **D**, which may destabilize the propagating radical in the "benzylic" position. We also found that these polymers exhibit enhanced solubility in polar solvents in comparison to the all-carbon analogs, which we ascribed to the increased polarity of the side groups and the presence of N-H moieties capable of hydrogen bonding. In related work, Staubitz reported high molecular weight polymers **F**,[35] which contain a methyl group in place of a hydrogen on N and elegantly demonstrated the effects of tacticity on the NMR spectral patterns. In addition, Klausen developed a gram scale synthesis of BN-substituted vinylnaphthalene polymers (**G**), both by free radical and syndiospecific Ziegler-Natta-type polymerization methods.[36, 37] They found that in free radical copolymerizations the reactivity of the respective BN-vinylnaphthalene monomer is somewhat lower but overall is in the same range as that of styrene, allowing for random incorporation into the copolymer products.[38] Importantly, they also demonstrated that the oxidative cleavage of the BN-naphthalene moieties results in poly(styrene-*co*-vinylalcohol) copolymers that are desirable as compatibilizers due to the additional polar functional groups.[38, 39]

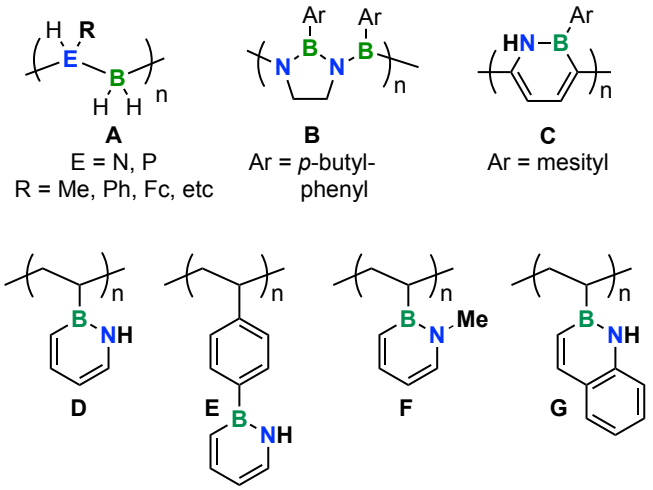

Figure 3-1. Examples of previously reported polymers that have C-C units replaced by B-N units (Fc = ferrocenyl, mesityl = 2,4,6-trimethylphenyl).

Our earlier observation that the parent BN-PS (**D**), while showing interesting solubility and thermal characteristics, can only be obtained in modest molecular weights prompted us to explore the effects of placing the B-N moiety in different positions relative to the polymer backbone on the polymerizability and the polymer physical properties. We report here the synthesis of a series of isomeric vinylazaborinine monomers, as well as their all-carbon counterparts. We also examine their polymerization activity in standard free radical polymerization and compare the physical properties of the resulting polymers with those of the all-carbon analogs.

3.2 Results and Discussion

Monomer Synthesis. We selected three isomeric azaborinines with the vinyl group attached to carbon at the 4-, 5-, or 6-position of the azaborinine as our targets (Scheme 3-1). The mesityl (Mes, 2,4,6-trimethylphenyl) group on the boron atom was attached to

provide robustness of the azaborinine heterocycle against water and oxygen. Other possible isomers with the mesityl groups in *ortho*-position to the polymerizable group (1- and 3-position) were not considered, as the steric bulk was presumed to prohibit polymerization. This assumption is supported by the fact that B-vinylborazines with Me or Ph groups attached to the nitrogens in *ortho*-position have been shown not to be amenable to polymerization whereas the parent B-vinylborazine does undergo thermal polymerization primarily at the vinyl group.[33, 40] In addition, *ortho*-mesitylstyrene (*o*MesSt), the respective all-carbon system, was prepared and found to only very slowly polymerize in the presence of 1,1′-azobisisobutyronitrile (AIBN) at 70 °C (Figures 3-S50-51).[41-43] The previously synthesized azaborinines **1**,[44] **3**,[44] and **6**[45] feature functional handles that enable the installation of the vinyl group via a late-stage Suzuki-Miyaura cross-coupling. Cross-coupling of borylated **1** with vinyl bromide followed by removal of the *N*-TBS group yielded the product, 4V-NBMes in 88% yield. Unexpectedly, the Suzuki coupling of the respective C(5)-borylated isomer 3 did not prove amenable to scale-up. However, C(5)-iodo-substituted azaborinine 4 allowed for the efficient Suzuki−Miyaura coupling with vinyl pinacol boronate ester to afford 5. Subsequent removal of the TBS group with tetra(n-butyl)-ammonium fluoride yielded the desired 5V-NBMes in 82% yield. Finally, the unprotected pinacolborane-functionalized compound 6 afforded under Suzuki−Miyaura cross-coupling conditions with vinyl bromide the final isomer 6V-NBMes in 71% yield. We also prepared meta-mesitylstyrene (*m*MesSt) as a direct all-carbon analogue of both 4V-NBMes and 6V-NBMes and para-mesitylstyrene (*p*MesSt) as an analogue of 5V-

NBMes. These monomers were readily obtained by Suzuki−Miyaura cross-coupling of 2-bromomesitylene and 3- or 4-vinylphenyl boronic acid, respectively.

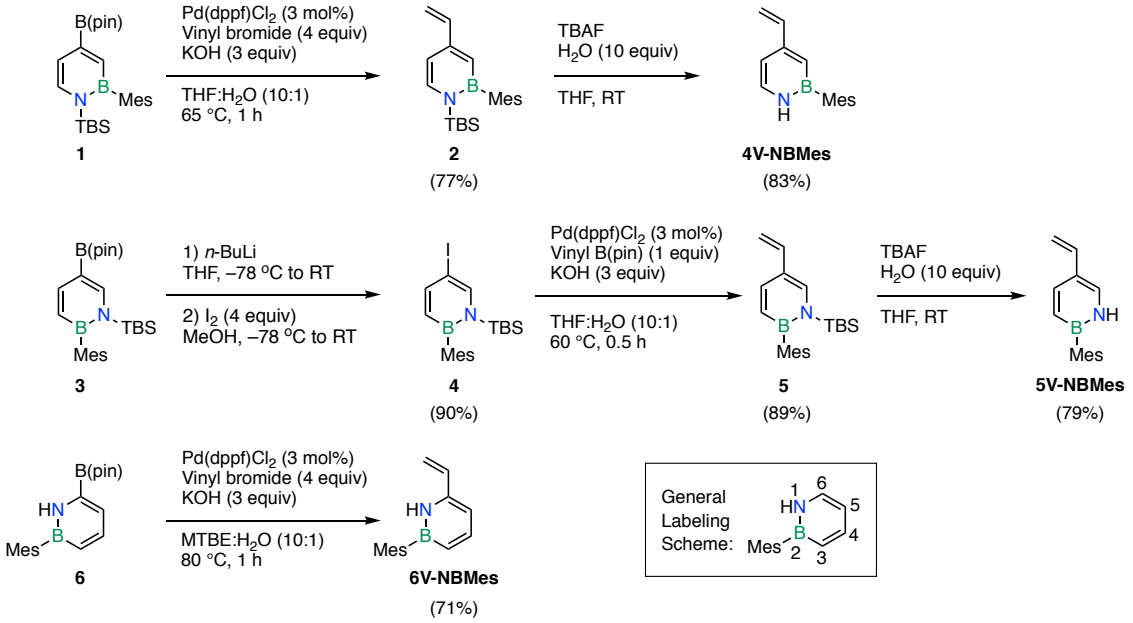

Scheme 3-1. Synthesis of the 4V-NBMes, 5V-NBMes and 6V-NBMes monomers (TBS = t-butyldimethylsilyl; dppf = 1,1'-bis(diphenylphosphino)ferrocene; MTBE = methyl t-butyl ether; TBAF = tetra-n-butylammonium fluoride; pin = pinacolato).

Electronic Structure Calculations. When considering the propensity of these different monomers to undergo polymerization it is important to recognize that each position on the azaborinine ring is electronically distinct.[19, 45-48] We performed electronic structure calculations of the azaborinine isomers as well as their corresponding all-carbon counterparts using the CAM-B3LYP hybrid exchange-correlation functional with the 6-311G(d,p) basis set (Figure 3-2). Electrostatic potential (ESP) maps show the charge distribution typical of aromatic compounds, with an electron-rich surface above and below the ring and an electron-deficient region around the C−H edge (Figure 3-2b). The

positioning of the vinyl group relative to the mesityl group does not significantly impact the charge distribution (Figure 3-2c) for the carbonaceous mMesSt and pMesSt or the C−H bond dissociation energies (BDEs, Figure 3-2d) of the respective ethyl-substituted derivatives. On the other hand, the positioning of the vinyl/ethyl group relative to the more electronegative nitrogen and less electronegative boron atoms in the azaborinine ring does influence both the charge distribution and the C−H BDEs. The C_{α}−H BDE values for the ethyl derivatives of 6V-NBMes, 5V-NBMes, and 4V-NBMes (80.1, 82.3, and 83.6 kcal mol−1, respectively) increase with an increasing distance from the nitrogen atom of the azaborinine ring in the order C_{α}−$H_{(6V\text{-}NBMes)}$ < C_{α}−$H_{(5V\text{-}NBMes)}$ < C_{α}−$H_{(4V\text{-}NBMes)}$. The higher stability of the radical derived from 6V-NBMes may also be related to the enhanced resonance stabilization because of conjugation with the butadiene system of the azaborinine moiety. We note that these differences are relatively modest as a much larger difference in BDEs is seen when comparing B-ethylazaborinine (C_{α}−H BDE of 88.2 kcal mol^{-1}) to ethylbenzene (C_{α}−H BDE of 83.0 kcal mol^{-1}), [38] indicating a significantly lower stability for the radical derived from B-vinylazaborinine that served as an intermediate in the synthesis of polymer **D** (see Figure 3-1). Furthermore, as can be seen from the Mulliken charge values (Figure 3-2c), the vinyl-bound intraring C6 carbon (+0.185 in 6V-NBMes) and C4 carbon (−0.028 in 4V-NBMes) in 1,2-azaborinines are relatively electron-deficient in comparison to the intraring *ipso*-carbon of the mesitylstyrene derivatives (∼−0.08 for *m*MesSt and *p*MesSt). On the other hand, the vinyl-bound intraring C5 carbon (−0.166 in 5V-NBMes) is significantly more electron-rich. The observed intraring charge distribution is consistent with the nitrogen atom exerting its inductive electron-withdrawing (−I)

influence. Importantly, the mesomeric electron-donating (+M) effect is carried over into the attached vinyl group, rendering the vinyl carbons of 5V-NBMes significantly more electron-rich than those of 4V-NBMes. Those of 6V-NBMes are also relatively electron-rich because of the linear conjugation with the butadiene group of the azaborinine moiety. The theoretically predicted differences in the Mulliken charges are nicely reflected in the ^{13}C NMR data of the azaborinine monomers. Specifically, the ^{13}C NMR data are consistent with the notion that the C_β carbon of 5V-NBMes (Mulliken charge −0.217, $\delta(^{13}C)$ = 109.6 ppm) is the most electron-rich and the C_β carbon of 4V-NBMes (Mulliken charge −0.201, $\delta(^{13}C)$ = 115.9 ppm) the least electron-rich in this series of isomeric compounds.

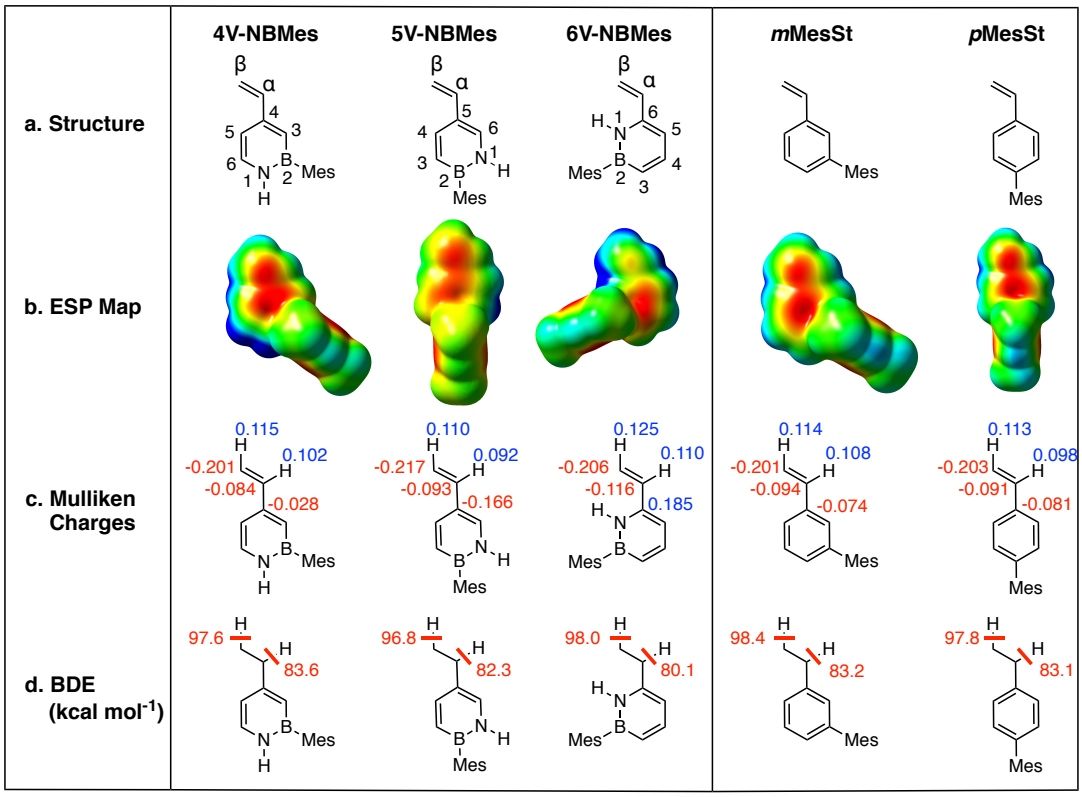

Figure 3-2. a) Structures of the B-mesitylazaborinine and mesitylstyrene compounds (the lowest energy conformers are shown); b) electrostatic potential (ESP) maps; c) Mulliken charges of selected atoms; d) calculated bond dissociation energies (BDEs).

Homopolymerizations. We investigated the free-radical polymerization of monomers 4V-NBMes, 5V-NBMes, and 6V-NBMes in anisole with AIBN (2 mol %) as the initiator (Scheme 3-2). The data are summarized in Table 3-1. After 24 h at 70 °C, ^{1}H NMR analyses showed that 76% of the monomer 4V-NBMes, 63% of 5V-NBMes, and 51% of 6V-NBMes were converted to the respective polymers. Gel permeation chromatography (GPC) analyses in tetrahydrofuran (THF) gave the estimated molecular weights of M_n = 26.9 kDa ($Đ$ = 4.84) for P4V-NBMes, M_n = 11.6 kDa ($Đ$ = 3.98) for P5V-NBMes, and M_n = 18.2 kDa ($Đ$ = 2.44) for P6V-NBMes relative to polystyrene standards. For comparison, the isosteric all-carbon analogues, *m*MesSt and *p*MesSt, were also converted to the corresponding polymers by free-radical polymerization under similar conditions as for the azaborinine monomers. The polymerizations proceeded much faster than in the case of the azaborinines, resulting in quantitative conversion to polymer within only 6.5 h at 70 °C. The fact that both *m*MesSt and *p*MesSt rapidly polymerized and the conversion for *m*MesSt was even higher than that for *p*MesSt suggests that steric factors play a relatively minor role. Furthermore, the conversion and the degree of polymerization (X_n) of 4V-NBMes, 5V-NBMes, and 6V-NBMes achieved were similar to those obtained in a control reaction with unsubstituted styrene (50% conversion, M_n = 11.5 kDa, $Đ$ = 1.86, X_n = 111), but much higher than that for the previously reported 1-hydro-2-vinyl-1,2-azaborinine (BN-St),[34] in which the vinyl group was attached to boron rather than carbon. BN-St was reported to give only sluggish (dimethylformamide, benzene) or no polymerization at all (THF) under

varying conditions (solvent, temperature, and initiator);[34] under conditions identical to those used for the polymerization of 4V-NBMes, 5V-NBMes, and 6V-NBMes, almost no conversion of BN-St was observed (4%; M_n = 1.1 kDa, $Đ$ = 1.49, X_n = 11). A reason could be that the propagating radical in the "benzylic" position is better stabilized when the vinyl group is attached to C rather than B as is the case for BN-St.

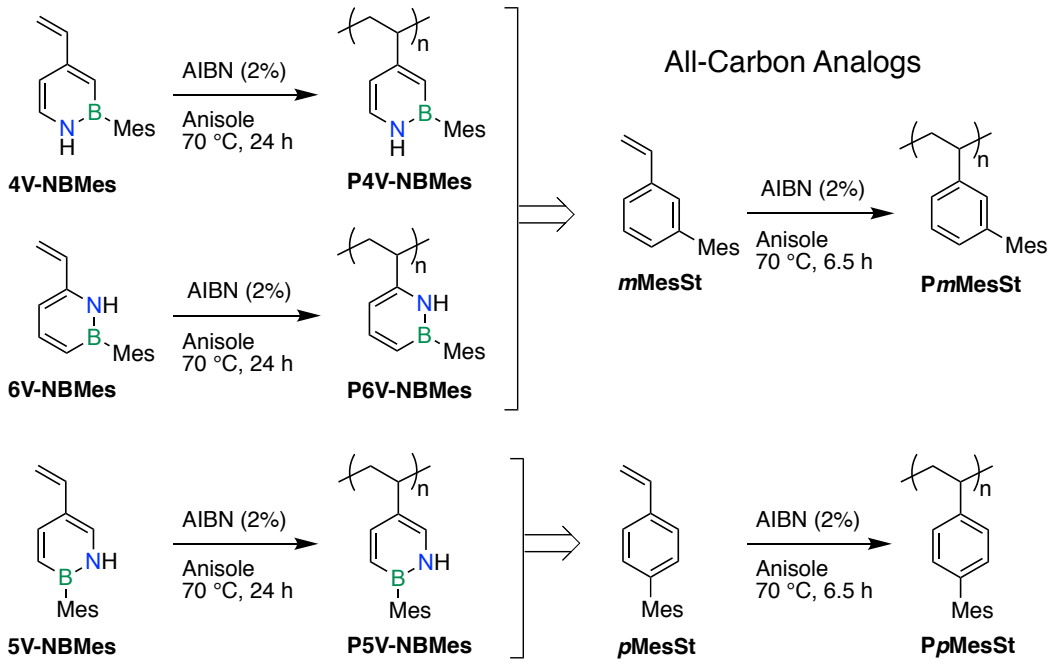

Scheme 3-2. Synthesis of the azaborinine polymers and their all-carbon analogs by free radical polymerization (AIBN = 1,1'-azobisisobutyronitrile).

Table 3-1. Data for the free radical polymerization of vinyl-functionalized azaborinines and their all-carbon analogs

Monomer	Feed ratio [a]	T / t (ºC / h)	Conv [b] (%)	M_n (kDa)[c]	M_w (kDa)[c]	$Đ$ [c]	X_n [c]
4V-NBMes	50:1	70 / 24	76	26.9	130.4	4.84	119
6V-NBMes	50:1	70 / 24	51	18.2	44.4	2.44	80
*m*MesSt	50:1	70 / 6.5	>95	29.7	61.3	2.07	134

5V-NBMes	50:1	70 / 24	63	11.6	46.1	3.98	52
*p*MesSt	50:1	70 / 6.5	82	21.6	42.1	1.95	97

[a] Feed ratio of [monomer]:[AIBN] in anisole, [M] = 4.5 M. [b] Conversion estimated based on ^{1}H NMR integration of residual monomer before purification relative to anisole standard. [c] Dispersity ($Đ$) and average degree of polymerization (X_n) based on GPC analysis of isolated product in THF relative to PS standards.

Polymer Characterization. The chemical structures of the new BN-substituted polystyrene derivatives were confirmed by multinuclear and two-dimensional (2D) NMR spectroscopy. The disappearance of the vinyl group signals and pronounced peak broadening in the ^{1}H and ^{13}C NMR spectra of 4V-NBMes, 5V-NBMes, and 6V-NBMes clearly indicate successful polymerization with the formation of polymers that are presumed to be atactic (Figure 3-3). The ^{11}B NMR spectra provide further evidence for the incorporation of the azaborinine moieties into the polymers P4V-NBMes, P5V-NBMes, and P6V-NBMes. For all the three polymers, a significant upfield shift from ca. 36 to 29 ppm was observed along with a strong signal broadening relative to the monomers (Figure 3-3). Such an upfield shift is commonly observed in the polymerization of borane-functionalized styrene derivatives and likely a result of shielding effects because of the neighboring groups along the polymer chain.[49-51] In the ^{1}H NMR spectra, the N−H protons were shifted to lower frequency upon polymerization, most dramatically for 6V-NBMes (8.02 to ca. 7.2 ppm) and 5V-NBMes (8.11 to ca. 7.3 ppm), and somewhat less pronounced for 4V-NBMes (7.70 to ca. 7.3 ppm). This difference is likely because of the fact that N−H is in closer proximity to the polymer main chain and the neighboring groups in P6V-NBMes and P5V-NBMes, but further removed in the case of P4V-NBMes. To further confirm the structural integrity of the azaborinine side groups and the absence of ring-

opening or rearrangements during polymerization, heteronuclear multiple-quantum correlation (HMQC) NMR spectra were acquired for the polymers and the corresponding monomers (Figures 3-S21, 25, 31 and 36 in the appendix). By comparing the HMQC data for the monomers and polymers, and by considering that B-bound carbons generally give rise to quadrupole-broadened signals for the monomers, we were able to fully assign and correlate the NMR signals to the polymer structures. Relatively sharp signals were detected for the mesityl groups in the aromatic region (indicated with "M" in Figure 3-3), and their chemical shifts changed little between monomers and polymers, or between different isomers. For the azaborinine moieties, a consistent upfield shift of the ^{1}H NMR resonances agrees well with our observations from the ^{11}B NMR data, but these signals were extremely broad, most likely because of tacticity and the neighboring group effects. Meanwhile, well-separated signals were detected in the ^{13}C NMR spectra, and the chemical shifts generally correlated nicely with those of the monomers, considering the slight differences because of the conversion of vinyl to alkyl substituents upon polymerization. Most notably, the carbons in 5-position, that is meta to N and para to B, appeared far upfield, except for those of 5V-NBMes/P5V-NBMes which contain the vinyl group/polymer chain in this position. In contrast, the carbons in 4-position, that is *meta* to B and para to N, appeared further downfield. This effect was even more pronounced for 4V-NBMes/P4V-NBMes because of the attachment of the vinyl group/polymer chain. Collectively, these data strongly support the notion that the azaborinine heterocycles remained intact during the free-radical polymerization.

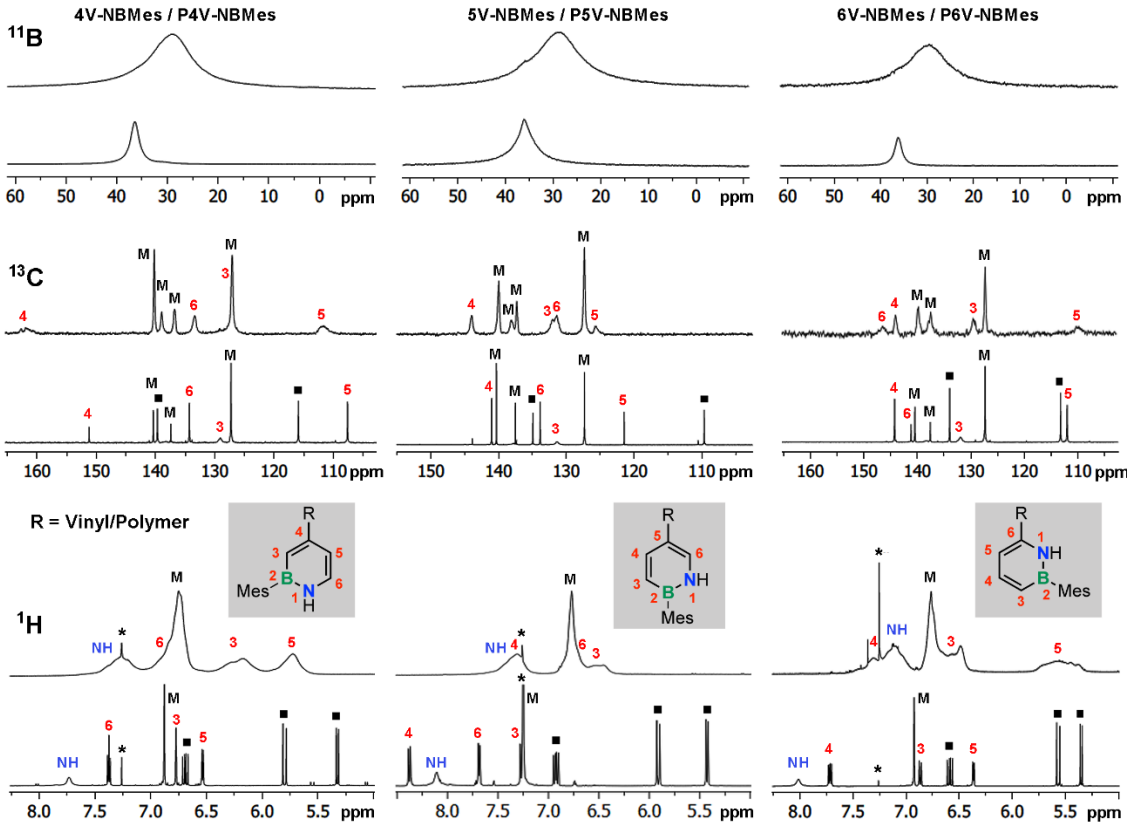

Figure 3-3. ^{1}H, ^{13}C (aromatic region), and ^{11}B NMR spectra of monomers (bottom) and polymers (top) in $CDCl_3$ (*). Vinyl groups are indicated with a black square, and signals attributed to the pendent mesityl groups with "M".

Copolymerizations. Although the higher conversion of 4V-NBMes relative to the other isomers in the homopolymerization experiments may suggest a relatively higher reactivity of this monomer, chain transfer and early termination because of trace impurities or side reactions may also play a role, as suggested by the relatively high dispersities for P4V-NBMes and P5V-NBMes. Another indication is that under otherwise identical conditions, the polymerization of the isosteric carbonaceous mesitylstyrene analogues goes to much higher conversion over a shorter period of time (Table 3-1). To better understand the differences in the polymerization rates, we investigated the free-radical copolymerization

of the azaborinine monomers with styrene as well as with the direct isosteric carbon analogues to produce the corresponding copolymers shown in Figure 3-4. Polymerizations were conducted with 1 mol% AIBN in anisole at a monomer concentration of [M1] = [M2] = 2.25 M for 20 h at 70 °C. The conversion of the monomers in each copolymerization experiment revealed that 4V-NBMes and 6V-NBMes in fact polymerize preferentially, but 5V-NBMes is incorporated at a lower rate than styrene (Table 3-2). This was further verified by elemental analyses of the isolated polymers, which were reasonably consistent with the conversion determined by ^{1}H NMR. To achieve an even more direct comparison of the B−N for C=C substitution that also takes into consideration the steric and electronic effects of the mesityl groups, we also copolymerized the azaborinine monomers with the respective isosteric monomers, *m*MesSt and *p*MesSt, respectively. The results were qualitatively similar, further confirming these reactivity trends.

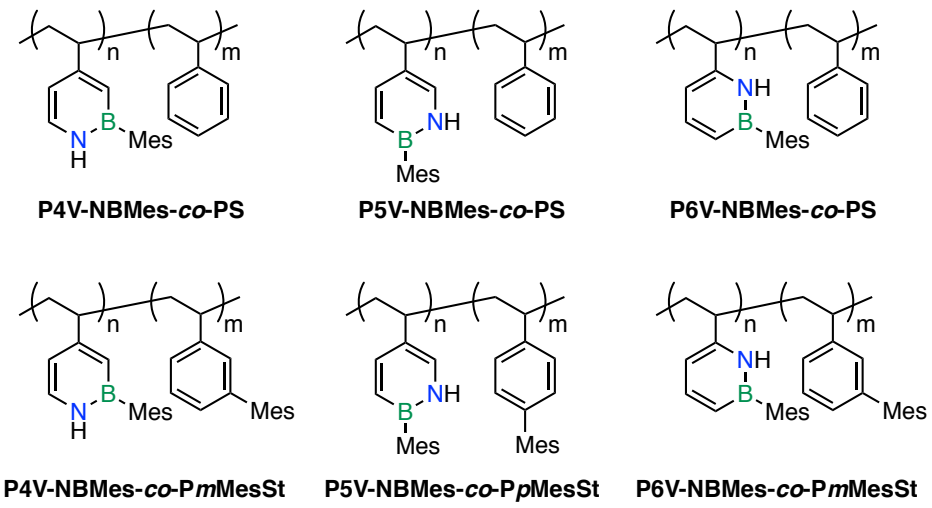

Figure 3-4. B-Mesitylazaborinine-(mesityl)styrene copolymer structures.

Table 3-2. Data for the free radical copolymerization of vinyl-functionalized azaborinines with styrene (St) and mesitylstyrene (MesSt)

Copolymer	Feed ratio [a]	T / t (°C / h)	Conv (BN)[b] (%)	Conv (St/MesSt)[c] (%)	M_n (kDa)[d]	M_w (kDa)[d]	$Đ$ [d]
P4V-NBMes-co-PS	50:50:1	70 / 20	57	50	15.6	50.7	3.25
P5V-NBMes-co-PS	50:50:1	70 / 20	41	63	19.6	39.8	2.02
P6V-NBMes-co-PS	50:50:1	70 / 20	57	40	10.9	32.8	3.02
P4V-NBMes-co-P*m*MesSt	50:50:1	70 / 10	65	66	19.2	54.8	2.85
P5V-NBMes-co-P*p*MesSt	50:50:1	70 / 10	32	54	28.9	59.3	2.05
P6V-NBMes-co-P*m*MesSt	50:50:1	70 / 10	26	15	8.8	24.4	2.77
P6V-NBMes-co-P*m*MesSt	50:50:1	70 / 24	41	14	16.0	56.7	3.55

[a] Feed ratio of [BN monomer]:[styrene]:[AIBN] in anisole, [M1] = [M2] = 2.25 M. [b] Conversion of azaborinine monomer (BN) estimated based on ^{1}H NMR integration of residual BN vinyl signal before purification relative to anisole standard. [c] Conversion of styrene/mesitylstyrene estimated based on ^{1}H NMR integration of residual styrene vinyl signal before purification relative to anisole standard. [d] On the basis of GPC analysis of isolated product in THF relative to PS standards.

The results of these experiments consistently indicate that at about 50% conversion 5V-NBMes with its vinyl group in metaposition to N and para-position to B is incorporated to a lesser extent than (mesityl)styrene, whereas 4V-NBMes and 6VNBMes are incorporated to a similar extent or even preferentially. This could be because of the differences in the tendency of an azaborinine-terminated polymer radical to add to another azaborinine monomer (azaborinine homopolymerization) and/or the tendency of a (mesityl)styrene-terminated polymer radical to add to the specific azaborinine monomer (crossover to azaborinine). In-depth reactivity ratio determinations would be necessary to further evaluate the relative monomer reactivities.[38, 52]However, we note that the relatively lower

incorporation of the 5V-NBMes isomer does not correlate well with the calculated BDE trends (see Figure 3-2), which suggested that the radical derived from 6V-NBMes is the most stabilized and that of 4V-NBMes the least stabilized (Table 3-1). The difference in reactivity for 5V-NBMes is therefore more likely related to a radical polarity mismatch[52] in that a nucleophilic benzylic radical is predicted to react more slowly with a relatively electron-rich monomer such as 5V-NBMes.

Polymer Properties. As a precaution, the azaborinine polymers were stored under N_2 atmosphere. However, based on ^{1}H and ^{11}B NMR analyses, the polymers proved to be perfectly stable over a period of over 1 week in air either as a solid or in aerated chloroform solution. The thermal stability of the polymers was established by thermogravimetric analysis (TGA), revealing the decomposition temperatures (onset) for P4V-NBMes and P6V-NBMes at 365 °C and for P5V-NBMes at 377 °C; they are very similar to those of the all-carbon analogues, P*m*MesSt and P*p*MesSt, at 372 and 379 °C, respectively (Figure 3-5A−C). The thermal characteristics were further examined by differential scanning calorimetry (DSC). Previously, we reported that the glass transition temperature of BN-PS (D, $T_{g,onset}$ = 93 °C) was significantly higher than that of PS of similar molecular weight (M_n = 2.0 kg mol^{-1}, $T_{g,onset}$ = 55−60 °C). We tentatively attributed this difference to the polarization of the B−N bonds and the possibility of N−H moieties engaged in hydrogen-bonding interactions. The glass transitions for P4V-NBMes ($M_{n,GPC}$ = 26.9 kg mol^{-1}), P5V-NBMes ($M_{n,GPC}$ = 11.6 kg mol^{-1}), and P6V-NBMes ($M_{n,GPC}$ = 18.2 kg mol^{-1}) were detected at $T_{g,onset}$ = 160, 167, and 138 °C, respectively (Figure 3-5D−F). The glass transitions of the respective all-carbon analogues PmMesSt ($M_{n,GPC}$ = 29.7 kg mol^{-1}) and PpMesSt

($M_{n,GPC}$ = 21.6 kg mol^{-1}) were found at 152 and 183 °C. They all are significantly higher than that for PS, which is ascribed to the steric effect of the bulky mesityl groups in the side chains. When comparing the T_g's of the isostructural polymers P4V-NBMes, P6V-NBMes, and P*m*MesSt to those of the isostructural polymers P5V-NBMes and P*p*MesSt, it is clearly evident that the positioning of the mesityl groups in the para-position leads to an increase in the glass transition temperature. Direct comparisons between the isostructural BN and CC systems are hampered by the differences in the molecular weight and dispersity. For instance, the higher molecular weight of P*p*MesSt may be responsible for the higher T_g in comparison to P5V-NBMes. The relatively higher T_g of P4V-NBMes in comparison to the isosteric P6V-NBMes could be a result of the less hindered environment around the N−H moiety which may facilitate hydrogen-bonding interactions, but the higher dispersity for P4V-NBMes makes it impossible to draw unambiguous conclusions. For the copolymers P4V-NBMes-co-PS, P5VNBMes-co-PS, and P6V-NBMes-co-PS, single glass transitions were observed at 152, 150, and 135 °C in between those recorded for the respective homopolymers and polystyrene (Figure 3-S64 in the appendix).

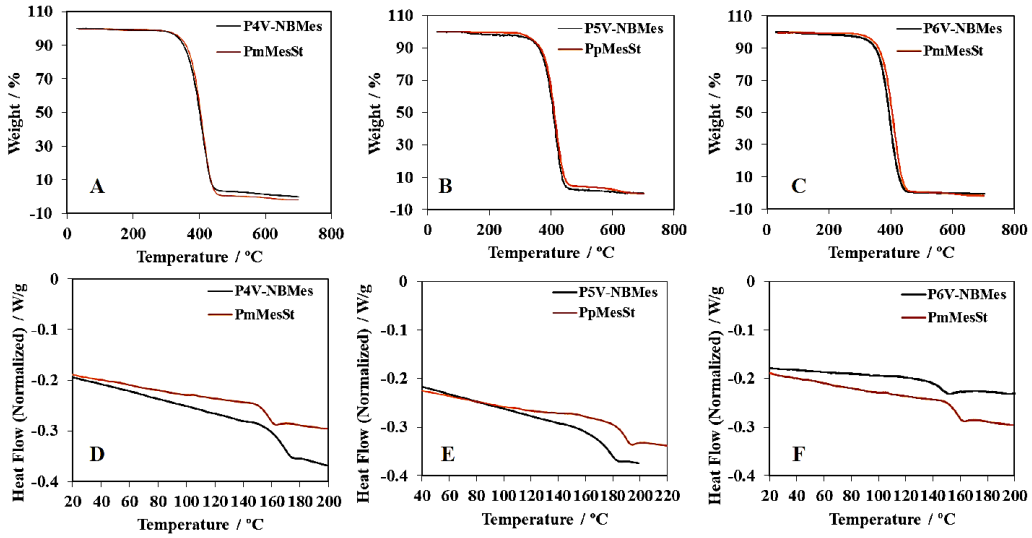

Figure 3-5. Comparisons of TGA traces (A-C) and DSC traces (D-F) for azaborinine polymers with those of the respective isosteric carbon analogs. TGA data were acquired at scan rates of 10 ºC min^{-1} and DSC data at 20 ºC min^{-1}.

Finally, we investigated the photophysical properties of the new polymers and their precursors. The monomers 4V-NBMes, 5V-NBMes, and 6V-NBMes showed the longest wavelength absorption maxima at 298, 299, and 303 nm, respectively, and a second higher energy absorption at ca. 240−250 nm. For the polymers, the longest wavelength absorptions were slightly blue-shifted to 273, 288, and 286 nm because of the smaller π-system of the chromophores (vinylazaborinine vs azaborinine) after polymerization (Figure 3-6). The longest wavelength absorption maxima of the BN compounds are red-shifted in relation to the CC compounds, a typical effect of BN/CC isosterism. [17] Among the isomeric azaborinine monomers and polymers, the absorption maxima are relatively similar. However, intriguingly, the 5V-NBMes monomer exhibits an absorption behavior that is distinct from the other isomers in that its lowest energy absorption peak at 299 nm has a significantly smaller extinction coefficient than its absorption peak at ∼260 nm.

Time-dependent density functional theory (TD-DFT) calculations are consistent with this observation, revealing that the oscillator strength of the first excited state of 5V-NBMes is significantly smaller than that of the other monomers and almost 1 order of magnitude smaller than its second excited state. The unusual absorption behavior of the 5V-NBMes isomer is perhaps because of the fact that it is the only isomer in which the vinyl group is linearly conjugated with the nitrogen lone pair.

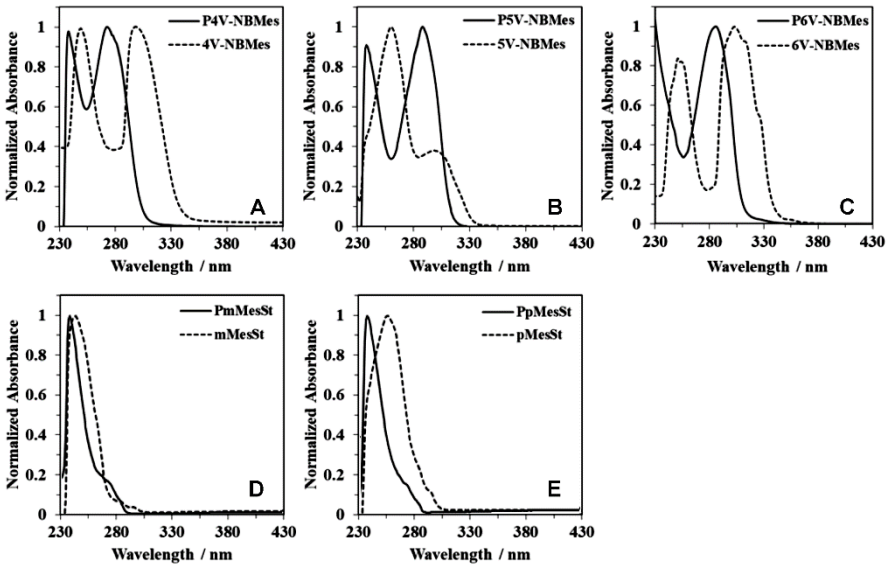

Figure 3-6. Comparison of UV-Vis spectra of B-mesityl azaborinine (A-C) and mesitylstyrene (D-E) homopolymers with those of the respective monomers in THF solution.

The TD-DFT calculations also revealed distinct differences in regard to the nature of the lowest energy absorptions of the isomeric vinyl azaborinine monomers and the respective ethyl derivatives that serve as models for the polymers (Figure 3-7). For 5V-NBMes, both the very weak lowest energy highest occupied molecular orbital (HOMO) to lowest unoccupied molecular orbital (LUMO) and the more intense higher energy HOMO to

LUMO + 1 transition are primarily because of the π−π* excitations localized on the vinylazaborinine moiety. However, the LUMO shows no contributions of the vinyl group, whereas the LUMO + 1 is primarily centered on the vinyl group and the empty p-orbital on boron. The S_0−S_1 transition for 5Et-NBMes is localized on the azaborinine moiety. A similar picture emerges for 6V-NBMes and 6Et-NBMes, except for that the higher energy absorption for 6V-NBMes involves a charge transfer to the mesityl group (LUMO + 3). In sharp contrast, for 4V-NBMes and 4Et-NBMes, which are identical to 5V-NBMes and 5Et-NBMes, other than that the positions of B and N in the ring system are switched, the lowest energy absorptions primarily result from charge transfer from the electron-rich mesityl group to the azaborinine moiety.

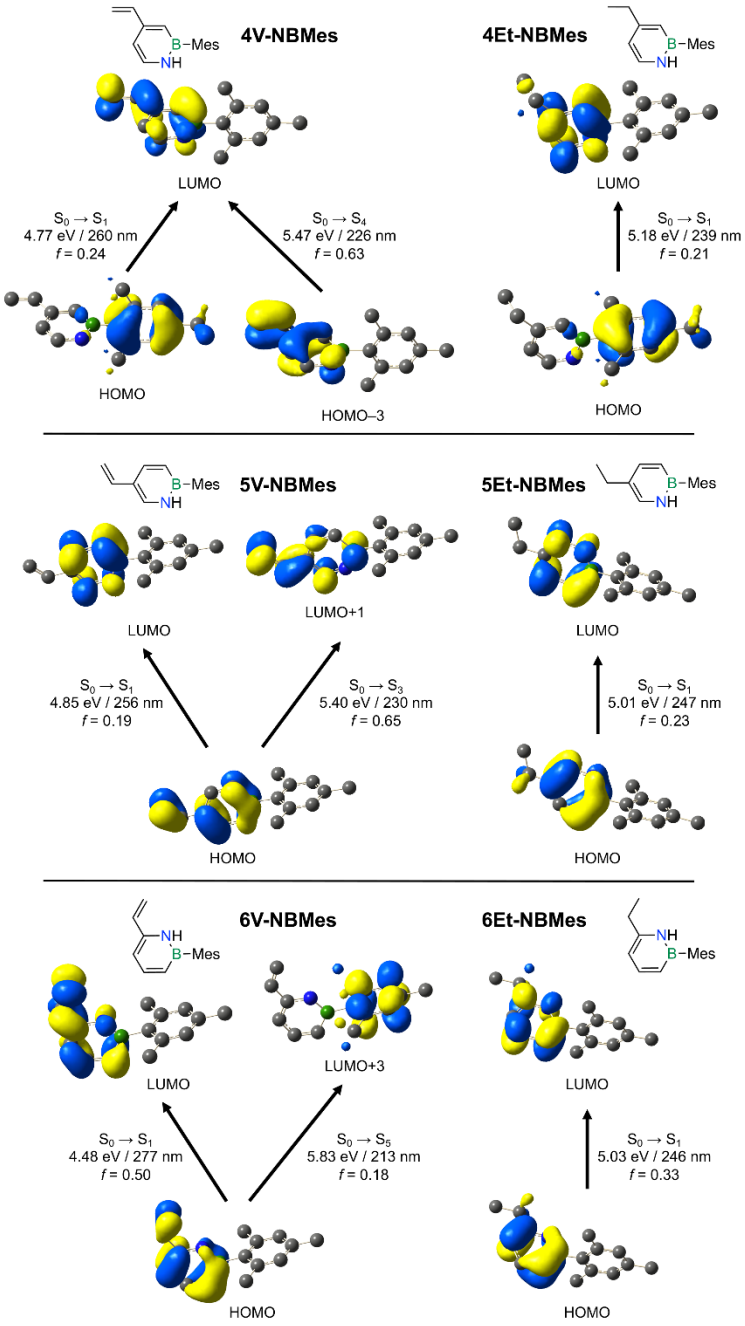

Figure 3-7. Illustration of the calculated electronic excitations for the isomeric vinyl azaborinine monomers (left) and the respective ethyl-substituted model compounds (right); only major contributions are shown.

3.3 Conclusions

To examine the influence of the vinyl group position on the polymerization activity and the polymer properties, we have synthesized three isomeric B-mesityl vinylazaborinines, as well as the carbon analogues with a mesityl group attached in the meta- or para-position of styrene. The monomers have all been successfully converted into high-molecular-weight polymers by AIBN-initiated standard free-radical polymerization. The polymer structures have been verified by multinuclear and multidimensional NMR experiments that unequivocally confirm the presence of the intact azaborinine heterocycles. The azaborinine polymers exhibit high thermal stability similar to the carbon analogues and, despite the presence of more polar B−N units, show good stability to air and moisture. Their glass transition temperatures are significantly higher than for polystyrene and in a similar range as the direct all-carbon analogues derived from mesitylstyrene. The absorptions for the BN polymers are red-shifted in relation to the CC compounds, a typical effect of BN/CC isosterism.

Computational studies demonstrate that the isomeric azaborinine monomers differ in terms of the stabilization of the propagating radical species (stability increases from *p*MesSt = *m*MesSt ≈ 4V-NBMes < 5V-NBMEs < 6V-NBMes) as well as the electron density on the vinyl carbons (electron density increases from 4V-NBMes ≈ *p*MesSt ≈ *m*MesSt < 5V-NBMes ≈ 6V-NBMes) and the vinyl-bearing ipso-carbons (electron density increases from 6V-NBMes < 4V-NBMEs < *p*MesSt ≈ *m*MesSt < 5V-NBMes). Copolymerization experiments with styrene and *m*MesSt/*p*MesSt reveal the preferential incorporation of 4V-NBMes and 6V-NBMes, but less effective incorporation of 5V-NBMes.

Overall, our results demonstrate that isomeric azaborinine monomers exhibit similar reactivity as the isosteric styrene analogues, while offering tunability as a result of attachment of the vinyl groups to different carbon atoms in the heterocyclic framework. The new polymers described herein add to a growing but still underdeveloped class of aromatic polymers, in which a C−C unit is replaced by an isoelectronic but polarized B−N unit. The favorable stability and facile copolymerization suggest that many new functional materials with azaborinine moieties replacing styrenic groups can be accessed.

3.4 Experimental

General Method. All oxygen- and moisture-sensitive manipulations were carried out under an inert atmosphere using either standard Schlenk techniques or a glove box.

NMR data were acquired at 25 ºC. 499.9 MHz ^{1}H and 160.4 MHz ^{11}B NMR data were recorded on a 500 MHz Bruker AVANCE spectrometer, 500.2 MHz ^{1}H and 125.8 MHz ^{13}C NMR data on a 500 MHz Bruker Auto AVANCE spectrometer, and 599.7 MHz ^{1}H, 150.8 MHz ^{13}C and 192.4 MHz ^{11}B NMR data on a Varian INOVA 600 spectrometer. ^{11}B NMR spectra were acquired with boron-free quartz NMR tubes either on the Varian INOVA 600 with a boron-free 5 mm dual broadband gradient probe (Nalorac, Varian Inc., Martinez, CA) or the 500 MHz Bruker Auto Avance with a 5mm PH SEX 500S1 11B-H/F-D probe. ^{1}H and ^{13}C NMR spectra were referenced internally to solvent signals ($CDCl_3$: 7.26 ppm for ^{1}H NMR, 77.16 ppm for ^{13}C NMR) and all other NMR spectra externally to $SiMe_4$ (0 ppm).

High-resolution mass spectrometry data were obtained at the Boston College mass spectrometry facility on a JEOL AccuTOF instrument (JEOL USA, Peabody, MA), equipped with a DART ion source (IonSense, Inc., Danvers, MA) in positive ion mode. GC-MS data were acquired on an Agilent HP6890 GC System with an HP-5MS 5% phenyl methyl siloxane column and Agilent 5973A inert XL EI/CI MSD using helium as the carrier gas at a flow rate of 1 mL/min. The initial oven temperature was 50 °C, after holding for 3 mins the temperature was increased with a 10 °C/min ramp to a final temperature of 220 °C, then held at 220 °C for 15 min (splitless mode of injection, total run time of 22.0 min). GPC-RI analyses were performed in THF (1.0 mL/min, 35 °C) using a Viscotek GPCmax with a VE 2001 GPC solvent/sample module, a 2600 UV-PDA detector, and a TDA 305 triple detector array. A set of two columns consisting of one PLgel 5 mm mixed-D and one PLgel 5 mm mixed-C column was used for separation and ten polystyrene standards (580 Da – 364000 Da, Polymer Laboratories, Varian Inc.) for calibration. Differential scanning calorimetry (DSC) measurements were performed on a TA Instruments Discovery Series system at a scan rate of 20 °C/min. The results reported are from the second heating cycle. Thermogravimetric analyses (TGA) were performed on a TA Instruments Discovery Series analyzer at a heating rate of 10 ºC min^{-1}. UV-visible absorption data were acquired on a Varian Cary 5000 UV-Vis/NIR spectrophotometer.

Materials. THF was distilled from Na/benzophenone, anisole and chlorinated solvents were distilled from CaH_2. Toluene and hexanes were purified using a solvent purification system (Innovative Technologies). Azobisisobutyronitrile (AIBN) initiator was recrystallized in methanol. Azaborinines **1**,[44] **3**,[44] and **6**[45] were prepared according to

previously reported procedures. 3-Vinylphenylboronic acid and 4-vinylphenylboronic acid were purchased from Combi Blocks and 2-bromomesitylene from Acros Organics. All other solvents and chemicals were purchased from commercial sources and used without further purification unless noted otherwise.

Syntheses of N-(tert-butyldimethylsilyl)-B-Mesityl-4-vinyl-1,2-dihydro-1,2-azaborinine (2). A 75 mL pressure vessel was charged with N-(tert-butyldimethylsilyl)-B-mesityl-4-(4,4,5,5-tetramethyl-1,3,2-dioxoborolanyl)-1,2-dihydro-1,2-azaborinine (1, 0.510 g, 1.20 mmol), bromo-ethylene 1.0 M THF solution (4.81 mL, 4.81 mmol), Pd(dppf)Cl_2 (0.044 g, 0.60 mmol), KOH (0.202 g, 3.61 mmol), H_2O (1.0 mL), and THF (5.0 mL). The KOH pellets were ground into a powder and the H_2O was sparged with argon for 1 hour prior to use. The reaction mixture was then heated at 70 ^{o}C for 1 hour. The organic layer was decanted, and the reaction mixture was concentrated under reduced pressure. The desired product was obtained as a yellow oil after purification by silica gel chromatography with 99:1 pentane:ether as the eluent (0.312 g, 77%). ^{1}H NMR (400 MHz, CD_2Cl_2) δ 7.45 (d, J = 7.1 Hz, 1H), 6.77 (s, 2H), 6.62 (m, 1H), 6.54 (m, 1H), 6.44 (s, 1H), 5.79 (dd, J = 17.6, 1.1 Hz, 1H), 5.30 (m, 1H), 2.26 (s, 3H), 2.06 (s, 6H), 0.91 (s, 9H), -0.00 (s, 6H). ^{13}C NMR (126 MHz, CD_2Cl_2) δ 149.67, 138.96, 138.94, 138.63, 136.23, 126.72, 115.67, 108.18, 27.13, 23.08, 20.81, 19.04, -3.69 (the carbons attached to boron were not observed). ^{11}B NMR (160 MHz, CD_2Cl_2) δ 40.00. HRMS (DART) calcd. for $C_{21}H_{32}BNSi$ ($[M+H]^+$) 338.2475, found 338.248.

Synthesis of N-(tert-butyldimethylsilyl)-B-mesityl-5-iodo-1,2-dihydro-1,2-azaborinine (4). A 100 mL round bottom flask was charged with THF (10 mL) and cooled to –78 ºC. n-butyllithium 2.5 M hexanes solution (0.89 mL, 2.2 mmol) was added via syringe. N-(tert-butyldimethylsilyl)-B-mesityl-5-(4,4,5,5-tetramethyl-1,3,2-dioxoborolanyl)-1,2-dihydro-1,2-azaborinine (3, 750 mg, 1.72 mmol) was dissolved in THF (5.0 mL) and added dropwise via syringe to the flask containing n-butyllithium. The reaction mixture was allowed to warm to room temperature, whereupon the formation of the borate was confirmed by ^{11}B NMR (δ 2.83). The reaction mixture was again cooled to –78 ºC. I_2 (1.75 g, 6.88 mmol) was dissolved in methanol (10 mL) and added via syringe to the flask containing the borate. The reaction mixture was allowed to stir at –78 ºC for 30 minutes, then was allowed to warm to room temperature over a period of 1 hour. The reaction mixture was quenched with aqueous Na_2SO_3 and then extracted with hexanes. The organic layer was then washed with brine. Finally, the organic layer was dried over $MgSO_4$, passed through a Buchner funnel lined with filter paper, and concentrated in vacuo. The desired product was obtained as a highly viscous yellow oil after purification by silica gel chromatography with hexanes as the eluent (676 mg, 90%). ^{1}H NMR (500 MHz, C_6D_6) δ 7.84 (s, 1H), 7.70 (dd, J = 11.5, 1.7 Hz, 1H), 6.79 (s, 2H), 6.53 (d, J = 11.5 Hz, 1H), 2.22 (s, 3H), 2.12 (s, 6H), 0.75 (s, 9H), -0.14 (s, 6H). ^{13}C NMR (126 MHz, CD_2Cl_2) δ 150.01, 143.41, 138.57, 136.63, 126.83, 109.99, 26.96, 23.07, 20.80, 18.96, -3.75. (the carbons adjacent to boron were not observed). ^{11}B NMR (160 MHz, C_6D_6) δ 38.96. HRMS (DART) calcd. for $C_{19}H_{30}BNSiI$ ($[M+H]^+$) 438.1285, found 438.1281.

Synthesis of N-(*tert*-butyldimethylsilyl)-B-Mesityl-5-vinyl-1,2-dihydro-1,2-azaborinine (5). A 150 mL pressure vessel was charged with N-(*tert*-butyldimethylsilyl)-B-mesityl-5-iodo-1,2-dihydro-1,2-azaborinine (**4**, 2.00 g, 4.57 mmol), 4,4,5,5-tetramethyl-2-vinyl-1,3,2-dioxaborolane (1.06 g, 6.86 mmol), Pd(dppf)Cl_2 (0.167 g, 0.229 mmol), KOH (0.77 g, 13.7 mmol), H_2O (2.8 mL), and THF (28 mL). The reaction mixture was heated at 60 ºC for 30 minutes. The organic layer was decanted, and volatiles were removed *in vacuo*. The product was obtained as a pale yellow oil after purification by silica gel chromatography with 99:1 pentane:ether as the eluent (1.38 g, 89%). ^{1}H NMR (500 MHz, CD_2Cl_2) δ 7.88 (dd, J = 11.2, 1.8 Hz, 1H), 7.42 (s, 1H), 6.77 (s, 2H), 6.59 (m, 2H), 5.52 (d, J = 17.6 Hz, 1H), 5.03 (d, J = 11.0 Hz, 1H), 2.27 (s, 3H), 2.06 (s, 6H), 0.92 (s, 9H), 0.02 (s, 6H). ^{13}C NMR (126 MHz, CD_2Cl_2) δ 139.52, 138.94, 138.59, 136.38, 135.50, 121.88, 109.99, 108.61, 27.11, 23.04, 20.81, 18.96, -3.66 (the boron-bound carbons were not observed). ^{11}B NMR (160 MHz, CD_2Cl_2) δ 40.32. HRMS (DART) calcd. for $C_{21}H_{33}BNSi$ ($[M+H]^+$) 338.2475, found 338.248.

Synthesis of B-Mesityl-4-vinyl-1,2-dihydro-1,2-azaborinine (4V-NBMes). A 100 mL round bottom flask was charged with N-(*tert*-butyldimethylsilyl)-B-mesityl-4-vinyl-1,2-dihydro-1,2-azaborinine (**2**, 1.28 g, 3.79 mmol), H_2O (0.683 g, 37.9 mmol) and THF (30 mL). The reaction mixture was allowed to stir at room temperature, and a 1.0 M solution of tetrabutylammonium fluoride in THF (3.79 mL, 3.79 mmol) was added dropwise via syringe. More H_2O was added and the crude product was extracted with diethyl ether. The organic layer was dried over magnesium sulfate, passed through a Buchner funnel lined with filter paper, then concentrated *in vacuo*. The product was obtained as a clear, colorless

oil after purification by silica gel chromatography with 99:1 pentane:ether as the eluent (0.70 g, 83%). ^{1}H NMR (599.7 MHz, $CDCl_3$) δ = 7.73 (s, 1H), 7.36 (t, *J* = 7.2 Hz, 1H), 6.88 (s, 2H), 6.77 (s, 1H), 6.71 (dd, *J* = 17, 11 Hz 1H), 6.54 (d, *J* = 6.6 Hz, 1H), 5.80 (d, *J* = 17 Hz, 1H), 5.32 (d, *J* = 11 Hz, 1H), 2.31 (s, 3H), 2.18 (s, 6H). ^{13}C NMR (150.8 MHz, $CDCl_3$) δ = 151.2, 140.4, 139.7, 137.4, 134.3, 129.1 (br), 127.3, 115.9, 107.6, 23.2, 21.3 (the mesityl carbon adjacent to boron was not observed). ^{11}B NMR (160.4 MHz, $CDCl_3$) δ = 36.3. HRMS (DART) calcd. for $C_{15}H_{19}BN$ ($[M+H]^+$) 224.1611, found 224.1621. UV-Vis (THF): λ_{max} = 298, 249 nm.

Synthesis of B-Mesityl-5-vinyl-1,2-dihydro-1,2-azaborinine (5V-NBMes). A 50 mL round bottom flask was charged with N-*tert*-butyldimethylsilyl-B-mesityl-5-vinyl-1,2-dihydro-1,2-azaborinine (**5**, 620 mg, 1.84 mmol), H_2O (331 mg, 18.4 mmol) and THF (12 mL). The reaction mixture was allowed to stir at room temperature and a 1.0 M solution of tetrabutylammonium fluoride in THF (1.84 mL, 1.84 mmol) was added dropwise via syringe. More H_2O was added, and the crude product was extracted with diethyl ether. The organic layer was dried over magnesium sulfate, passed through a Buchner funnel lined with filter paper, and concentrated *in vacuo*. The product was obtained as a clear, colorless oil after purification by silica gel chromatography with 99:1 pentane:ether as the eluent (325 mg, 79%). ^{1}H NMR (599.7 MHz, $CDCl_3$) δ = 8.38 (d, *J* = 13 Hz, 1H), 8.11 (s, 1H), 7.69 (d, *J* = 7.8 Hz, 1H), 7.27 (m, 1H), 7.25 (s, 2H), 6.92 (dd, *J* = 17, 11 Hz, 1H), 5.91 (d, *J* = 18 Hz, 1H), 5.43 (d, *J* = 11 Hz, 1H), 2.68 (s, 3H), 2.54 (s, 6H). ^{13}C NMR (150.8 MHz, $CDCl_3$) δ = 141.0, 140.3, 137.5, 134.9, 133.7, 131.3 (br), 127.3, 121.4, 109.6, 23.1, 21.3. (the mesityl carbon adjacent to boron was not observed). ^{11}B NMR (160.4 MHz, $CDCl_3$) δ

= 36.1. HRMS (DART) calcd. for $C_{15}H_{19}BN$ ([M+H]$^+$) 224.1611, found 224.1621. UV-Vis (THF): λ_{max} = 299, 260 nm.

Synthesis of B-Mesityl-6-vinyl-1,2-dihydro-1,2-azaborinine (6V-NBMes). A sealed reaction vessel was charged with B-mesityl-6-(4,4,5,5-tetramethyl-1,3,2-dioxoborolanyl) -1,2-dihydro-1,2-azaborinine (**6**, 1.50 g, 4.64 mmol), bromoethylene solution (1.0 M THF solution, 18.6 mL, 18.6 mmol), Pd(dppf)Cl_2 (0.102 g, 0.139 mmol), KOH (0.782 g, 13.9 mmol), H_2O (5.0 mL), and MTBE (45 mL). The KOH pellets were ground into a powder and the H_2O was purged with argon for 1 hour prior to use. The reaction mixture was then heated at 80 ºC for 1 hour. The organic layer was decanted, and the reaction mixture was concentrated under reduced pressure. The desired product was obtained as a yellow oil after purification by silica gel chromatography with 95:5 pentane:dichloromethane as the eluent (0.74 g, 71%). ^{1}H NMR (599.7 MHz, $CDCl_3$) δ = 8.02 (br s, 1H), 7.72 (dd, *J* = 11, 6.6 Hz, 1H), 6.92 (s, 2H), 6.87 (d, J = 11 Hz, 1H), 6.59 (dd, *J* = 17, 11 Hz, 1H), 6.37 (d, *J* = 6.6, 1H), 5.57 (d, *J* = 18 Hz, 1H), 5.35 (d, *J* = 11 Hz, 1H), 2.34 (s, 3H), 2.22 (s, 6H). ^{13}C NMR (151 MHz, CD_2Cl_2) δ = 144.2, 141.2, 140.5, 138.3 (br), 137.6, 134.0, 132.0 (br), 127.3, 113.2, 112.0, 23.3, 21.3. ^{11}B NMR (160.4 MHz, $CDCl_3$) δ = 36.3. HRMS (DART) calcd. for $C_{15}H_{19}BN$ ([M+H]$^+$) 224.1611, found 224.1607. UV-Vis (THF): λ_{max} = 303, 251 nm.

Synthesis of *meta*-Mesitylstyrene (*m*MesSt, all-carbon analogue to 4V-NBMes and 6V-NBMes). A 500 mL two-neck Schlenk flask was charged with *meta*-vinylphenylboronic acid (2.66 g, 18.1 mmol), 2-bromomesitylene (3.00 g, 15.1 mmol) and

Na_2CO_3 (6.40 g, 60.4 mmol). Toluene (100 mL), ethanol (20 mL), and H_2O (70 mL) were then added to the reaction vessel. The reaction mixture was purged with N_2 for 20 min. A suspension of $Pd(PPh_3)_4$ (0.52 g, 0.45 mmol) in toluene (10 mL) was then added by syringe. The reaction mixture was heated to 95 °C for 16 hours under nitrogen flow. After cooling to room temperature, water was added to the reaction mixture, and the mixture extracted with dichloromethane. The organic layer was collected, washed with water, and the solvent removed under reduced pressure. The product was obtained as a colorless oil by column chromatography (silica gel, hexanes). Yield: 1.25 g (37%). ^{1}H NMR (500.0 MHz, $CDCl_3$): 7.37 (m, 2H), 7.20 (s, 1H), 7.04 (m, 1H), 6.95 (s, 2H), 6.74 (dd, J = 18, 11 Hz, 1H), 5.75 (d, J = 18 Hz, 1H), 5.25 (d, J = 11 Hz, 1H), 2.33 (s, 3H), 2.01 (s, 6H). ^{13}C NMR (125.8 MHz, $CDCl_3$) δ = 141.4, 138.8, 137.6, 137.0, 136.7, 136.0, 128.9, 128.6, 128.1, 127.2, 124.5, 113.8, 21.0, 20.8. GC-MS (retention time 20 min) calcd. for $C_{17}H_{18}$ (m/z) 222.1, found 222.2. UV-Vis (THF): λ_{max} = 244 nm.

Synthesis of *ortho*-Mesitylstyrene (*o*MesSt). A 250 mL three-neck Schlenk flask was charged with *ortho*-vinylphenylboronic acid (0.88 g, 7.68 mmol), 2-bromomesitylene (1.00 g, 5.02 mmol) and Na_2CO_3 (2.13 g, 0.02 mol). Toluene (20 mL), ethanol (20 mL), and H_2O (70 mL) were then added. The mixture was purged with N_2 for 20 min. A suspension of $Pd(PPh_3)_4$ (0.17 g, 0.15 mmol) in toluene (10 mL) was then added by syringe. The mixture was heated to 95 °C for 16 hours under nitrogen flow. After cooling to room temperature, water was added to the reaction mixture, and the mixture extracted with dichloromethane. The organic layer was collected, washed with water, and the solvent removed under reduced pressure. The residue was purified by column chromatography (silica gel, hexanes),

giving the product as a colorless oil. Yield: 0.35 g (31%). ^{1}H NMR (500.0 MHz, $CDCl_3$): 7.68 (d, J = 7.0 Hz, 1H), 7.32 (m, 2H), 7.05 (d, J = 7.0 Hz, 1H), 6.94 (s, 2H), 6.33 (dd, J = 18, 11 Hz, 1H), 5.64 (d, J = 18 Hz, 1H), 5.07 (d, J = 11 Hz, 1H), 2.35 (s, 3H), 1.92 (s, 6H). ^{13}C NMR (125.8 MHz, $CDCl_3$) δ = 139.9, 137.4, 136.8, 136.3, 136.0, 134.8, 129.9, 128.1, 128.0, 127.3, 125.0, 114.4, 21.2, 20.4. GC-MS (retention time 13 min) calcd. for $C_{17}H_{18}$ (m/z) 222.1, found 222.2.

FREE RADICAL HOMOPOLYMERIZATION EXPERIMENTS

General Procedure for the Free Radical polymerization of Azaborinine Monomers. Into a 10 mL Schlenk tube were loaded the azaborinine monomer (50.0 mg, 224 μmol), 20 μL of an 0.37 M AIBN solution in anisole, and 30 μL of anisole ([azaborinine]/[AIBN] = 50/1). After 3 freeze-pump-thaw cycles, the tube was fully immersed in a 70 °C oil bath and kept stirring for 24 h. The tube was placed in liquid nitrogen to terminate the reaction. One drop of the polymerization solution was taken for ^{1}H NMR measurement to determine the monomer conversion. The polymers were then precipitated in a 10-fold volume of hexanes at -20 °C, redissolved in toluene, precipitated in a 10-fold volume of cold hexanes again, and freeze-dried in benzene. After drying in high vacuum, the azaborinine polymers were obtained as off-white powders.

General Procedure for the Free Radical Copolymerization of Mesitylstyrene Monomers. Into a 10 mL Schlenk tube were loaded the mesitylstyrene monomer (100 mg, 448 μmol), 20 μL of an 0.45 M AIBN solution in anisole, and 80 μL of anisole

([mesitylstyrene]/[AIBN] = 50/1). The scale was doubled for *para*-mesitylstyrene (*p*MesSt). After 3 freeze-pump-thaw cycles, the tube was fully immersed in a 70 °C oil bath and kept stirring for 6.5 h (for *o*MesSt the mixture was heated for 21 h). The tube was placed in liquid nitrogen to terminate the reaction. One drop of the polymerization solution was taken for ^{1}H NMR measurement to determine the monomer conversion (>95%). The polymer was then precipitated in a 10-fold volume of hexanes, redissolved in toluene, precipitated in a 10-fold volume of cold hexanes again, and freeze-dried in benzene. After drying in high vacuum, the mesitylstyrene polymers were obtained as off-white powders.

Homopolymerization of Azaborinine Monomer 4V-NBMes.

Scale: 50 mg of Monomer 4V-NBMes, [4V-NBMes]/[AIBN] = 50/1.

Monomer conversion: 63%; from ^{1}H NMR integration of residual vinyl group signals of monomer relative to Me group of anisole.

Isolated yield for P4V-NBMes: 22.0 mg (44%).

^{11}B NMR (160.4 MHz, $CDCl_3$): δ = 29.1.

^{13}C NMR (150.8 MHz, $CDCl_3$): ^{13}C NMR (150.8 MHz, $CDCl_3$) δ = 161.9, 140.2, 139.0, 136.8, 133.4, 127.1, 111.8, 42.8, 23.3, 21.3.

GPC-RI: $M_{n,GPC}$ = 26900 g mol^{-1}, $M_{w,GPC}$ = 130400 g mol^{-1}, $Đ$ = 4.84. $X_{n\ GPC}$ = 119.

UV-Vis (THF): λ_{max} = 273, 238 nm.

Homopolymerization of Azaborinine Monomer 5V-NBMes.

Scale: 50 mg of Monomer 5V-NBMes, [5V-NBMes]/[AIBN] = 50/1.

Monomer conversion: 63%; from ^{1}H NMR integration of residual vinyl group signals of monomer relative to Me group of anisole.

Isolated yield: 21.0 mg (42%).

^{11}B NMR (160.4 MHz, $CDCl_3$): δ = 28.9.

^{13}C NMR (150.8 MHz, $CDCl_3$): δ = 144.0, 140.0, 138.1, 137.3, 132.0, 131.3, 127.3, 125.7, 41.4, 38.3, 23.2, 21.2.

GPC-RI: $M_{n,GPC}$ = 11600 g mol^{-1}, $M_{w,GPC}$ = 46100 g mol^{-1}, $Đ$ = 3.98. $X_{n\ GPC}$ = 52.

UV-Vis (THF): λ_{max} = 288, 238 nm.

Homopolymerization of Azaborinine Monomer 6V-NBMes.

Scale: 50 mg of Monomer 6V-NBMes, [6V-NBMes]/[AIBN] = 50/1.

Monomer conversion: 51%; from ^{1}H NMR integration of residual vinyl group signals of monomer relative to Me group of anisole.

Isolated yield: 16.1 mg (32%).

^{11}B NMR (160.4 MHz, $CDCl_3$): δ = 29.5.

^{13}C NMR (150.8 MHz, $CDCl_3$): δ = 146.7, 144.1, 140.0, 137.6, 129.5, 127.4, 109.8, 41.3, 23.4, 21.3.

GPC-RI: $M_{n,GPC}$ = 18200 g mol^{-1}, $M_{w,GPC}$ = 44400 g mol^{-1}, $Đ$ = 2.44, $X_{n,GPC}$ = 80.

UV-Vis (THF): λ_{max} = 286 nm.

Homopolymerization of *meta*-Mesitylstyrene (*m*MesSt).

Scale: 100 mg of Monomer *m*MesSt, [*m*MesSt]/[AIBN] = 50/1.

Monomer conversion: >95%; from ^{1}H NMR integration of residual vinyl group signals of monomer relative to Me group of anisole.

Isolated yield: 56.1 mg (56%).

^{13}C NMR (125.8 MHz, $CDCl_3$): δ = 146.0, 145.0, 144.6, 140.8, 139.2, 136.1, 135.8, 128.0, 126.7, 40.5, 21.2, 20.8.

GPC-RI: $M_{n,GPC}$ = 29700 g mol^{-1}, $M_{w,GPC}$ = 61300 g mol^{-1}, $Đ$ = 2.07. $X_{n\ GPC}$ = 134.

UV-Vis (THF): λ_{max} = 239 nm.

Homopolymerization of *para*-Mesitylstyrene (*p*MesSt).

Scale: 200 mg of Monomer *p*MesSt, [*p*MesSt]/[AIBN] = 50/1.

Monomer conversion: 82%; from ^{1}H NMR integration of residual vinyl group signals of monomer relative to Me group of anisole.

Isolated yield: 103.0 mg (51%).

^{13}C NMR (125.8 MHz, $CDCl_3$): δ = 144.9, 143.5, 142.8, 139.1, 138.5, 136.3, 136.0, 129.0, 128.1, 40.6, 21.1, 20.8.

GPC-RI: $M_{n,GPC}$ = 21600 g mol^{-1}, $M_{w,GPC}$ = 42000 g mol^{-1}, $Đ$ = 1.95. $X_{n\ GPC}$ = 97.

UV-Vis (THF): λ_{max} = 239 nm.

Homopolymerization of *ortho*-Mesitylstyrene (*o*MesSt).

Scale: 100 mg of Monomer *o*MesSt, [*o*MesSt]/[AIBN] = 50/1. The reaction time was extended to 21 h.

Monomer conversion: 27%; from ^{1}H NMR integration of residual vinyl group signals of monomer relative to Me group of anisole.

Isolated yield: ca. 5 mg.

GPC-UV: $M_{n,GPC}$ = 5000 g mol^{-1}, $M_{w,GPC}$ = 7000 g mol^{-1}, $Đ$ = 1.39. $X_{n\ GPC}$ = 22.

FREE RADICAL COPOLYMERIZATION EXPERIMENTS

General Procedure for the Free Radical Copolymerization of Azaborinine Monomers with Styrene. Into a 10 mL Schlenk tube were loaded the azaborinine monomer (50 mg, 224 μmol), styrene monomer (23.3 mg, 224 μmol), 40 μL of an 0.11 M AIBN solution in

anisole, and 60 μL of anisole ([azaborinine]/[St]/[AIBN] = 50/50/1). After 3 freeze-pump-thaw cycles, the tube was fully immersed in a 70 °C oil bath and the mixture kept stirring for 20 h. The tube was placed in liquid nitrogen to terminate the reaction. One drop of the polymerization solution was taken for ^{1}H NMR measurement to determine the conversion of the monomers. The polymer was then precipitated in a 10-fold volume of hexanes, redissolved in toluene, precipitated in a 10-fold volume of cold hexanes again, and freeze-dried in benzene. After drying in high vacuum, the copolymers were obtained as off-white powders. They were analyzed by ^{1}H NMR, elemental analysis, GPC-RI, and DSC.

General Procedure for the Free Radical Copolymerization of Azaborinine Monomers with Mesitylstyrene Derivatives. Into a 10 mL Schlenk tube were loaded the azaborinine monomer (50 mg, 224 μmol), MesSt monomer (50.0 mg, 224 μmol), 40 μL of an 0.11 M AIBN solution in anisole, and 60 μL of anisole ([azaborinine]/[MesSt]/[AIBN] = 50/50/1). After 3 freeze-pump-thaw cycles, the tube was fully immersed in a 70 °C oil bath and kept stirring for 10 h. The tube was placed in liquid nitrogen to terminate the reaction. One drop of the polymerization solution was taken for ^{1}H NMR measurement to determine the conversion of the monomers. The polymer was then precipitated in a 10-fold volume of hexanes, redissolved in toluene, precipitated in a 10-fold volume of cold hexanes again, and freeze-dried in benzene. After drying in high vacuum, the copolymers were obtained as off-white powders. They were analyzed by ^{1}H NMR, elemental analysis, and GPC-RI.

Copolymerization of 4V-NBMes and styrene.

Scale: 50 mg of each monomer, [azaborinine]/[St]/[AIBN] = 50/50/1.

Monomer conversion: 4V-NBMes: 57%; styrene: 50% from ^{1}H NMR integration of residual vinyl group signals of monomers relative to Me group of anisole.

Isolated yield: 40.0 mg.

GPC-RI: $M_{n,GPC}$ = 15600 g mol^{-1}, $M_{w,GPC}$ = 50700 g mol^{-1}, $Đ$ = 3.25.

Elemental analysis: Calcd for $(C_{15}H_{18}B_1N_1)_n(C_8H_8)_m$ with n/m = 1.14/1 (from monomer conversion by ^{1}H NMR integration): C 84.09; H 8.02; N 4.45. Found: C 83.39; H 7.96; N 4.64.

Copolymerization of 5V-NBMes and styrene.

Scale: 50 mg of each monomer, [azaborinine]/[St]/[AIBN] = 50/50/1.

Monomer conversion: 5V-NBMes: 41%; styrene: 63% from ^{1}H NMR integration of residual vinyl group signals of monomers relative to Me group of anisole.

Isolated yield: 43.0 mg.

GPC-RI: $M_{n,GPC}$ = 19600 g mol^{-1}, $M_{w,GPC}$ = 39800 g mol^{-1}, $Đ$ = 2.02.

Elemental analysis: Calcd for $(C_{15}H_{18}B_1N_1)_n(C_8H_8)_m$ with n/m = 0.65/1 (from monomer conversion by ^{1}H NMR integration): C 85.56; H 7.97; N 3.65. Found C 85.53; H 7.88; N 3.44.

Copolymerization of 6V-NBMes and styrene.

Scale: 50 mg of each monomer, [azaborinine]/[St]/[AIBN] = 50/50/1.

Monomer conversion: 6V-NBMes: 57%; styrene: 40% from ^{1}H NMR integration of residual vinyl group signals of monomers relative to Me group of anisole.

Isolated yield: 34.4 mg.

GPC-RI: $M_{n,GPC}$ = 10900 g mol^{-1}, $M_{w,GPC}$ = 32800 g mol^{-1}, $Đ$ = 3.02.

Elemental analysis: Calcd for $(C_{15}H_{18}B_1N_1)_n(C_8H_8)_m$ with n/m = 1.42/1 (from monomer conversion by ^{1}H NMR integration): C 83.59; H 8.04; N 4.72. Found C 82.00; H 7.84; N 4.85.

Copolymerization of 4V-NBMes and *meta*-mesitylstyrene (*m*MesSt)

Scale: 50 mg of each monomer, [azaborinine]/[MesSt]/[AIBN] = 50/50/1.

Monomer conversion: 4V-NBMes: 65%; *m*MesSt: 66% from ^{1}H NMR integration of residual vinyl group signals of monomers relative to Me group of anisole.

Isolated yield: 58.0 mg (58%).

GPC-RI: $M_{n,GPC}$ = 19200 g mol^{-1}, $M_{w,GPC}$ = 54800 g mol^{-1}, $Đ$ = 2.85.

Elemental analysis: Calcd for $(C_{15}H_{18}B_1N_1)_n(C_{17}H_{18})_m$ with n/m = 1/1 (from monomer conversion by ^{1}H NMR integration): C 86.28; H 8.15; N 3.14. Found C 84.91; H 8.12; N 3.12.

Copolymerization of 5V-NBMes and *para*-mesitylstyrene (*p*MesSt).

Scale: 50 mg of each monomer, [azaborinine]/[MesSt]/[AIBN] = 50/50/1.

Monomer conversion: 5V-NBMes: 32%; *p*MesSt: 54% from ^{1}H NMR integration of residual vinyl group signals of monomers relative to Me group of anisole.

Isolated yield: 71.6 mg (72%).

GPC-RI: $M_{n,GPC}$ = 28900 g mol^{-1}, $M_{w,GPC}$ = 59300 g mol^{-1}, $Đ$ = 2.05.

Elemental analysis: Calcd for $(C_{15}H_{18}B_1N_1)_n(C_{17}H_{18})_m$ with n/m = 0.59/1 (from monomer conversion by ^{1}H NMR integration): C 87.71; H 8.15; N 2.33. Found C 87.71; H 8.15; N 2.20.

Copolymerization of 6V-NBMes and *meta*-mesitylstyrene (*m*MesSt).

Scale: 50 mg of each monomer, [azaborinine]/[MesSt]/[AIBN] = 50/50/1.

Monomer conversion: 6V-NBMes: 26%; *m*MesSt: 15% from ^{1}H NMR integration of residual vinyl group signals of monomers relative to Me group of anisole after 10 hours. In another experiment the polymerization time was extended to 24 h (monomer conversion**:** 6V-NBMes: 41%; *m*MesSt: 14% from ^{1}H NMR integration). All analytical data provided correspond to the experiment with a 10 h reaction time.

Isolated yield: 27.6 mg (28%).

GPC-RI: $M_{n,GPC}$ = 8800 g mol^{-1}, $M_{w,GPC}$ = 24400 g mol^{-1}, $Đ$ = 2.77.

Elemental analysis: Calcd for $(C_{15}H_{18}B_1N_1)_n(C_{17}H_{18})_m$ with n/m = 1.73/1 (from monomer conversion by ^{1}H NMR integration): C 84.80; H 8.14; N 3.98. Found C 85.71; H 8.12; N 3.52. Note that the elemental analysis is more consistent with a ratio of n/m = 1.25/1.

3.5 References

1.Liu, Z. Q.; Marder, T. B., B-N versus C-C: How similar are they? *Angew. Chem. Int. Ed.* **2008,** *47* (2), 242-244.

2.Bosdet, M. J. D.; Piers, W. E., B-N as a C-C substitute in aromatic systems. *Can. J. Chem.* **2009,** *87* (1), 8-29.

3.Campbell, P. G.; Marwitz, A. J. V.; Liu, S. Y., Recent Advances in Azaborine Chemistry. *Angew. Chem. Int. Edit.* **2012,** *51* (25), 6074-6092.

4.Narita, A.; Wang, X. Y.; Feng, X. L.; Müllen, K., New advances in nanographene chemistry. *Chem. Soc. Rev.* **2015,** *44* (18), 6616-6643.

5.Helten, H., B=N Units as Part of Extended pi-Conjugated Oligomers and Polymers. *Chem.-Eur. J.* **2016,** *22* (37), 12972-12982.

6.Bélanger-Chabot, G.; Braunschweig, H.; Roy, D. K., Recent Developments in Azaborinine Chemistry. *Eur. J. Inorg. Chem.* **2017,** (38-39), 4353-4368.

7.Stępień, M.; Gońka, E.; Żyła, M.; Sprutta, N., Heterocyclic Nanographenes and Other Polycyclic Heteroaromatic Compounds: Synthetic Routes, Properties, and Applications. *Chem. Rev.* **2017,** *117* (4), 3479-3716.

8.Giustra, Z. X.; Liu, S. Y., The State of the Art in Azaborine Chemistry: New Synthetic Methods and Applications. *J. Am. Chem. Soc.* **2018,** *140* (4), 1184-1194.

9.Baggett, A. W.; Guo, F.; Li, B.; Liu, S. Y.; Jäkle, F., Regioregular Synthesis of Azaborine Oligomers and a Polymer with a syn Conformation Stabilized by N-H center dot center dot center dot pi Interactions. *Angew. Chem. Int. Ed.* **2015,** *54* (38), 11191-11195.

10.Lee, H.; Fischer, M.; Shoichet, B. K.; Liu, S. Y., Hydrogen Bonding of 1,2-Azaborines in the Binding Cavity of T4 Lysozyme Mutants: Structures and Thermodynamics. *J. Am. Chem. Soc.* **2016,** *138* (37), 12021-12024.

11.Hatakeyama, T.; Hashimoto, S.; Seki, S.; Nakamura, M., Synthesis of BN-Fused Polycyclic Aromatics via Tandem Intramolecular Electrophilic Arene Borylation. *J. Am. Chem. Soc.* **2011,** *133* (46), 18614-18617.

12.Wang, X. Y.; Wang, J. Y.; Pei, J., BN Heterosuperbenzenes: Synthesis and Properties. *Chem.-Eur. J.* **2015,** *21* (9), 3528-3539.

13.Zhao, R. Y.; Dou, C. D.; Xie, Z. Y.; Liu, J.; Wang, L. X., Polymer Acceptor Based on BN Units with Enhanced Electron Mobility for Efficient All-Polymer Solar Cells. *Angew. Chem. Int. Ed.* **2016,** *55* (17), 5313-5317.

14.Zhang, W. D.; Li, G. P.; Xu, L. T.; Zhuo, Y.; Wan, W. M.; Yan, N.; He, G., 9,10-Azaboraphenanthrene-containing small molecules and conjugated polymers: synthesis and their application in chemodosimeters for the ratiometric detection of fluoride ions. *Chem. Sci.* **2018,** *9* (19), 4444-4450.

15.Zhang, J. Y.; Liu, F. D.; Sun, Z.; Li, C. L.; Zhang, Q.; Zhang, C.; Liu, Z. Q.; Liu, X. G., Synthesis, characterization and properties of aryl-fused bis-BN dihydropyrenes. *Chem. Commun.* **2018,** *54* (59), 8178-8181.

16.Mellerup, S.; Wang, S., Boron-Doped Molecules for Optoelectronics. *Trends Chem.* **2019**, 1, 77−89.

17.McConnell, C. R.; Campbell, P. G.; Fristoe, C. R.; Memmel, P.; Zakharov, L. N.; Li, B.; Darrigan, C.; Chrostowska, A.; Liu, S. Y., Synthesis and Characterization of 1,2-Azaborine-Containing Phosphine Ligands: A Comparative Electronic Structure Analysis. *Eur. J. Inorg. Chem.* **2017,** *2017* (15), 2207-2210.

18.Knack, D. H.; Marshall, J. L.; Harlow, G. P.; Dudzik, A.; Szaleniec, M.; Liu, S. Y.; Heider, J., BN/CC Isosteric Compounds as Enzyme Inhibitors: N- and B-Ethyl-1,2-azaborine Inhibit Ethylbenzene Hydroxylation as Nonconvertible Substrate Analogues. *Angew. Chem. Int. Edit.* **2013,** *52* (9), 2599-2601.

19.Vlasceanu, A.; Jessing, M.; Kilburn, J. P., BN/CC isosterism in borazaronaphthalenes towards phosphodiesterase 10A (PDE10A) inhibitors. *Bioorgan. Med. Chem.* **2015,** *23* (15), 4453-4461.

20.Manners, I., Synthetic Metal-Containing Polymers. Wiley-VCH: 2004.

21.Priegert, A. M.; Rawe, B. W.; Serin, S. C.; Gates, D. P., Polymers and the p-block elements. *Chem. Soc. Rev.* **2016,** *45* (4), 922-953.

22.Gon, M.; Tanaka, K.; Chujo, Y., Recent progress in the development of advanced element-block materials. *Polym. J.* **2018,** *50* (1), 109-126.

23.Baumgartner, T.; Jäkle, F., *Main group strategies towards functional hybrid materials*. John Wiley & Sons: Hoboken, NJ, 2018.

24.van de Wouw, H. L.; Klausen, R. S., BN Polystyrenes: Emerging Optical Materials & Versatile Intermediates. *J. Org. Chem.* **2019,** 84,1117−1125.

25.Jäkle, F., Borylated Polystyrenes as Versatile Functional Materials. In *New Polymeric Materials Based on Element-Blocks* Chujo, Y., Ed. Springer Nature: Singapore, 2019; pp 59-76.

26.Vidal, F.; Jäkle, F., Functional Polymeric Materials Based on Main Group Elements. *Angew. Chem. Int. Ed.* **2019**, 58, 5846−5870.

27.Staubitz, A.; Hoffmann, J.; Gliese, P. J., Group 13–Group 15 Element Bonds Replacing Carbon–Carbon Bonds. In *Main Group Polyolefin Analogs in Smart Inorganic Polymers*, Hey-Hawkins, E.; Hissler, M., Eds. Wiley: Weinheim, **2019**.

28.Staubitz, A., Generation of High-Molecular-Weight Polymers with Diverse Substituents: An Unusual Metal-Free Synthesis of Poly(aminoborane)s. *Angew. Chem. Int. Ed.* **2018,** *57* (21), 5990-5992.

29.Staubitz, A.; Robertson, A. P. M.; Manners, I., Ammonia-Borane and Related Compounds as Dihydrogen Sources. *Chem. Rev.* **2010,** *110* (7), 4079-4124.

30.Staubitz, A.; Robertson, A. P. M.; Sloan, M. E.; Manners, I., Amine- and Phosphine-Borane Adducts: New Interest in Old Molecules. *Chem. Rev.* **2010,** *110* (7), 4023-4078.

31.Resendiz-Lara, D. A.; Stubbs, N. E.; Arz, M. I.; Pridmore, N. E.; Sparkes, H. A.; Manners, I., Boron-nitrogen main chain analogues of polystyrene: poly(B-aryl) aminoboranes via catalytic dehydrocoupling. *Chem. Commun.* **2017,** *53* (85), 11701-11704.

32.Ayhan, O.; Eckert, T.; Plamper, F. A.; Helten, H., Poly(iminoborane)s: An Elusive Class of Main-Group Polymers? *Angew. Chem. Int. Ed.* **2016,** *55* (42), 13321-13325.

33.Su, K.; Remsen, E. E.; Thompson, H. M.; Sneddon, L. G., Syntheses and Properties of Poly(B-vinylborazine) and Poly(styrene-co-B-vinylborazine) Copolymers. *Macromolecules* **1991,** *24*, 3760-3766.

34.Wan, W. M.; Baggett, A. W.; Cheng, F.; Lin, H.; Lamm, A. N.; Liu, S. Y.; Jäkle, F., Synthesis by free radical polymerization and properties of BN-polystyrene and BN-poly(vinylbiphenyl). *Chem. Commun.* **2016,** *52* (93), 13616-13619.

35.Thiedemann, B.; Gliese, P. J.; Hoffmann, J.; Lawrence, P. G.; Sönnichsen, F. D.; Staubitz, A., High molecular weight poly(N-methyl-B-vinylazaborine) – a semi-inorganic B–N polystyrene analogue. *Chem. Commun.* **2017,** *53*, 7258-7261

36.van de Wouw, H. L.; Lee, J. Y.; Klausen, R. S., Gram-scale free radical polymerization of an azaborine vinyl monomer. *Chem. Commun.* **2017,** *53* (53), 7262-7265.

37.Mendis, S. N.; Zhou, T.; Klausen, R. S., Syndioselective Polymerization of a BN Aromatic Vinyl Monomer. *Macromolecules* **2018,** *51* (17), 6859-6864.

38.van de Wouw, H. L.; Awuyah, E. C.; Baris, J. I.; Klausen, R. S., An Organoborane Vinyl Monomer with Styrene-like Radical Reactivity: Reactivity Ratios and Role of Aromaticity. *Macromolecules* **2018,** *51* (16), 6359-6368.

39.van de Wouw, H. L.; Lee, J. Y.; Awuyah, E. C.; Klausen, R. S., A BN Aromatic Ring Strategy for Tunable Hydroxy Content in Polystyrene. *Angew. Chem. Int. Ed.* **2018,** *57* (6), 1673-1677.

40.Jackson, L. A.; Allen, C. W., Alkenylborazines. *Phosphorus Sulfur* **1989,** *41* (3-4), 341-346.

41.*ortho*-Phenyl-substituted styrene derivatives have been subjected to polymerization (see refs 42 and 43), but orthomesitylstyrene or other 2,6-disubstituted *ortho*-phenylstyrene derivatives have never been polymerized.

42.Zhang, Q. K.; Tian, H. J.; Li, C. F.; Zhu, Y. F.; Liang, Y. R.; Shen, Z. H.; Fan, X. H., Synthesis and phase behavior of a new 2-vinylbiphenyl-based mesogen-jacketed liquid crystalline polymer with a high glass transition temperature and low threshold molecular weight. *Polym. Chem.* **2014,** *5* (15), 4526-4533.

43.Qu, W.; Zhu, X. Q.; Chen, J. H.; Niu, L.; Liang, D. H.; Fan, X. H.; Shen, Z. H.; Zhou, Q. F., Synthesis and Characterization of a Mesogen-Jacketed Polyelectrolyte. *Macromolecules* **2014,** *47* (8), 2727-2735.

44.McConnell, C. R.; Haeffner, F.; Baggett, A. W.; Liu, S.-Y. 1,2-Azaborine's Distinct Electronic Structure Unlocks Two New Regioisomeric Building Blocks via Resolution Chemistry. J. Am. Chem. Soc. **2019**, *141*(22), 9072-9078.

45.Baggett, A. W.; Vasiliu, M.; Li, B.; Dixon, D. A.; Liu, S. Y., Late-Stage Functionalization of 1,2-Dihydro-1,2-azaborines via Regioselective Iridium-Catalyzed C-H Borylation: The Development of a New N,N-Bidentate Ligand Scaffold. *J. Am. Chem. Soc.* **2015,** *137* (16), 5536-5541.

46.Marwitz, A. J. V.; Matus, M. H.; Zakharov, L. N.; Dixon, D. A.; Liu, S. Y., A Hybrid Organic/Inorganic Benzene. *Angew. Chem. Int. Ed.* **2009,** *48* (5), 973-977.

47.Daly, A. M.; Tanjaroon, C.; Marwitz, A. J. V.; Liu, S. Y.; Kukolich, S. G., Microwave Spectrum, Structural Parameters, and Quadrupole Coupling for 1,2-Dihydro-1,2-azaborine. *J. Am. Chem. Soc.* **2010,** *132* (15), 5501-5506.

48.Chrostowska, A.; Xu, S. M.; Lamm, A. N.; Maziere, A.; Weber, C. D.; Dargelos, A.; Baylere, P.; Graciaa, A.; Liu, S. Y., UV-Photoelectron Spectroscopy of 1,2-and 1,3-Azaborines: A Combined Experimental and Computational Electronic Structure Analysis. *J. Am. Chem. Soc.* **2012,** *134* (24), 10279-10285.

49.Parab, K.; Doshi, A.; Cheng, F.; Jäkle, F., Synthesis and Characterization of Luminescent Polystyrene Derivatives with Sterically Protected Fluorenyl- and Carbazolylborane Moieties. *Macromolecules* **2011,** *44*, 5961-5967.

50.Parab, K.; Venkatasubbaiah, K.; Jäkle, F., Luminescent Triarylborane-Functionalized Polystyrene: Synthesis, Photophysical Characterization, and Anion-Binding Studies. *J. Am. Chem. Soc.* **2006,** *128* (39), 12879-12885.

51.Cheng, F.; Bonder, E. M.; Jäkle, F., Electron-Deficient Triarylborane Block Copolymers: Synthesis by Controlled Free Radical Polymerization and Application in the Detection of Fluoride Ions. *J. Am. Chem. Soc.* **2013,** *135* (46), 17286-17289.

52.Hiemenz, P. C.; Lodge, T. P., *Polymer Chemistry*. Second Edition ed.; CRC Press: Boca Raton, Fl, 2007.

3.6 Appendix

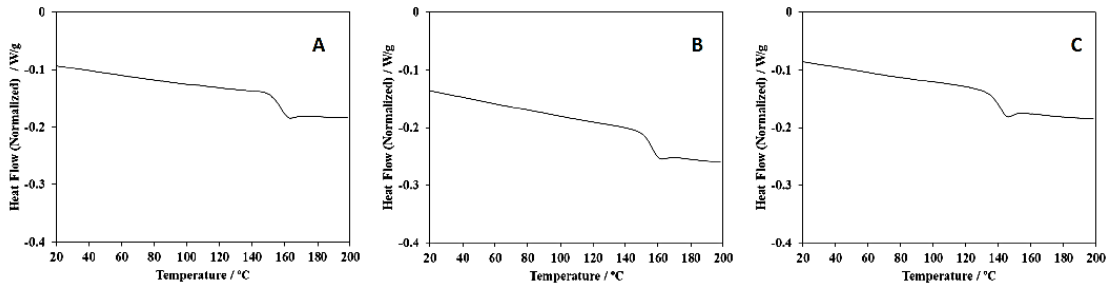

Figure 3-S1. DSC traces of (A) P4V-NBMes-co-PS, (B) P5V-NBMes-co-PS, and (C) P6V-NBMes-co-PS.

Table 3-S1. Comparison of copolymer glass transition temperatures to predicted values based on the relative composition using the Fox equation $1/T_{g,calc} = (w_{BN}/T_{g,BN}) + (w_{St}/T_{g,St})$ where w_{BN} and w_{St} are the weight fractions of vinyl azaborinine and styrene respectively as determined from the monomer conversion

	$T_{g,\,obs}$ (K)	$T_{g,\,calcd}$ (K)	w_{BN}	w_{St}	$T_{g,BN}$ (K)	$T_{g,St}$ (K)
P4V-NBMes-co-PS	425	413	0.71	0.29	433	371
P5V-NBMes-co-PS	423	408	0.58	0.42	440	371

P6V-NBMes-co-PS	408	399	0.72	0.28	411	371

Note: The slightly lower calculated values may be a reflection of the fact that the measured $T_{g,BN}$ for the azaborinine homopolymers is lower than that at infinite molecular weight.

Table 3-S2. HOMO - LUMO orbital plots for B-mesityl vinylazaborinines (cam-b3lyp/6-311g(d,p))

	4V-NBMes	4Et-NBMes
LUMO	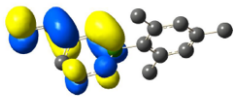 -0.04 eV	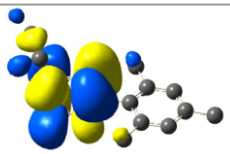 0.63 eV
HOMO	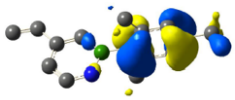 -7.53 eV	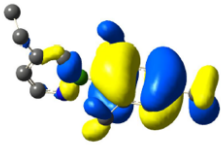 -7.48eV

	5V-NBMes	5Et-NBMes
LUMO	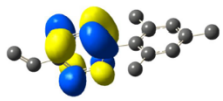 0.46 eV	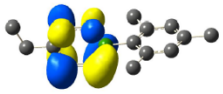 0.60 eV
HOMO	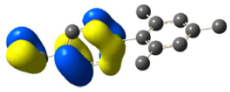 -7.18 eV	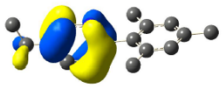 -7.41 eV

	6V-NBMes	6Et-NBMes
LUMO	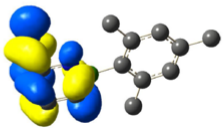 -0.30 eV	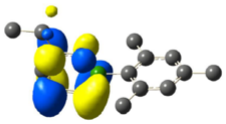 0.60 eV
HOMO	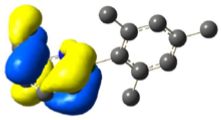 -7.36 eV	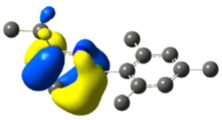 -7.42eV

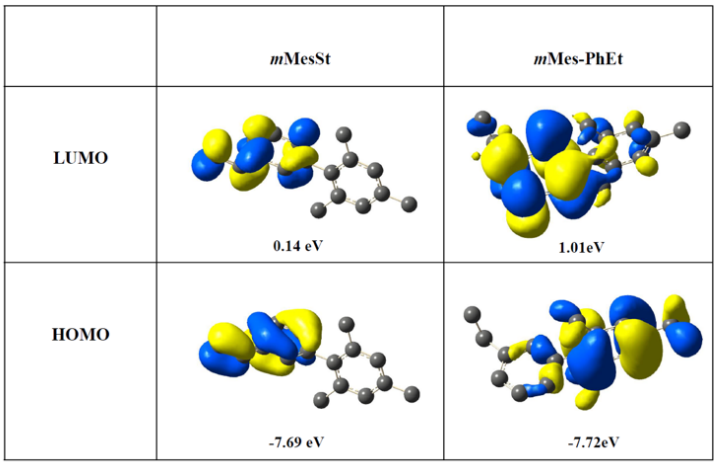

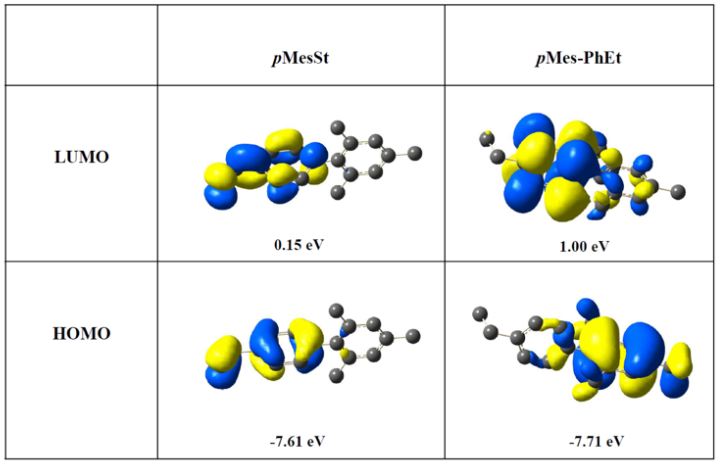

Table 3-S3. Summary of TD-DFT data (cam-b3lyp/6-311g(d,p))

Compound	Transition [a]	E_{ex} (eV)	λ (nm)	Oscillator strength f	Assignment (%)
4V-NBMes	$S_0 \rightarrow S_1$	4.77	260.1	0.242	H-3 → L (0.12) H → L (0.67)
	$S_0 \rightarrow S_4$	5.47	226.5	0.632	H-3 → L (0.67) H-1 → L+1 (0.10) H → L (-0.11)
4Et-NBMes	$S_0 \rightarrow S_1$	5.18	239.5	0.209	H-3 → L+3 (-0.14) H → L (0.68)
	$S_0 \rightarrow S_3$	5.86	211.7	0.130	H-2 → L+2 (0.34) H-1 → L (-0.10) H-1 → L+1 (0.60)
5V-NBMes	$S_0 \rightarrow S_1$	4.85	255.7	0.191	H → L (0.66) H → L+1 (0.19)

	$S_0 \rightarrow S_3$	5.40	229.5	0.645	H-3 → L (-0.13) H → L (-0.18) H → L+1 (0.65)
5Et-NBMes	$S_0 \rightarrow S_1$	5.01	247.3	0.228	H-3 → L+3 (0.12) H → L (0.69)
	$S_0 \rightarrow S_4$	5.85	211.9	0.140	H-2 → L+2 (0.34) H-1 → L+1 (0.61)
	$S_0 \rightarrow S_5$	6.25	198.3	0.250	H-3 → L (-0.29) H-2 → L (-0.16) H-2 → L+2 (-0.11) H → L+3 (0.59)
6V-NBMes	$S_0 \rightarrow S_1$	4.48	277.0	0.499	H → L (0.69) H → L+3 (0.10)
	$S_0 \rightarrow S_5$	5.83	212.7	0.177	H-3 → L (-0.34) H-2 → L (-0.17) H → L (-0.11) H → L+3 (0.56)
	$S_0 \rightarrow S_6$	5.85	211.8	0.113	H-3 → L (-0.11) H-2 → L (-0.11) H-2 → L+2 (0.33) H-1 → L+1 (0.60)
6Et-NBMes	$S_0 \rightarrow S_1$	5.03	246.4	0.327	H-3 → L+3 (-0.12) H → L (0.68)
	$S_0 \rightarrow S_4$	5.86	211.7	0.109	H-2 → L+2 (0.35) H-1→ L+1 (-0.22)
	$S_0 \rightarrow S_5$	6.31	196.5	0.184	H-3 → L (0.27) H-2 → L (-0.22) H-2 → L+2 (-0.10) H → L+1 (-0.15) H → L+3 (0.56)
*m*MesSt	$S_0 \rightarrow S_1$	5.11	242.8	0.233	H-3 → L (-0.38) H → L (0.44) H → L+1 (-0.37)
	$S_0 \rightarrow S_2$	5.19	238.9	0.296	H-3 → L (0.34) H → L (0.53) H → L+1 (0.27)
	$S_0 \rightarrow S_5$	5.93	209.2	0.197	H-3 → L (-0.10) H-2 → L (0.11) H-2 → L+3 (-0.34) H-1 → L+2 (0.57) H → L+1 (0.13)
	$S_0 \rightarrow S_6$	6.21	199.7	0.193	H-3 → L (0.16) H-2 → L (0.65) H-1 → L+2 (-0.11) H → L+1 (-0.13)
*m*Mes-PhEt	$S_0 \rightarrow S_1$	5.35	231.6	0.000	H-1 → L+2 (0.48) H → L (-0.19)

					H → L+3 (-0.45)
	$S_0 \rightarrow S_3$	5.94	208.8	0.112	H-1 → L (0.15) H-1 → L+3 (0.34) H → L+1 (-0.16) H → L+2 (0.55)
*p*MesSt	$S_0 \rightarrow S_1$	5.04	246.0	0.536	H-3 → L (-0.21) H → L (0.59) H → L+1 (-0.27)
	$S_0 \rightarrow S_2$	5.20	238.2	0.273	H-3 → L (0.42) H → L (0.35) H → L+1 (0.40)
*p*Mes-PhEt	$S_0 \rightarrow S_1$	5.35	231.7	0.000	H-1 → L+2 (0.49) H → L (0.20) H → L+3 (-0.46)
	$S_0 \rightarrow S_3$	5.93	209.1	0.188	H-2 → L+1 (-0.19) H-1 → L (-0.14) H-1 → L+3 (0.33) H → L+2 (0.57)
	$S_0 \rightarrow S_4$	6.07	204.1	0.124	H-3 → L (-0.36) H-2 → L+1 (0.55) H-1 → L (-0.12) H-1 → L+3 (0.15)

Spectral Data for Isolated Compounds

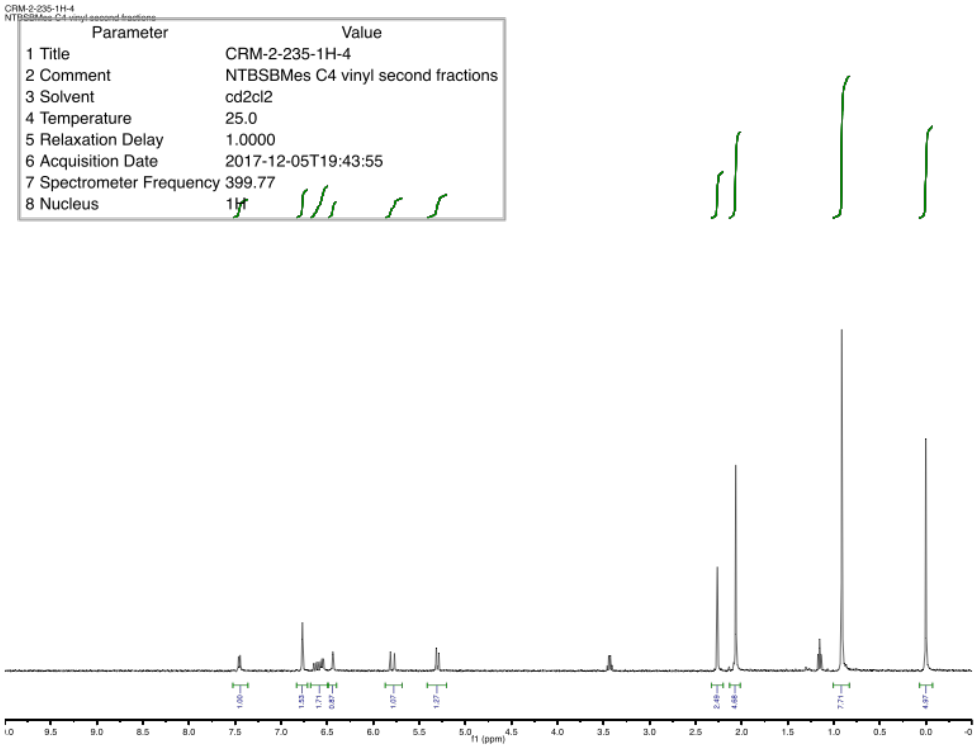

Figure 3-S2. ^{1}H NMR spectrum of 2 in CD_2Cl_2.

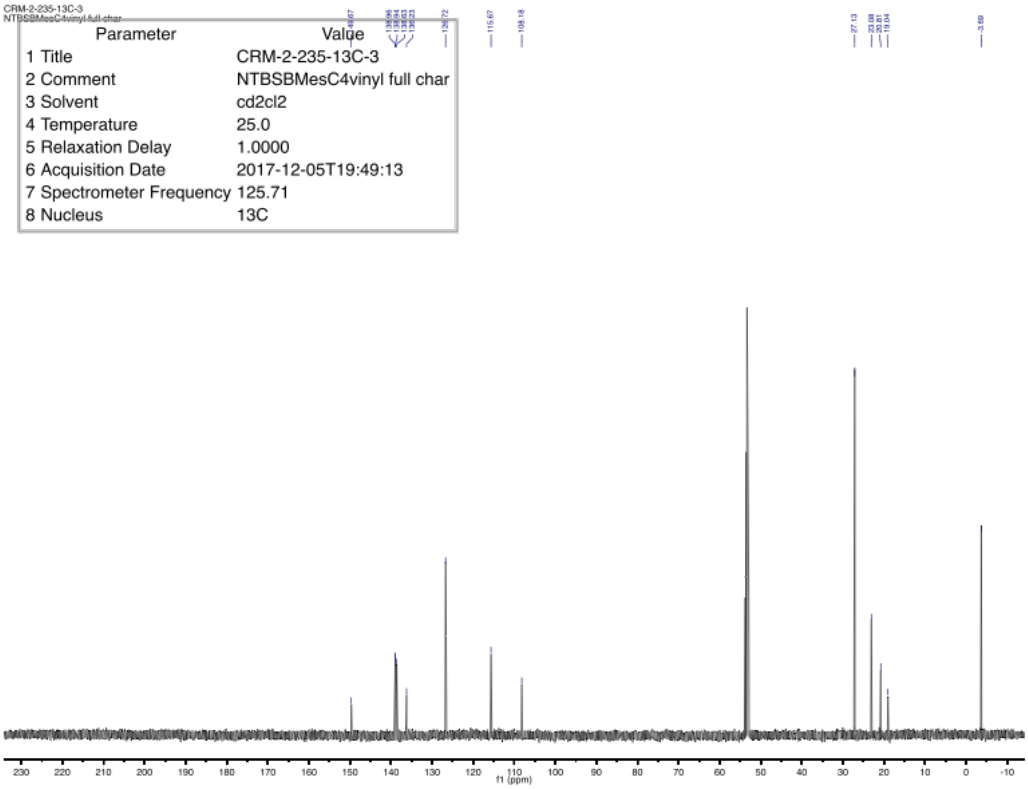

Figure 3-S3. ^{13}C NMR spectrum of 2 in CD_2Cl_2.

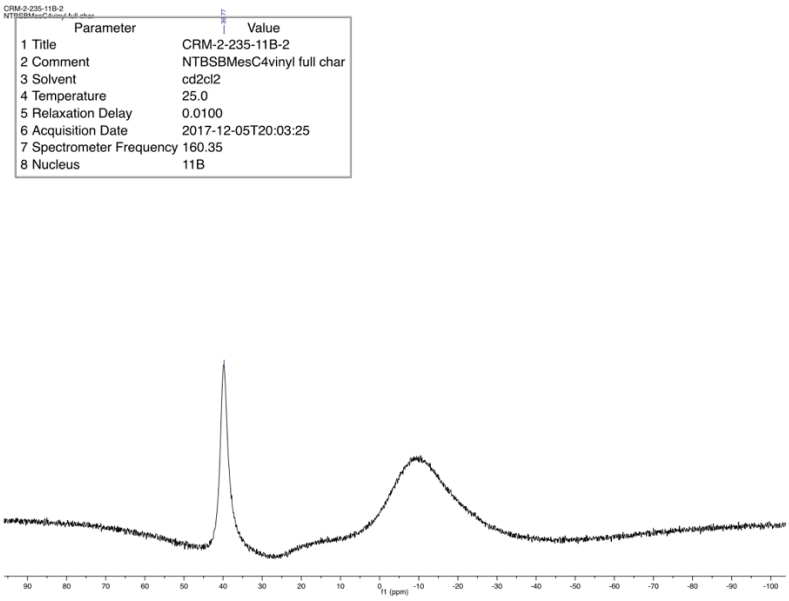

Figure 3-S4. ^{11}B NMR spectrum of **2** in CD_2Cl_2.

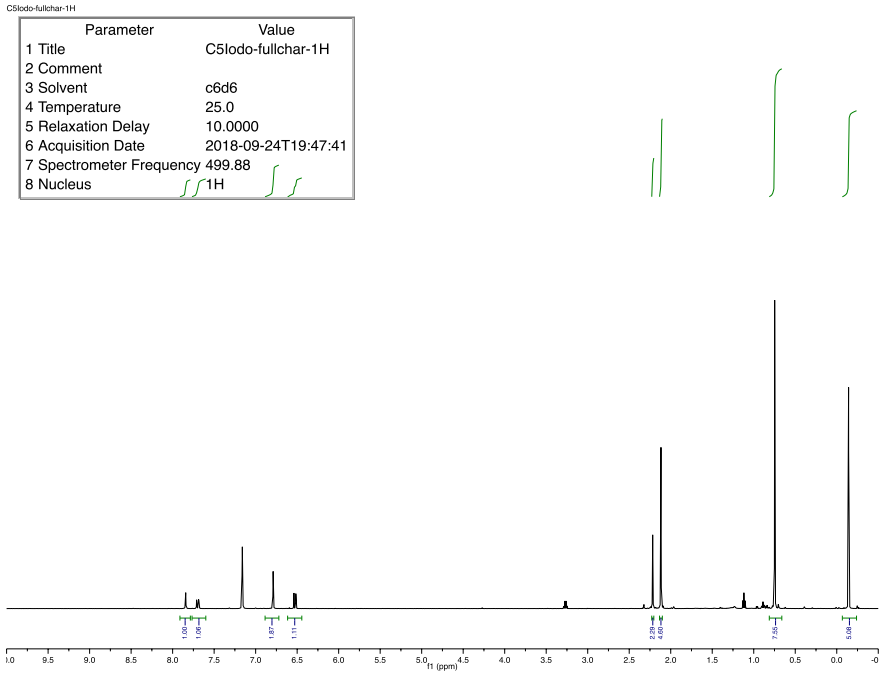

Figure 3-S5. ^{1}H NMR spectrum of **4** in C_6D_6.

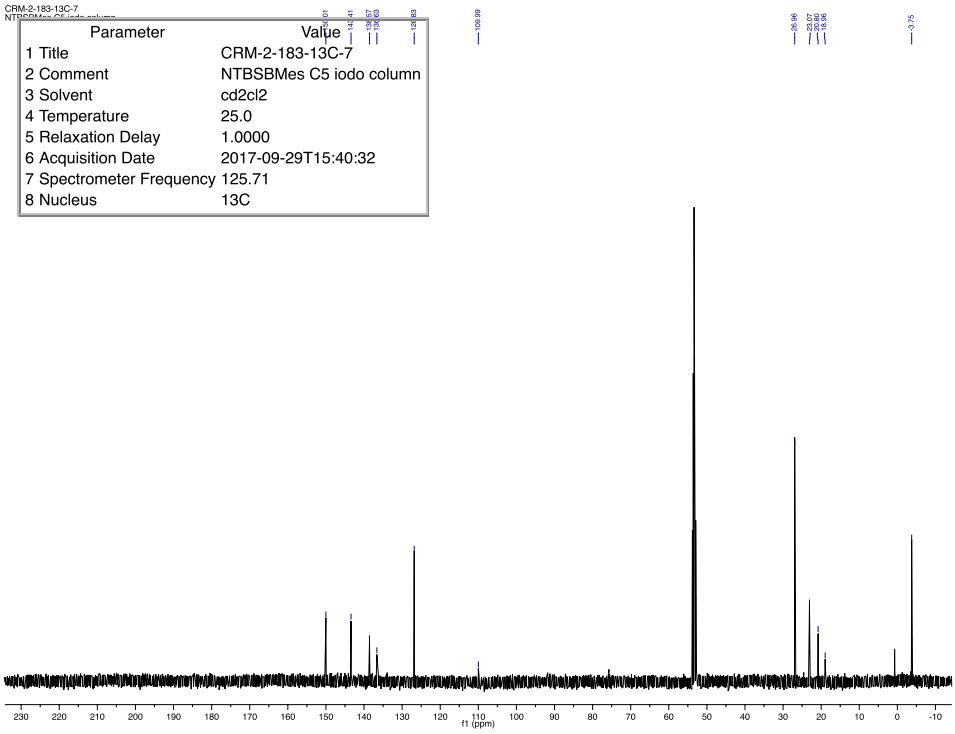

Figure 3-S6. ^{13}C NMR spectrum of **4** in C_6D_6.

C5Iodo-fullchar-11B

Parameter	Value
1 Title	C5Iodo-fullchar-11B
2 Comment	
3 Solvent	c6d6
4 Temperature	25.0
5 Relaxation Delay	0.0100
6 Acquisition Date	2018-09-24T19:42:15
7 Spectrometer Frequency	160.35
8 Nucleus	11B

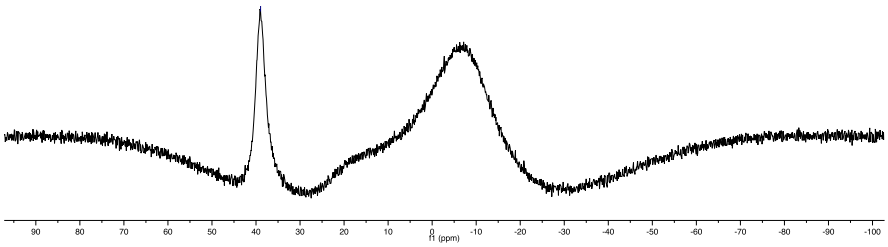

Figure 3-S7. ^{11}B NMR spectrum of **4** in C_6D_6.

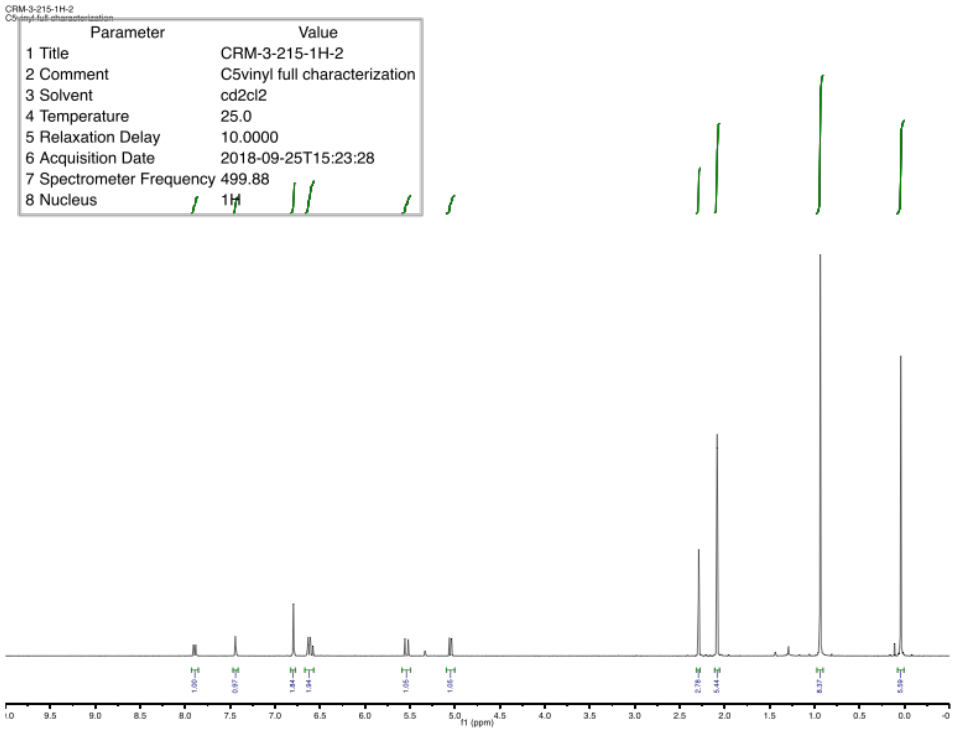

Figure 3-S8. ^{1}H NMR spectrum of **5** in CD_2Cl_2.

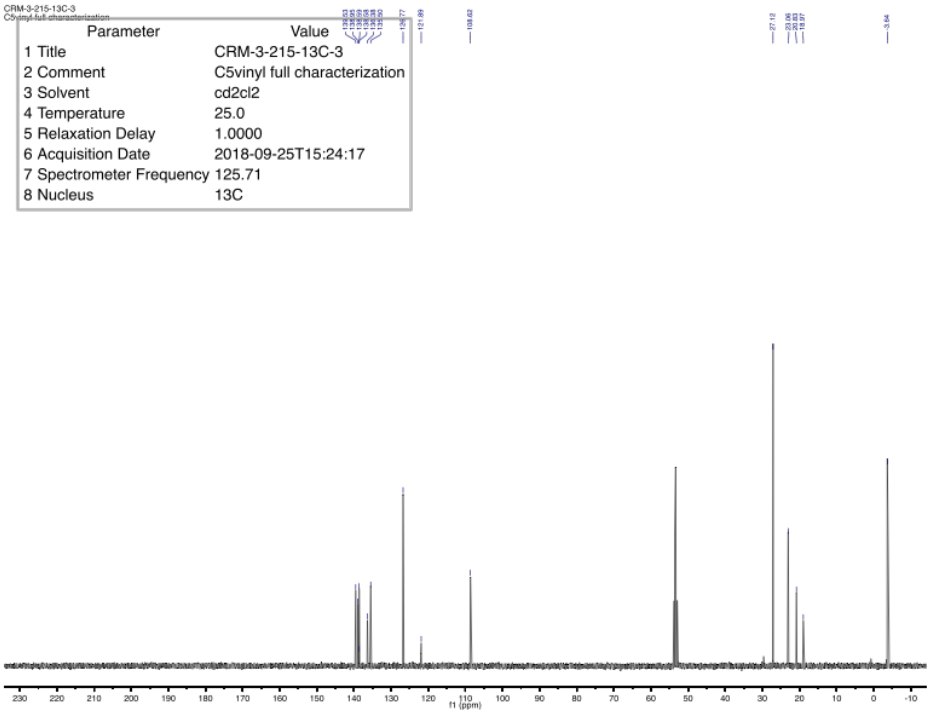

Figure 3-S9. ^{13}C NMR spectrum of **5** in CD_2Cl_2.

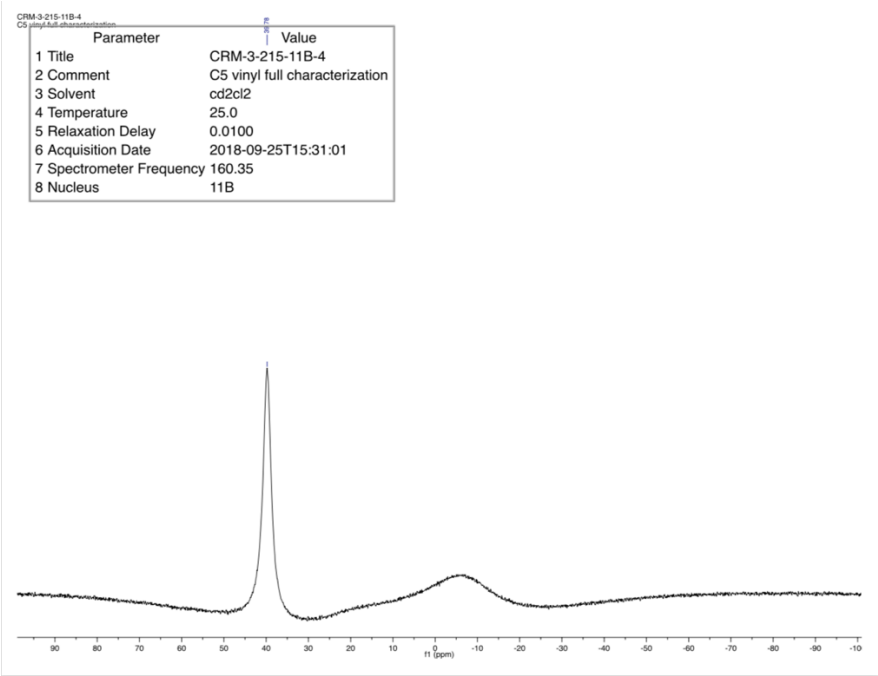

Figure 3-S10. ^{11}B NMR spectrum of **5** in CD_2Cl_2.

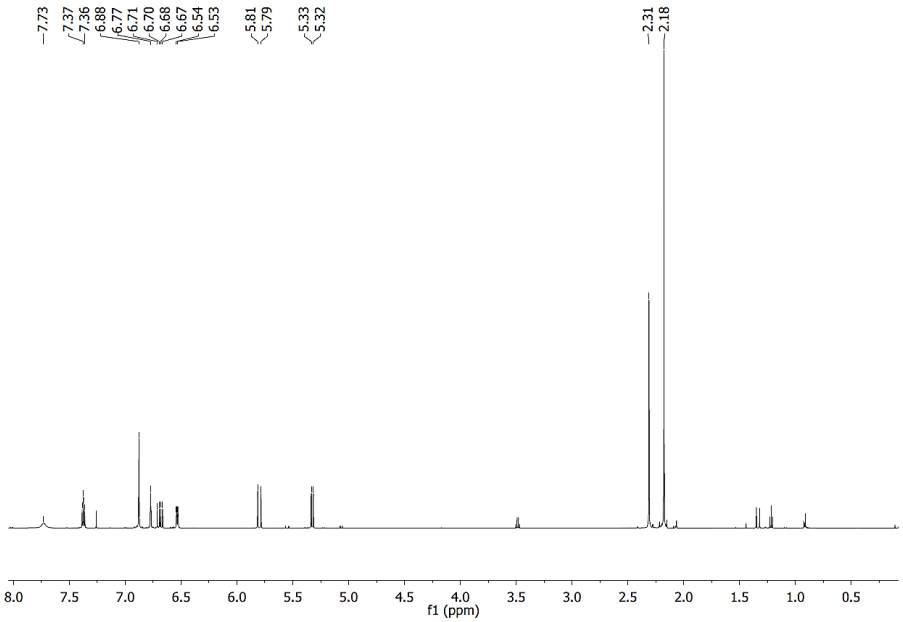

Figure 3-S11. ^{1}H NMR spectrum of 4V-NBMes monomer in $CDCl_3$.

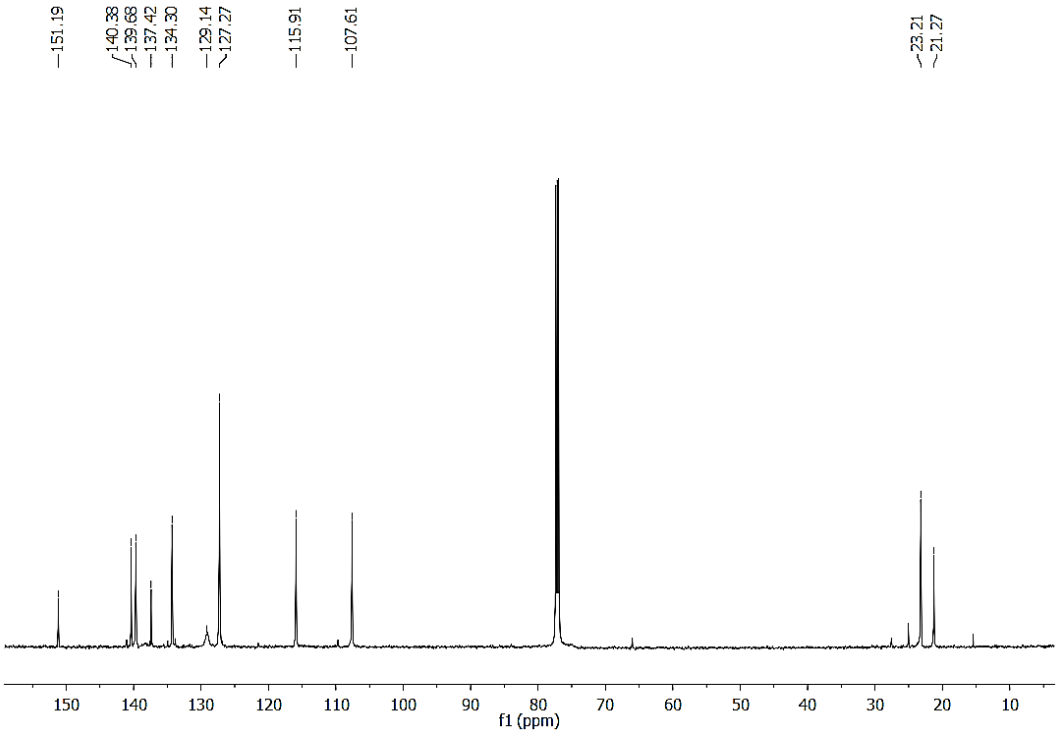

Figure 3-S12. ^{13}C NMR spectrum of 4V-NBMes monomer in $CDCl_3$.

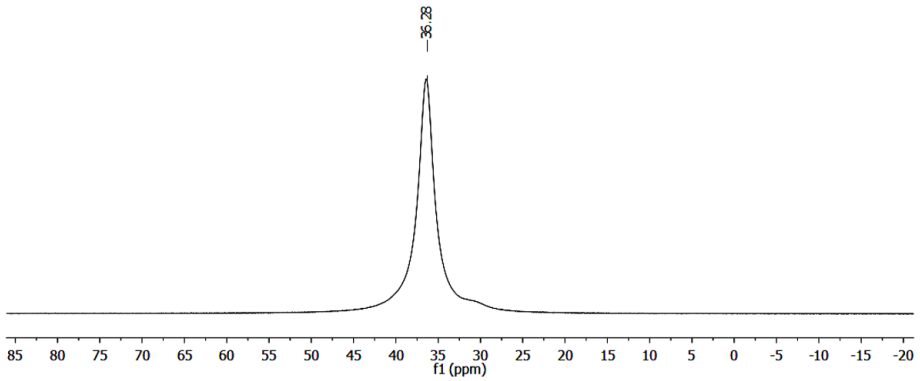

Figure 3-S13. ^{11}B NMR spectrum of 4V-NBMes monomer in $CDCl_3$ (B-free NMR tube).

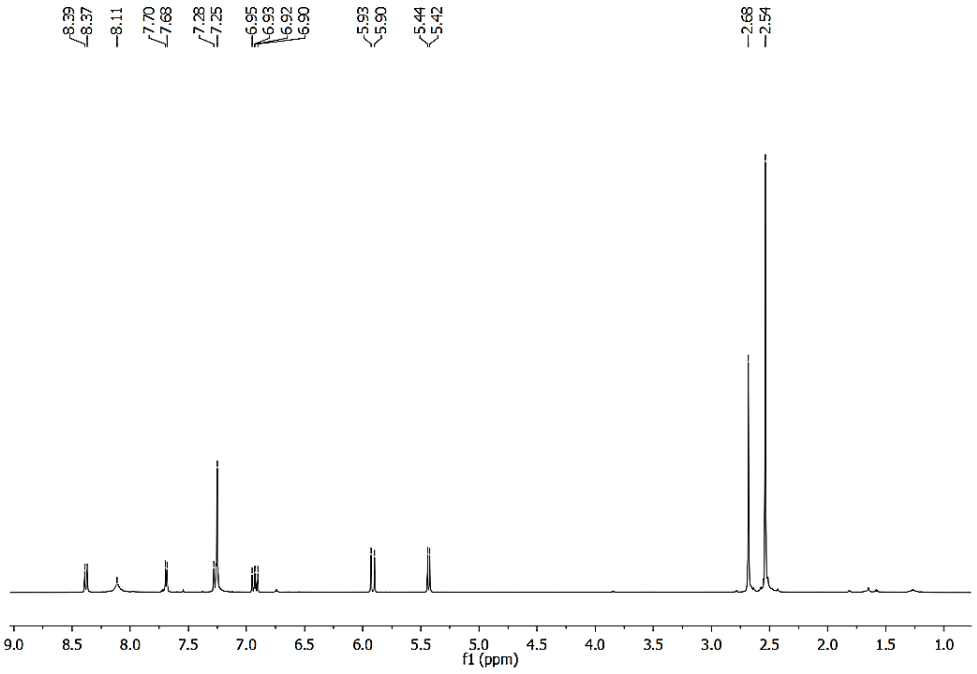

Figure 3-S14. ^{1}H NMR spectrum of 5V-NBMes monomer in $CDCl_3$.

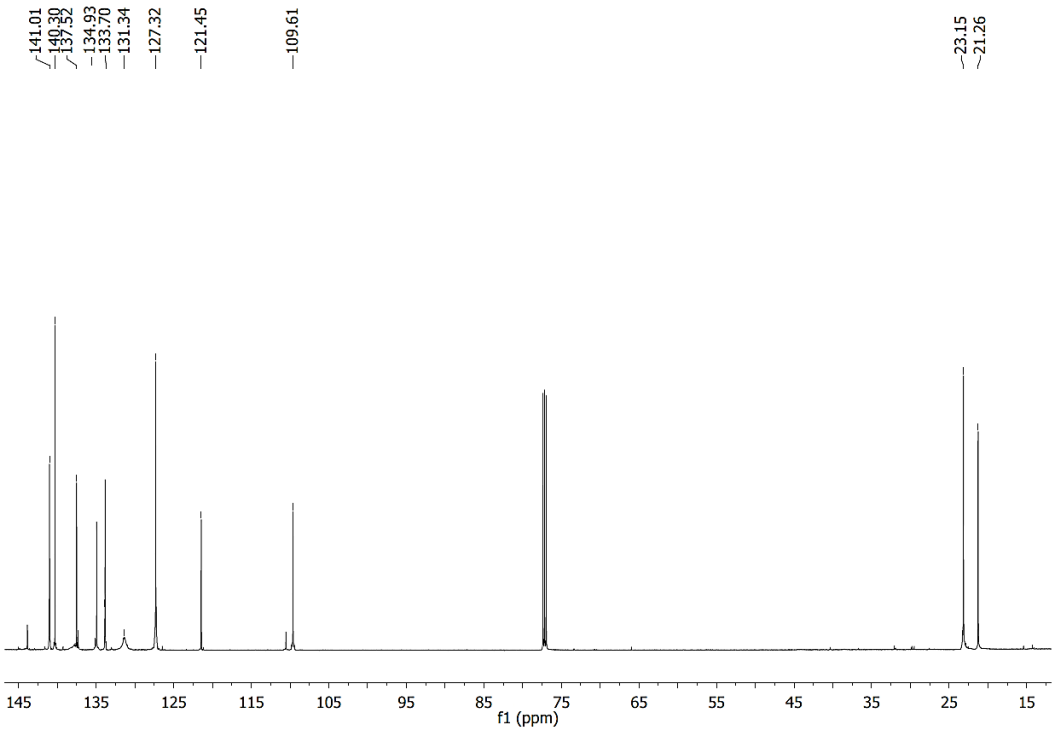

Figure 3-S15. ^{13}C NMR spectrum of 5V-NBMes monomer in $CDCl_3$.

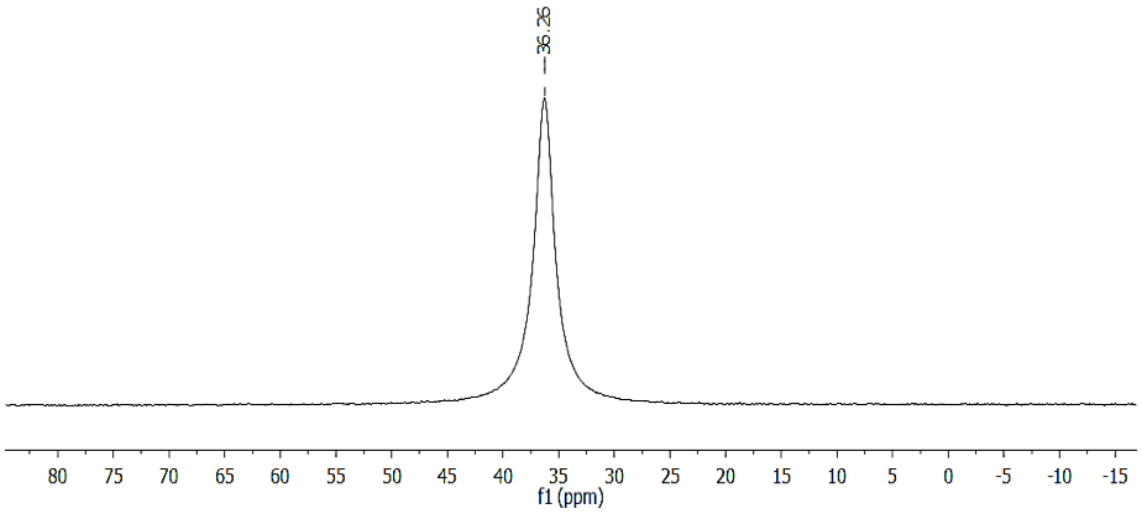

Figure 3-S16. ^{11}B NMR spectrum of 5V-NBMes monomer in $CDCl_3$ (B-free NMR tube).

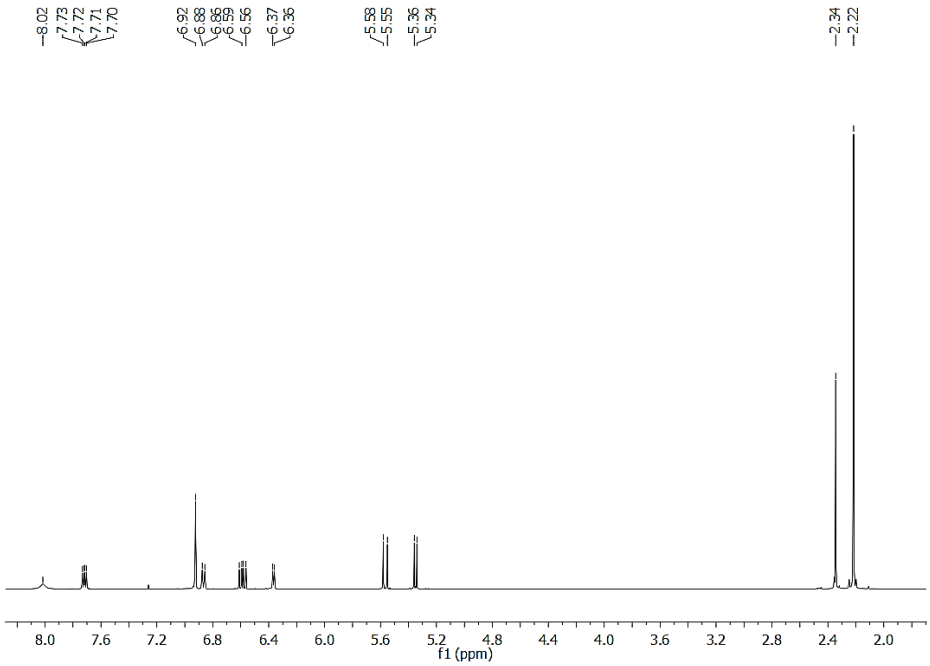

Figure 3-S17. ^{1}H NMR spectrum of 6V-NBMes monomer in $CDCl_3$.

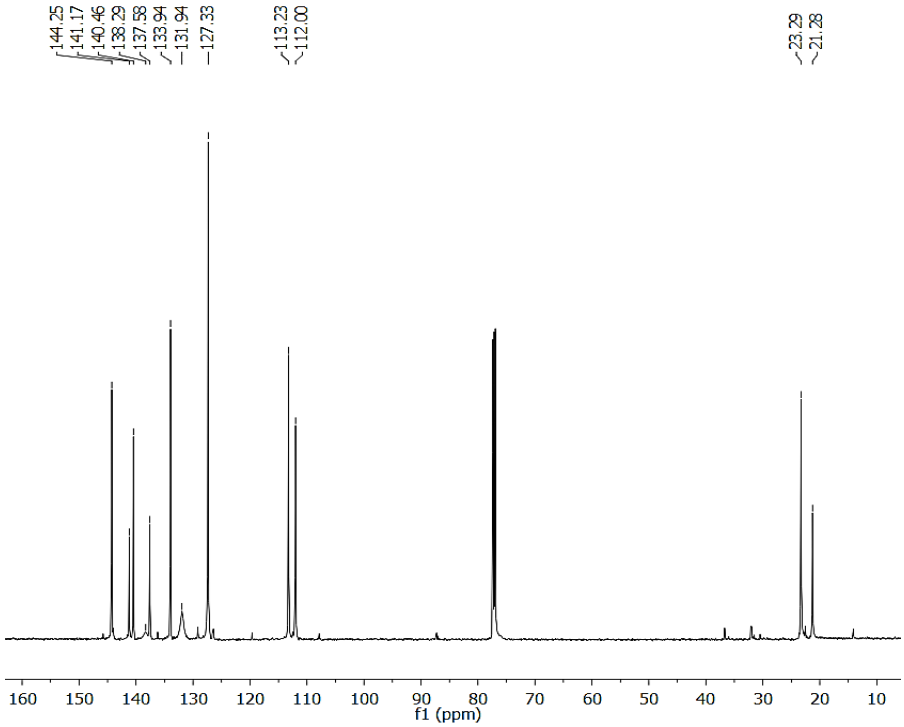

Figure 3-S18. ^{13}C NMR spectrum of 6V-NBMes monomer in $CDCl_3$.

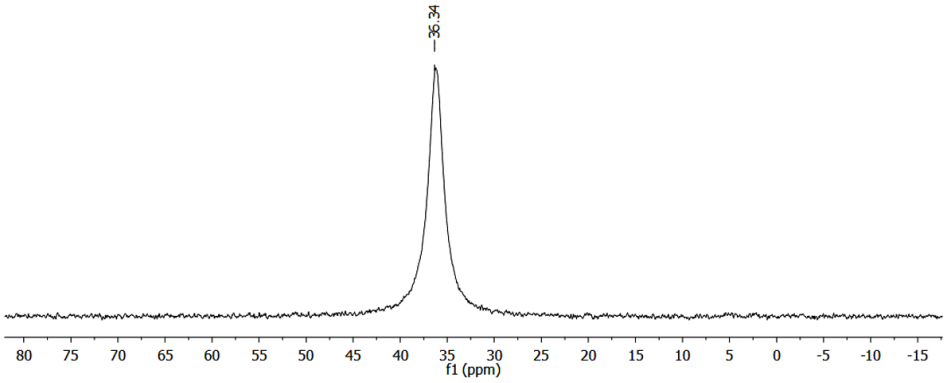

Figure 3-S19. ^{11}B NMR spectrum of 6V-NBMes monomer in $CDCl_3$ (B-free NMR tube).

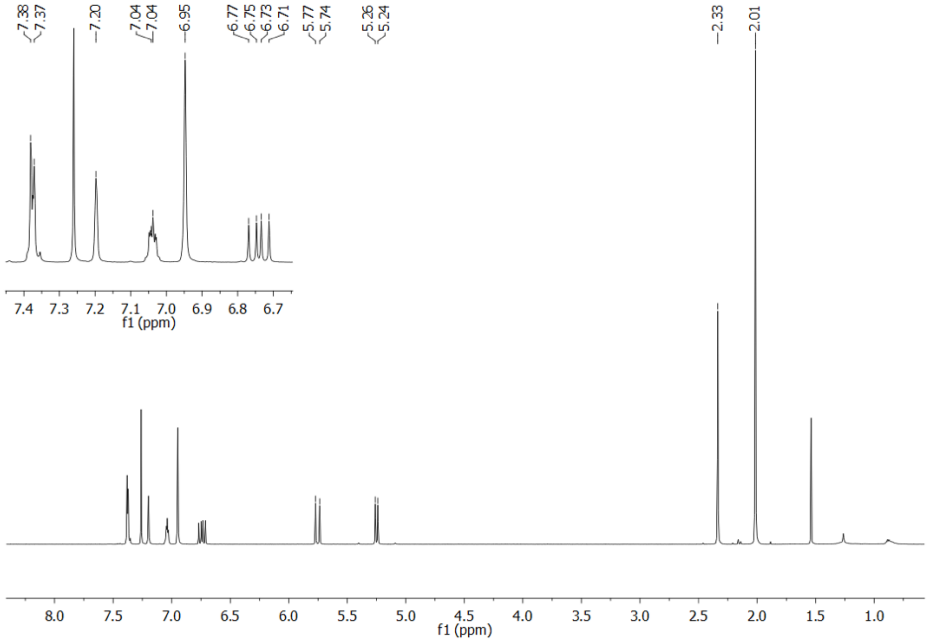

Figure 3-S20. ^{1}H NMR spectrum *meta*-mesitylstyrene (*m*MesSt) in $CDCl_3$.

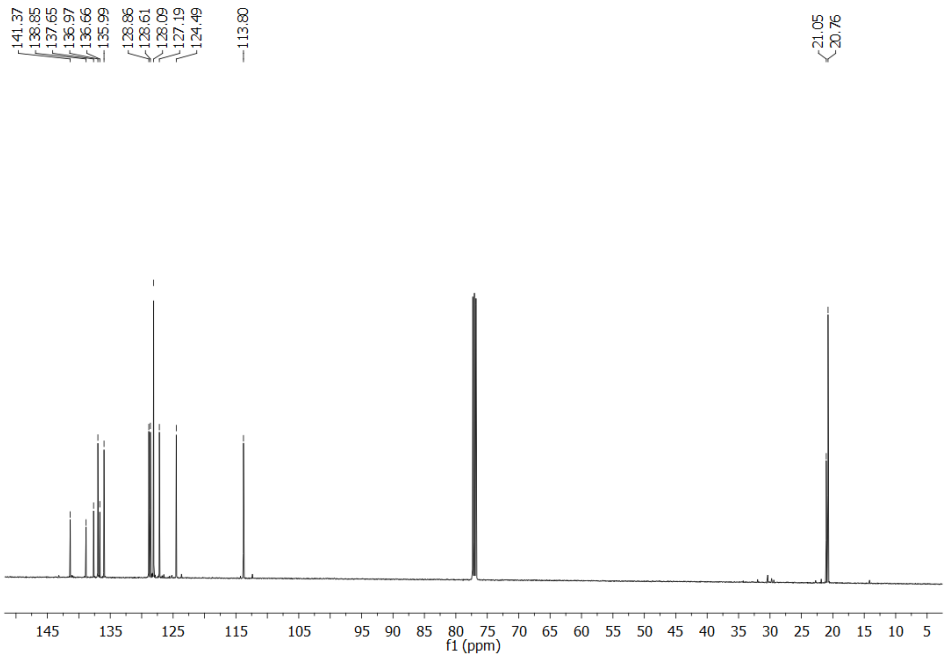

Figure 3-S21. ^{13}C NMR spectrum of *meta*-mesitylstyrene (*m*MesSt) in $CDCl_3$.

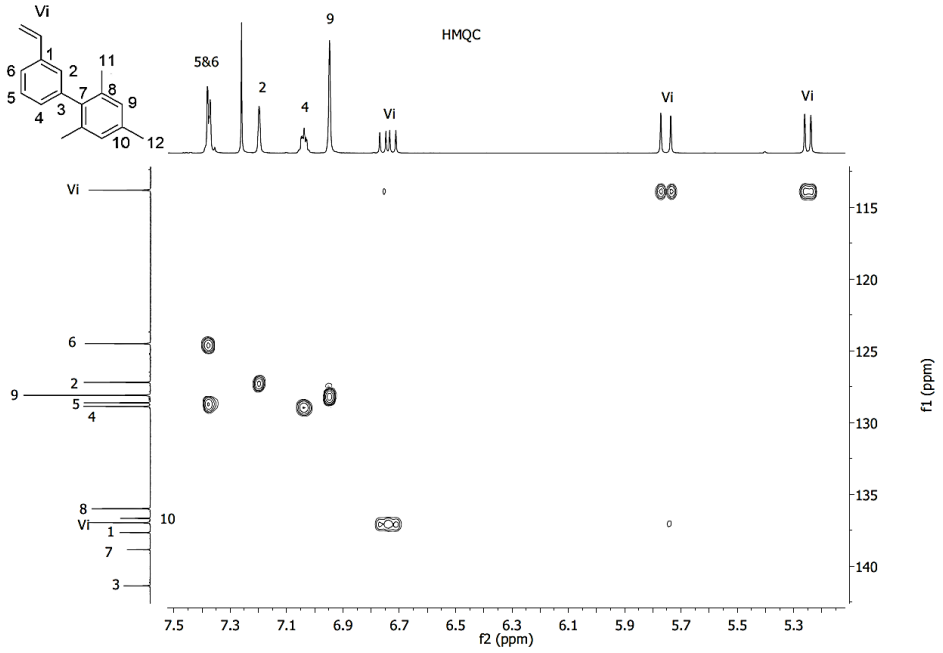

Figure 3-S22. ^{1}H,^{13}C-HMQC NMR spectrum of *m*MesSt in $CDCl_3$.

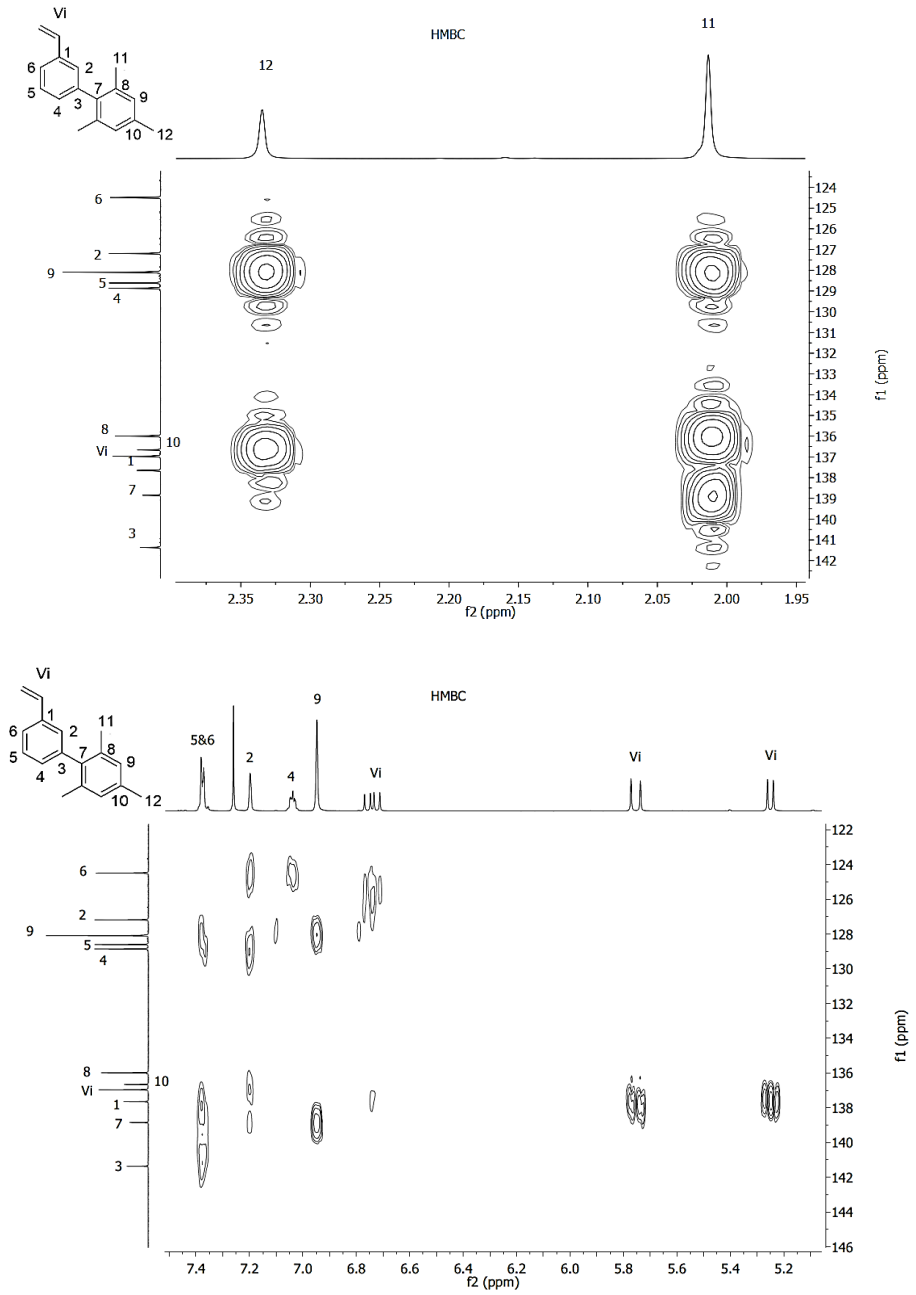

Figure 3-S23. $^{1}H,^{13}C$-HMBC NMR spectrum of *m*MesSt in $CDCl_3$.

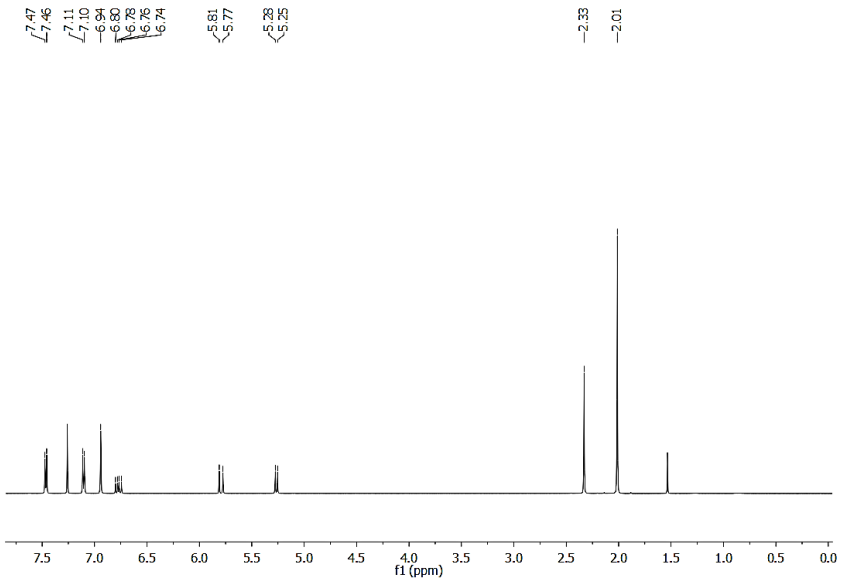

Figure 3-S24. ^{1}H NMR spectrum of *para*-mesitylstyrene (*p*MesSt) in $CDCl_3$.

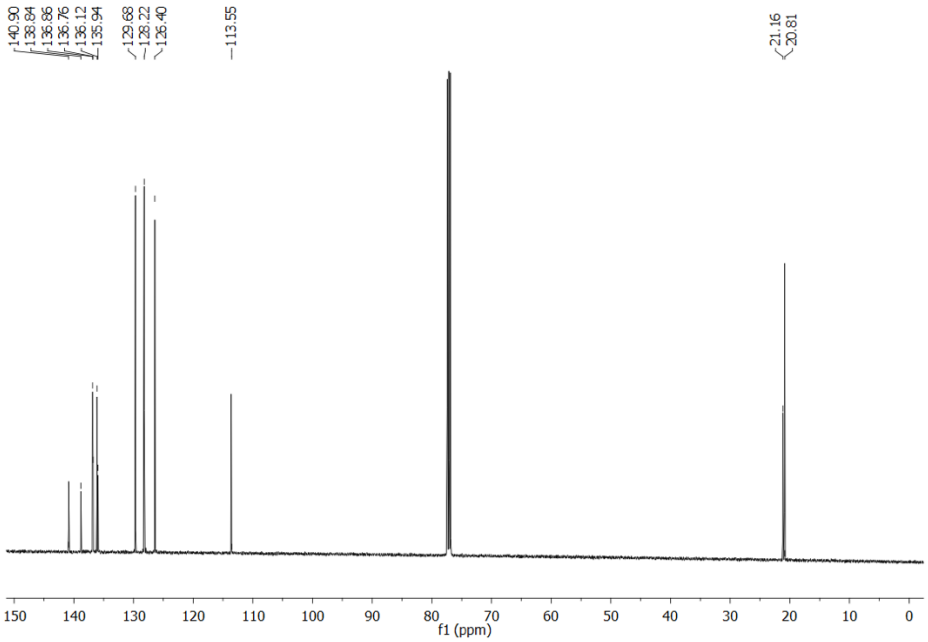

Figure 3-S25. ^{13}C NMR spectrum of *para*-mesitylstyrene (*p*MesSt) in $CDCl_3$.

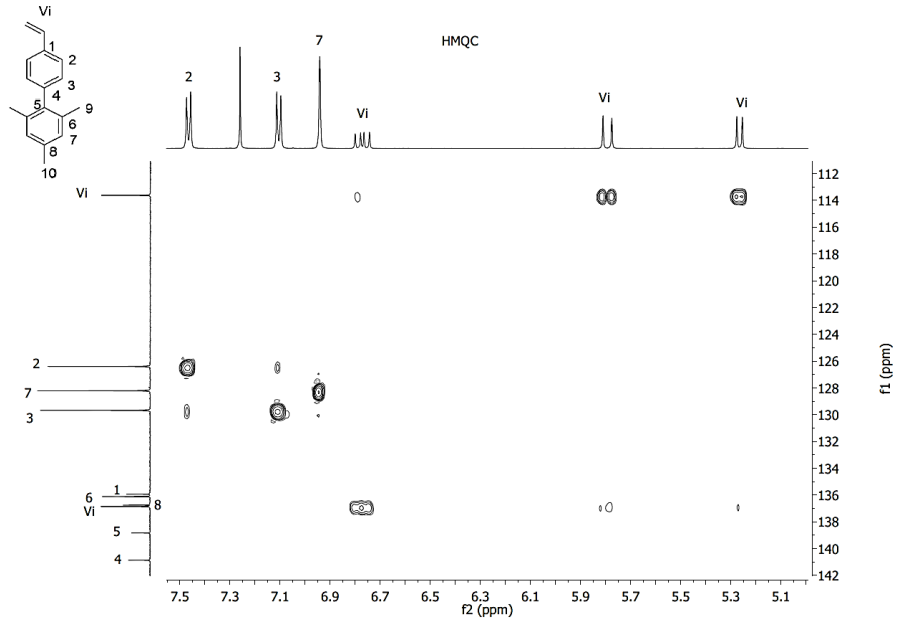

Figure 3-S26. $^{1}H,^{13}C$-HMQC NMR spectrum of *p*MesSt in $CDCl_3$.

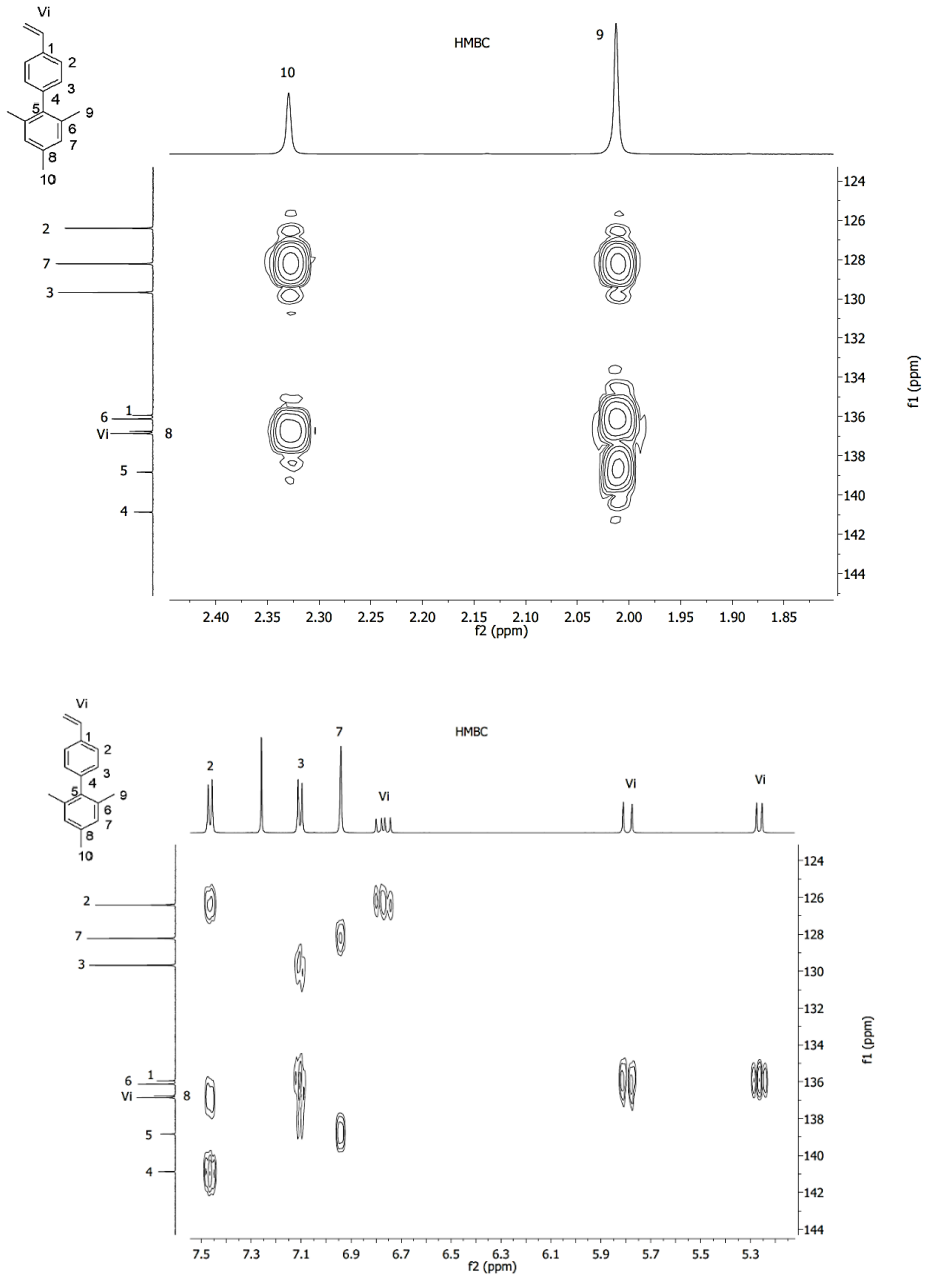

Figure 3-S27. $^{1}H,^{13}C$-HMBC NMR spectrum of *p*MesSt in $CDCl_3$.

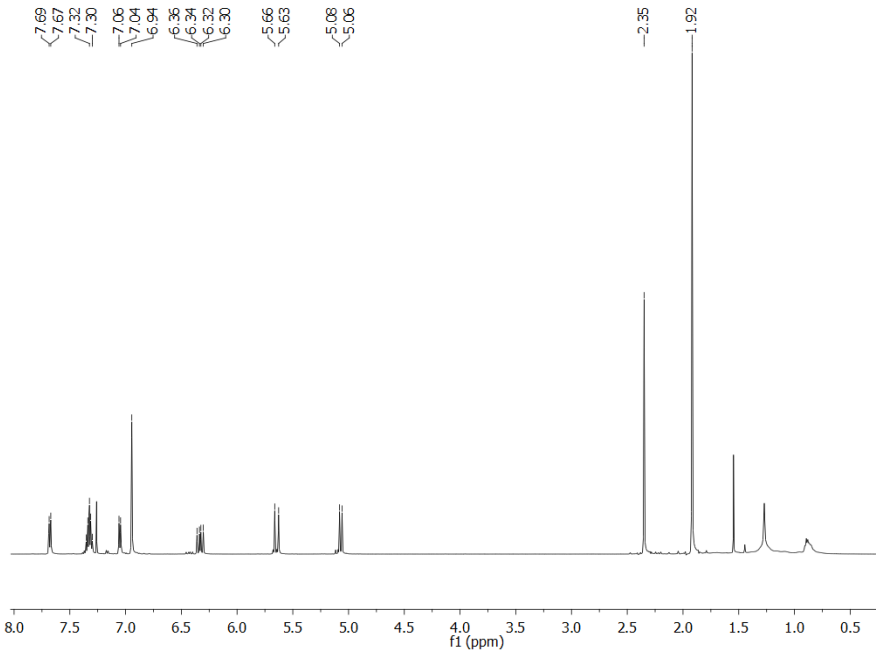

Figure 3-S28. ^{1}H NMR spectrum of *ortho*-mesitylstyrene (*o*MesSt) in $CDCl_3$.

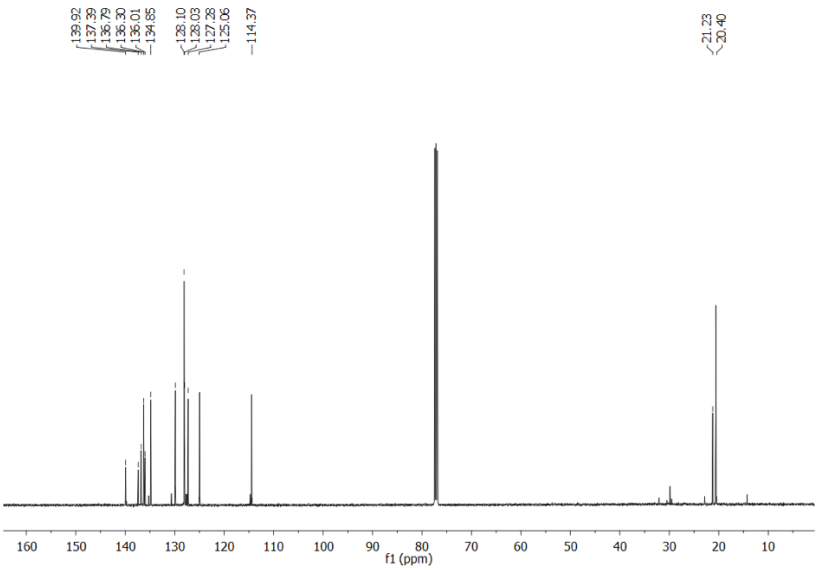

Figure 3-S29. ^{13}C NMR spectrum of *ortho*-mesitylstyrene (*o*MesSt) in $CDCl_3$.

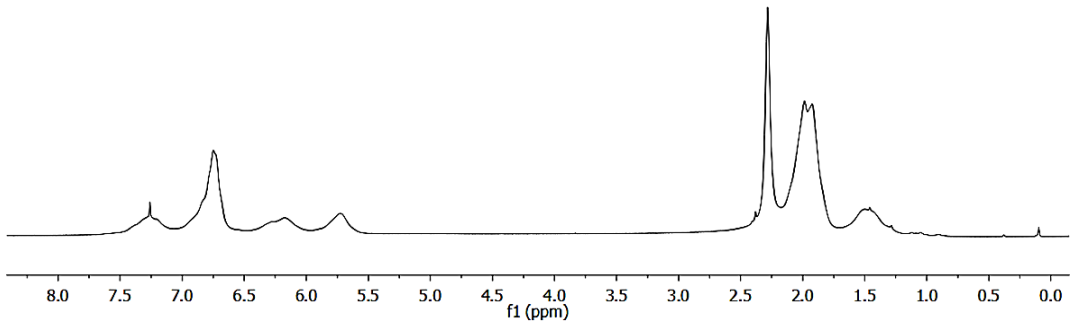

Figure 3-S30. ^{1}H NMR spectrum of P4V-NBMes polymer in $CDCl_3$.

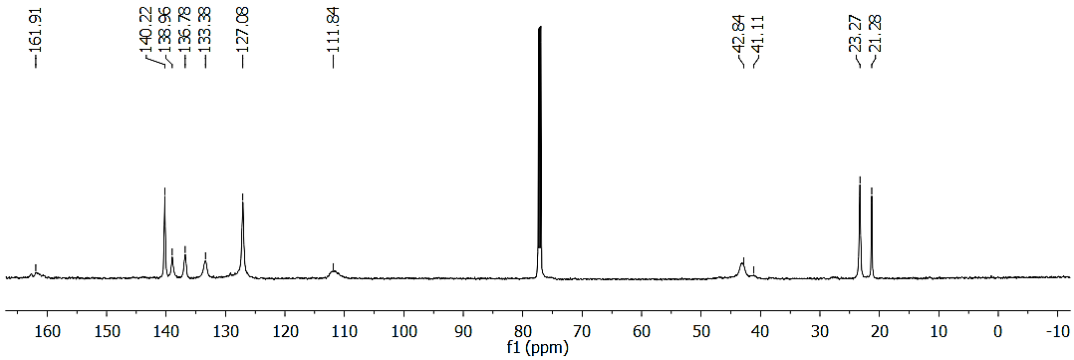

Figure 3-S31. ^{13}C NMR spectrum of P4V-NBMes polymer in $CDCl_3$.

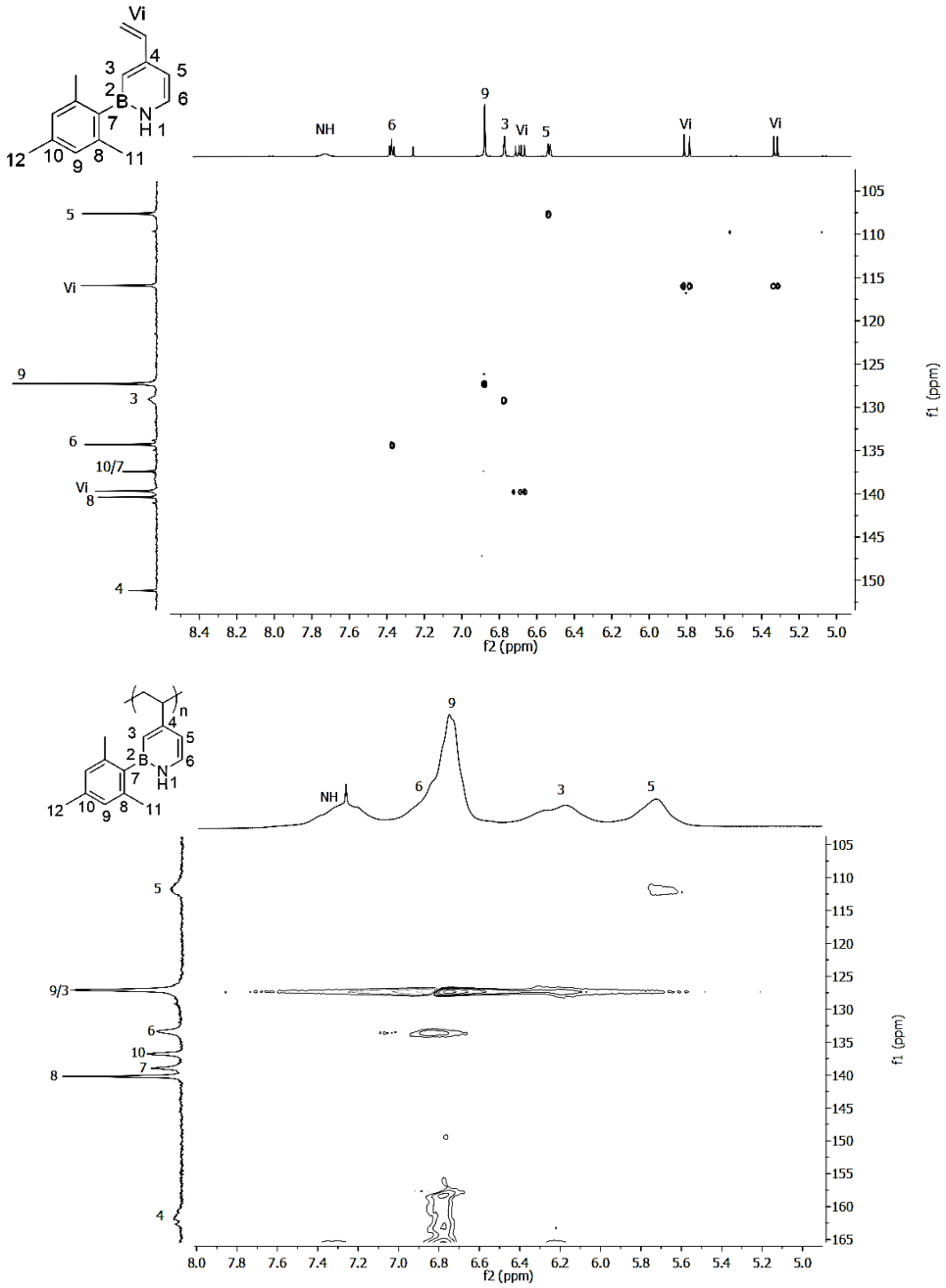

Figure 3-S32. Comparison of $^{1}H,^{13}C$-HMQC NMR spectra of 4V-NBMes and P4V-NBMes in $CDCl_3$.

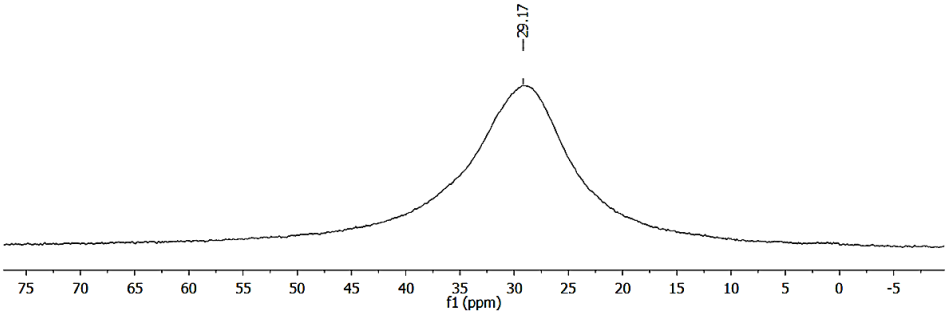

Figure 3-S33. ^{11}B NMR spectrum of P4V-NBMes polymer in $CDCl_3$ (B-free NMR tube).

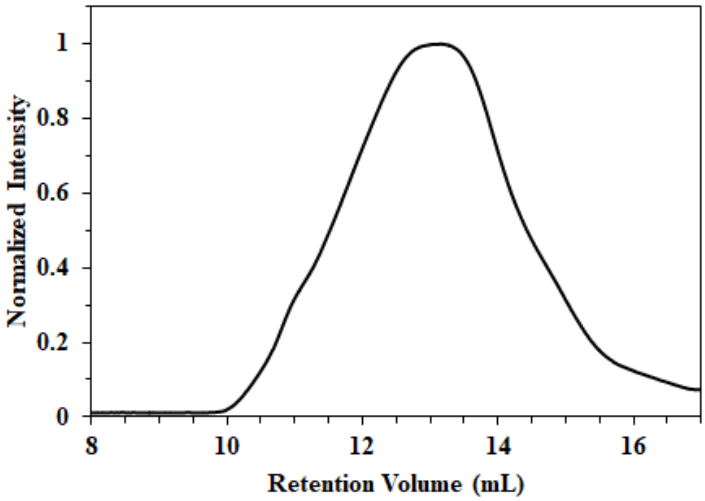

Figure 3-S34. GPC-RI trace of P4V-NBMes; eluent: THF, 1 mL min^{-1}.

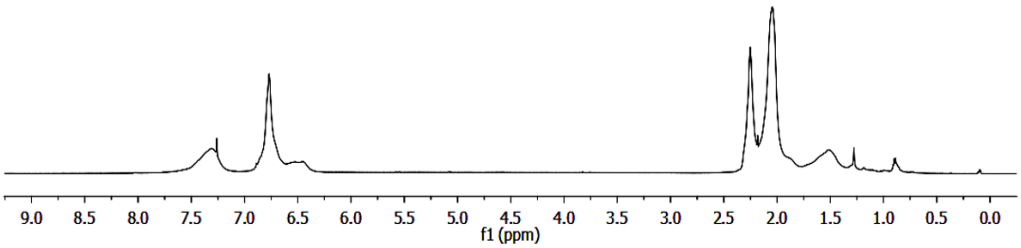

Figure 3-S35. ^{1}H NMR spectrum of P5V-NBMes polymer in $CDCl_3$.

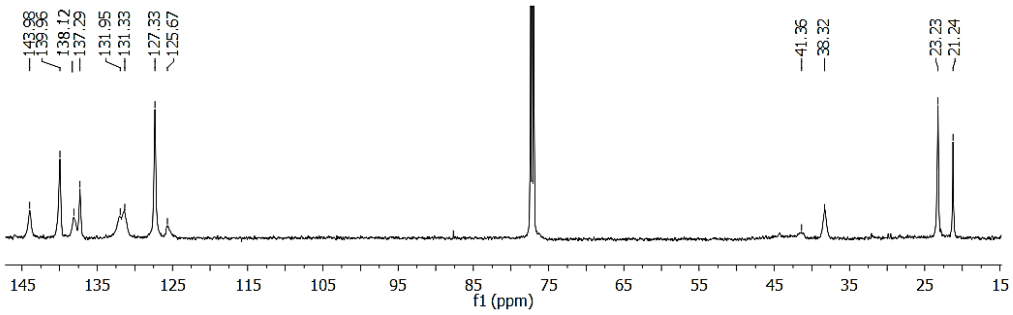

Figure 3-S36. ^{13}C NMR spectrum of P5V-NBMes polymer in $CDCl_3$.

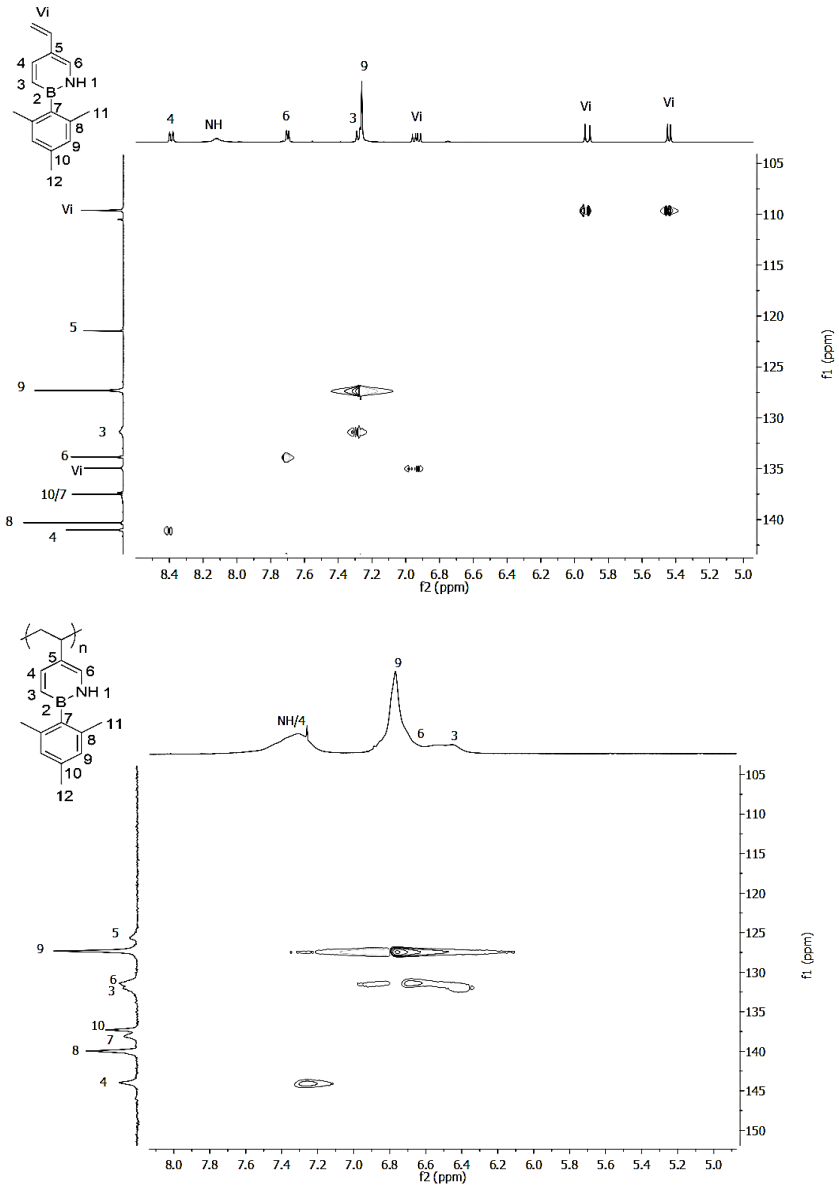

Figure 3-S37. Comparison of $^{1}H,^{13}C$-HMQC NMR spectra of 5V-NBMes and P5V-NBMes in $CDCl_3$.

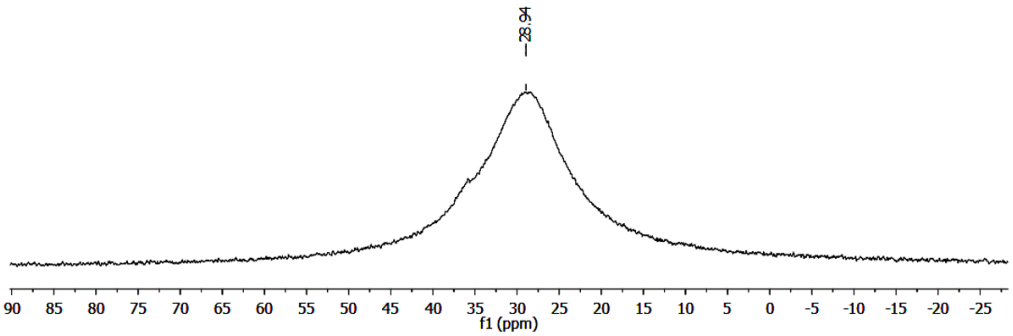

Figure 3-S38. ^{11}B NMR spectrum of P5V-NBMes polymer in CDCl3 (B-free NMR tube).

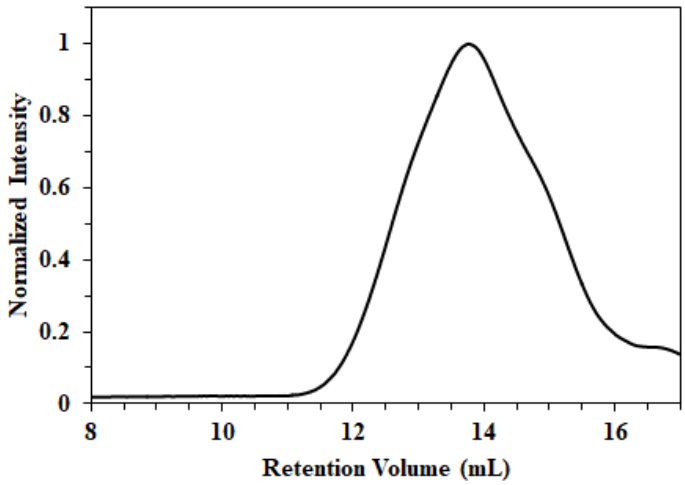

Figure 3-S39. GPC-RI trace of P5V-NBMes; eluent: THF, 1 mL min^{-1}.

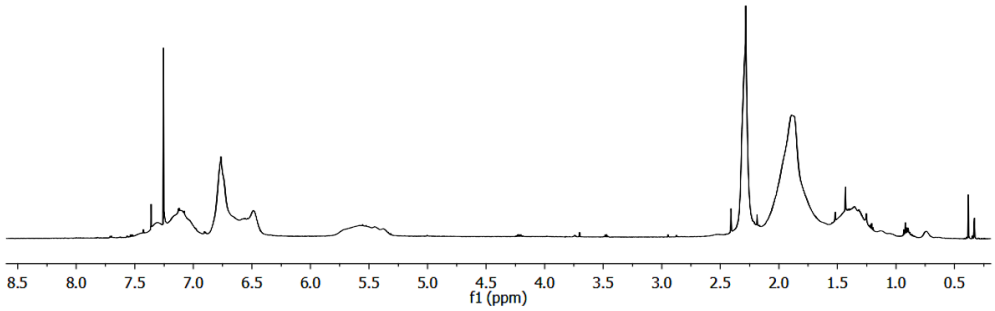

Figure 3-S40. ^{1}H NMR spectrum of P6V-NBMes polymer in $CDCl_3$.

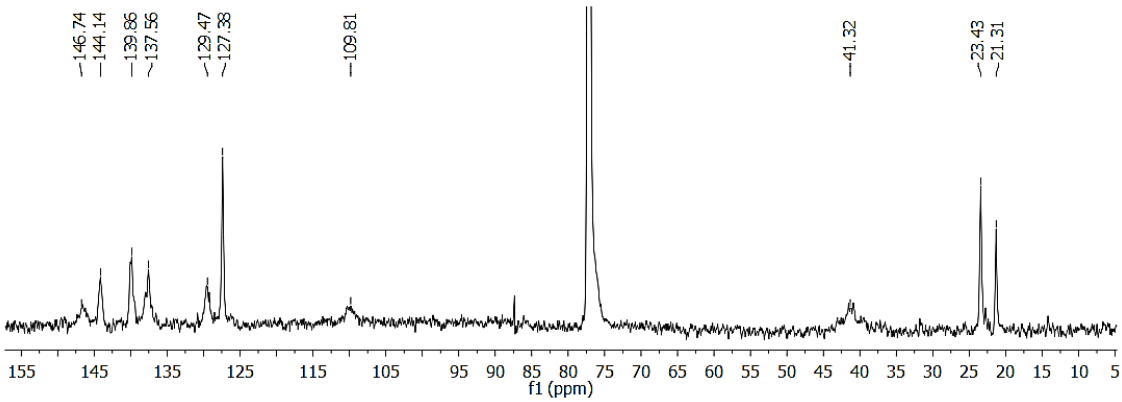

Figure 3-S41. ^{13}C NMR spectrum of P6V-NBMes polymer in $CDCl_3$.

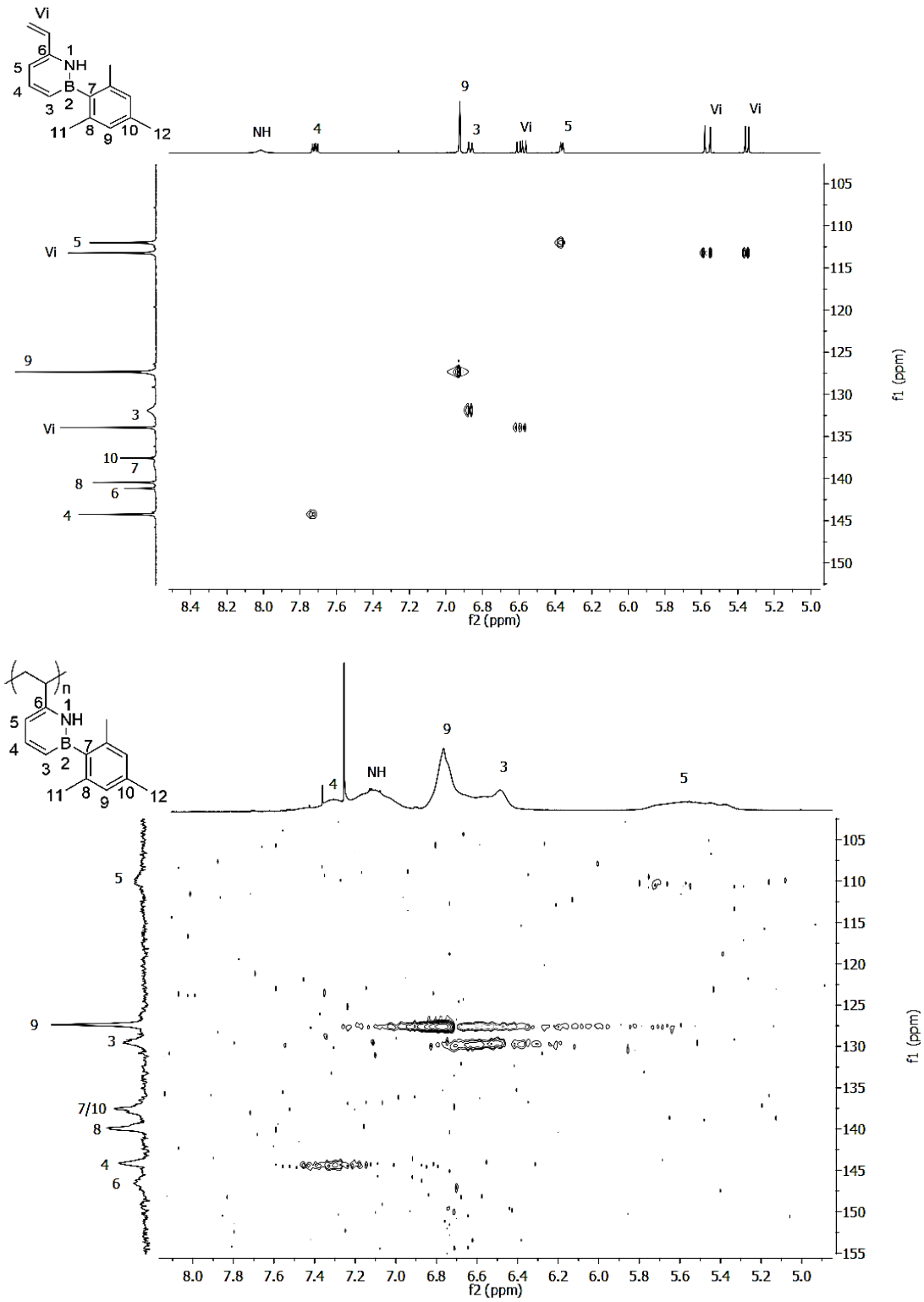

Figure 3-S42. Comparison of $^{1}H,^{13}C$-HMQC NMR spectra of 6V-NBMes and P6V-NBMes in $CDCl_3$.

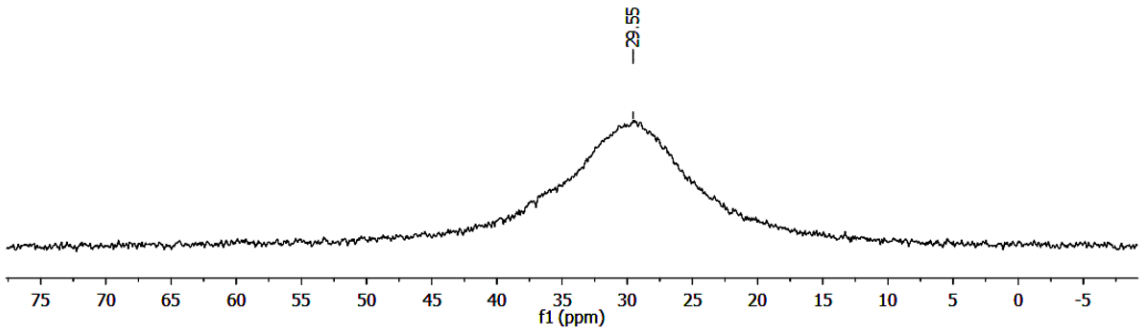

Figure 3-S43. ^{11}B NMR spectrum of P6V-NBMes polymer in $CDCl_3$ (B-free NMR tube).

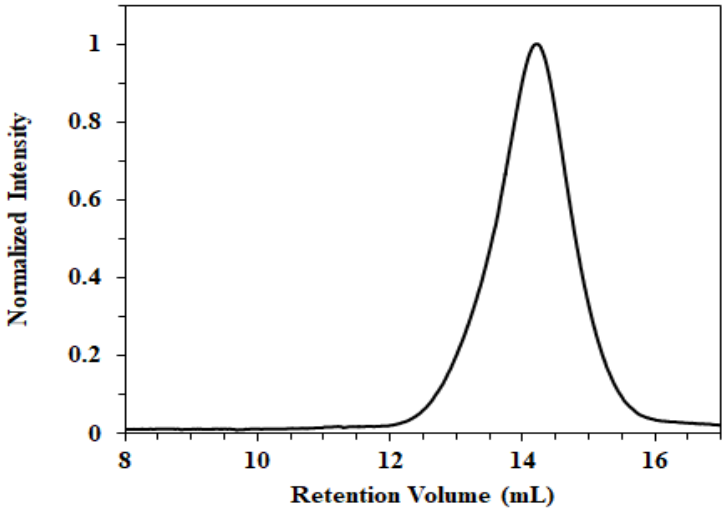

Figure 3-S44. GPC-RI trace of P6V-NBMes; eluent: THF, 1 mL min^{-1}.

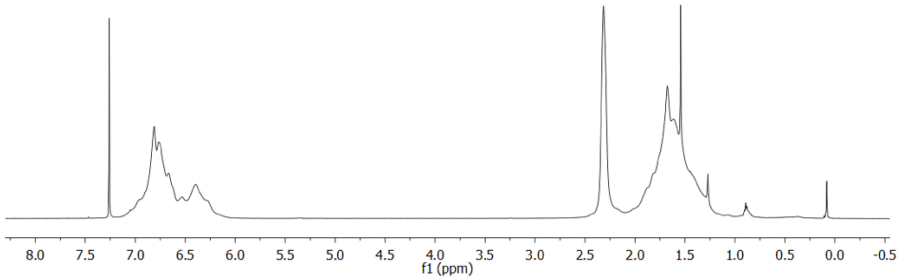

Figure 3-S45. ^{1}H NMR spectrum of mMesSt polymer in $CDCl_3$.

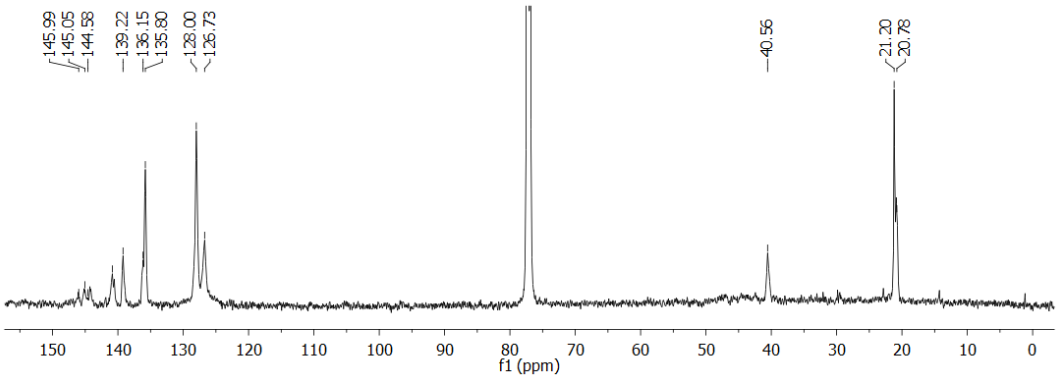

Figure 3-S46. ^{13}C NMR spectrum of *m*MesSt polymer in $CDCl_3$.

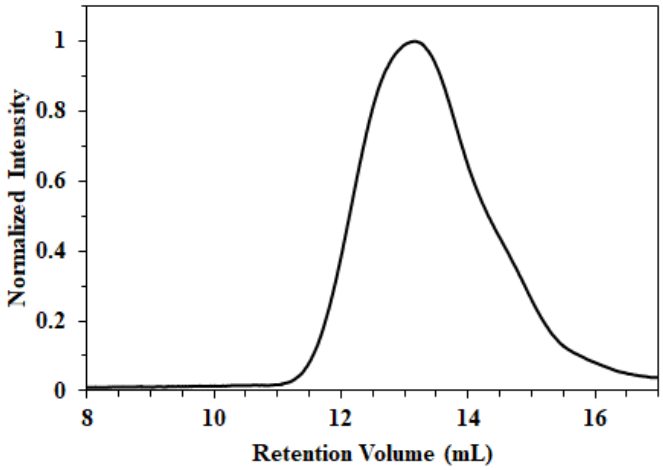

Figure 3-S47. GPC-RI trace of *m*MesSt polymer; eluent: THF, 1 mL min^{-1}.

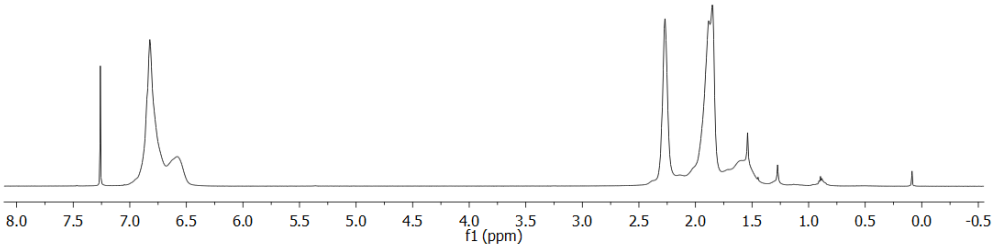

Figure 3-S48. ^{1}H NMR spectrum of *p*MesSt polymer in $CDCl_3$.

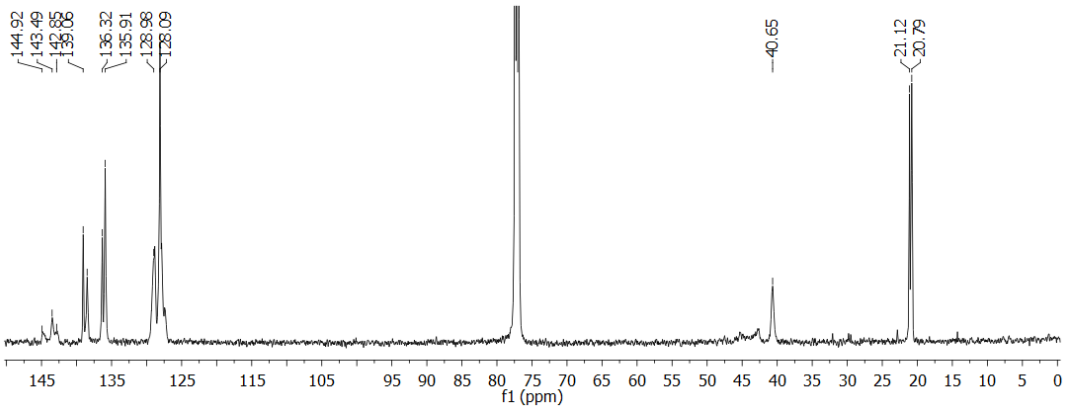

Figure 3-S49. ^{13}C NMR spectrum of *p*MesSt polymer in $CDCl_3$.

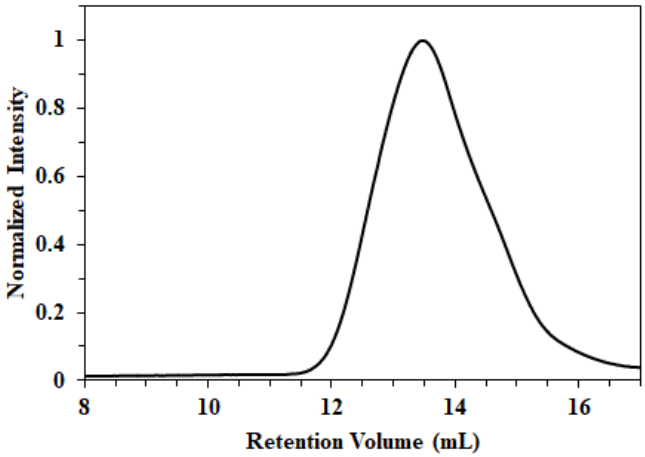

Figure 3-S50. GPC-RI trace of *p*MesSt polymer; eluent: THF, 1 mL min^{-1}.

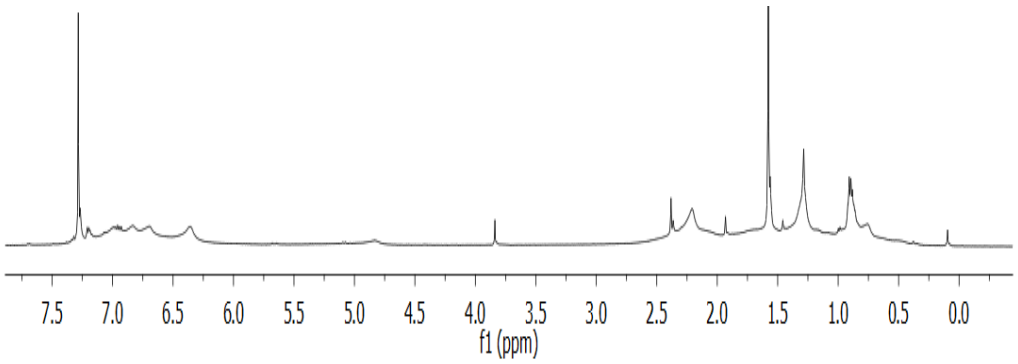

Figure 3-S51. ^{1}H NMR spectrum of *o*MesSt polymer in $CDCl_3$.

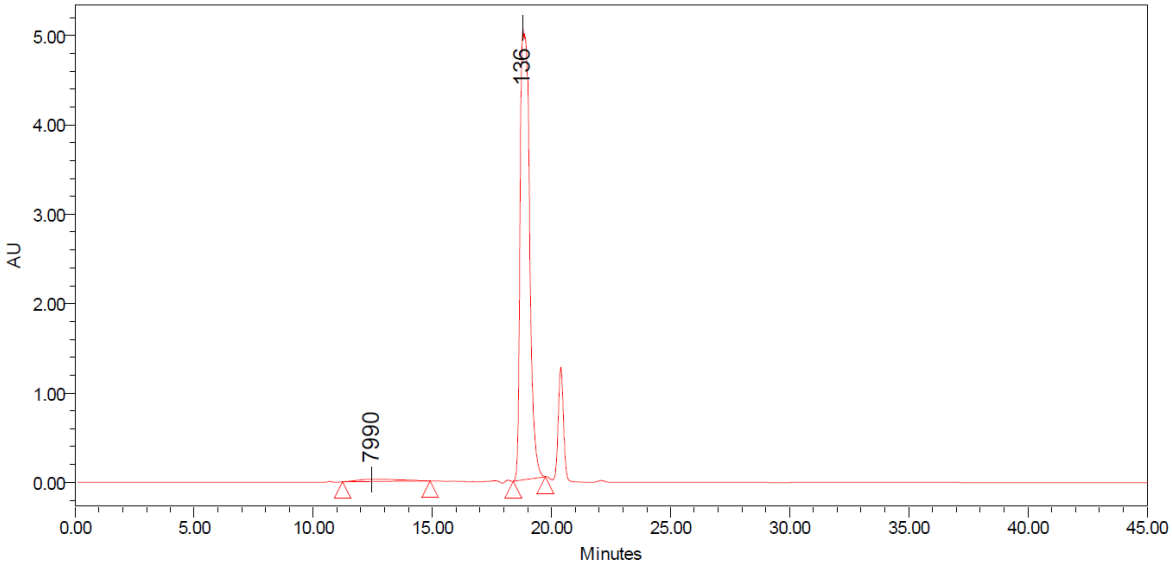

Figure 3-S52. GPC-UV trace of crude mixture for *o*MesSt polymerization; eluent: THF, 1 mL min^{-1} (peak at 136 Da corresponds to residual monomer).

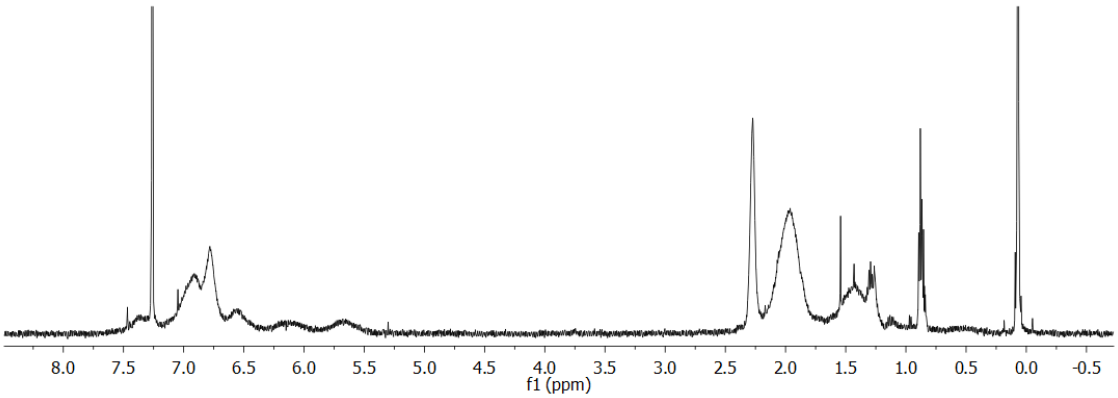

Figure 3-S53. ^{1}H NMR spectrum of isolated P4V-NBMes-co-PS in $CDCl_3$.

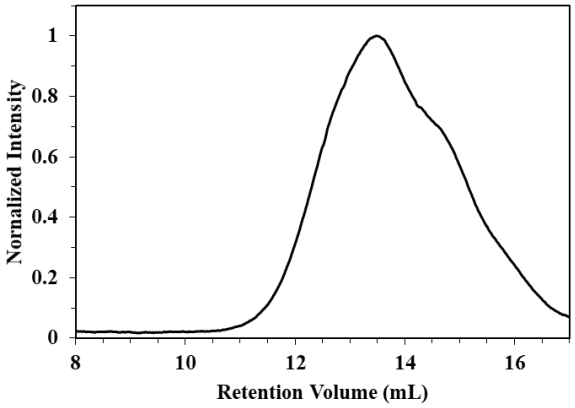

Figure 3-S54. GPC trace of isolated P4V-NBMes-co-PS; eluent: THF, 1 mL min^{-1}.

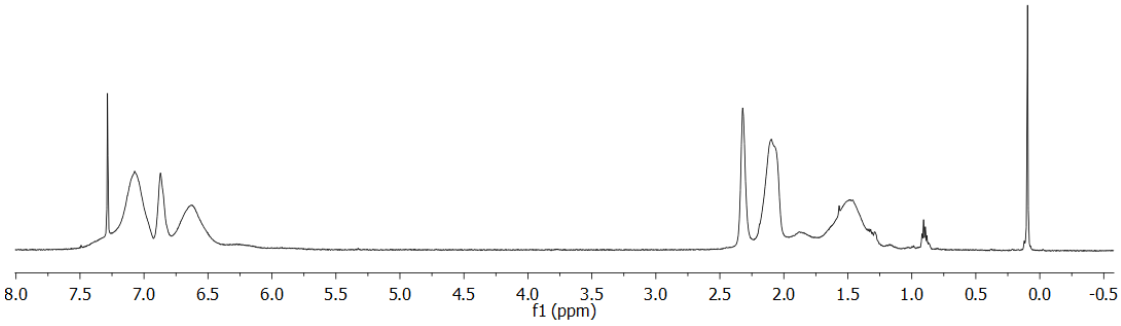

Figure 3-S55. ^{1}H NMR spectrum of P5V-NBMes-co-PS polymer in $CDCl_3$.

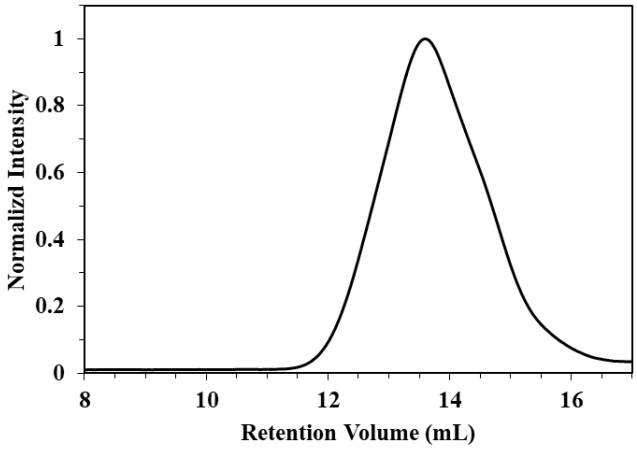

Figure 3-S56. GPC trace of P5V-NBMes-co-PS; eluent: THF, 1 mL min^{-1}.

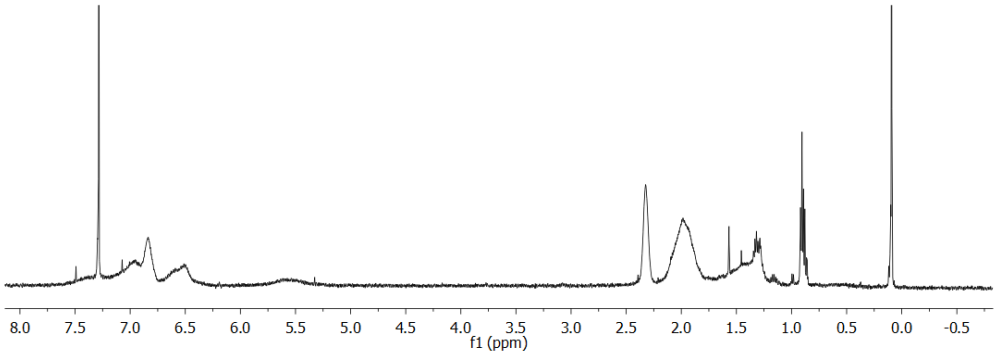

Figure 3-S57. ^{1}H NMR spectrum of P6V-NBMes-co-PS polymer in $CDCl_3$.

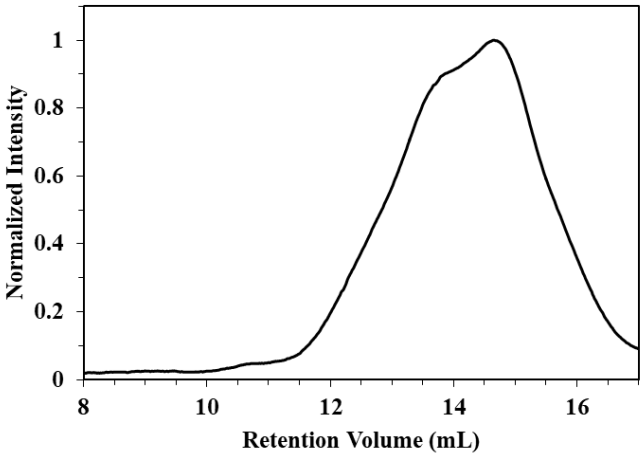

Figure 3-S58. GPC trace of P6V-NBMes-co-PS; eluent: THF, 1 mL min^{-1}.

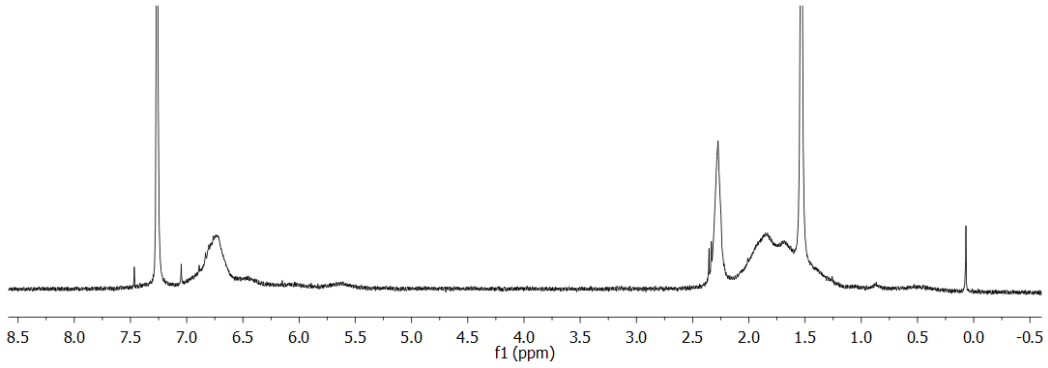

Figure 3-S59. ^{1}H NMR spectrum of P4V-NBMes-co-P*m*MesSt polymer in $CDCl_3$.

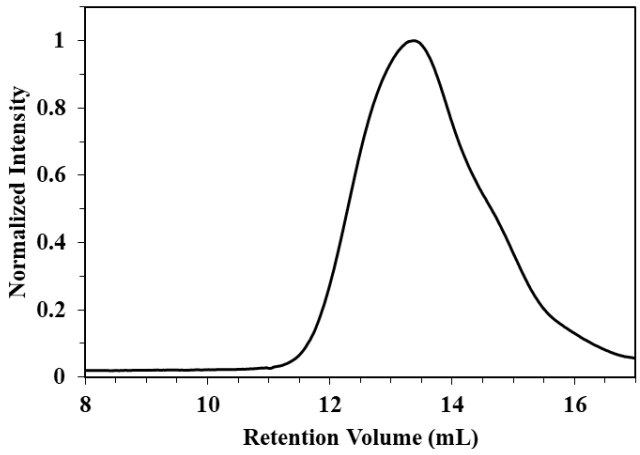

Figure 3-S60. GPC trace of P4V-NBMes-co-P*m*MesSt; eluent: THF, 1 mL min^{-1}.

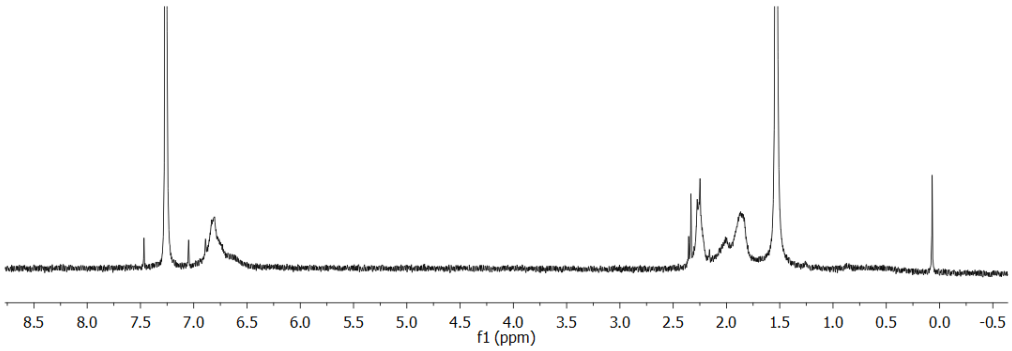

Figure 3-S61. ^{1}H NMR spectrum of P5V-NBMes-co-P*p*MesSt polymer in $CDCl_3$.

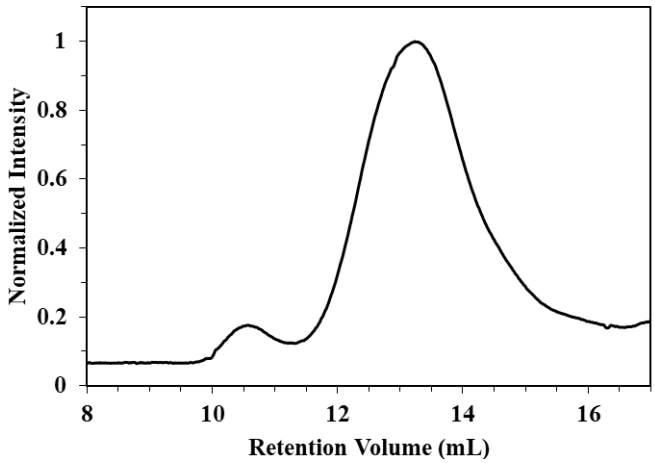

Figure 3-S62. GPC trace of P5V-NBMes-co-P*p*MesSt; eluent: THF, 1 mL min^{-1}.

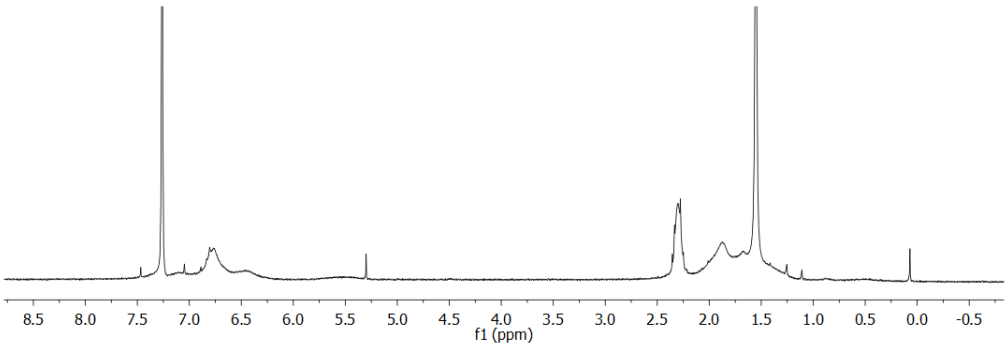

Figure 3-S63. ^{1}H NMR spectrum of P6V-NBMes-co-P*m*MesSt polymer in $CDCl_3$.

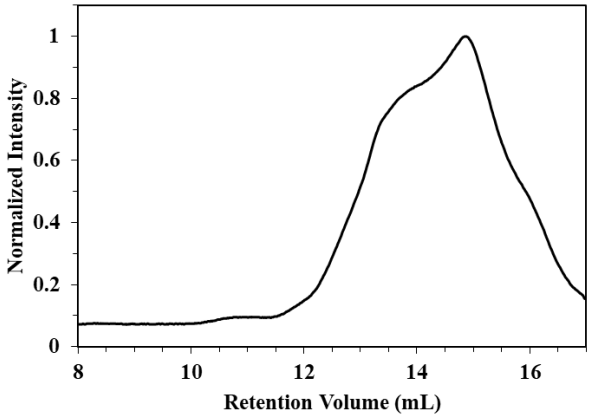

Figure 3-S64. GPC trace of P6V-NBMes-co-P*m*MesSt; eluent: THF, 1 mL min^{-1}.

Chapter 4 Ring Opening Metathesis Polymerization (ROMP) of the Dewar Isomer of a 1,2-Azaborinine

4.1 Introduction

Dewar benzene, first synthesized in 1963 by Tamelen *via* photoisomerization of cis-1,2-dihydrophthalic anhydride followed by decarboxylation with lead tetraacetate,[1] consists of two strained cyclobutene rings that are fused together. Due to the reversibility of the Dewar benzene formation, suitably substituted derivatives are promising as energy storage materials. For instance, in the hexamethyl benzene (HMB) – hexamethyl Dewar benzene (HMDB) pair, photoisomerization converts HMB to high-energy HMDB, which is sufficiently stable to release thermal energy only on demand.[2] In materials science, Hawker, Stucky and coworkers applied Dewar benzene derivatives embedded into cross-linked polymeric materials for holographic 3D-information storage, taking advantage of quantum-amplification effects of the photoisomerization.[3] Recently, Dewar benzene has also been embedded into the main chain of polymers as a means to achieve new reconfigurable materials that undergo highly efficient main-chain structural transformations via valence isomerization. As demonstrated by Swager and coworkers, the free radical 1,4-polymerization of Dewar-*o*-xylylene yields a poly(Dewar-*o*-xylylene) that is composed of Dewar benzene units stitched together by ethylene.[4] Triggered by heat or a photoredox process this unique polymer can be quantitatively converted into poly(*o*-xylylene).

While the materials discussed above consist solely of carbon atoms in their backbone, heteroarenes with B-N units embedded in the aromatic framework provoke ever increasing

interest due to the extensive applications that are emerging in biochemistry and pharmacology, materials science, and catalysis.[5] The isosteric replacement of C=C for B-N units in benzene to furnish 1,2-azaborinines has proved to be a particularly effective approach. Importantly, azaborinines exhibit significant differences in the aromatic delocalization from benzene. As a consequence, they present distinct reactivity at different ring positions that allows for selective functionalization.[5] In a remarkable recent development, Bettinger and Liu discovered that 1,2-dihydro-1-tert-butyldimethylsilyl-2-mesityl-1,2-azaborinine (**A**) undergoes photoconversion into the corresponding Dewar valence isomer (**B**) upon irradiation with UV light (> 280 nm) (Scheme 4-1). The kinetically stable **B** can be converted back to **A** by a thermal electrocyclic ring-opening reaction that requires an activation energy of (27.0 ± 1.2) kcal mol^{-1}. In the presence of the Wilkinson catalyst, the ring-opening occurs rapidly and exothermically at room temperature.[6] Bettinger and Liu proposed that the energy that is reversibly stored in this Dewar valence isomer could be utilized in molecular solar-thermal system applications. Pursuing new synthetic pathways that take advantage of the facile formation of highly functional BN-Dewar benzene derivatives, Liu and coworkers also developed a new strategy to 1,2-substituted cyclobutane derivatives (**E**) via hydrogenation and subsequent ring-opening of the 4-membered B-N heterocycle.[7]

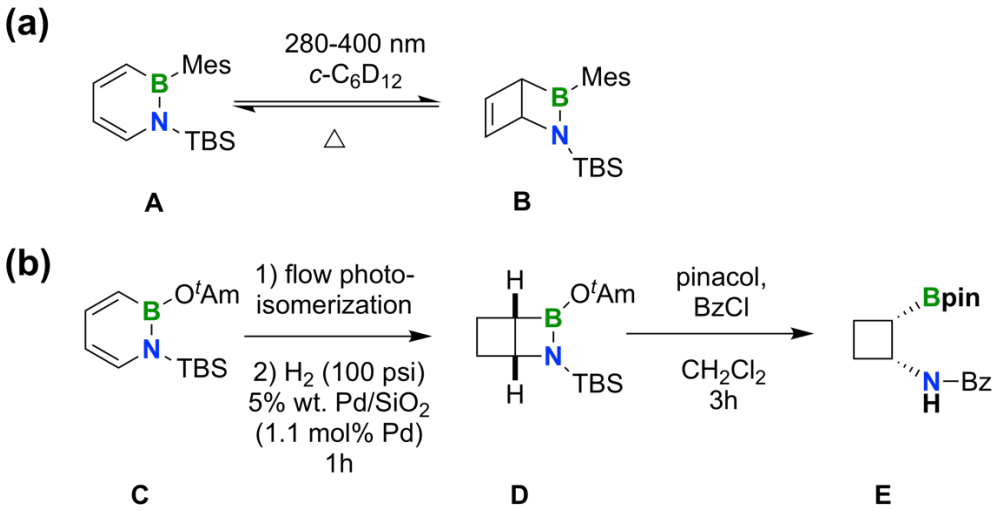

Scheme 4-1. (a) Photoisomerization of **A** to the Dewar isomer **B** (TBS = t-butyldimethylsilyl, Mes = 2,4,6-trimethylphenyl). (b) Sequential isomerization/hydrogenation of **C** to azaborabicyclohexane **D** and subsequent ring opening to form aminoborylated cyclobutane **E**.

Inspired by these results, we hypothesized that the presence of a strained cyclobutene ring system in BN Dewar isomers may provide an avenue to new classes of highly functionalized polyolefins via ring-opening metathesis polymerization (ROMP). The ROMP of strained cyclobutenes has been widely studied and is typically accomplished using Grubbs 2nd (G2) and 3rd (G3), or Hoveyda-Grubbs 2nd (HG2) generation catalysts. For instance, Bielawski and coworkers reported the ROMP of a dibromo derivative of Dewar benzene, which upon elimination and rapid isomerization was converted into *trans*-poly(acetylene) (Scheme 4-2).[8] More recently, Xia and coworkers demonstrated the ROMP synthesis of poly(ladderene)s and poly(benzoladderene)s that could be mechanochemically transformed into polyacetylene derivatives.[9, 10] Different from these polymeric materials, in which rearrangements are triggered by ring-opening of cyclobutene or multiple fused cyclobutane rings, the ROMP of BN-Dewar isomers is expected to result in novel classes of polyolefins that contain both amine and borane moieties that potentially can be further

transformed into many other functional groups. Herein we report the first synthesis of poly(BN-Dewar benzene) *via* ROMP as a versatile new route to highly desirable functional polyolefins that contain both amine and alcohol functional groups separated by ethylene spacers. This unique class of polymers with amine and alcohol functional groups attached in regular sequence directly to the polymer backbone would be exceedingly difficult to access through any other synthetic routes.

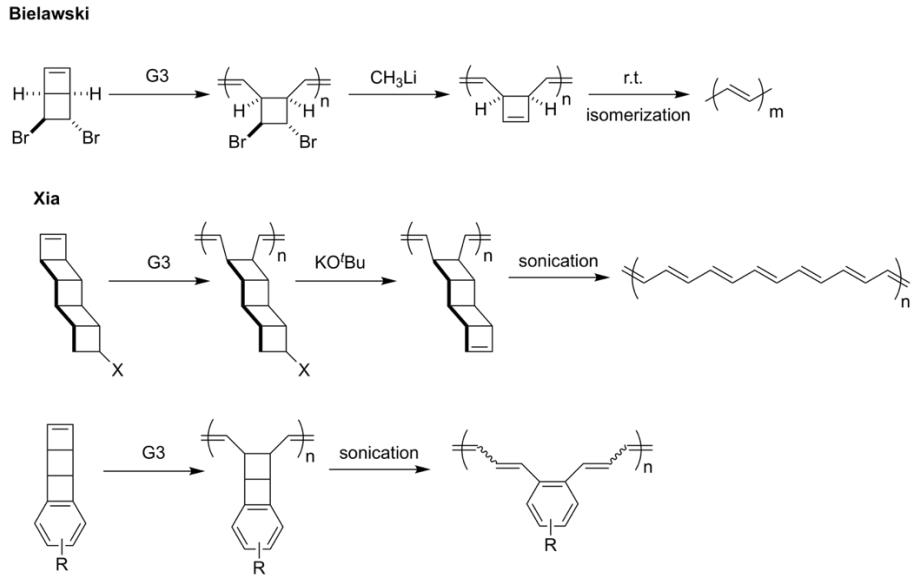

Scheme 4-2. Selected examples of ROMP of strained cyclobutenes.

4.2 Results and Discussion

The Dewar isomer **1** was prepared as previously reported by photoisomerization of B—mesityl-N-(*t*-butyldimethylsilyl)azaborinine (**A**) as described in Scheme 4-1.[6] We explored different generations of Grubbs and Hoveyda Grubbs catalysts for the ROMP of monomer **1** (Scheme 4-3). The monomer conversion was determined by ^{1}H NMR integration and the results are summarized in Table 4-1. Grubbs 3rd generation catalyst (G3) is one of the most

widely used ruthenium initiators for ROMP. In comparison to 2nd generation catalysts (G2, HG2), G3 exhibits very fast initiation rates, which typically enables the formation of polymers with very narrow dispersities and an excellent control over their molecular weights.[11] However, G3 was found to be not very effective at converting Dewar isomer **1** to polymer **2**. At 0.1 M monomer concentration, G3 gave only low monomer conversion even after very long reaction times at either room temperature or 0 ºC (Table 4-1, entry 1, 2). This contrasts the successful controlled polymerization of other cyclobutene derivatives reported in the literature.[8] A possible reason could be that the polymerization is slow due to steric effects of the bulky Mes and TBS groups or electronic effects[12, 13] of the electron-deficient borane group, which in combination with the relatively low stability of G3 may result in backbiting or early termination processes over the longer reaction times needed. Another possibility might be that the pyridine base liberated during the initiation step may interfere by binding to the boron centers.[14] As such, we explored the ROMP of **1** with G2 and HG2, which do not contain unhindered basic pyridine ligands and are known to exhibit improved thermal stability, oxygen- and moisture-tolerance.[15] Although G2 and HG2 are usually not suitable for living polymerization due to the slow initiation and small initiation/propagation rate ratio (k_i/k_p), they have been successfully applied to the polymerization of cyclobutenes when other catalysts gave poor results.[14, 16] Performing the ROMP of **1** at room temperature with either G2 or HG2 proved to be more effective, resulting in higher monomer conversion (>90%) over a shorter time period of 7-9 hours (Table 4-1, entry 3-4). As seen in entries 5 and 6, higher monomer concentration (0.3 M) promoted propagation, further shortening the reaction time to 4.5 h. HG2 consistently gave

slightly higher conversions, indicating a faster rate of polymerization. To explore the effect of raising the temperature on the ROMP of **1** polymerizations were attempted at 50 ºC using G3, G2 and HG2 at 0.1 M initial monomer concentration. Under these conditions we found increased amounts of thermal ring opening of Dewar isomer **1** back to the parent 1,2-azaborinine. In addition, we carried out a polymerization with the *cis*-selective catalyst HGM2001 (Table 4-1, entry 7). ^{1}H NMR data (Figure 4-S7) revealed sharper peaks at 5.70, 5.41, and 4.90 ppm, indicative of enhanced stereoselectivity of the polymerization. However, the conversion proved to be relatively low (33%) even after an extended reaction time of 24 h.

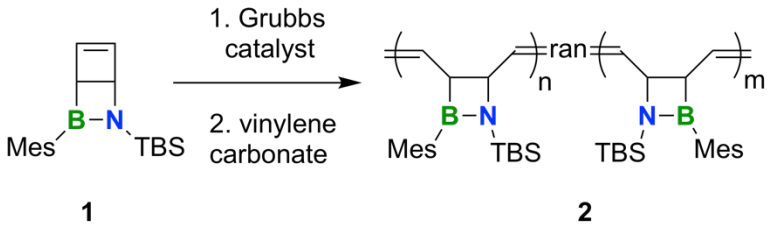

Scheme 4-3. ROMP Synthesis of polymer **2**.

Table 4-1. Ring-opening metathesis polymerization condition of Dewar isomer **1**.

Entry	Catalyst	Feed ratio	[**1**] (M)	Solvent	*T* / t (ºC / h)	Conv (%)	M_n [a] (Da)	M_w [a] (Da)	*Đ* [a]	DP_n or DP_w
1 [b]	G3	50:1	0.1	C_6D_6	r.t. / 120	47%	4300	7500	1.74	14
2 [b]	G3	50:1	0.1	CD_2Cl_2	0 / 48	51%	5200	8700	1.67	17
3 [c]	G2	100:1	0.1	C_6H_6	r.t. / 9	92%	8100	14400	1.76	26
								24100 [d]	1.74 [d]	77 [d]
4 [c]	HG2	100:1	0.1	C_6H_6	r.t. / 7	>99%	6000	9200	1.54	19
								14600 [d]	1.44 [d]	47 [d]

5 [c]	G2	100:1	0.3	C_6H_6	r.t. / 4.5	80%	9600	18000	1.88	31
								31300 [d]	1.41 [d]	100 [d]
6 [c]	HG2	100:1	0.3	C_6H_6	r.t. / 4.5	93%	7600	15700	2.08	24
								28600 [d]	1.31 [d]	92 [d]
7 [c]	HGM2001	100:1	0.1	C_6D_6	r.t. / 24	33%	4200	6200	1.46	13

[a] Analyzed by gel permeation chromatography with refractive index (GPC-RI) detection relative to narrow polystyrene standards unless otherwise stated; $Đ = M_w / M_n$. [b] Conversion estimated for the crude product based on ^{1}H NMR integration of the *t*-butyl H NMR signal of the residual monomer relative to the *t*-butyl H signal of the polymer; GPC analysis of crude product in THF. [c] Conversion estimated for the crude product based on ^{1}H NMR integration of the olefinic signals of the residual monomer relative to anisole as a reference; GPC analysis of isolated product in THF. [d] Analyzed by gel permeation chromatography with right-angle light scattering (GPC-RALS) detection (dn/dc = 0.168 mL/g).

The polymerizations were quenched with a large excess of vinyl carbonate, the volatiles removed in vacuo, and the polymers isolated by repeated precipitation from benzene into MeCN. The molecular weight distributions were analyzed by gel permeation chromatography (GPC) in tetrahydrofuran (THF) with a refractive index detector (GPC-RI) relative to narrow polystyrene (PS) standards and/or using a right-angle light scattering detector (GPC-RALS). GPC-RI analysis for the polymer obtained with G2 (1 mol%) at 0.1 M monomer concentration (entry 3) gave a monomodal molecular weight (MW) distribution with a number average molecular weight of M_n = 8100 Da and a dispersity ($Đ$) of 1.76. A similar result was obtained for HG2 (entry 4), which gave M_n = 6000 Da and a dispersity ($Đ$) of 1.54. The theoretically predicted molecular weights are significantly higher (31100 at 100% conversion), suggesting that these data are likely underestimated because of the use of structurally different narrow PS standards. Indeed, molecular weights derived from RALS detection were consistently higher.

To further study the controlled nature of the ROMP of **1** with G2 and HG2 as catalysts we carried out detailed kinetic experiments at 0.3 M monomer concentration (Table 1, entries 5, 6 and Figure 4-S1). For both G2 and HG2, the monomer conversion reached >80% in 4.5 hours at room temperature in benzene. The conversion of Dewar isomer **1** with G2 followed first-order kinetics, illustrated by a linear plot of ln([M_0]/[M]) vs time with a calculated $k_{obsd,G2}$ = 0.38 M^{-1} s^{-1}. Meanwhile, HG2 showed very fast conversion over the first 30 minutes, but then followed a similar first-order kinetics as seen for G2 with $k_{obsd,HG2}$ = 0.41 M^{-1} s^{-1} (Figure 4-1). This may suggest that HG2 more rapidly initiates polymerization than G2.

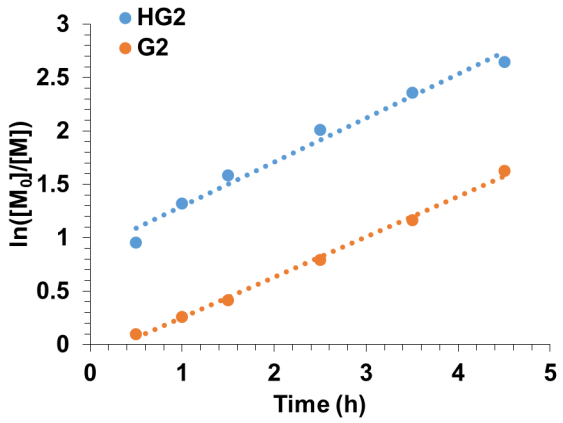

Figure 4-1. First order kinetic plot for ROMP of Dewar isomer **1** with G2/HG2. ROMP conditions: [M_0] = 0.3 M; conversion determined by ^{1}H NMR integration.

GPC-RI analyses revealed monomodal distributions with slight low molecular weight shoulders for which average molecular weights of M_n = 9600 Da ($Đ$ = 1.88) for entry 5 and M_n = 7600 Da ($Đ$ = 2.08) for entry 6 were estimated (Figure 4-2). The GPC-RALS analyses gave weight-average molecular weights of M_w = 31300 Da (entry 5) and M_w = 28600 Da (entry 6) that are close to the predicted molecular weight based on the monomer to initiator

ratio (31100 at complete conversion). The RALS analyses also indicated the presence of a very small amount of cross-linked high molecular weight polymers, which are not detected by using RI detection (Figure 4-S2). Overall, G2 shows better first-order kinetics behavior, thus we chose G2 as catalyst in our subsequent studies.

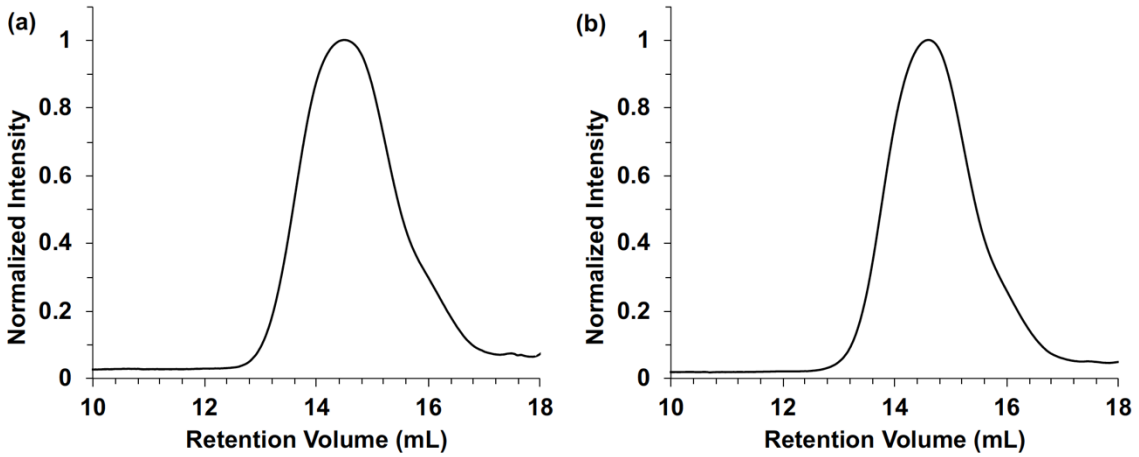

Figure 4-2. GPC-RI traces of polymers obtained with G2 (a) and HG2 (b); eluent: THF, 1 mL min^{-1}.

The chemical structure of the new polymer was confirmed by ^{1}H, ^{11}B, and two-dimensional (2D) NMR spectroscopy. The disappearance of the olefinic group signals and pronounced peak broadening in the ^{1}H NMR spectra clearly indicate successful ROMP of the strained cyclobutene rings in Dewar isomer **1** with the formation of polymers that are presumed to be regiorandom (Figure 4-3a). In the ^{11}B NMR spectra, a significant upfield shift from ca. 53 to 45 ppm and concomitant peak broadening provides further evidence for the successful polymerization (Figure 4-3b). A slight upfield shift is frequently observed upon polymerization of borane monomers as a result of shielding effects of the neighboring groups along the polymer chain.[17, 18] To further confirm the connectivity between the four-

membered BN-heterocycles and vinylene groups in the polymer main chain, heteronuclear single-quantum correlation (HSQC), heteronuclear multiple-quantum correlation (HMBC), and nuclear Overhauser effect spectroscopy (NOESY) NMR data were acquired. The HSQC and HMBC data show the expected cross peaks for the mesityl and *tert*-butyldimethylsilyl groups (Figure 4-S4, 4-S5).

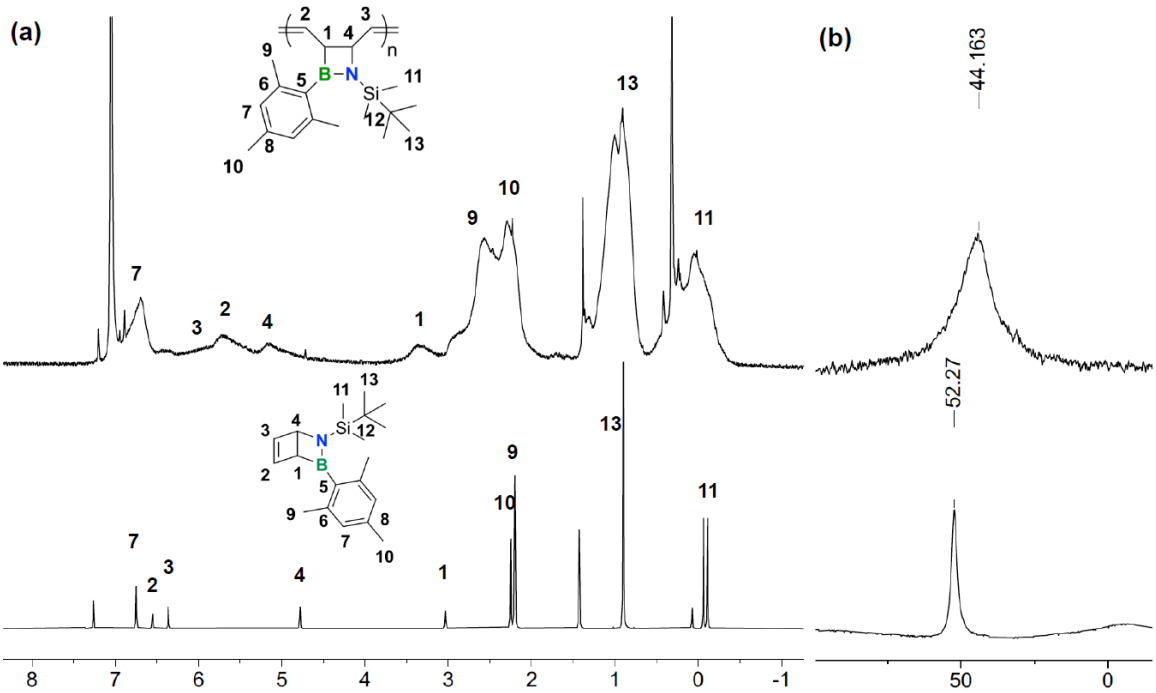

Figure 4-3. (a) ^{1}H and (b) ^{11}B NMR spectra of monomer (bottom) and polymer (top) in C_6D_6.

The strongly broadened backbone protons of the polymer in the range from 3.0 - 6.5 ppm are based on a NOESY NMR analysis (Figure 4-4 and Figure 4-S6). To gain insights into the relative distances between protons we used DFT methods to optimize the geometry of head-to-tail model dimers with vinyl as end groups, both *cis*-vinylene and *trans*-vinylene-

linked structures, with the nonaromatic methine protons H1 and H4 *cis* relative to one another as expected based on the geometry of the Dewar-azaborinine precursor. The calculated Gibbs free energy is 20.8 kJ mol^{-1} higher for the *cis*- than the *trans*-isomer, which indicates that the *trans*-isomer is significantly more favorable (Figure 4-S7; Tables 4-S1, 4-S2). The structure of the more favorable *trans*-isomer is displayed in Figure 4-4a, illustrating some of the closest intramolecular H···H distances. The distances in this model dimer were then used to assign the NOE peaks in the NOESY spectrum of the polymer (Figure 4-4b). The allylic methine protons H1 and H4 are expected more upfield than H2 and H3. The upfield signal at 3.4 ppm was assigned to H1 as it shows the expected cross peak 3.4/5.8 ppm due to its proximity to the boron-bound mesityl groups (H9). The *ortho*-mesityl protons (H9) are also in close proximity to H2 resulting in another very dominant cross peak at δ = 5.8/2.6 ppm. A third strong cross peak at δ = 3.4/5.2 ppm is attributed to the NOE between H1 and H4 which are in adjacent positions and share the same orientation. Finally, the assignment of H3 at 6.0 ppm is based on a cross-peak with H2 at δ = 6.0/5.8 ppm. The separation of H2 and H3 within a single trans-vinylene unit is large, but H2 can come in close contact to H3 in the next vinylene repeating unit and vice versa. We note that additional weaker broad ^{1}H NMR peaks may indicate the presence of a smaller extent of *cis*-vinylene linkage or possibly head-to-head arrangements of the BN four-membered heterocycles.

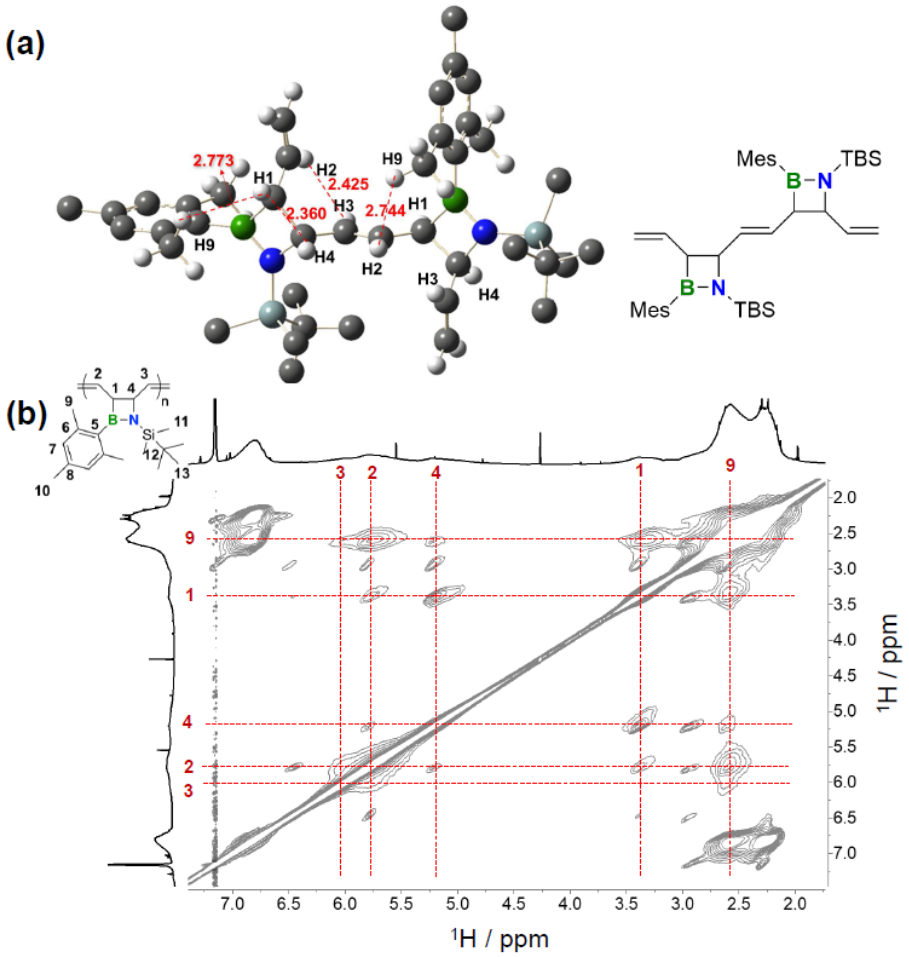

Figure 4-4. (a) Structure of head-to-tail *trans*-vinylene bridged model dimer (one isomer shown, multiple isomer possible due to chirality at C1 and C4). (b) Section of ^{1}H-^{1}H NOESY spectrum of polymer **2** in C_6D_6.

The structural integrity of the four-membered BN-heterocycle was further verified by comparison of the FT-IR spectra of the monomer and the polymer (Figure 4-5). The IR bands for poly(1,2-azaborining) **2** were assigned based on comparisons with results from theoretical calculations (B3LYP/6-31g(d)) of Dewar isomer **1** and the *trans*-vinylene-linked head-to-tail model dimer (see Figure 4-4a and Table 4-2), as well as previous reported experimental data for **1**.[6, 19] Strong BN stretching modes (ca. 1354 / 1361 cm^{-1}) are observed in both the monomer and polymer spectra. The characteristic C-H bending

modes in the BN heterocycle of **1** (ca. 1179, 1136 and 979 cm^{-1}) as well as the C-B stretching (ca. 1038 cm^{-1}) and C-N stretching modes (ca. 1252 cm^{-1}), are also seen in the poly(1,2-azaborinine) **2**, with some peak broadening, further confirming the integrity of the BN-heterocycle. For the Dewar isomer **1**, an additional set of strong bands is found at 1275, 1228, 1158, 1120-1106 and 941-883 cm^{-1} and assigned to C-H bending modes in the cyclobutene ring. The disappearance of these bands in poly(1,2-azaborinine) **2** confirms the ring opening of the cyclobutene ring during polymerization. Collectively, these data strongly support the polymer structure with four-membered heterocycles embedded in the backbone (for the complete spectrum see Figure 2-S8 in the appendix).

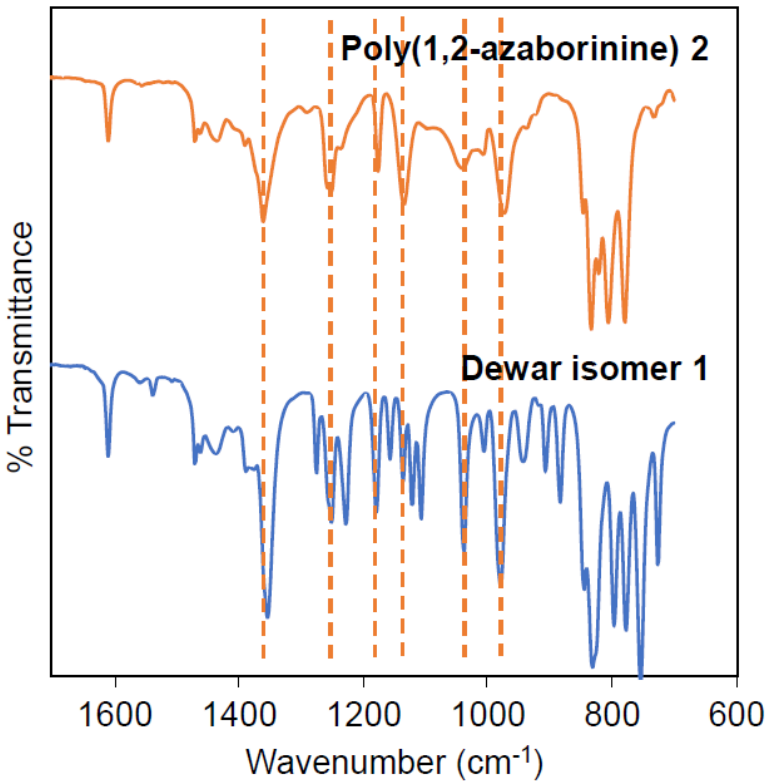

Figure 4-5. FT-IR spectrum of Dewar isomer **1** and poly(1,2-azaborinine) **2**.

Table 4-2. Comparison of vibrational frequencies and calculated absorptions for Dewar isomer **1** and poly(1,2-azaborinine) **2**.

1	**1_{th}**			**2**	**Model $Dimer_{th}$**		
υ_{exp} [cm^{-1}]	ω_{theor} [cm^{-1}]	Intensity	Assignment	υ_{exp} [cm^{-1}]	ω_{theor} [cm^{-1}]	Intensity	Assignment
2953.6 - 2855.6	3092 3116 3164	365.3 295.0 129.0	υ(CH)	2953.6-2855.7	3092 3108 3124	546.5 531.3 585.0	υ(CH)
1610.1	1668	65.8	υ(CC in Mes)	1610.0	1668	168.8	υ(CC in Mes)
1470.6 - 1436.3	1492	129.5	υ(CC in TBS)	1470.6-1435.3	1492	378.6	υ(CC in TBS)
1354.0	1388	983.9	υ(BN)	1360.9	1388	1081.3	υ(BN)
1275.2	1324	123.4	δ(CH in CC ring in-plane)				
1251.6	1276	80.6	υ(CN) δ(BN ring)	1249.6	1268	289.4	υ(CN) δ(BN ring)
1228.0	1268	111.7	δ(CH in CC ring in-plane)				
1179.0	1212	91.6	δ(CH in BN ring in-plane)	1176.0	1212	259.1	δ(CH in BN ring in-plane)
1157.9	1180	69.3	δ(CH in CC ring)				
1136.1	1164	58.9	δ(CH in BN ring out-of-plane)	1133.9	1164	483.5	δ(CH in BN ring out-of-plane)
1120.4 1106.9	1140 1132	171.8 71.56	δ(CH in CC ring)				
1037.5	1076	115.2	υ(CB)	1041.4	1108	346.4	υ(CB)

			δ(BN ring)				δ(BN ring)
979.7	996	273.3	δ(CH in BN ring in-plane)	971.9	996	510.9	δ(CH in BN ring in-plane)
941.1 906.3 883.2	964 932 908	53.0 51.4 54.9	δ(CH in CC ring)				
831.2	860	356.0	δ(CH in BN ring out-of-plane)	833.1	852	802.6	δ(CH in BN ring out-of-plane)

Finally, the thermal stability of the polymer was established by thermogravimetric analysis (TGA), revealing an onset of decomposition for **2** at 231 °C (Figure 4-6).

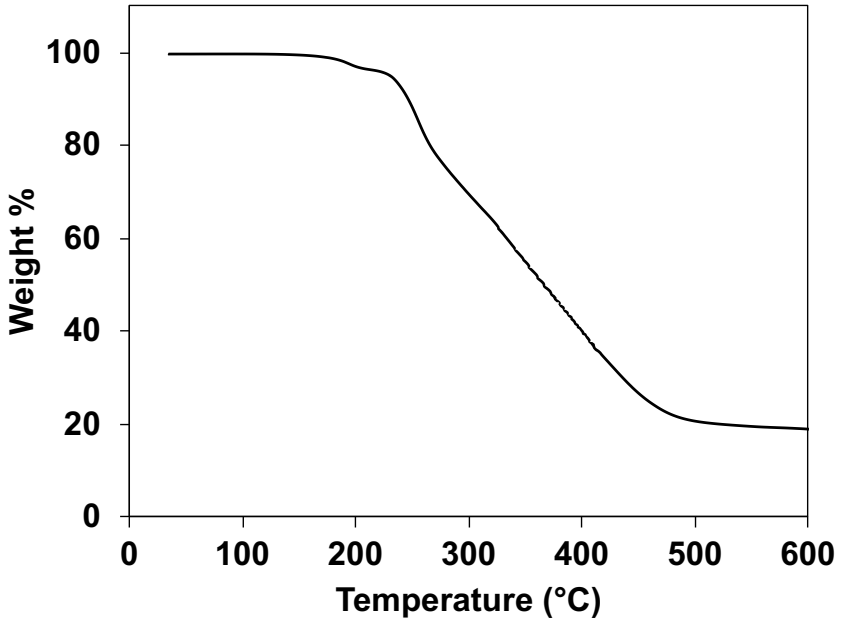

Figure 4-6. TGA trace of poly(1,2-azaborinine) **2** acquired at a scan rate of 10 °C min^{-1}.

4.3 Conclusion

In summary, we have successfully synthesized polymer **2** by ROMP of Dewar isomer **1** with Grubbs or Hoveya Grubbs 2nd generation catalysts. The polymer features four-membered BN-heterocycles alternating with vinylene groups in the main chain. The unique structure of **2** was verified by GPC analysis, 2-dimensional NMR, and FT-IR measurements. The presence of the B-N four-membered rings may be exploited in the preparation of new functional polymers via chemoselective organoborane oxidation and/or hydrogenation of the double bonds in the backbone. This strategy may open up a new pathway to highly desirable functional polyolefins that contain both amine and alcohol groups separated by ethylene spacers. Such a polymer would be difficult to access through any other synthetic routes.

4.4 Experimental

General Method. All oxygen- and moisture-sensitive manipulations were carried out under an inert atmosphere using either standard Schlenk techniques or a glove box.

NMR data were acquired at 25 ºC. 499.9 MHz ^{1}H and 160.4 MHz ^{11}B NMR data were recorded on a 500 MHz Bruker AVANCE spectrometer, 500.2 MHz ^{1}H NMR data on a 500 MHz Bruker Auto AVANCE spectrometer, and 599.7 MHz ^{1}H, 150.8 MHz ^{13}C and 192.4 MHz ^{11}B NMR data on a Varian INOVA 600 spectrometer. ^{11}B NMR spectra were acquired with boron-free quartz NMR tubes either on the Varian INOVA 600 with a boron-free 5 mm dual broadband gradient probe (Nalorac, Varian Inc., Martinez, CA) or the 500 MHz Bruker Auto Avance with a 5mm PH SEX 500S1 11B-H/F-D probe. ^{1}H and ^{13}C spectra were referenced internally to solvent signals (C_6D_6: 7.16 ppm for ^{1}H NMR, 128.06

ppm for ^{13}C NMR) and ^{11}B NMR spectra externally to $SiMe_4$ (0 ppm). The Fourier transform infrared (FTIR) spectra were collected on a Thermo Electron Corporation Nicolet 6700 FT-IR with 128 scans and spectral resolution of 8 cm^{-1}; cells with CaF_2 windows were used (pathway length 0.0164 mm).

GPC-RI analyses were performed in THF (1.0 mL/min, 35 °C) using a Malvern Viscotek GPCmax with a VE 2001 GPC solvent/sample module, a 2600 UV-PDA detector, and a TDA 305 triple detector array. A set of two columns consisting of one PLgel 5 mm mixed-D and one PLgel 5 mm mixed-C column was used for separation and ten polystyrene standards (580 Da – 364000 Da, Polymer Laboratories, Varian Inc.) for calibration. GPC-RALS analyses were performed using the built-in right-angle light scattering detector. A dn/dc value of 0.168 mL/g for polymer **2** in THF was determined by assuming 100% mass elution from the columns.

Materials. All solvents and chemicals were purchased from commercial sources and used without further purification unless noted otherwise. C_6H_6 and C_6D_6 were distilled from Na/K alloy. CD_2Cl_2, anisole and acetonitrile were distilled from CaH_2. Dewar isomer **1** was prepared according to previously reported procedures.[6]

General Procedure for ROMP of 1 using Grubbs or Hoveyda Grubbs Catalysts (Table 1, entries 1-4). In a typical polymerization, a 20 mL vial capped was charged with 1,2-dihydro-1-*tert*-butyldimethylsilyl-2-mesityl-1,2-azaborinine (100 mg, 0.32 mmol), 1.8 mL of anhydrous C_6H_6, and 0.1 mL of a 0.8 M of solution of anisole in benzene as internal standard. The mixture was stirred to ensure homogeneity, and a few drops of the solution

were removed for NMR analysis to define the concentration of monomers present at t = 0 relative to the anisole internal standard. Under stirring, the reaction was then initiated by the addition of 0.1 mL of a 0.032 M solution of Grubbs catalyst in benzene. The reaction mixture was kept stirring at room temperature for as predetermined time. The conversion of the monomer was determined by integration of the ^{1}H NMR peak at 4.18 ppm (1H) for the monomer in comparison to the anisole reference peak at 3.34 ppm (3H). The final reaction solution was quenched by addition of a large excess of vinyl carbonate (0.1 mL). The solutions were concentrated in *vacuo.* The polymer was then precipitated into 100 mL of dry MeCN and redissolved in benzene, precipitated in MeCN again, and freeze-dried in benzene. After drying in high vacuum, the polymer was obtained as an off-white powder. Yield: 64 mg (64%).

Kinetic Studies (Table 1, entries 5 and 6). The reaction was set up in a manner similar to that described above. 50 μL aliquots of the polymerization solution were analyzed periodically by NMR (samples were injected into vials containing 0.05 mL vinylene carbonate and 0.4 mL C_6D_6) until the conversion of the monomers exceeded 80%. The mixture was then quenched by addition of a large excess of vinyl carbonate (0.1 mL), stirred for one hour, and then concentrated to 1 mL. The polymer solution was precipitated into 100 mL of dry MeCN and the supernatant decanted from the polymer. The polymer was dried on a high-vacuum line at ambient temperature for at least 24 h to remove volatiles.

^{1}H NMR (C_6D_6, 499.9 MHz): δ 6.81 (br, mesityl aromatic protons), 6.07, 5.75, 5.21, 3.35 (br, backbone protons), 2.59 (br, mesityl *ortho*-Me), 2.27 (br, mesityl *para*-Me), 1.01 (br,

Si-*t*-Bu), 0.02 (br, Si-Me). ^{13}C NMR (C_6D_6, 150.8 MHz): δ 138.7, 137.3, 27.1, 23.1, 21.4, 18.8, 4.5. ^{11}B NMR (C_6D_6, 160.4 MHz): δ 44 ppm.

4.5 References

1.van Tamelen, E. E.; Pappas, S. P., Bicyclo [2.2.0]hexa-2,5-diene. *Journal of the American Chemical Society* **1963,** *85* (20), 3297-3298.

2.Schäfer, W.; Hellmann, H., Hexamethyl(Dewar Benzene) (Hexamethylbicyclo[2.2.0]hexa-2,5-diene). *Angewandte Chemie International Edition in English* **1967,** *6* (6), 518-525.

3.Khan, A.; Stucky, G. D.; Hawker, C. J., High-Performance, Nondiffusive Crosslinked Polymers for Holographic Data Storage. *Advanced Materials* **2008,** *20* (20), 3937-3941.

4.Zhu, R.; Swager, T. M., Polymer Valence Isomerism: Poly(Dewar-o-xylylene)s. *Journal of the American Chemical Society* **2018,** *140* (15), 5211-5216.

5.Giustra, Z. X.; Liu, S.-Y., The State of the Art in Azaborine Chemistry: New Synthetic Methods and Applications. *Journal of the American Chemical Society* **2018,** *140* (4), 1184-1194.

6.Edel, K.; Yang, X.; Ishibashi, J. S. A.; Lamm, A. N.; Maichle-Mössmer, C.; Giustra, Z. X.; Liu, S.-Y.; Bettinger, H. F., The Dewar Isomer of 1,2-Dihydro-1,2-azaborinines: Isolation, Fragmentation, and Energy Storage. *Angew Chem.Int.Ed* **2018,** *57* (19), 5296-5300.

7.Giustra, Z. X.; Yang, X.; Chen, M.; Bettinger, H. F.; Liu, S.-Y., Accessing 1,2-Substituted Cyclobutanes through 1,2-Azaborine Photoisomerization. *Angew Chem.Int.Ed* **2019,** *58* (52), 18918-18922.

8.Seo, J.; Lee, S. Y.; Bielawski, C. W., Unveiling a Masked Polymer of Dewar Benzene Reveals trans-Poly(acetylene). *Macromolecules* **2019,** *52* (8), 2923-2931.

9.Su, J. K.; Feist, J. D.; Yang, J.; Mercer, J. A. M.; Romaniuk, J. A. H.; Chen, Z.; Cegelski, L.; Burns, N. Z.; Xia, Y., Synthesis and Mechanochemical Activation of Ladderene–Norbornene Block Copolymers. *Journal of the American Chemical Society* **2018,** *140* (39), 12388-12391.

10.Yang, J.; Horst, M.; Romaniuk, J. A. H.; Jin, Z.; Cegelski, L.; Xia, Y., Benzoladderene Mechanophores: Synthesis, Polymerization, and Mechanochemical Transformation. *Journal of the American Chemical Society* **2019,** *141* (16), 6479-6483.

11.Walsh, D. J.; Lau, S. H.; Hyatt, M. G.; Guironnet, D., Kinetic Study of Living Ring-Opening Metathesis Polymerization with Third-Generation Grubbs Catalysts. *Journal of the American Chemical Society* **2017,** *139* (39), 13644-13647.

12.Charvet, R.; Novak, B. M., New Functional Monomers for Well-Controlled ROMP Polymerizations. *Macromolecules* **2001,** *34* (22), 7680-7685.

13.Leroux, F.; Pascual, S.; Montembault, V.; Fontaine, L., 1,4-Polybutadienes with Pendant Hydroxyl Functionalities by ROMP: Synthetic and Mechanistic Insights. *Macromolecules* **2015,** *48* (12), 3843-3852.

14.Seo, J.; Lee, S. Y.; Bielawski, C. W., Dewar lactone as a modular platform to a new class of substituted poly(acetylene)s. *Polymer Chemistry* **2019,** *10* (47), 6401-6412.

15.Vougioukalakis, G. C.; Grubbs, R. H., Ruthenium-Based Heterocyclic Carbene-Coordinated Olefin Metathesis Catalysts. *Chemical Reviews* **2010,** *110* (3), 1746-1787.

16.Kim, K. O.; Shin, S.; Kim, J.; Choi, T.-L., Living Polymerization of Monomers Containing endo-Tricyclo[4.2.2.02,5]deca-3,9-diene Using Second Generation Grubbs and Hoveyda–Grubbs Catalysts: Approach to Synthesis of Well-Defined Star Polymers. *Macromolecules* **2014,** *47* (4), 1351-1359.

17.Lin, H.; McConnell, C. R.; Jilus, B.; Liu, S.-Y.; Jäkle, F., Changing up BN-Polystyrene: Effect of Substitution Pattern on the Free-Radical Polymerization and Polymer Properties. *Macromolecules* **2019,** *52* (12), 4500-4509.

18.Parab, K.; Venkatasubbaiah, K.; Jäkle, F., Luminescent Triarylborane-Functionalized Polystyrene: Synthesis, Photophysical Characterization, and Anion Binding Studies. *J. Am. Chem. Soc.* **2006,** *128*, 12879-12885.

19.Brough, S. A.; Lamm, A. N.; Liu, S.-Y.; Bettinger, H. F., Photoisomerization of 1,2-Dihydro-1,2-Azaborine: A Matrix Isolation Study. *Angew Chem.Int.Ed* **2012,** *51* (43), 10880-10883.

4.6 Appendix

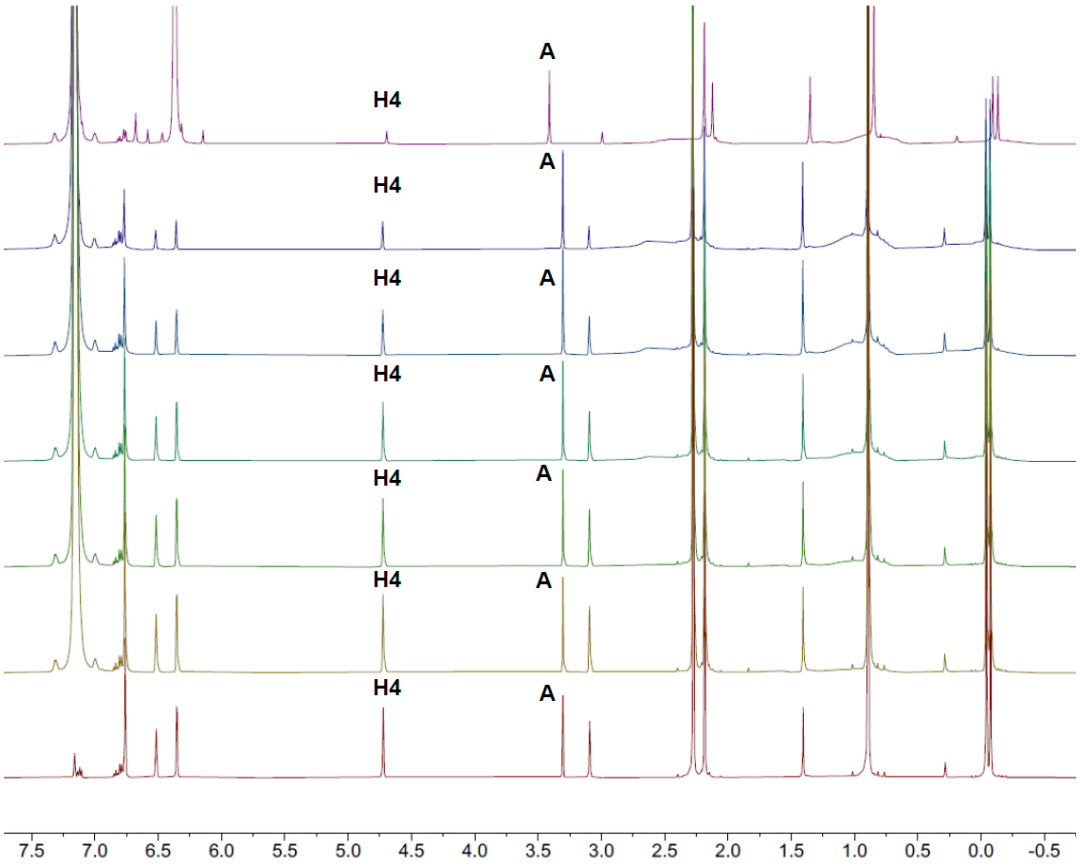

Figure. 4-S1. Figure 4-S1. Stacked ^{1}H NMR spectra at different time points during ROMP of Dewar isomer **1** (0, 0.5, 1, 1.5, 2.5, 3.5, 4.5 hours from bottom to top). "H4" represents the proton in 4-position of the monomer and the anisole reference standard is labeled with "A".

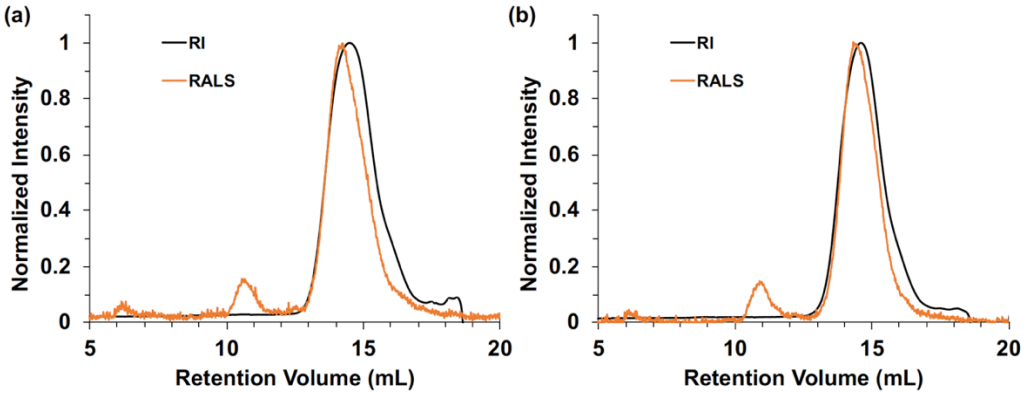

Figure. 4-S2. Overlay of GPC-RI and RALS traces for polymers obtained with G2 (a) and HG2 (b); eluent: THF, 1 mL min^{-1}.

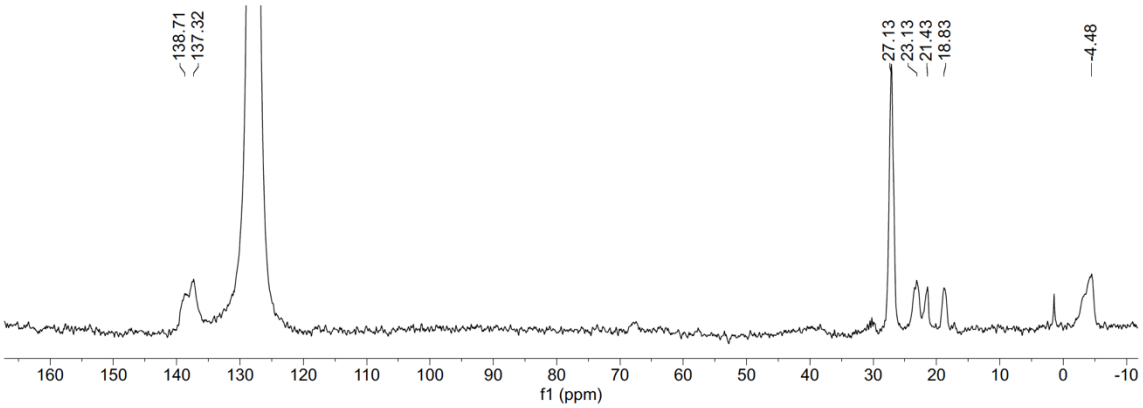

Figure. 4-S3. ^{13}C NMR spectrum of poly(1,2-azaborinine) in C_6D_6.

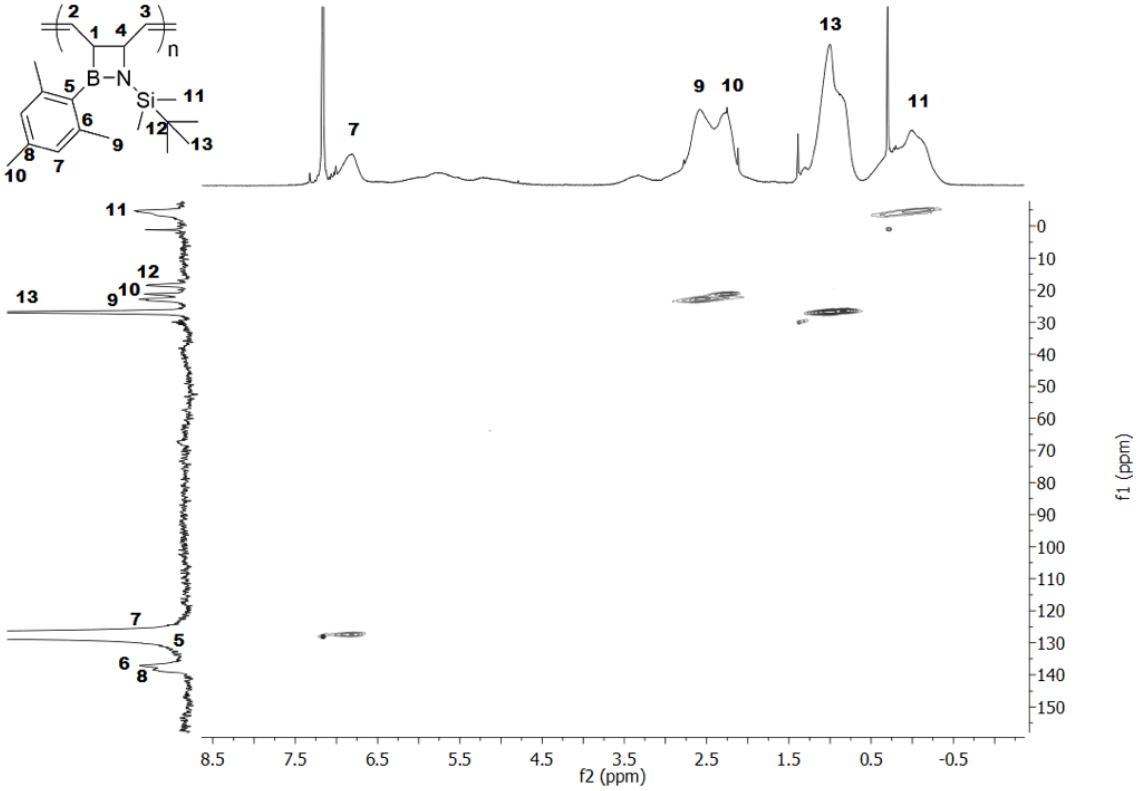

Figure. 4-S4. ^{1}H, ^{13}C-HSQC NMR spectrum of poly(1,2-azaborinine) in C_6D_6.

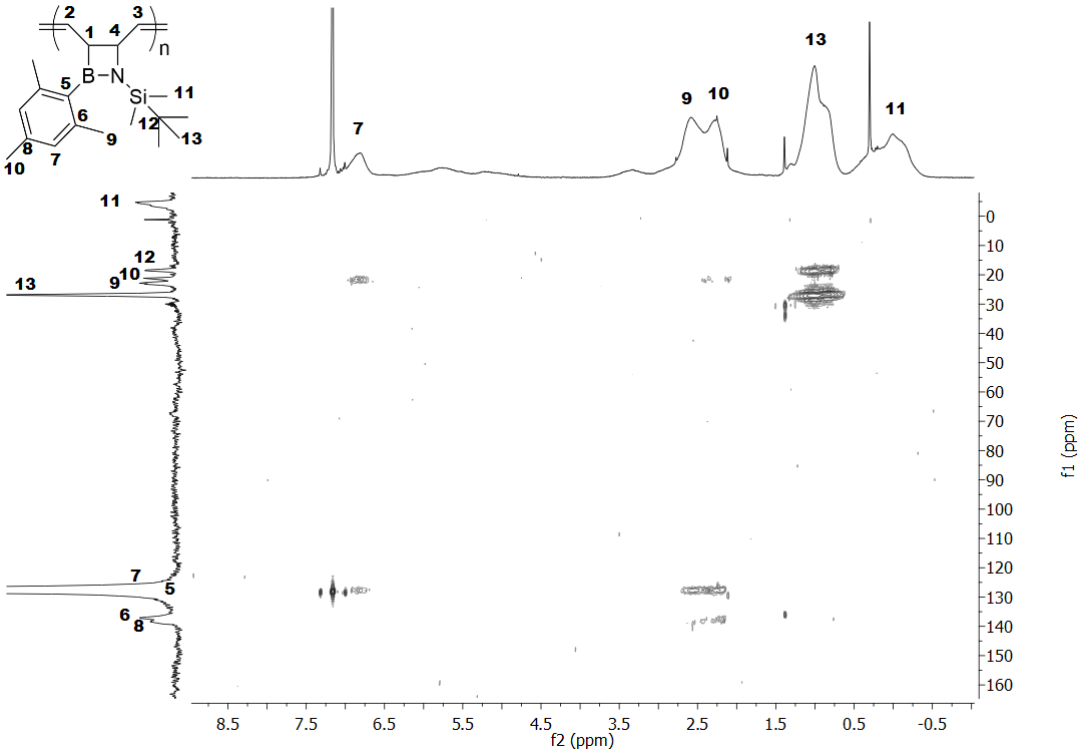

Figure. 4-S5. ^{1}H, ^{13}C-HMBC NMR spectrum of poly(1,2-azaborinine) in C_6D_6.

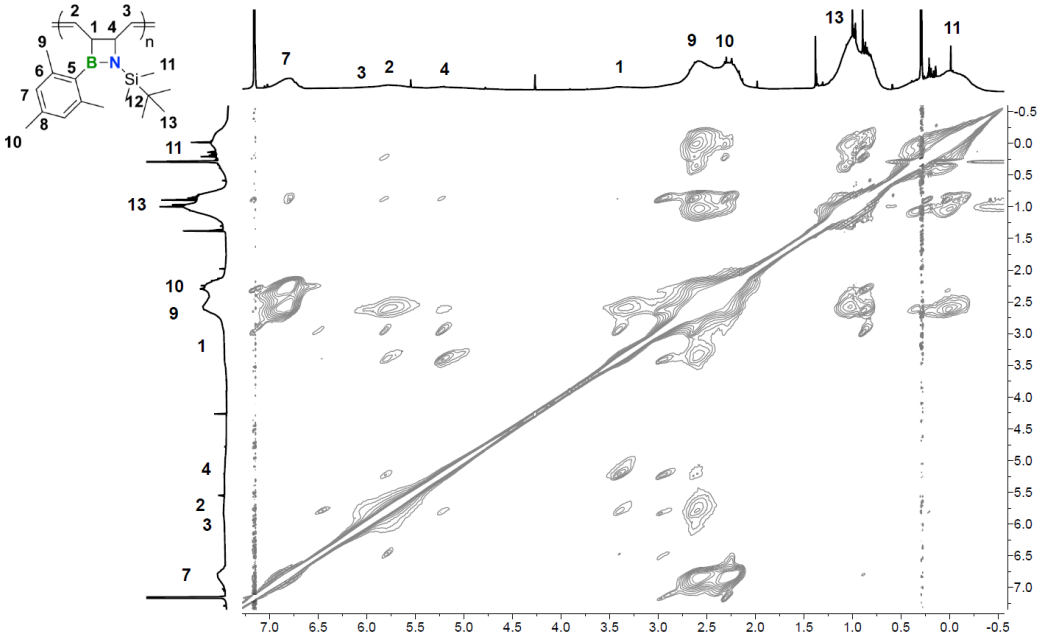

Figure. 4-S6. Full NOESY NMR spectrum of poly(1,2-azaborinine) in C_6D_6.

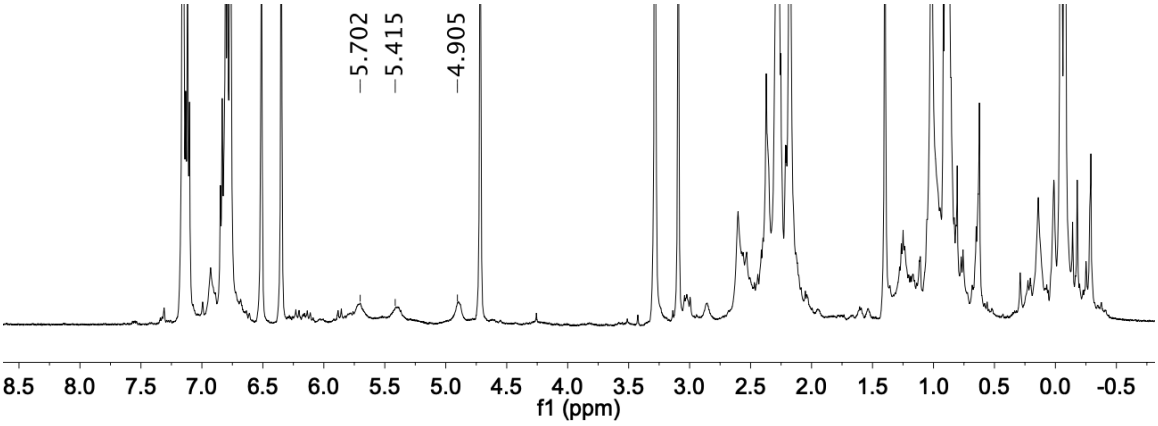

Figure. 4-S7. ^{1}H NMR spectrum of ROMP of 1 with the cis-selective catalyst HGM2001in C_6D_6.

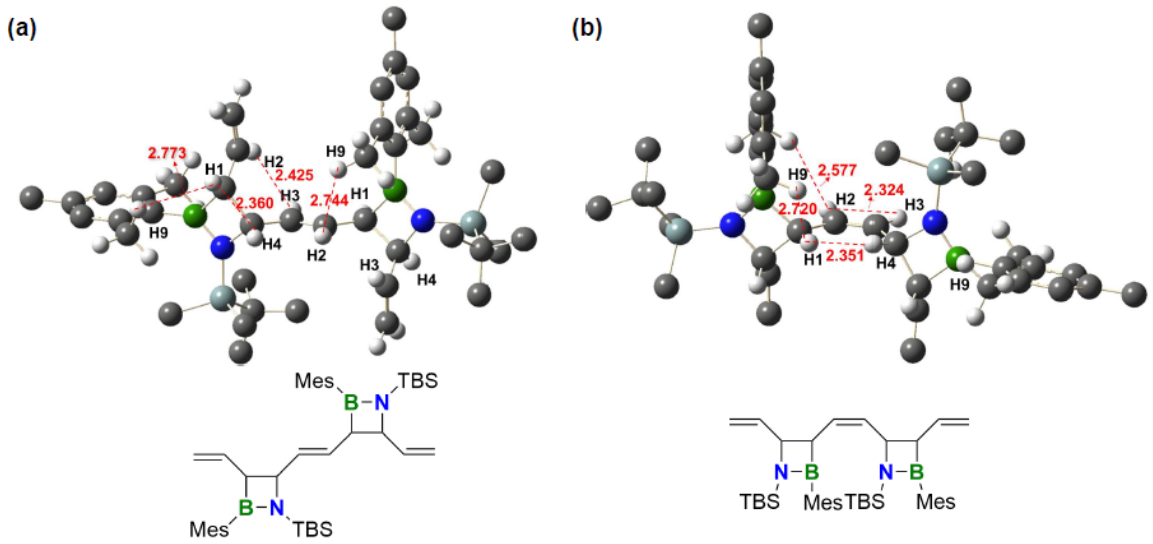

Figure. 4-S8. Optimized structures of (a) trans-dimer, (b) cis-dimer (Gaussian 16; rb3lyp/6-31g(d)). C dark grey, B green, N blue, Si light blue-grey; only selected H atoms are shown.

Table 4-S1. Comparison of the ground state energies for head-to-tail *trans*- and *cis*-dimer, optimized at rb3lyp/6-31g(d) level of theory.

Compound	S_0 (Hartree)
trans-dimer	-2300.281945
cis-dimer	-2300.274024

Table 4-S2. Comparison of the distances between hydrogens (distances in Å) in head-to-tail *trans* and *cis*-dimer obtained from DFT calculations (Gaussian 09; rb3lyp/6-31g(d))

	trans-dimer	*cis*-dimer
H1-H2	**3.09**	**3.09**
H1-H3	2.43[a]	3.80
H1-H4	**2.36**	**2.35**
H2-H3	**2.43 (intra-unit)**	**2.32 (inter-unit)**
H2-H4	2.33[a]	3.87
H3-H4	**3.09**	**3.08**
H1-H9	**2.70**	**2.72**
H2-H9	**2.74**	**2.58**
H3-H9	4.22	3.64
H4-H9	3.78	3.83

[a] Strong NOE peaks between H1/H3 and H2/H4 are not seen, but this could be due to conformational differences in solution relative to the computed structure. Considering the computational results, a *trans*-configuration is still more likely than a *cis*-configuration, although the latter cannot be fully ruled out.

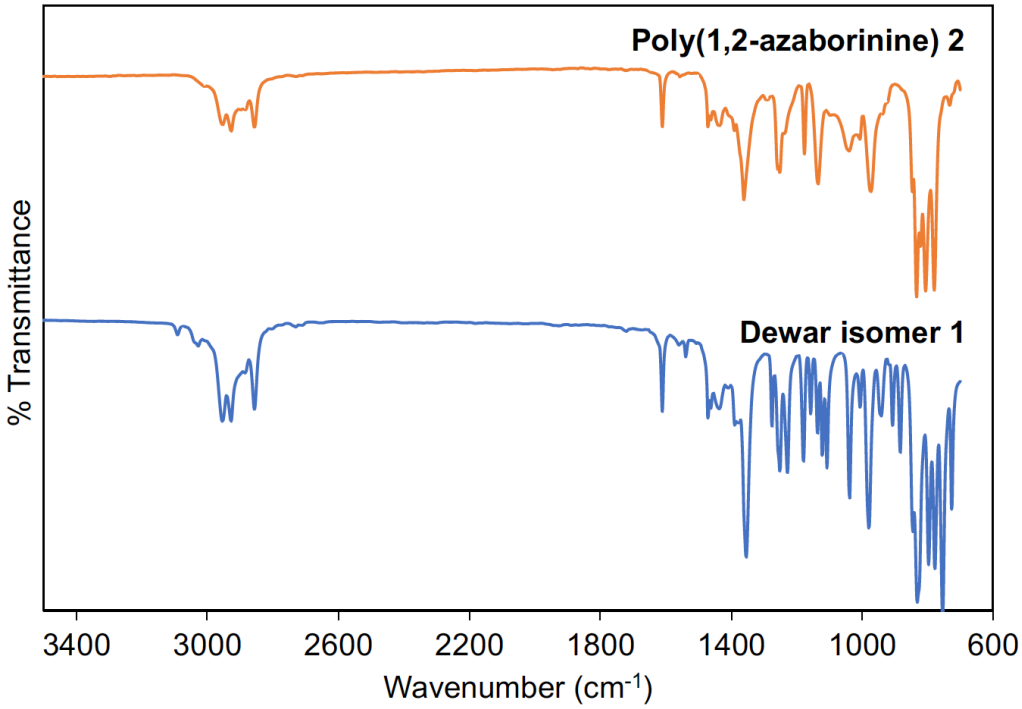

Figure. 4-S9. Full FT-IR spectrum of Dewar isomer **1** and poly(1,2-azaborinine) **2**.

Overall Conclusions

In this thesis, the applications of new polymeric triarylboranes in catalysis and luminescent materials have been investigated. We also explored new azaborine-substituted polymers to expand the diversity and functionality of polystyrenes via B-N for C-C substitution.

Two novel polymeric Lewis acids and their corresponding model compounds have been prepared. By introducing two *ortho*-methyl or a single *ortho*-chlorine substituent to boron moiety, we were able to tune Lewis acidity for efficient catalysis with an expanded substrate scope. We also discovered that all compounds display strong luminescence in solution and TADF due to the twisted intramolecular charge transfer state. This study presented the strong potential of structurally fine-tuned polymer-supported Lewis acids as catalysts in the hydrosilylation of C=X bonds (X = O, N) with excellent recyclability, whereas the intriguing emissive properties suggest potential utility as luminescent materials.

A variety of azaborinine-substituted polymers with B-N units in different positions relative to the polymer backbone have been synthesized via free radical polymerization. The isomeric azaborinine monomers offer tunable reactivity as a result of the attachment of the vinyl groups to different carbon atoms in the heterocyclic framework. Computational studies offered insights into the subtle electronic effects that result in this differential reactivity. The azaborinine polymers exhibit favorable stability and high glass transition temperatures relative to PS. The absorptions for the BN polymers are red-shifted in relation to the CC compounds as a typical effect of BN/CC isosterism. The new polymers described

herein add to a growing but still underdeveloped class of aromatic polymers, in which a C−C unit is replaced by an isoelectronic but polarized B−N unit.

Finally, we succeeded in the synthesis of a new type of poly(Dewar-1,2-azaborinine) by ROMP with G2 and HG2 as catalysts. For both G2 and HG2, the polymerization followed first-order kinetics. The unique polymer structure, verified by GPC analysis, 2D NMR, and FT-IR, encompasses four-membered heterocycles embedded in the backbone. The presence of the B-N four-membered rings may be exploited in the preparation of new functional polymers via chemoselective organoborane oxidation and/or hydrogenation of the double bonds in the backbone.

All the work presented in this thesis has advanced our understanding of the unique properties of boron-containing polymers, and some of them have shown to be promising for future applications in catalysis and material chemistry.